
Dissertation zur Erlangung des Doktorgrades
der Fakultät für Chemie und Pharmazie
der Ludwig-Maximilians-Universität München

*Click Chemistry for Enhanced and Emerging
Biological Applications: From Novel Dyes for Cell Proliferation
Assays to mRNA-Based Vaccination*

Luis Montiel Campanón

aus

Torredembarra, Spanien

2023

Erklärung

Diese Dissertation wurde im Sinne von §7 der Promotionsordnung von 28. November 2011 von Herrn Prof. Dr. Thomas Carell betreut.

Eidesstattliche Versicherung

Diese Dissertation wurde selbstständig, ohne unerlaubte Hilfe erarbeitet.

München, 03.08.2023

Luis Montiel Campanón

Dissertation eingereicht am:

03.08.2023

1. Gutachter:

Prof. Dr. Thomas Carell

2. Gutachter:

Dr. Pavel Kielkowski

Mündliche Prüfung am:

19.09.2023

“Investigad, interesaos por los fenómenos de la naturaleza. Pero lo más importante: salid, socializad y, sobre todo, pasadlo bien.”

José A. Altemir

Table of Contents

Publication List	I
Conference Attendance	I
Acknowledgements	II
Abbreviation List	V
Abstract	VIII
1 Introduction.....	1
1.1 The Concept of Click Chemistry	1
1.1.1 Huisgen's Cycloaddition.....	2
1.1.2 Copper-Catalyzed Azide Alkyne Cycloaddition (CuAAC).....	3
1.1.3 Strain-Promoted Azide Alkyne Cycloaddition (SPAAC).....	5
1.1.4 The 2022 Nobel Prize in Chemistry.....	6
1.2 Click Chemistry to Chemically Modify Nucleic Acids.....	6
1.3 Incorporation of Click-Chemistry-Functionalities into Nucleic Acids.....	8
1.4 Applications of Click-Chemistry-Modified Nucleic Acids	10
1.4.1 Small Molecule and Dendritic Structure Labeling	10
1.4.2 Cellular Metabolic Labeling	12
1.4.3 Assembly of Oligonucleotide Sequences.....	13
1.4.4 Other Applications: Antisense Oligonucleotides, Single-Guide RNA, Nanomaterials and Cyclic DNA.....	15
2 Aims of the Thesis	16
3 Published Work.....	17
3.1 Divergent Synthesis of Ultrabright and Dendritic Xanthenes for Enhanced Click-Chemistry-Based Bioimaging.....	19

4 Unpublished Work	27
4.1 Synthesis and Validation of Clickable Multimeric Mannose Ligands for Dendritic Cell Targeting	27
4.1.1 Prolog: Targeted Delivery of Nucleic Acid Therapeutics	27
4.1.2 Results and Discussion	29
4.2 Application of Multimeric Mannose Targeting Ligands in an mRNA-Based SARS-CoV-2 Vaccine Candidate	37
4.2.1 Prolog: The COVID-19 Pandemic	37
4.2.2 Results and Discussion	40
5 Conclusions and Outlook	45
6 Experimental Section for Unpublished Work	49
6.1 General Experimental Methods and Materials	49
6.2 Chemical Synthesis	52
6.2.1 Synthesis of TBDPS-Protected Mannose Derivative (63)	52
6.2.2 Synthesis of Diantennary-Mannose Targeting Ligand (68)	53
6.2.3 Synthesis of Tetraantennary-Mannose Targeting Ligand (73)	57
6.2.4 Synthesis of Mannotriose Targeting Ligand (75)	61
6.2.5 Synthesis of Triantennary-GalNac Targeting Ligand (77)	62
6.2.6 General Procedure for Click-Chemistry-Conjugation of Targeting Ligands with Fluorescein Azide	64
6.3 Minimum Energy Geometry Optimization of Fluorescent Conjugates	65
6.4 Solution Stability Study of Fluorescent Conjugates	66
6.5 Synthesis of IVT mRNA	67
7 References	70
8 Appendices	83
8.1 Supporting Information for Published Work	83
8.2 NMR Spectra for Unpublished Work	130

Publication List

- 2) **Montiel, L.**; Spada, F.; Crisp, A.; Wiedemann, S.; Carell, T.; Frischmuth, T. Synthesis and Validation of Clickable Multimeric Mannose Ligands for Dendritic Cell Targeting. *ACS Omega*, submitted.

(Highlighted as Hot Topic: Click Chemistry)

- 1) **Montiel, L.**; Spada, F.; Crisp, A.; Serdjukow, S.; Carell, T.; Frischmuth, T. Divergent Synthesis of Ultrabright and Dendritic Xanthenes for Enhanced Click-Chemistry-Based Bioimaging. *Chem. - A Eur. J.* **2023**, *29* (5), e202202633.

Conference Attendance

- 5) Oral Presentation. *Fluorescent multivalent dendrimers for enhanced bioimaging*. **3rd LightDyNAMics Week**, Virtual Symposium. July 2021.
- 4) Poster presentation. *Modified-mRNA SARS-CoV-2 Vaccine Development for Targeted Delivery*. **2021 RNA Therapeutics: From Concept to Clinic**, University of Massachusetts Chan Medical School, Worcester, USA (Virtual Symposium). June 2021.
- 3) Poster presentation. *Development of a SARS-CoV-2 Vaccine Containing modified mRNA*. **8th International mRNA Health Conference**. Boston, USA (Virtual Symposium). November 2020.
- 2) Oral Presentation. *Development of a SARS-CoV-2 vaccine containing modified mRNA*. **2nd LightDyNAMics Week**. Slovenian NMR Centre, National Institute of Chemistry, Ljubljana, Slovenia (Virtual Symposium). October 2020.
- 1) Oral Presentation. *Chemical Amplification of Fluorescently Click-labeled DNA*. **1st LightDyNAMics Week**. Department of Industrial Chemistry Toso Montanari, University of Bologna, Bologna, Italy. June 2019.

Acknowledgements

Throughout the journey of completing this doctoral dissertation, a number of individuals have had a profound impact on its development, to whom I would like to express my sincere gratitude.

First and foremost, I would like to thank Dr. Thomas Frischmuth for providing me with the opportunity to pursue my doctoral studies at baseclick GmbH. I would also like to express my heartfelt appreciation to Prof. Dr. Thomas Carell for welcoming me as an external PhD student to his research group at the LMU facilities.

Moreover, I want to express my sincere gratitude to all the remarkable individuals I had the pleasure of meeting at baseclick GmbH. I am particularly thankful to Dr. Sascha Serdjukow for his helpful advice and guidance during my initial year as a newly minted PhD student. Additionally, I owe a tremendous debt of gratitude to Dr. Antony Crisp and Dr. Fabio Spada, as their contributions were crucial in the success of my doctoral work. Their expertise, constant advice, motivation, and guidance have been invaluable throughout both my laboratory experiments and writing process. Having such skilled and dedicated scientists by my side has been an incredible asset. I extend my warmest thanks for their unwavering support, which has enabled me to achieve this significant milestone.

This doctoral thesis would not have been the same without the extraordinary companionship of Dr. Stefano Croce and Eva Schönegger in the laboratories of baseclick. Our coffee breaks, mutual assistance in overcoming PhD-related challenges, and the friendship we have developed have made this experience all the more fulfilling. Special thanks are also extended to my master's student, Tianqi Zhang, for her remarkable enthusiasm and dedication throughout her internship with me. I am grateful for her hard work, which has contributed to the progress of my research objectives.

I also wish to express my gratitude to all the people I encountered in the Carell group. Their presence has made this experience truly remarkable, especially in those memorable parties that made this journey more enjoyable and manageable. I want to extend special thanks to Giacomo Ganazzoli, Filipp Streshnev, and Samuele Stazzoni for our friendship and joint experiences during this time. Additionally, I acknowledge the exceptional contributions of Dr. Markus Müller in providing valuable corrections to this thesis, which have outstandingly enhanced the quality of this work.

I express my appreciation to all members of the LightDynamics Marie Curie network. It has been an absolute pleasure to connect with you and to share memorable experiences during our meetings and training events!

I want to extend special thanks to my awesome former flat mates, Gemma Comas, Celina González, and Chris Schimpf. Living together in our apartment was a blast! From our daily lives to our parties, we had such a great time. Getting to know all of you was truly a highlight.

I wish to thank my friends from both my hometown, Torredembarra, and Rovira i Virgili University, in Tarragona. I am deeply grateful for the countless shared experiences we have had, even after I moved to Munich. Special thanks go to Gerard Lozano, Gerard Magriñá, Arnau Ribera, Cristina Pueyo, Cristina Miracle, Enric Petrus and Alejandro Bara for visiting me during these years. For the rest who did not have the chance to come yet, we still have a pending Oktoberfest!

One individual who has had a significant impact on my academic journey is my high school chemistry teacher, José Antonio Altemir. His exceptional dedication and passion for teaching chemistry played a crucial role in cultivating my interest in the subject, which ultimately led me to pursue this doctoral thesis. I will never forget one of his many valuable pieces of advice, which I have applied throughout the course of my doctoral work: *Do your research, be interested in the phenomena of nature. But most importantly: go out, socialize and above all, have fun.*

Another person I am deeply grateful to is Sara Herzog. Thank you, Sara, for your invaluable assistance during the initial stages of this journey, particularly when I faced one of the most challenging hurdles. As the first person to extend a helping hand when I arrived in Munich, you played a pivotal role in laying the foundation that ultimately led to the culmination of this remarkable journey. I will never forget your advice, memorable experiences, and engaging discussions we shared during that incredible month and a half we spent together in late 2018. Thank you very much, Sara!

The most significant acknowledgements are saved for the end. First and foremost, I would like to express my heartfelt appreciation for the relentless support of my family: my parents and my sister. I am profoundly grateful for their unconditional backing and constant motivation, especially during moments of weakness when I doubted my ability to persevere. Their belief in me has been a driving force throughout this adventure and I cannot thank them enough for their unwavering presence and encouragement.

Last but certainly not least, I want to extend my deepest gratitude to my beloved girlfriend, Isabel Kellermann. Your firm support and remarkable perseverance have been a constant source of strength and motivation. When I found myself lost and unsure, you knew exactly how to calm my anxieties and inspire me to keep pushing forward. Your unconditional encouragement has been the cornerstone of my success, and I am truly grateful beyond words. Thank you for being my strongest pillar of support throughout these years.

Abbreviation List

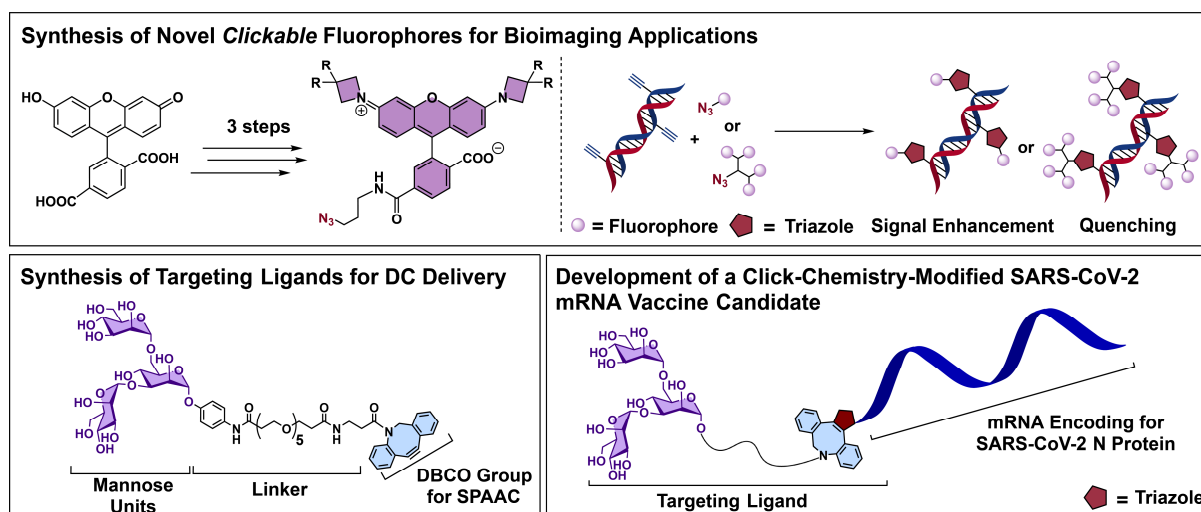
AmdU	5-(azidomethyl)-2'-deoxyuridine
ARCA	Anti-Reverse Cap Analog
ARDS	Acute Respiratory Distress Syndrome
ASGPR	Asialoglycoprotein Receptor
ASO	Antisense Oligonucleotide
AzddATP	3'-azido-2',3'-dideoxyadenosine Triphosphate
bis-MPA	2,2-bis(methylol)propionic Acid
Boc	<i>tert</i> -butyloxycarbonyl
BrdU	5-bromo-2'-deoxyuridine
cDNA	Complementary DNA
COSY	Correlated Spectroscopy
COVID-19	Coronavirus Disease 2019
CTL	C-Type Lectin
CTLD	CTL Binding Domain
CuAAC	Copper-Catalyzed Azide Alkyne Cycloaddition
DAPI	4',6-diamidino-2-phenylindole
dba	Dibenzylideneacetone
DBCO	Dibenzocyclooctyne/Dibenzoazacyclooctyne
DBCO-PEG-5-NHS	Dibenzoazacyclooctyne-penta(ethylene glycol)-propanoic Acid Succinimidyl Ester
DC	Dendritic Cell
DCIR	Dendritic Cell Immunoreceptor
DC-SIGN	Dendritic Cell-Specific Intercellular Adhesion Molecule-3- Grabbing Nonintegrin
DMAP	4-(Dimethylamino)pyridine
DMF	<i>N,N</i> -dimethylformamide
DMSO	Dimethyl Sulfoxide
DNA	Deoxyribonucleic Acid
dNTP	Deoxynucleoside Triphosphate
DSC	<i>N,N'</i> -disuccinimidyl Carbonate
EA	2-ethynyl Adenosine

EDTA	Ethylenediaminetetraacetic Acid
EdU	5-ethynyl-deoxyuridine
EdUTP	5-ethynyl-deoxyuridine Triphosphate
ESI	Electrospray Ionization
EU	5-ethynyl-uridine
EWG	Electron Withdrawing Group
FITC	Fluorescein Isothiocyanate
FRET	Förster/Fluorescence Resonance Energy Transfer
GalNAc	<i>N</i> -acetylgalactosamine
HMBC	Heteronuclear Multiple Bond Correlation
HSQC	Heteronuclear Single Quantum Coherence
IR	Infrared
IVT	<i>in vitro</i> Transcribed
LNA	Locked Nucleic Acid
LNP	Lipid Nanoparticle
MALDI	Matrix-Assisted Laser Desorption/Ionization
MERS-CoV	Middle East Respiratory Syndrome-Related Coronavirus
MGL	Macrophage Galactose/ <i>N</i> -acetylgalactosamine Specific C-Type Lectin
MR	Mannose Receptor
mRNA	Messenger RNA
MS	Mass Spectrometry
Mϕ	Macrophage
<i>N</i>⁶pA	<i>N</i> ⁶ -propargyladenosine
NGS	Next Generation Sequencing
NHS	<i>N</i> -hydroxysuccinimide
NMR	Nuclear Magnetic Resonance
OdU	5-(1,7-octadiynyl)-deoxyuridine
ORF	Open Reading Frame
PAP	Poly(A) Polymerase
pDNA	Plasmid DNA
PET	Photoinduced Electron Transfer
PMDTA	Pentamethyldiethylenetriamine

Py	Pyridine
R_f	Retention Factor
RNA	Ribonucleic Acid
RNAP	RNA Polymerase
RNP	Helical Ribonucleoprotein
ROS	Reactive Oxygen Species
RP-HPLC	Reverse Phase High-Performance Liquid Chromatography
R_t	Retention Time
SARS-CoV	Severe Acute Respiratory Syndrome Coronavirus (1/2)
sgRNA	Single Guide RNA
SPAAC	Strain-Promoted Azide Alkyne Cycloaddition
TAE	Tris-Acetate-EDTA
TBDMS	<i>tert</i> -butyldimethylsilyl
TBDPS	<i>tert</i> -butyldiphenylsilyl
TBDPSCI	<i>tert</i> -butyldiphenylsilyl Chloride
TBTA	tris[(1-benzyl-1H-1, 2, 3-triazol-4-yl)methyl]amine
Tf₂O	Trifluoromethanesulfonic Anhydride
TFA	Trifluoroacetic Acid
THF	Tetrahydrofuran
THPTA	tris[(1-hydroxypropyl-1H-1,2,3-triazol-4-yl)methyl]amine
TLC	Thin-Layer Chromatography
Tris-HCl	Tris(hydroxymethyl)aminomethane Hydrochloride
UTR	Untranslated Region
WHO	World Health Organization
YFP	Yellow Fluorescent Protein
ε	Extinction Coefficient
λ_{abs}	Absorption Wavelength
λ_{em}	Emission Wavelength
φ	Quantum Yield
ΨTP	Pseudouridine Triphosphate

ABSTRACT

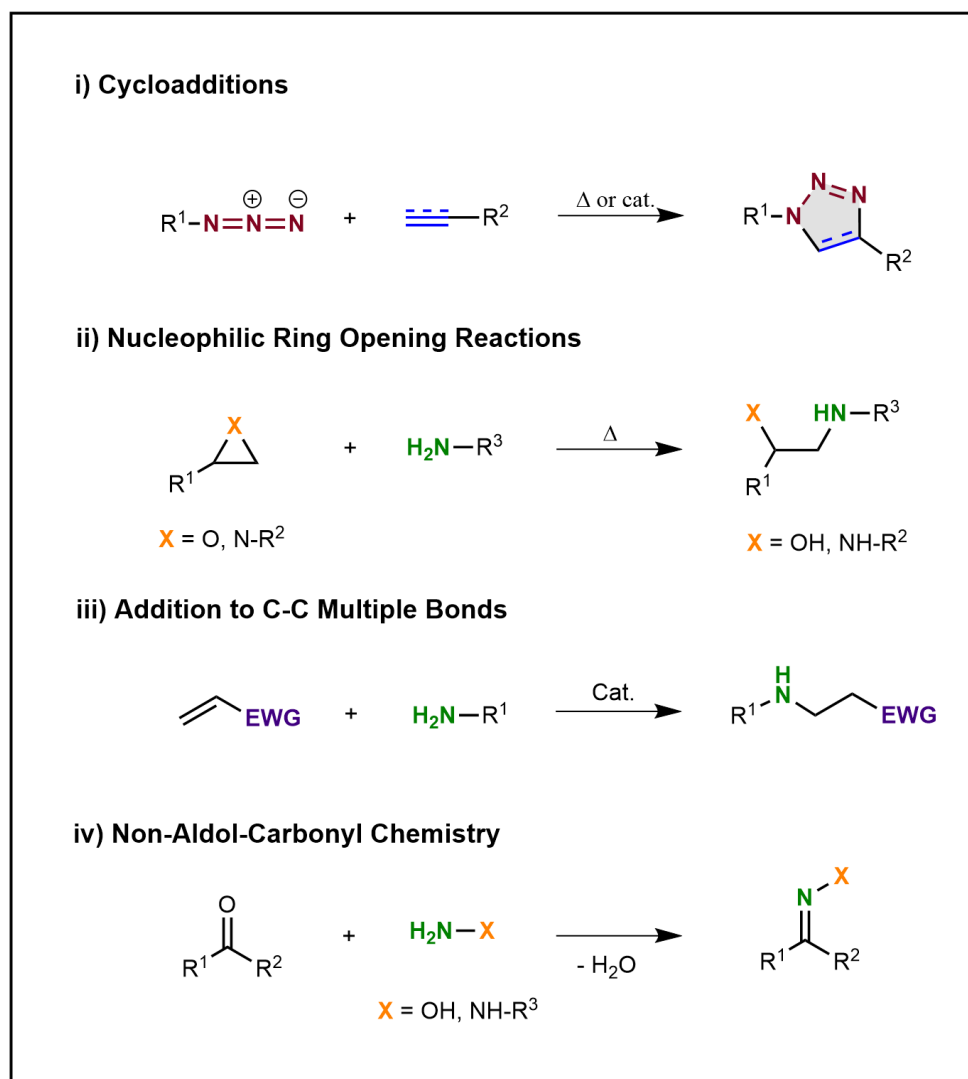
The present dissertation represents a focused endeavor aimed at broadening click-chemistry-based applications in the field of nucleic acids. The principal objective is to extend the synthetic utility of bioorthogonal click chemistry by delving into the following diverse, yet equally crucial areas of research: DNA fluorescent-labeling for bioimaging purposes and ligand development for nucleic acid cell-targeting in emerging therapeutics. We aimed to develop new fluorescent probes to improve detection sensitivity and quality of imaging methods. To achieve this, we established a divergent synthetic pathway that produced *ready-to-click*, pH-insensitive rhodamine dyes with outstanding brightness, which were proven to be a superior alternative in EdU cell proliferation assays. Furthermore, we prepared a group of fluorescein- and rhodamine-based multivalent dendrons by branching click chemistry, which exhibited self-quenching effects and demonstrated potential application as FRET quenchers. Additionally, in an effort to develop emerging therapeutics using click chemistry, particularly in vaccination and cancer immunotherapies, we synthesized three distinct *ready-to-click* mannose-functionalized ligands with the aim of targeting dendritic cells (DCs). Our analyses confirmed the uptake of the ligands' fluorescent conjugates into DCs through endocytosis. Finally, spurred by the COVID-19 pandemic, baseclick GmbH took on the task of developing a SARS-CoV-2 vaccine candidate. To this aim, we utilized our DC-targeting ligands and baseclick's mRNA labeling technology to successfully synthesize a mannose-mRNA conjugate. At present, pharmacokinetics and pharmacodynamics of the vaccine are under investigation. The promising *in vitro* results, nevertheless, instills optimism in our efforts to establish a framework for future exploration of cell-targeted, click-chemistry-based nucleic acid therapies.



1 INTRODUCTION

1.1 The Concept of Click Chemistry

The concept of *Click Chemistry*, first conceived by Kolb, Finn and Sharpless in 2001,^[1] refers to a synthetic approach that draws inspiration from nature's molecular assembly principles of efficiency, selectivity, and simplicity. Thereby, Click Chemistry defines a set of reactions that are modular, broad in scope, high-yielding, stereospecific, and no or minimal byproduct-producing. Furthermore, the term *click* implies specific reaction conditions defined by ease of execution, use of readily available starting materials, aqueous- or non-solvent compatibility, and simple product isolation.^[1,2] These reactions, thus, are highly sought-after



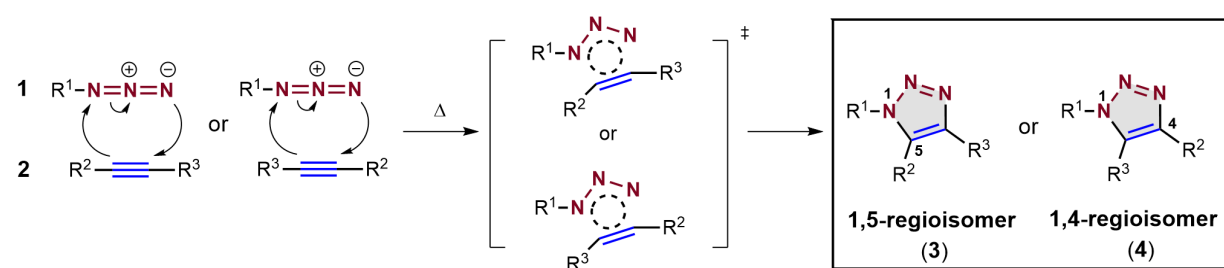
Scheme 1. Selected click reactions defined by Kolb, Finn and Sharpless. EWG = electron withdrawing group.

in synthetic chemistry due to their exceptional properties and are currently divided in four groups (**Scheme 1**): i) cycloadditions (e.g. 1,3-dipolar cycloadditions, Diels-Alder reaction), ii) nucleophilic ring-opening reactions (e.g. ring-opening of epoxides and aziridines), iii) additions to C-C multiple bonds (e.g. Michael addition of Nu-H reactants, epoxidation, aziridination, dihydroxylation), and iv) non-aldol-carbonyl chemistry (e.g. amide-, hydrazone- and oxime formation).^[1,2]

The Huisgen reaction, a 1,3-dipolar cycloaddition that involves alkynes and azides, was already a well-established technique for the synthesis of heterocyclic compounds. The advent of click chemistry, nonetheless prompted further advancements of this reaction and led to the development of a transition metal-catalyzed version, becoming the most important exponent of click chemistry.^[3]

1.1.1 Huisgen's Cycloaddition

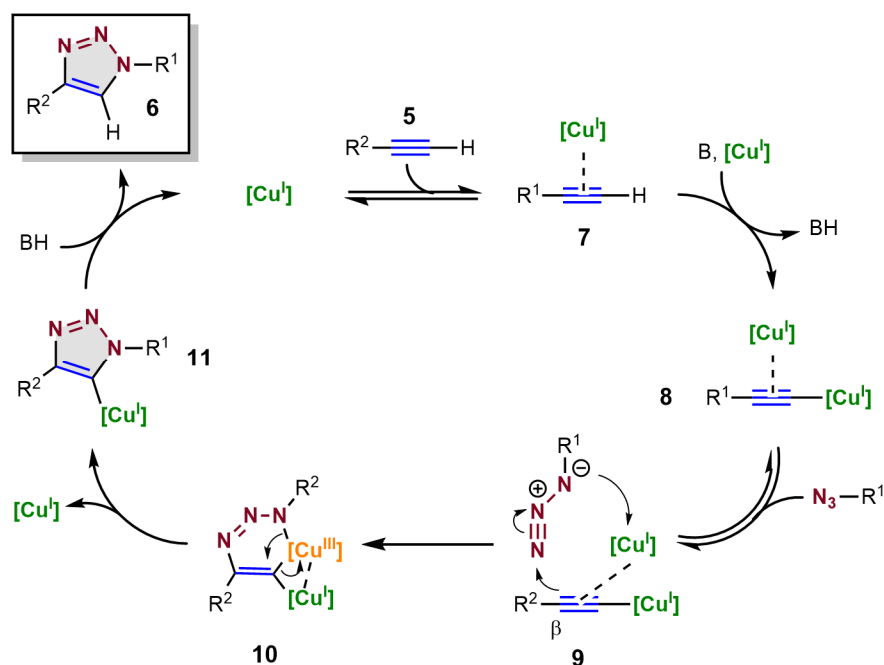
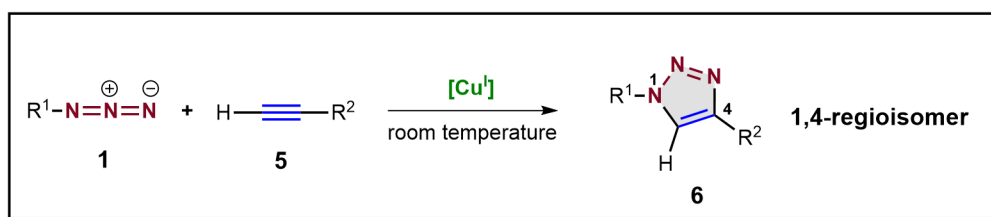
1,3-dipolar cycloadditions between alkynes and azides have been reported as early as 1893, when the first synthesis of a 1,2,3-triazole was described by Arthur Michael.^[4] In the mid-20th century, Rolf Huisgen performed an extensive systematic study of this reaction, in which he proposed a concerted pericyclic mechanism between a 1,3-dipole (azide **1**) and a dipolarophile (alkyne **2**).^[5] This reaction, known as Huisgen's cycloaddition,^[6,7] has been utilized over years in various fields of chemistry for the synthesis of five-membered heterocyclic compounds.^[3] The practical application of this cycloaddition, however, has been limited due to the requirement for high temperatures, extended reaction times, and the formation of both 1,5- and 1,4-regioisomers (**3** and **4**, respectively).^[8]



Scheme 2. Huisgen's cycloaddition.

1.1.2 Copper-Catalyzed Azide Alkyne Cycloaddition (CuAAC)

The limitations of Huisgen's cycloaddition were addressed through the independent findings of Meldal^[9] and of Sharpless and Fokin.^[10] These studies, reported in 2002, showed that the use of a Cu(I) catalyst accelerates the reaction kinetics by activation of terminal alkynes (**5**), provides only a regioselective 1,4-disubstituted triazole adduct **6**, and enables the reaction to proceed at room temperature. This reaction, known as Copper-catalyzed Azide Alkyne Cycloaddition (CuAAC), is characterized by its simplicity, efficiency, broad applicability and compatibility with a variety of functional groups and water-containing solvent mixtures, thereby embodying the core principles of click chemistry.^[9,10] Common Cu(I) sources include Cu(II) salts together with reducing agents (such as sodium ascorbate), direct use of Cu(I) compounds, and oxidation of Cu(0) precatalysts.^[11] In all cases, the species that catalyzes the



Scheme 3. Overview of CuAAC and catalytic mechanism proposed by Fokin et al.^[12]. B = base (usually Et₃N, DIPEA or ligand).^[13,14]

reaction involves Cu(I).^[9,10,13] CuAAC, considered the flagship of click chemistry, has been extensively employed in a myriad of fields including bioconjugation,^[15] dendrimer and polymer chemistry,^[16,17] material science^[18–20] and drug design.^[21,22]

The mechanism of the Cu(I) catalyzed reaction is different from the concerted Huisgen reaction and is characterized as a non-concerted stepwise process.^[10] Initially, it was postulated that the catalytic activity was exerted by Cu(I) mononuclear species^[10,14,23] but, after further kinetic studies and DFT calculations, it became apparent that simultaneously occurring dinuclear complexes prompted a more kinetically favored route.^[12,24,25] This latter mechanism involves a series of complex steps, beginning with the formation of a Cu(I)-alkyne π -complex **7**. The initial coordination of a Cu(I) species, which lowers the pKa of the terminal alkyne by 10 units, promotes subsequent deprotonation and σ -binding of a second Cu(I) species (**8**). After reversible coordination of the azide, a nucleophilic attack of the acetylide's β -carbon to the azide's distal nitrogen gives rise to a Cu(III) metallacycle (**10**). Subsequent ring contraction forms a triazolyl-copper compound (**11**) and the Cu(III) metal center is reduced to Cu(I). In the last step, compound **11** undergoes protolysis followed by release of the triazole product **6** to complete the catalytic cycle.

The relative nonreactivity of alkynes and azides towards biomolecules and their stability under biological reaction conditions establishes CuAAC as a *bioorthogonal* method.^[26,27] The use of coordinating ligands, moreover, stabilizes Cu(I) species and improves reaction kinetics and yields.^[28,29] Further optimization of these ligands have also led to the use of low micromolar catalyst concentrations, thus minimizing cytotoxicity.^[30] Polydentate amines, particularly those based on the tris(triazolylamine) scaffold,^[31] represent an important group of these ligands and various derivatives such as TBTA,^[32] THPTA,^[33] BTAA,^[30] BTES,^[34] TEOTA,^[35] BTTP^[36] and BTTPS^[37] have been synthesized to improve reaction biocompatibility (**Figure 1**). Other ligands, such as phosphines,^[31] nitrogen donors,^[38–40] aminoacids^[41] and phosphoramidites^[42] have also been employed as ligands to accelerate CuAAC.

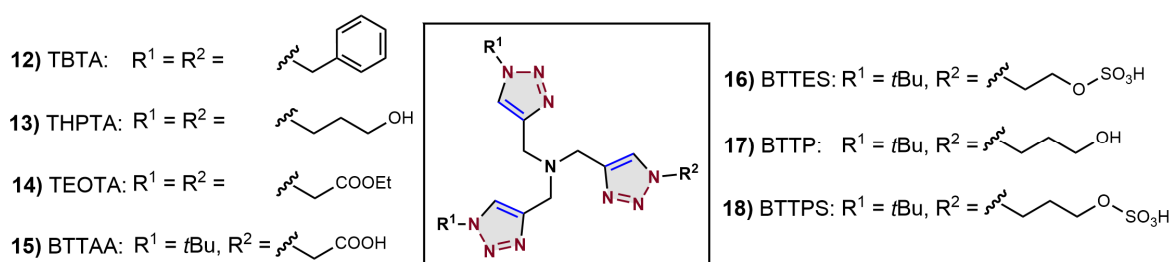
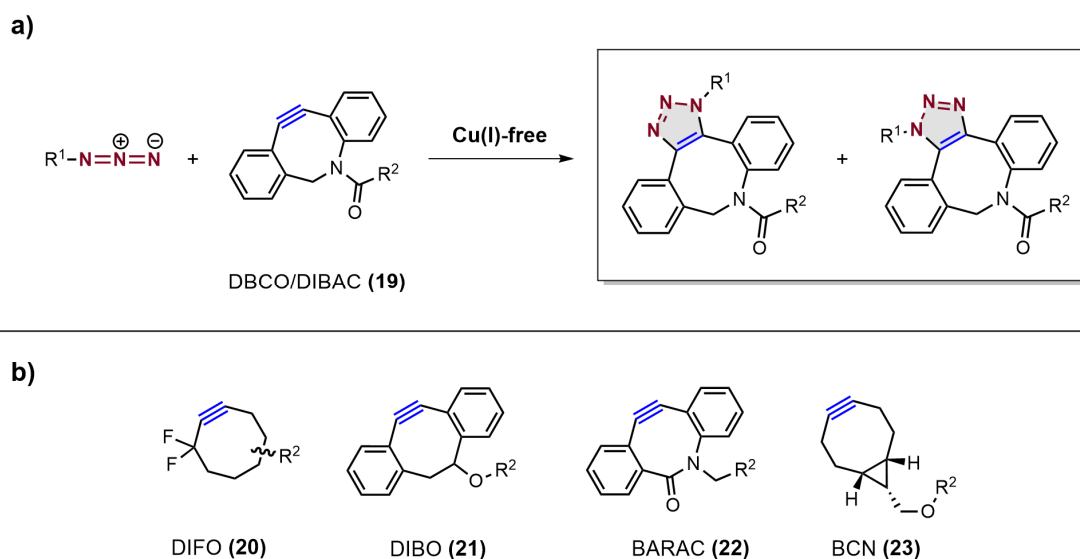


Figure 1. Structure of CuAAC-accelerating ligands based on the tris(triazolylamine) motif.

1.1.3 Strain-Promoted Azide Alkyne Cycloaddition (SPAAC)

The Strain-Promoted Azide-Alkyne Cycloaddition (SPAAC), first introduced by Bertozzi in 2004,^[43] is another prominent approach that builds upon the utility of CuAAC reactions. SPAAC involves the reaction between a strained cyclooctyne and an organic azide. Unlike CuAAC, the driving force behind SPAAC is the ring strain introduced into the alkyne reactants. To further improve SPAAC, various cyclooctyne derivatives have been developed to enhance reaction kinetics^[44–46] (**Scheme 4**).

SPAAC is a strategy that has been broadly used for bioorthogonal labeling and detection, as it eliminates the need for a Cu(I) catalyst. The utilization of SPAAC has been demonstrated in a variety of labeling applications, ranging from the surface of cells to living organisms such as zebrafish, *C. elegans*, and mice.^[47–49] Despite its benefits, SPAAC also has some drawbacks, including much slower reaction rates compared to the rate of CuAAC and the formation of regioisomeric triazoles.^[29,50]



Scheme 4. a) SPAAC reaction overview. DBCO/DIBAC = dibenzocyclooctyne/dibenzo-aza-cyclooctyne (**19**). b) Other known cyclooctynes for bioconjugation: DIFO = difluorocyclooctyne (**20**); DIBO = dibenzocyclooctyne (**21**); BARAC = biarylazacyclooctynone (**22**); BCN = Bicyclo[6.1.0]non-4-yne (**23**). Most typically, DBCO, DIBO, and BCN are employed for biological applications.^[44]

1.1.4 The 2022 Nobel Prize in Chemistry

Click chemistry and bioorthogonal chemistry have had a profound impact across the fields of chemistry, biology, and related research areas. As a result and in recognition of their seminal contributions, Carolyn R. Bertozzi, Morten Meldal, and K. Barry Sharpless were awarded the 2022 Nobel Prize in Chemistry.^[51]

1.2 Click Chemistry to Chemically Modify Nucleic Acids

Deoxyribonucleic acid (DNA) and ribonucleic acid (RNA) have fundamental roles in storage and transmission of genetic information. The differences in chemical structure of DNA and RNA (**Figure 2**) confer variations in stability, reactivity and roles in the cell.^[52]

Strategies for chemically modifying DNA and RNA with small molecules are essential resources in diverse research fields. The first adopted approach for such modifications

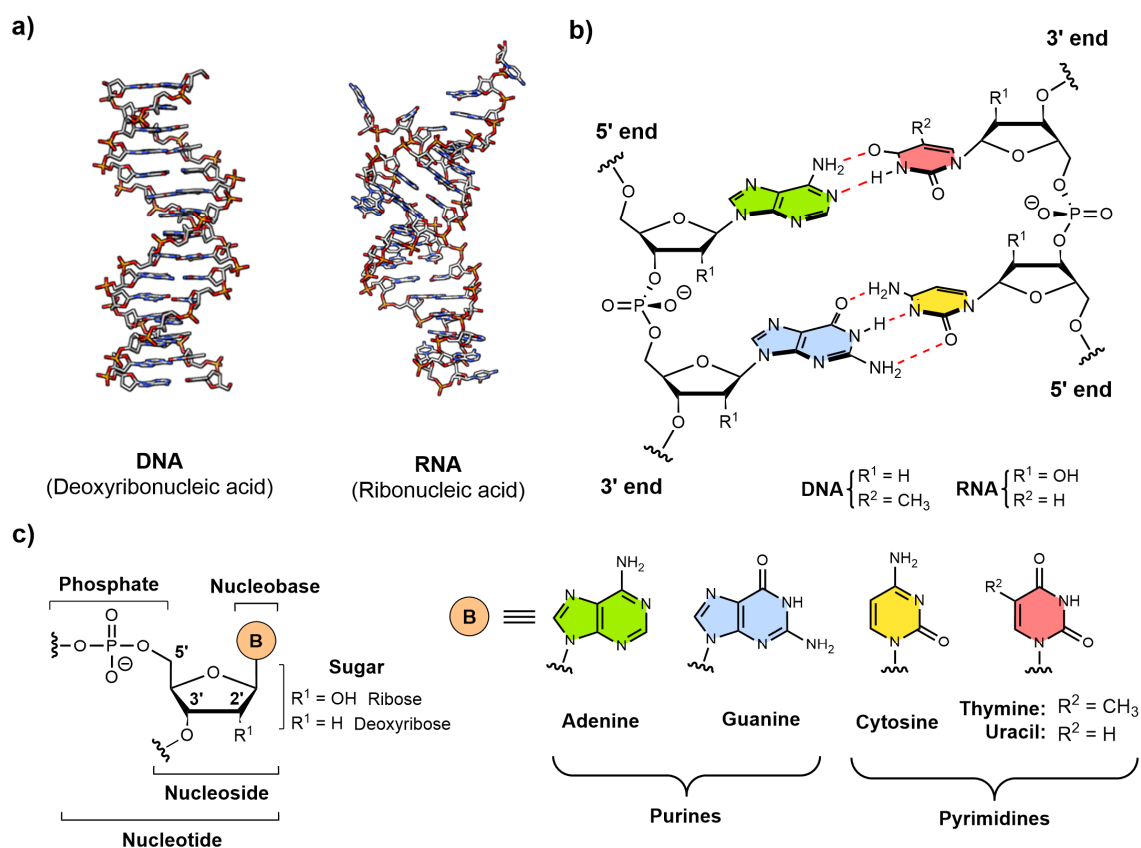
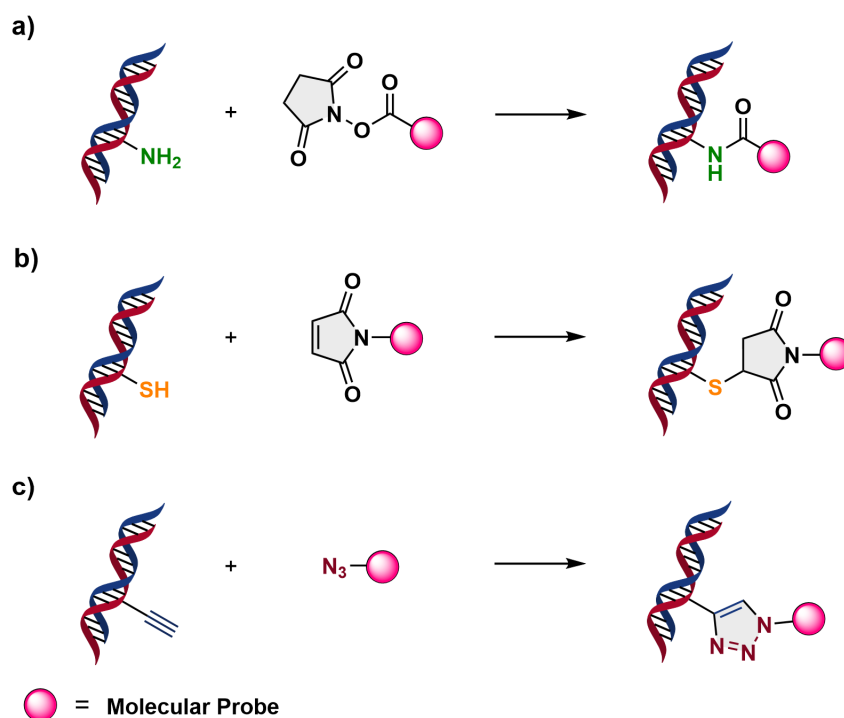


Figure 2. General concepts of nucleic acids: a) DNA and RNA structure, b) base pairing and c) chemical structure of nucleotides and nucleobases.

comprises the coupling of amine-containing oligonucleotides to active esters, such as NHS esters (**Scheme 5a**). These molecular probes, however, are unstable in reaction alkaline buffers ($\text{pH} > 8$) and are prone to decompose in moisture-containing environments or over extended storage periods. An alternative involves the use thiol-labeled oligonucleotides with maleimide- or iodoacetamide-presenting molecules (**Scheme 5b**). This strategy has also limitations due to electrophile instability and the proclivity of thiols to dimerize. In contrast, organic azides and alkynes have high chemical stability and react only with each other, remaining orthogonal to most functional groups. Subsequently, the implementation of CuAAC and SPAAC in the field of nucleic acids (**Scheme 5c**) has enabled the creation of a diverse array of tools and applications with extensive use in biology, biochemistry, and biotechnology, paving the way for groundbreaking advancements in these fields. Specifically, the impact of click chemistry as a potent technique for covalent conjugation presents a highly efficient and cost-effective approach, in comparison to traditional chemical and enzymatic techniques, for the labeling, ligation, and cyclization of DNA and RNA oligonucleotides.^[53]



Scheme 5. Main strategies to chemically modify nucleic acids. a) Coupling reaction involving amines and active esters. b) Michael-type reaction between maleimide/iodoacetamide and thiols. c) Azide-Alkyne Cycloaddition.

1.3 Incorporation of Click-Chemistry-Functionalities into Nucleic Acids

The incorporation of click modifications into DNA and RNA structures has become a well-established practice, especially due to the widespread commercial availability and synthetic routes of modified phosphoramidite monomers^[54–60] and nucleoside triphosphates,^[61–67] which are required for solid phase and enzymatic nucleic acid synthesis, respectively.

The high reactivity between organic azides and P(III) groups, as a consequence of the Staudinger reaction,^[68] proves challenging for the use of azide-containing phosphoramidites in solid-phase synthesis. Therefore, utilizing alkyne-containing phosphoramidites is the most common approach for the introduction of click chemistry functionalities (**Figure 3**). Due to their uncomplicated synthesis, alkyne-containing 2'-deoxyuridine derivatives are among the most utilized building blocks in both solid-phase synthesis and PCR applications, especially 5-ethynyl-deoxyuridine (EdU, **24**) and 5-(1,7-octadiynyl)-deoxyuridine (OdU, **25**).

OdU is a highly useful building block in phosphoramidite oligonucleotide synthesis as it does not require silyl protection of the terminal alkyne.^[70] It is also a reliable modification for the

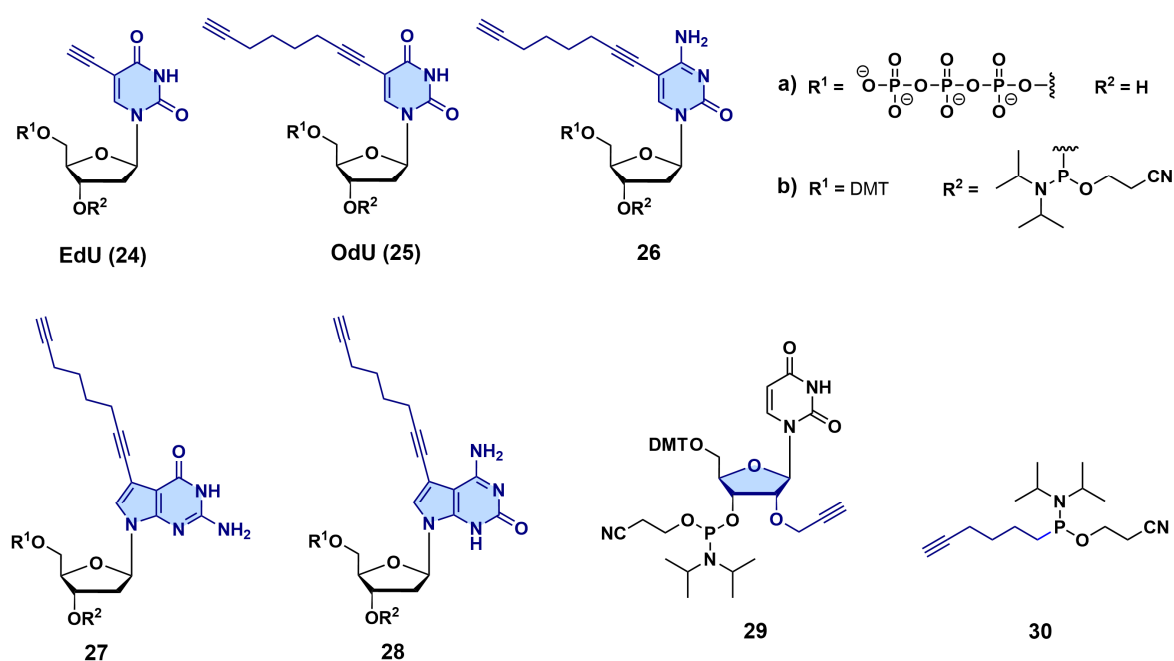


Figure 3. Examples of alkyne-modified nucleosides used as a) triphosphates for PCR and b) phosphoramidite monomers for DNA and RNA solid-phase synthesis. Non-nucleoside phosphoramidites such as hexynyl phosphoramidite^[69] (**30**) are also employed to introduce click-chemistry-functionalities into nucleic acids. DMT = dimethoxytrityl.

postsynthetic labeling of oligonucleotides with high modification density, that is, several alkyne-containing nucleotides in a synthetic strand.^[71,72] Alternatively, EdU triphosphate (EdUTP) is widely used in PCR experiments. EdUTP is an excellent substrate for DNA polymerases, comparable to natural deoxynucleotide triphosphates (dNTPs), and is superior to OdUTP when used for amplifying long DNA templates. EdU and its derivatives are also efficient metabolic labels that can be used to track DNA and RNA synthesis in living cells and *in vivo* in animal tissue models.^[73–75]

Enzymatic approaches utilizing alkyne- and azide-modified nucleosides have been employed to functionalize RNA with click chemistry groups for CuAAC and SPAAC labeling (**Figure 4**). Das and co-workers^[76] used 5'-azidoguanosine (**31**) together with T7 RNA polymerase or 3'-azido-2',3'-dideoxyadenosine (**32**) along with poly(A) polymerase (PAP) to modify RNA's 5'- and 3'-ends, respectively. Jäschke and colleagues^[77,78] utilized OdUpG dinucleotide (**33**) along with a number of bacteriophage RNA polymerases (RNAPs) and C-2' azido-modified ATP (**34**) combined with PAP enzymes for enzymatic labeling of RNA 5'- and 3'-ends, in that order. More interestingly, after introduction of **33** and **34**, the 5'- and 3'-OH groups remain available for further enzymatic modifications. Other strategies to chemoenzymatically label RNA 5'- and 3'-ends involve the use of O-propargyl-guanosine-5'-monophosphate (**35**) with T7 RNA polymerase and alkynylated 3',5'-uridine bisphosphate (**36**) through T4 RNA ligase, respectively. The application of **36** was further extended to label RNA at internal positions.^[79]

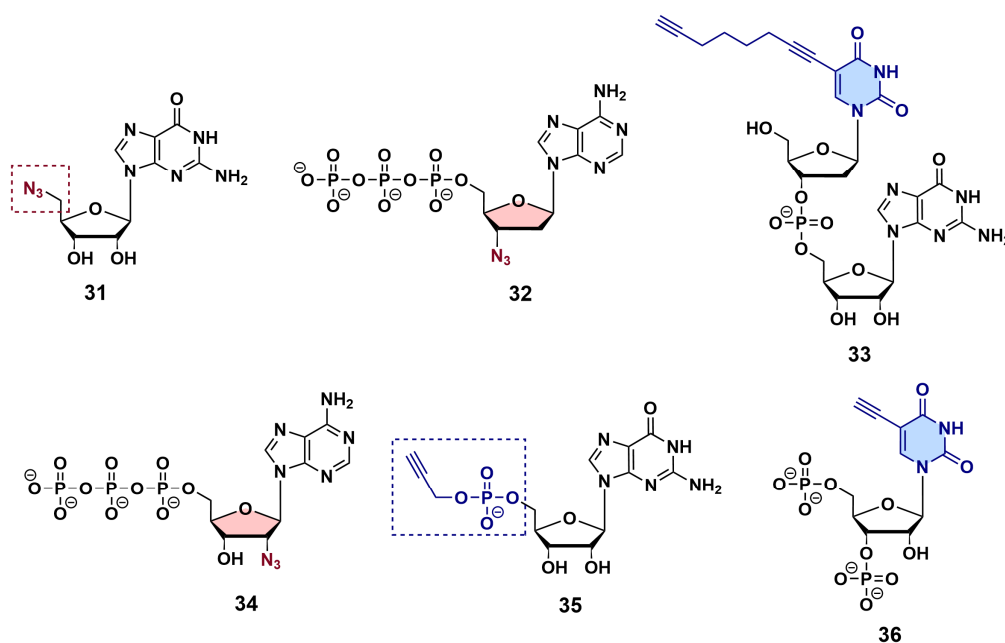


Figure 4. Building blocks to enzymatically incorporate alkyne and azide functionalities into RNA.

1.4 Applications of Click-Chemistry-Modified Nucleic Acids

1.4.1 Small Molecule and Dendritic Structure Labeling

Fluorescent dye labeling remains the most important approach of nucleic acid modification, owing to its fundamental role in nucleic acid sequencing, diagnostic procedures, forensic investigations, and genetic analysis.^[80–82] Despite the existence of numerous dyes, most of these probes are obtained from a small number of core structures (**Figure 5a**),^[83] such as fluoresceins (**37**), rhodamines (**38**), coumarins (**39**), cyanines (**40**), and BODIPY dyes (**41**).^[84–90] Advancements of novel fluorophores, therefore, is of paramount importance to augment sensitivity and quality of applications in which they are employed. Aiming to obtain probes with amplified fluorescent properties, the use of dendritic architectures containing multiple branched fluorophores has been explored (**Figure 5b**). Despite some problems related to

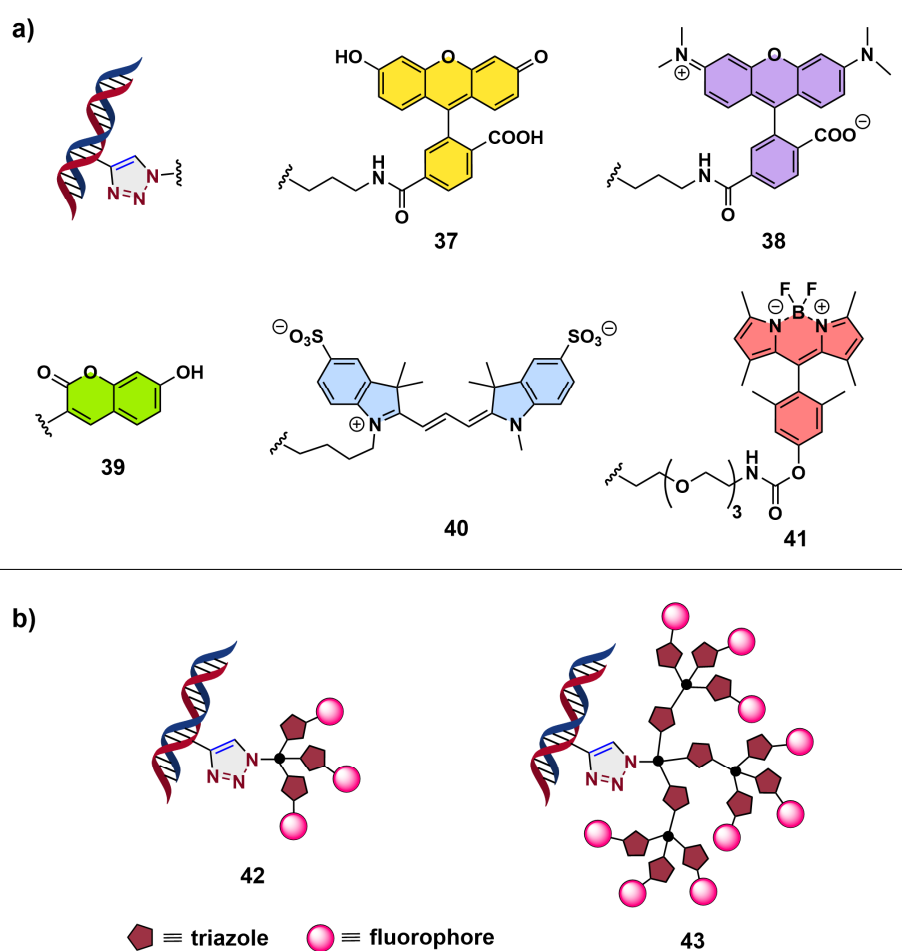


Figure 5. a) Typically employed fluorescent dyes for nucleic acid labeling and (b) dendrimer-based approach for fluorescence amplification.

self-quenching in a number of cases,^[91–93] fluorescence intensity has been successfully enhanced in antibody- and DNA-conjugates.^[91,94,95] As a remarkable case in point, Carell and coworkers^[96] developed click-chemistry-based dendritic constructs (**42** and **43**) that show significantly improved signal intensities and signal-to-noise ratios in EdU-based cell proliferation assays.

Besides fluorophores, nucleic acids have been covalently attached to other small molecules such as cholesterol, fatty acids, and receptor specific ligands — e.g., folate and carbohydrates — to enhance cellular uptake of oligonucleotide-based therapeutics.^[97–99] To give an example, the Carell group^[100] used cholesterol (**44**), folate (**45**), and anandamide (**46**) to click them at the 3'-end of siRNA molecules and induce their delivery to specific cell types (**Figure 6a**). Notoriously, anandamide conjugation exhibited efficient delivery to neuronal and immune cells. Carbohydrates have also gained attention as effective ligands for improving cellular uptake in different cell types and tissues, as evidenced by the prominent success of the marketed hepatocyte-targeting *N*-acetylgalactosamine (GalNAc)-conjugated siRNA therapeutics Givosiran, Lumasiran and Inclisiran.^[101–103] Interestingly, in line with this

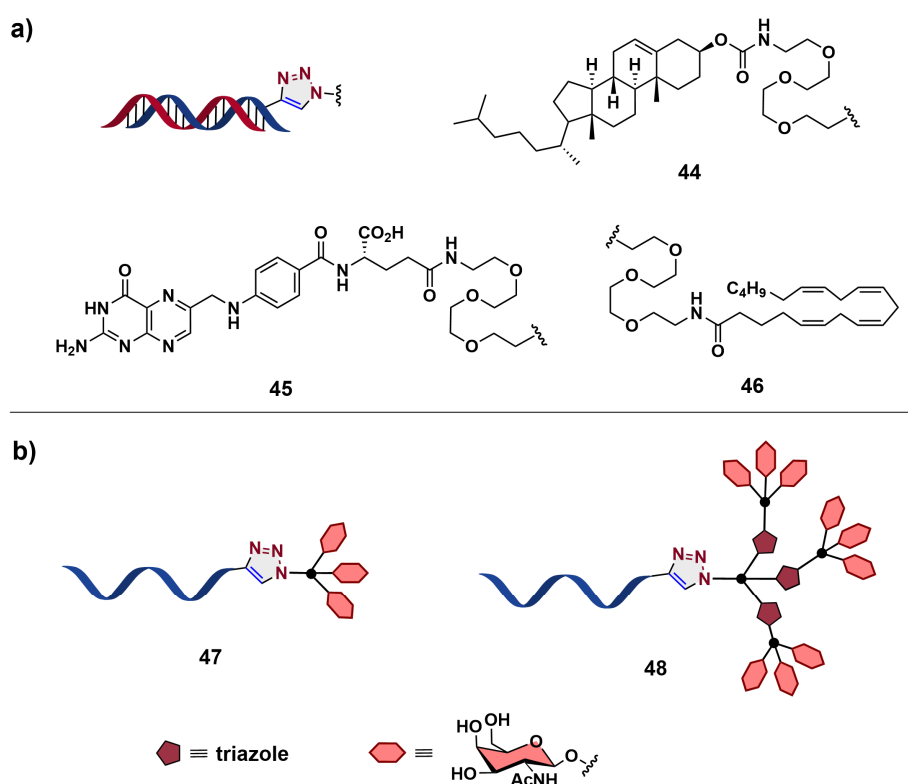


Figure 6. a) Conjugation of nucleic acids with biologically active molecules such as cholesterol (**44**), folate (**45**) and anandamide (**46**) for enhanced cellular uptake. b) Oligonucleotide–GalNAc dendrimer conjugates for *in vivo* hepatocyte targeting.

approach and following a click-chemistry-based strategy, Zatsepin and colleagues^[104] have reported a simple and fully-automated solid-phase CuAAC procedure for the preparation of 5'-end GalNAc-modified oligonucleotides as well as oligonucleotide–GalNAc dendrimer conjugates for *in vivo* hepatocyte targeting (**Figure 6b**). Furthermore, significant advancements have been made by utilizing alternative types of carbohydrates, such as mannose, in conjunction with click chemistry, to conjugate different payloads or carriers for the targeting of immunocompetent cells within the field of cancer immunotherapies and vaccination.^[105,106]

1.4.2 Cellular Metabolic Labeling

Traditional labeling strategies for cellular DNA^[107,108] and RNA^[109,110] analysis, based on the incorporation of tritiated or halogenated thymidine analogs, suffer from limitations related to radioactivity or cellular and tissue toxicity, respectively. The utilization of click chemistry overcomes these constraints and is especially valuable in *in vitro* and *in vivo* studies of DNA and RNA synthesis, cellular proliferation, and cell cycle dynamics.

In DNA metabolic labeling, incorporation of EdU (**24**) and subsequent efficient CuAAC coupling to fluorescent azides is the gold standard labeling strategy in DNA bioimaging experiments.^[73] EdU, however, presents certain inherent cytotoxicity and induces perturbation

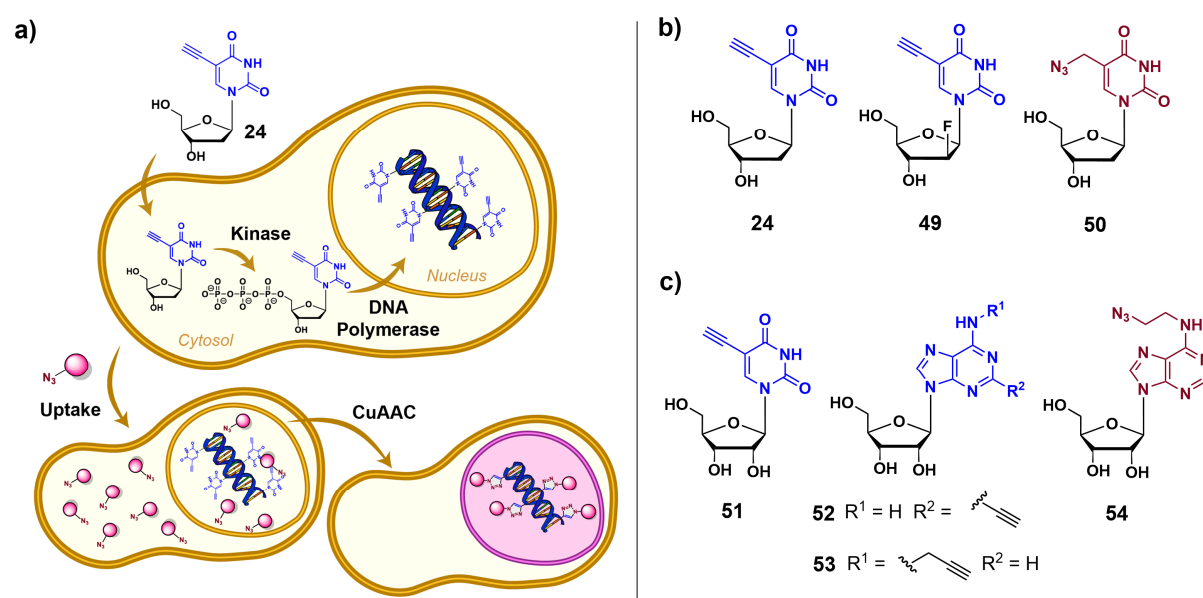


Figure 7. a) Example of metabolic DNA EdU-labeling. EdU (**24**) is phosphorylated via kinases into cells and incorporated by polymerases in the genome. Figure adapted from Fantoni et al.^[53] b) Modified deoxythymidine derivatives used for cellular metabolic labeling of DNA. c) Selected modified ribonucleoside derivatives used for cellular metabolic labeling of RNA.

of biological processes in cells, posing a significant limitation in assays that require long term physiological function of the tissue under study.^[111] F-*ara*-EdU (**49**), an arabinofuranosyl-ethynyluracil derivative, presents a viable alternative due to its reduced toxicity, permitting its detection through CuAAC fluorescence staining. This feature makes it an appropriate candidate for metabolic labeling studies that necessitate long-term cell viability.^[75] Alternatively, the integration of azido nucleoside analogs, such as 5-(azidomethyl)-2'-deoxyuridine (AmdU, **50**),^[112] enables the extension of click labeling to SPAAC, which eliminates the use of cytotoxic Cu(I) catalysts.

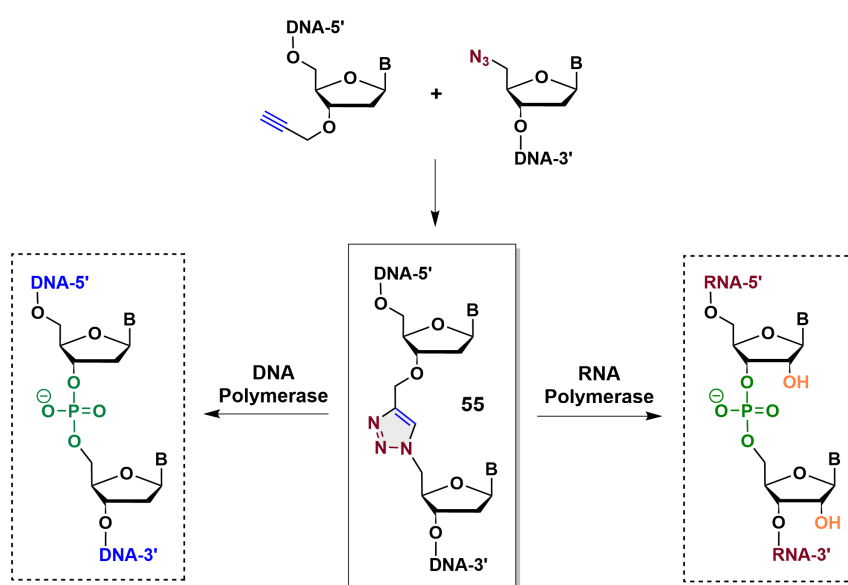
Analogous to DNA, RNA can be metabolically modified with the ribose derivative of EdU, 5-ethynyl-uridine (EU, **51**), to monitor transcriptional activity in cells.^[113] These nucleosides are incorporated by RNA polymerases during transcription. Other alkyne-modified ribonucleosides, including 2-ethynyl adenosine (EA, **52**)^[114] and *N*⁶-propargyladenosine (*N*⁶pA, **53**),^[115] have also been developed for transcription tracking and monitoring poly(A) tail dynamics. Incorporating alkyne nucleosides into RNA restricts the posttranscriptional labeling approach to CuAAC. Therefore, posttranscriptional SPAAC coupling can also be accomplished by introducing azido nucleosides into RNA, such as adenosine analog **54**.^[116] Alternatively, functional groups for CuAAC or SPAAC can be incorporated into RNA strands through site-specific introduction of native or engineered methyltransferases.^[117–120]

1.4.3 Assembly of Oligonucleotide Sequences

Chemical ligation of nucleosides provides several benefits compared to enzymatic methods commonly used in the synthesis of long genetic constructs. Enzymatic synthesis involves multiple cycles of PCR amplification, mismatch repair, cloning, sequencing, and selection, which can be time-consuming and yield low quantities of DNA and RNA strands. Additionally, problematic site-specific incorporation of modifications also hinders the production of large amounts of nucleic acid strands for research and industrial purposes. While DNA solid phase synthesis is an alternative approach, it has limitations due to the inefficient coupling reactions beyond 200 nucleotides and high error rates during phosphoramidite coupling reactions.^[121] To overcome these challenges, click chemistry has been explored as a biocompatible strategy to chemically synthesize long nucleic acid analogs.

Brown and colleagues have conducted research on the biocompatibility of various triazoles as phosphodiester surrogates,^[122,123] demonstrating that triazole linkages containing 5'-azide and

3'-propargyl modified oligonucleotides (**55**) can be successfully amplified *in vitro* by DNA polymerases. Correct replication and biocompatibility of triazole-containing genes was also evaluated in *E. coli*.^[124] Moreover, this particular triazole linkage has been utilized to generate clicked DNA templates to successfully transcribe them into RNA *in vitro* using T7 RNA polymerase.^[123] Click-mediated ligation of oligonucleotides, thus, represents a viable chemical strategy for gene assembly and the creation of extended RNA structures, offering potential utility in the fields of synthetic biology and industrial biotechnology.



Scheme 6. Assembly of oligonucleotide sequences via click ligation and subsequent amplification or transcription to obtain extended DNA or RNA sequences, respectively.

Despite the exceptional advantages of click chemistry for the synthesis of long nucleic acid analogs, these reactions typically require a splint-mediated approach to overcome the electrostatic repulsion between negatively charged DNA strands, preorganize the reaction partners, and facilitate efficient reaction progress.^[125,126] The use of splint oligonucleotides, however, adds complexity and cost to the experimental setup and purification and limits the applicability of the technique to known sequences. Interestingly, Serdjukow and colleagues reported the addition of Mg²⁺ ions to the catalyst/ligand mixture, under optimized reaction conditions, to significantly enhance click ligation without requiring splint templating.^[127] Thereby, this approach expands the scope of known and novel applications in splint-free versions, such as methods for complementary DNA (cDNA) library preparation in Next Generation Sequencing (NGS).^[128]

1.4.4 Other Applications: Antisense Oligonucleotides, Single-Guide RNA, Nanomaterials and Cyclic DNA

Incorporation of triazole modifications in antisense oligonucleotides (ASOs) enhance their therapeutic properties by improving stability against nucleases and reducing the anionic charge of the oligonucleotide, potentially facilitating cellular uptake. Additionally, G-clamp nucleobases^[129] and conformationally restricted locked nucleic acid (LNA) modifications^[130–132] are utilized to enhance the base pairing around the click modification (**Figure 8a**).

Likewise, a recent application of click chemistry is found in the field of CRISPR-Cas gene editing (**Figure 8b**). Both CuAAC and SPAAC have been utilized to generate pools of single guide RNAs (sgRNAs), which recognize and bind to specific DNA sequences, programming and directing the cleaving properties of the Cas enzyme.^[133,134]

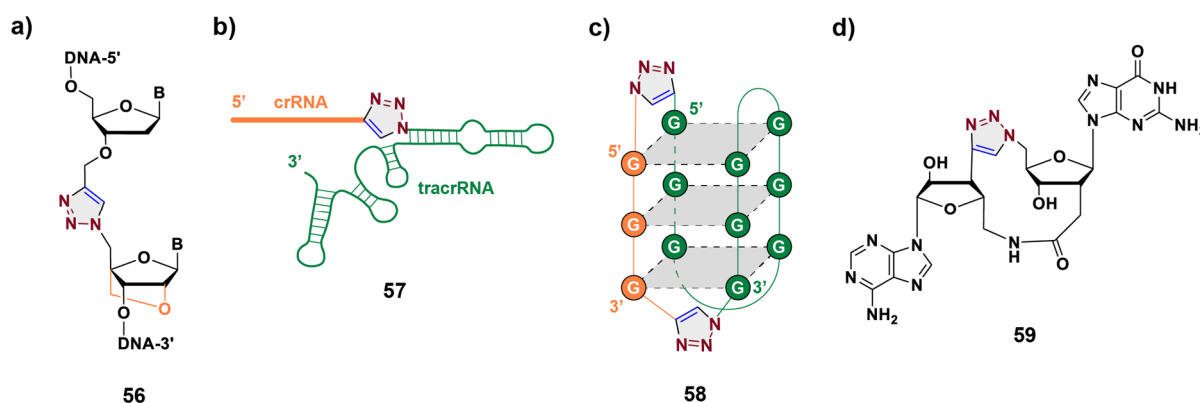


Figure 8. Applications of click chemistry in a) ASOs synthesis, b) sgRNAs production, c) nanomaterials and d) cyclic DNA scaffolds. crRNA = CRISPR RNA; tracrRNA = trans-activating CRISPR RNA.

Click ligation has also been utilized in the field of DNA nanomaterials and nanotechnology (**Figure 8c**), where precise hydrogen-bonding and base stacking interactions are critical for the assembly and stability of DNA nanoarrays. To overcome stability-related challenges, application of CuAAC has enabled the assembly of complex DNA tertiary structures such as duplexes,^[135] triplexes,^[136] and quadruplexes.^[137]

Lastly, click chemistry has been used to synthesize small cyclic DNA scaffolds (**Figure 8d**) for applications in drug–DNA binding analysis and as potential therapeutics, including cyclic mini-duplexes^[138–140] and cyclic dinucleotides.^[141] Besides, formation of large dsDNA catenanes has been also achieved through click ligation.^[142]

2 AIMS OF THE THESIS

The central focus of this doctoral thesis is to conduct in-depth investigations within the field of click chemistry as applied to nucleic acids. Specifically, this study seeks to extend the synthetic utility of bioorthogonal click chemistry by exploring diverse and crucial research areas and developing cutting-edge techniques and products with applications in biology, biochemistry, and biotechnology.

The primary goal of this thesis is directed towards the design and synthesis of innovative fluorophores for use in click chemistry-based bioimaging techniques. In pursuit of enhancing detection sensitivity and quality of bioimaging methods, novel fluorescent dyes exhibiting outstanding brightness would need to be developed. Furthermore, we would also consider the use of dendritic structures, such as dendrons, to be functionalized with multiple dye units and produce extremely bright fluorophores. To assess the applicability of these synthesized fluorescent probes, we would perform baseclick's EdU cell proliferation assays as a model system.

The second objective of this doctoral work is aimed at the development of emerging nucleic acid therapeutics, particularly on the fields of vaccination and cancer immunotherapy. To this end, we would synthesize a set of carbohydrate-based targeting ligands that could be utilized for specific delivery of nucleic acid drugs to immunocompetent cells. These ligands would contain a clickable functional group to allow for their modular bioconjugation to the desired cargo via click chemistry. The targeting properties of these ligands would be evaluated using an appropriate cell model to test their applicability in specific cell delivery.

The third and ultimate aim is to apply our targeting ligands to develop a novel nucleic acid therapeutic, such an mRNA-based vaccine. The insights acquired from this research would contribute to expanding the field of click chemistry and pave the way for future investigations into the advancement of state-of-the-art, cell-specific drug delivery systems.

The general goal of this thesis is to contribute to the advancement of knowledge in the context of click chemistry applied to nucleic acids, with special emphasis in the development of new technologies and products of high value to the scientific community and broader society.

3 PUBLISHED WORK

TITLE: Divergent Synthesis of Ultrabright and Dendritic Xanthenes for Enhanced Click-Chemistry-Based Bioimaging.

AUTHORS: Montiel, L.; Spada, F.; Crisp, A.; Serdjukow, S.; Carell, T.; Frischmuth, T

JOURNAL, YEAR, VOLUME, AND PAGE NO.:

Chem. - A Eur. J. **2023**, 29 (5), e202202633

SUMMARY:

The utilization of fluorescent small molecules for nucleic acid labeling has proven to be an effective method for diagnostic and biomedical purposes, especially in 5-ethynyl-2'-deoxyuridine (EdU)-based assays. The detection sensitivity and quality of the method can be improved by augmentation of fluorescent signal. Therefore, a novel rapid, divergent synthetic procedure has been established to produce *ready-to-click*, pH-insensitive rhodamine dyes that exhibit outstanding brightness. The new 3,3-difluoroazetidene rhodamine azide proved to be a superior alternative in imaging experiments when compared to popular commercially available fluorophores, such as 5-TAMRA-azide. Additionally, a group of fluorescein- and rhodamine-based multivalent dendrons were prepared by branching click chemistry. The photophysical properties of these dendritic structures revealed self-quenching effects, suggesting potential application as FRET quenchers.

PERSONAL CONTRIBUTIONS:

- Conceptualization of the project, synthesis design, preparation of all reported compounds and characterization of their chemical properties.
- Photophysical characterization (λ_{abs} , λ_{em} , ϵ , ϕ , brightness, photobleaching) of reported fluorophores at different pH values.
- Lead contribution to data curation, writing and preparation of the original manuscript.
- Edition and revision of the manuscript together with all co-authors.

PERMISSION AND LICENSING

Material from: Montiel et al., Divergent Synthesis of Ultrabright and Dendritic Xanthenes for Enhanced Click-Chemistry-Based Bioimaging, *Chem. - A Eur. J.*, published 2023, Wiley-VCH GmbH, Weinheim. This article was reprinted with permission from John Wiley and Sons ([CC BY 4.0](https://creativecommons.org/licenses/by/4.0/)).

Divergent Synthesis of Ultrabright and Dendritic Xanthenes for Enhanced Click-Chemistry-Based Bioimaging

Luis Montiel,^[a, b] Fabio Spada,^[a] Antony Crisp,^[a] Sascha Serdjukow,^[a] Thomas Carell,^[b] and Thomas Frischmuth*^[a]

Abstract: Biorthogonal labelling with fluorescent small molecules is an indispensable tool for diagnostic and biomedical applications. In dye-based 5-ethynyl-2'-deoxyuridine (EdU) cell proliferation assays, augmentation of the fluorescent signal entails an overall enhancement in the sensitivity and quality of the method. To this end, a rapid, divergent synthetic procedure that provides *ready-to-click* pH-insensitive rhodamine dyes exhibiting outstanding brightness was established. Compared to the shortest available synthesis of related high quantum-yielding rhodamines, two fewer synthetic steps are required. In a head-to-head imaging comparison involving

copper(I)-catalyzed azide alkyne cycloaddition reactions with *in vitro* administered EdU, our new 3,3-difluoroazetidine rhodamine azide outperformed the popular 5-TAMRA-azide, making it among the best available choices when it comes to fluorescent imaging of DNA. In a further exploration of the fluorescence properties of these dyes, a set of bis-MPA dendrons carrying multiple fluorescein or rhodamine units was prepared by branching click chemistry. Fluorescence self-quenching of fluorescein- and rhodamine-functionalized dendrons limited the suitability of the dyes as labels in EdU-based experiments but provided new insights into these effects.

Introduction

In the field of bioimaging and diagnostics, fluorescent labelling has emerged as a potent tool for the elucidation of structures, dynamics, interactions and functions of biomolecules such as proteins,^[1] nucleic acids,^[2] polysaccharides^[3] and lipids.^[4] Furthermore, efficient fluorescence resonance energy transfer (FRET)-compatible fluorophores and quenchers are increasingly sought after for their use in real-time PCR applications, including as components of molecular beacons,^[5] TaqMan probes,^[6] and Scorpion primers.^[7] In the context of cell proliferation detection, fluorescence labelling of nucleic acids helps to assess genotoxicity of new pharmaceuticals and to evaluate anticancer drugs.^[8] In order to obtain an effective image and produce high signal-to-noise ratios, probes must exhibit strong fluorescent signals. A known disadvantage of fluorescent labels over traditional radioactive labels is their moderately lower sensitivity.^[9] This difference can lead to undesirable results, especially in the framework of oncology,

where slowly proliferating cancerogenic cells have been reported to escape detection.^[10] Upon chemical functionalization with multiple dyes to enhance fluorescence signal, proteins and other biomolecules can become inactivated due to their large structural alteration.^[11] Fluorescence brightness, that is, the product of a fluorophore's extinction coefficient and fluorescence quantum yield ($\epsilon \cdot \phi$), is used to compare the fluorescent properties of different dyes.^[12] Therefore, to overcome concerns related to fluorescence intensity and biomolecule alteration, fluorophores with enhanced brightness values are highly desirable.

Click chemistry remains the gold standard labelling strategy used in imaging experiments to attach fluorophores to the biomolecule of interest,^[13] with EdU-based assays being particularly useful for cell proliferation detection, and where the clickable thymidine analogue EdU is metabolically incorporated during active DNA synthesis.^[14,15] Unlike halogenated thymidine analogues such as 5-bromo-2'-deoxyuridine (BrdU), EdU assays do not require harsh DNA denaturing conditions, thus preserving cellular and tissue integrity.^[14,16]

In this study, we disclose a facile, three-step synthesis of highly bright *ready-to-click* rhodamine dyes and systematically explore their photophysical properties. Moreover, we demonstrate the applicability of these dyes in the framework of EdU-based assays. In a further exploration of their synthetic utility and fluorescent properties, we prepare dendrons containing multiple branched fluorophores with the aim of augmenting fluorescence signal without increasing the number of labelling-sites within a given alkyne-modified DNA molecule.^[17] The use of related, but not identical constructs has been demonstrated to enable a wide variety of applications, particularly in drug and gene delivery,^[18] cancer therapy^[19] and tissue engineering.^[20] Controlled synthesis of large dendritic scaffolds remains a

[a] L. Montiel, Dr. F. Spada, Dr. A. Crisp, Dr. S. Serdjukow, Dr. T. Frischmuth
Baseclick GmbH
Floriensbogen 2–4, 82061 Neuried (Munich) (Germany)
E-mail: t.frischmuth@baseclick.eu

[b] L. Montiel, Prof. Dr. T. Carell
Department of Chemistry
Institut für Chemische Epigenetik München (ICEM)
Ludwig-Maximilians-Universität München (LMU)
Butenandtstr. 5–13, 81377 Munich (Germany)

Supporting information for this article is available on the WWW under <https://doi.org/10.1002/chem.202202633>

© 2022 baseclick GmbH. Chemistry - A European Journal published by Wiley-VCH GmbH. This is an open access article under the terms of the Creative Commons Attribution License, which permits use, distribution and reproduction in any medium, provided the original work is properly cited.

considerable challenge, particularly where structural characterization is concerned, thus prompting the need for new and improved synthetic strategies. In the context of fluorescent scaffolds, self-quenching has also proven problematic.^[9,21,22] In certain instances, fluorescence intensity in antibody- and DNA-conjugates has nonetheless been successfully enhanced, prompting us to investigate this approach ourselves.^[9,23,24]

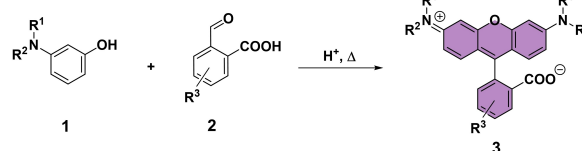
To such an end, we demonstrate the synthesis by means of click chemistry, of a set of bis-MPA dendrons carrying either multiple fluorescein units, or our best-performing rhodamine. After subsequent characterization of the photophysical properties of these fluorogenic compounds, we evaluate their suitability as fluorescent labels for EdU-based experiments as well as other potential applications.

Results and Discussion

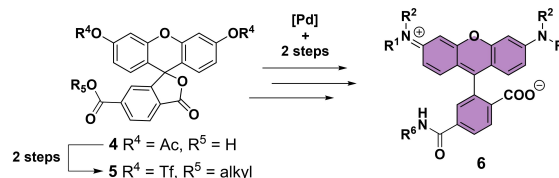
Rhodamines, first described in the 1880s,^[25] are a family of xanthene dyes which exhibit excellent brightness, exceptional photostability and low pH-sensitivity.^[26,27] Traditionally, rhodamine dyes (3) have been synthesized by means of an acid-catalyzed condensation reaction between a phthalic anhydride (1) and an aminophenol (2) (Scheme 1.1). This reaction is, however, characterized by harsh conditions, low yields, mixtures of regioisomers and incompatibilities with several functional groups.^[26,28–30] With the aim to omit this step, Lavis and co-workers reported a synthesis based on the use of fluorescein ditriflates (5) as key intermediates and a Pd-catalyzed cross coupling for the formation of C–N bonds (Scheme 1.2).^[28,31] Following this strategy, milder reaction conditions, higher yields and the use of a wide range of nitrogen nucleophiles were successfully carried out. In this work, the latter methodology has been modified for the synthesis of *ready-to-click* rhodamine dyes in a facile and straightforward manner for bioconjugation with DNA via click chemistry. This new route only comprises 3 synthetic steps and a late-stage formation of fluorescein azide ditriflate 9, which enables a divergent synthesis of different rhodamine dyes through Buchwald–Hartwig cross-coupling (Scheme 1.3).

The synthetic pathway starts with 6-carboxyfluorescein (7) as an inexpensive, isomerically pure starting material. The 6-carboxyl group was converted *in situ* in an *N*-hydroxysuccinimide (NHS) ester using a catalytic amount of 4-(Dimethylamino)pyridine (DMAP), triethylamine and *N,N*-disuccinimidyl carbonate (DSC) as a coupling reagent. Upon activation as an NHS ester, the bifunctional linker azidopropan-1-amine was added to provide **fluorescein azide** (8) as a bright orange solid in 70% yield. The next step involved conversion of the phenolic groups into triflates using trifluoromethanesulfonic anhydride (Tf₂O) and pyridine to yield fluorescein azide ditriflate 9 in 81% yield as the key intermediate of the synthesis. Subsequent Buchwald–Hartwig cross-couplings were performed using Pd₂(dba)₃/XPhos as the catalytic system and Cs₂CO₃ as base. In a similar approach as previously reported in the literature,^[30,32] catalyst and ligand loadings were increased to suppress triflate hydrolysis, which represented the main side-reaction of this

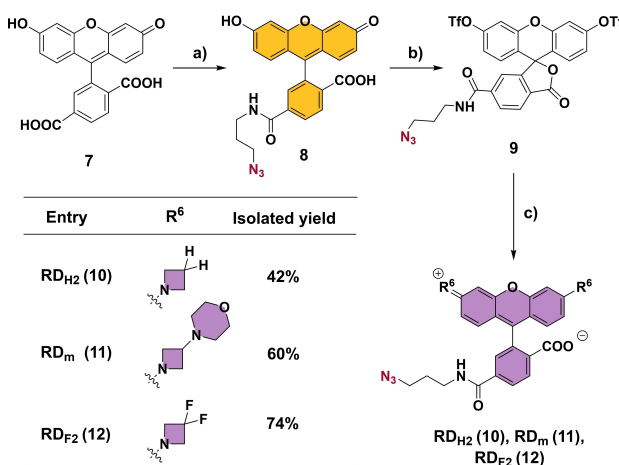
1) Rhodamine synthesis via condensation



2) Lavis and co-workers (2011, 2017)



3) This work



Scheme 1. Different strategies for the synthesis of rhodamine dyes. a) DSC, DMAP, Et₃N, DMF, 1 h, rt, then 3-azidopropan-1-amine, 2 h, rt, 70%, b) Py, Tf₂O, CH₂Cl₂, 16 h, 0 °C → rt, 81%, c) amine·HCl, Pd₂(dba)₃, XPhos, Cs₂CO₃, dioxane, 4 h, 100 °C, 42–74%. DSC = *N,N*'-disuccinimidyl carbonate. DMAP = 4-dimethylaminopyridine. DMF = *N,N*-dimethylformamide. Py = pyridine. Tf₂O = trifluoromethanesulfonic anhydride. dba = dibenzylideneacetone.

step. Different 3-substituted azetidines were used as nitrogen nucleophiles in the cross-coupling reaction since rhodamine dyes containing azetidine rings were found to exhibit considerable quantum yields.^[28,31] In this manner, dyes RD_{H2} (10), RD_m (11), and RD_{F2} (12) were successfully synthesized as pink-to-purple solids in 42%, 60% and 74% yield, respectively. A study of the photophysical properties of these dyes was performed by UV-Vis and fluorescence spectroscopic techniques at different pH values (Table 1). In order to observe the properties of the zwitterionic and cationic forms of the rhodamines,^[26] measurements were taken at close-to physiological (pH = 7.3) and acidic (pH = 1.9) pH values, respectively (see Supporting Information, Figures S19–21 for the calculated pK_a values). As for the absorption and emission maxima (λ_{abs}, λ_{em}), the synthesized dyes absorb green and green-to-yellow light (λ_{abs} = 530–556 nm) and emit green-to-yellow and yellow light (λ_{em} = 554–580 nm). A larger hypsochromic 5(blue) shift in both λ_{abs} and λ_{em} was observed when using azetidine derivatives containing

Table 1. Photophysical properties of the synthesized rhodamine dyes.

Fluorophore	pH 7.3 ^[a]			pH 1.9 ^[b]				
	$\lambda_{\text{abs}}/\lambda_{\text{em}}$ [nm]	ϵ_{max} ^[c] [M ⁻¹ cm ⁻¹]	φ ^[d]	$\epsilon_{\text{max}} \cdot \varphi$ [M ⁻¹ cm ⁻¹]	$\lambda_{\text{abs}}/\lambda_{\text{em}}$ [nm]	ϵ_{max} ^[c] [M ⁻¹ cm ⁻¹]	φ ^[d]	$\epsilon_{\text{max}} \cdot \varphi$ [M ⁻¹ cm ⁻¹]
RD _{H2}	554/576	64000	0.74	47360	556/580	63000	0.67	42210
RD _m	547/569	53000	0.67	35510	536/560	55000	0.86	47300
RD _{F2}	530/554	60000	0.89	53400	533/558	68000	0.87	59160

[a] Measurements were taken in 10 mM HEPES, pH 7.3 buffer at room temperature. [b] Measurements were taken in 0.1% TFA aqueous solution at room temperature. [c] Maximum extinction coefficients (ϵ_{max}) were calculated by a linear regression analysis obeying the Beer-Lambert law. [d] Quantum yields (φ) were determined using the comparative method and rhodamine 6G ($\varphi = 0.95$ in EtOH)^[33] as reference.

more electron-withdrawing groups. Thus, λ_{abs} and λ_{em} of these dyes obey the following tendency: $\text{RD}_{\text{H2}} > \text{RD}_{\text{m}} > \text{RD}_{\text{F2}}$. This set of rhodamine dyes showed high ϵ_{max} values ($\epsilon_{\text{max}} = 53000$ to $68000 \text{ M}^{-1} \text{ cm}^{-1}$) with low pH sensitivity. Likewise, the rhodamines showed high to very high quantum yield values ($\varphi = 0.67$ to 0.89) with minimal pH-dependent effects, except for RD_{m} ($\varphi = 0.67$ at pH 7.3 and $\varphi = 0.86$ at pH 1.9). This quenching behavior, as described in the literature,^[28,34,35] is indicative of an intramolecular photoinduced electron transfer (PeT) due to the presence of unprotonated morpholino amines. Consequently, the quantum yield value of RD_{m} increased dramatically at pH 1.9.

Given its remarkably high extinction coefficient, quantum yield and low pH-dependence, RD_{F2} dye ($\epsilon_{\text{max}} = 60000 \text{ M}^{-1} \text{ cm}^{-1}$ and $\varphi = 0.89$ at pH 7.3) stood as the best-performing dye in terms of fluorescence brightness. With this in mind, we assessed the applicability of RD_{F2} to an EdU cell proliferation assay (Figure 1a). HEK-293T cells were pulsed for 2 h with EdU, fixed, permeabilized and Cu-catalyzed *in situ* click reactions were performed in parallel with RD_{F2} and the well-established 5-TAMRA-PEG3-azide. After image acquisition by fluorescence microscopy (Figure 1b), both dyes provided images with characteristic nuclear patterns of DNA replication and similar fluorescence intensity. The emission filter used in this assay, however, exhibited an acquisition window overlapping more extensively the emission spectrum of TAMRA in detriment of that of RD_{F2} . This indicates, therefore, that RD_{F2} performs at least as robustly as the well-established TAMRA dye upon click-mediated *in situ* EdU labelling.

Encouraged by these results, we investigated the use of dye-containing dendrons as fluorescent labels to further amplify the fluorescence signal without increasing the number of labelling-sites on DNA (Scheme 2). We therefore synthesized and characterized the photophysical properties of a family of fluorescein-based dendritic dyes carrying two (**FD2**, **12**), four (**FD4**, **13**) and eight (**FD8**, **14**) branched fluorescein substituents. In order to synthesize these multivalent fluorescent dyes, we chose a set of 2,2-bis(methylol)propionic acid (bis-MPA) polyester dendrons as functional, biodegradable and low-cytotoxic polymeric scaffolds suitable for biological applications.^[17] The present strategy consisted of functionalizing the different dendritic structures with units of **fluorescein azide** via a copper-catalyzed click reaction to yield **FD2**, **FD4** and **FD8** in 61%, 67% and 40% yield, respectively. **FD8** was further functionalized to include an azide moiety into its focal point to

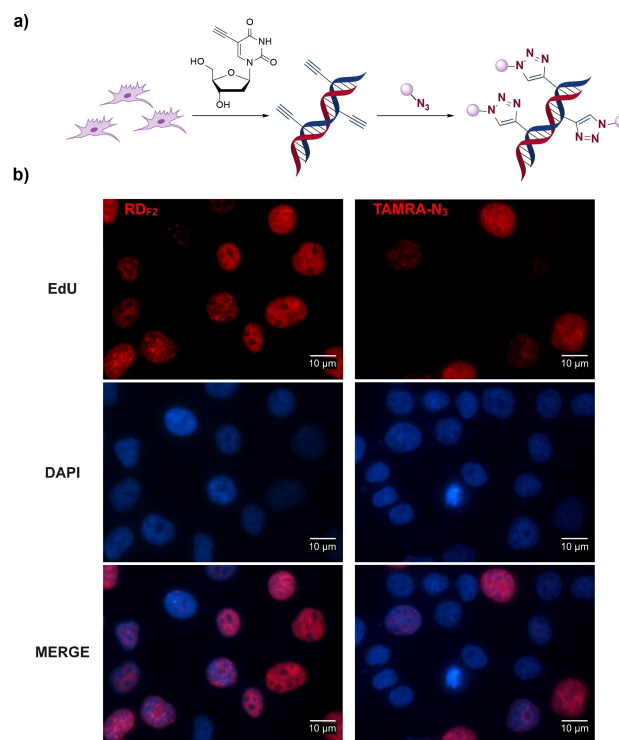
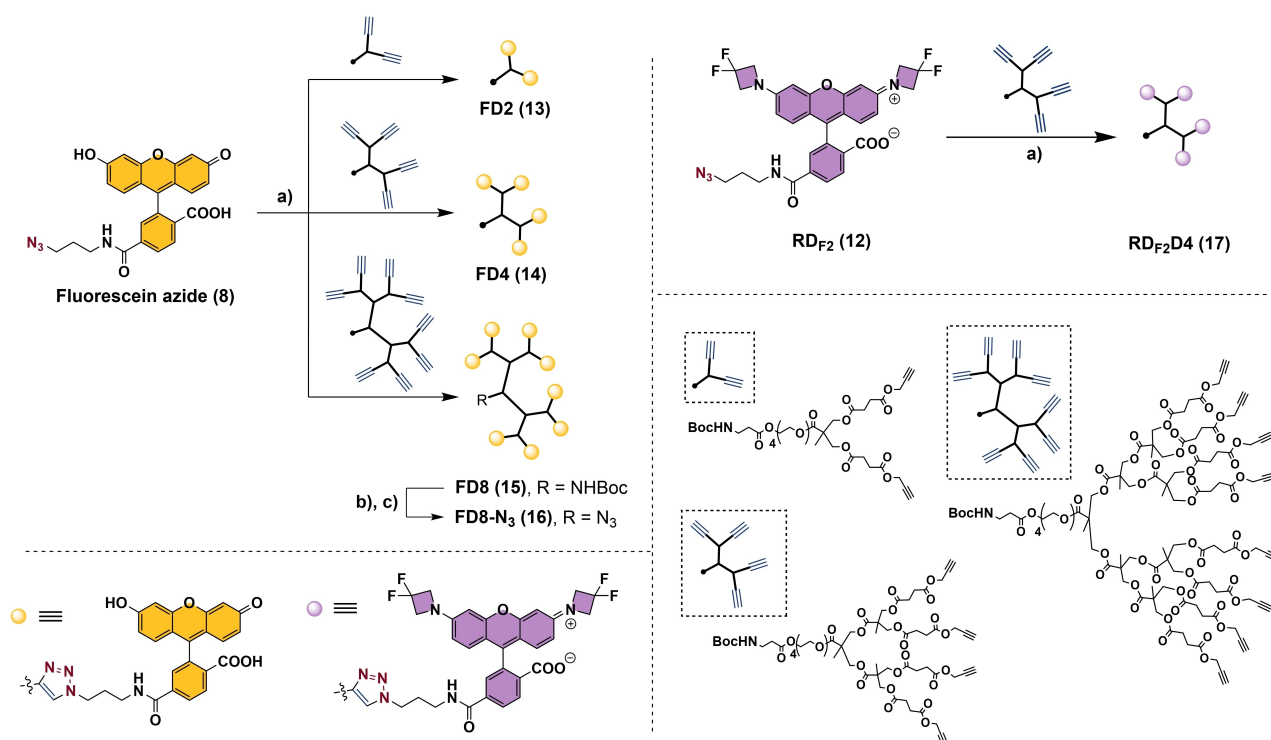


Figure 1. EdU cell proliferation assays with RD_{F2} and 5-TAMRA-PEG3-Azide. a) Schematic workflow of the EdU cell proliferation assay. Cells were grown and incubated with EdU. After cell fixation, the alkyne-modified DNA was bioconjugated with RD_{F2} or 5-TAMRA-PEG3-azide via Cu-catalyzed click reaction and detected by fluorescence microscopy. b) Fluorescence microscopy images of EdU-pulsed HEK-293T cells after click reactions with RD_{F2} (red, left panels) and 5-TAMRA-PEG3-azide (red, right panels). Blue signals represent nuclear counterstaining with DAPI.

enable a possible bioconjugation via click chemistry. Upon treatment of **FD8** with trifluoroacetic acid, the Boc-protected amine was released in quantitative yields. The subsequent coupling reaction with the NHS ester of an azide-containing linker afforded **FD8-N₃** (**16**) in 67% yield.

In an analogous approach to that of the synthesized rhodamine dyes, the photophysical properties of these dendrons were evaluated at different pH values (Table 2 and Figure 2). The spectral properties of fluorescein are known to be pH-sensitive, especially due to the equilibrium between the mono- and dianion forms with a pK_a of 6.4,^[37] the dianion being the most fluorescent species.^[37,38] For this reason, measurements were taken at close-to physiological (pH = 7.3) and basic (pH =



Scheme 2. Synthesis and structure of fluorescein- and rhodamine-based dendritic dyes. a) CuBr, PMDTA, DMF, 45 °C, 4 h, 61 % (FD2), 67 % (FD4), 40 % (FD8), 85 % (RD_{F2}D4). b) TFA, 2 h, rt, quantitative yield. c) Azido-PEG4-NHS ester, Et₃N, DMF, 1 h, 67%. PMDTA = pentamethyldiethylenetriamine. DMF = *N,N*-dimethylformamide. TFA = trifluoroacetic acid. Azido-PEG4-NHS = 15-Azido-4,7,10,13-tetraoxa-pentadecanoic acid succinimidyl ester.

Table 2. Photophysical properties of fluorescein azide and fluorescein-based dendritic fluorophores at different pH values.

Fluorophore	pH 7.3 ^[a]				pH 9.1 ^[b]			
	$\lambda_{\text{abs}}/\lambda_{\text{em}}$ [nm]	$\epsilon_{\text{max}}^{[c]}$ [M ⁻¹ cm ⁻¹]	$\varphi^{[d]}$	$\epsilon_{\text{max}} \cdot \varphi$ [M ⁻¹ cm ⁻¹]	$\lambda_{\text{abs}}/\lambda_{\text{em}}$ [nm]	$\epsilon_{\text{max}}^{[c]}$ [M ⁻¹ cm ⁻¹]	$\varphi^{[d]}$	$\epsilon_{\text{max}} \cdot \varphi$ [M ⁻¹ cm ⁻¹]
Fluorescein azide	495/517	61000	0.77	46970	495/517	71000	0.91	64610
FD2	497/519	80000	0.13	10400	498/520	123000	0.26	31980
FD4	497/519	116000	0.04	4640	498/520	202000	0.05	10100
FD8	492/519	168000	< 0.01	1176	498/519	375000	< 0.01	2225
RD _{F2} D4	532/555	33000	0.13	4290	537/558 ^[e]	57000 ^[e]	0.14 ^[e]	7980 ^[e]

[a] Measurements were taken in 10 mM HEPES, pH 7.3 buffer at room temperature. [b] Measurements were taken in 10 mM sodium borate, pH 9.1 buffer at room temperature. [c] Maximum molar extinction coefficients (ϵ_{max}) were calculated by a linear regression analysis obeying the Beer-Lambert law. [d] Quantum yields (φ) were determined using the comparative method and fluorescein ($\varphi = 0.91$ in 0.1 M aqueous NaOH)^[36] as reference. [e] Measurements were taken in 0.1% v/v TFA aqueous solution (pH = 1.9) at room temperature. Quantum yields (φ) were determined using the comparative method and rhodamine 6G ($\varphi = 0.95$ in EtOH)^[33] as reference.

9.1) pH values to study the impact of this equilibrium in our family of fluorescein-based fluorophores.

As for the absorption properties, absorbance rose with the number of dyes. The maximum molar extinction coefficients (ϵ_{max}) for **fluorescein azide**, **FD2**, **FD4** and **FD8** at pH 7.3 were 61000 ($\lambda_{\text{max}} = 495$ nm), 80000 ($\lambda_{\text{max}} = 497$ nm), 116000 ($\lambda_{\text{max}} = 497$ nm) and 168000 M⁻¹ cm⁻¹ ($\lambda_{\text{max}} = 492$ nm), respectively. Upon normalization, the ratio of the dyes' respective ϵ_{max} values was therefore, 1/1.3/1.9/2.8. At pH 9.1, the fluorophores exhibited ϵ_{max} values of 71000 ($\lambda_{\text{max}} = 495$ nm), 123000 ($\lambda_{\text{max}} = 498$ nm), 202000 ($\lambda_{\text{max}} = 498$ nm) and 375000 M⁻¹ cm⁻¹ ($\lambda_{\text{max}} = 498$ nm) for **fluorescein azide**, **FD2**, **FD4** and **FD8**, in that order. The ϵ_{max} ratio was, in this case, 1/1.8/2.9/5.4, showing an important pH-dependent escalation of the absorption proper-

ties and approaching to the number of fluorescein units, that is 1:2:4:8.

Regarding the emission of the fluorophores, a decrease of the fluorescence quantum yield (φ) was observed along with the increasing number of fluorescein units (Table 2). More specifically, quantum yields at pH 7.3 for **fluorescein azide**, **FD2**, **FD4** and **FD8** were, in that order, 0.77, 0.13, 0.04 and < 0.01. Analogously, the decay in quantum yield was observed at pH 9.1 although a wide variation as a function of pH was noted, particularly for **fluorescein azide** and **FD2**. Thus, the quantum yield values at pH 9.1 were 0.91, 0.26, 0.05 and < 0.01 for **fluorescein azide**, **FD2**, **FD4** and **FD8**, respectively.

The fluorescence brightness (Table 2) diminished upon increasing the number of dyes per molecule at both pH values.

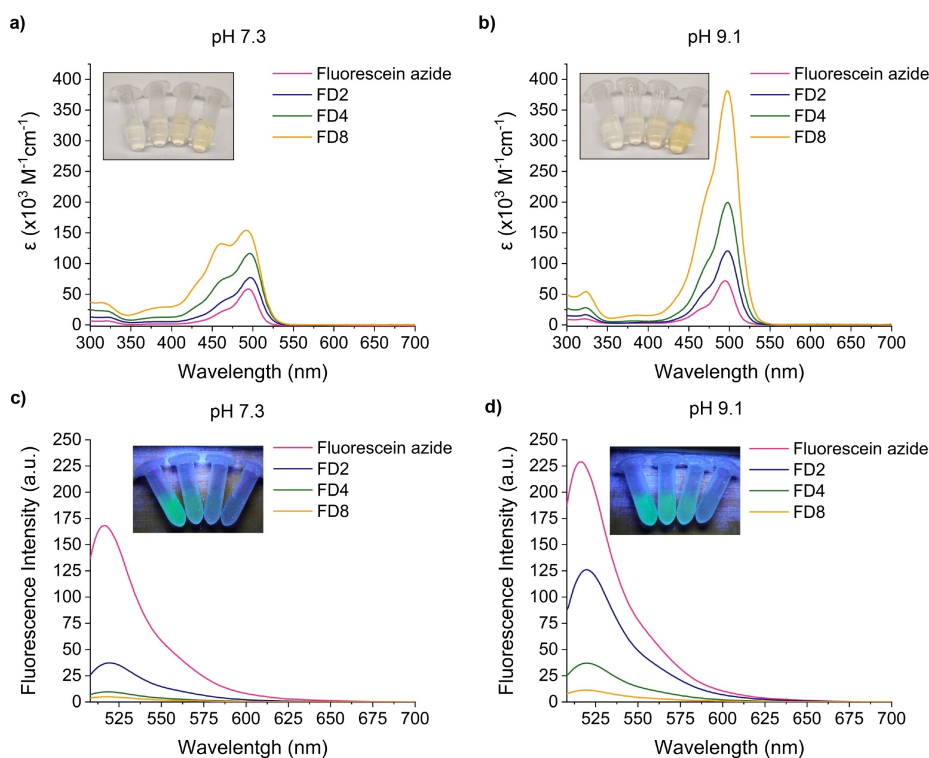


Figure 2. Absorption and emission spectra of fluorescein azide, FD2, FD4 and FD8 at different pH values. a) Absorption spectra measured in 10 mM HEPES, pH 7.3 buffer at a concentration of 2 μM . b) Absorption spectra measured in 10 mM sodium borate, pH 9.1 buffer at a concentration of 2 μM . c) Emission spectra measured in 10 mM HEPES, pH 7.3 buffer at a concentration of 0.2 μM . $\lambda_{\text{exc}} = 495 \text{ nm}$ (fluorescein azide), 497 nm (FD2 and FD4) and 492 nm (FD8). d) Emission spectra measured in 10 mM sodium borate, pH 9.1 buffer at a concentration of 0.2 μM . $\lambda_{\text{exc}} = 495 \text{ nm}$ (fluorescein azide) and 498 nm (FD2, FD4 and FD8). Inset: Solutions in the photographs correspond, from left to right, to fluorescein azide, FD2, FD4 and FD8 at 2 μM (absorbance) or 0.2 μM (emission). Absorbance and emission scans are averages ($n = 3$). All measurements were taken at room temperature.

Therefore, even though the absorption increased upon increasing the number of fluorescein moieties, the strong decay in quantum yield rendered a decrease in the fluorescence intensity. This behavior is confirmed by the fluorescence spectra shown in Figure 2. This decrease in fluorescence intensity was attributed to self-quenching, presumably resulting from the relatively small Stokes shift of fluorescein and the proximity of the dyes within the dendritic structures.^[9,38,39] It is noteworthy to mention the bimodal shape of the absorbance spectrum of **FD8** at pH 7.3. In comparison to the other analogous dendrons, **FD8** exhibited a hypsochromic shift in which a second absorption band arose at 462 nm. This was suggestive of the formation of H-aggregates caused by π - π interactions between the different dye units.^[23,40–42] These interactions were less prevalent at pH 9.1 with the more polar and water-soluble dianion form of fluorescein.^[43,44] Hence, the absorption spectrum recovered the original pattern.

After evaluating the fluorescein-based family of dendritic fluorophores, we concluded that the macromolecules are ill-suited for use in nucleic acid detection compared with their individual monomeric substituents. The strong interactions between the different dye units led to self-quenching, which was evidently undesirable for the synthesis of dendron-based fluorescence amplifiers.

Raddaoui, Stazzoni et al.^[24] developed a TAMRA-functionalized dendritic fluorophore which was bioconjugated to EdU-labelled DNA via click chemistry and achieved fluorescence amplification. Inspired by this work, we focused our efforts on the preparation of a rhodamine-based dendritic fluorophore using our model dye **RD_{F2}**. In the event, after functionalizing an alkyne-presenting bis-MPA dendron via copper-catalyzed click chemistry, **RD_{F2}D4** was afforded as a bright, pink powder in 85% yield (Scheme 2). Once the photophysical properties were measured (Table 2 and Figure 3), **RD_{F2}D4** was found to exhibit absorption and emission wavelengths very similar to **RD_{F2}** at both pH 7.3 and pH 1.9. As for the extinction coefficient, lower values than those of **RD_{F2}** were noted as well as an important pH-dependence ($\epsilon_{\text{max}} = 33000 \text{ M}^{-1} \text{ cm}^{-1}$ at pH 7.3 and $\epsilon_{\text{max}} = 57000 \text{ M}^{-1} \text{ cm}^{-1}$ at pH 1.9). In terms of quantum yield, an important decay of the fluorescence emission was observed with a negligible effect of pH ($\phi = 0.13$ at pH 7.3 and $\phi = 0.14$ at pH 1.9). Therefore, as shown in Figure 3, the fluorescence intensity of **RD_{F2}D4** did not surpass that of **RD_{F2}**. The most plausible explanation of this behavior is, once again, the self-quenching caused by the relatively small Stokes shift of **RD_{F2}** as well as the relative proximity of the dye units within the dendron. A tendency of **RD_{F2}D4** to form H-aggregates in aqueous solution is also observed by the presence, at both pH values, of an additional shoulder at 505 nm (pH = 7.3) or

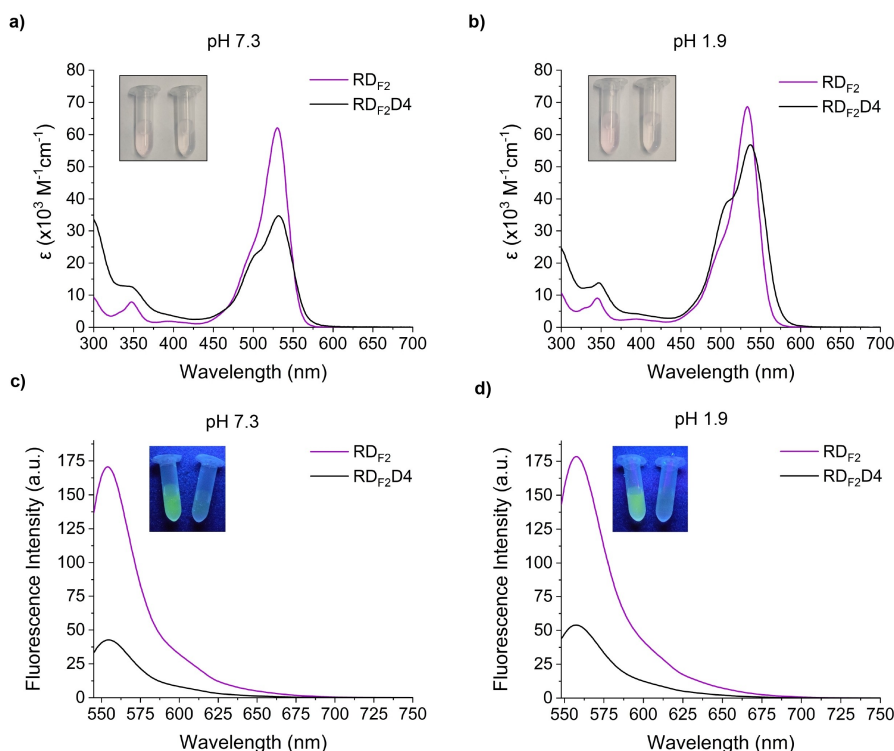


Figure 3. Absorption and emission spectra of RD_{F_2} and $\text{RD}_{\text{F}_2\text{D}_4}$ at different pH values. a) Absorption spectra measured in 10 mM HEPES, pH 7.3 buffer at a concentration of 2 μM . b) Absorption spectra measured in 0.1% v/v TFA aqueous solution (pH = 1.9) at a concentration of 2 μM . c) Emission spectra measured in 10 mM HEPES, pH 7.3 buffer at a concentration of 0.2 μM . $\lambda_{\text{ex}} = 530 \text{ nm}$ (RD_{F_2}) and 532 nm ($\text{RD}_{\text{F}_2\text{D}_4}$). d) Emission spectra measured in 0.1% v/v TFA aqueous solution (pH = 1.9) at a concentration of 0.2 μM . $\lambda_{\text{ex}} = 533 \text{ nm}$ (RD_{F_2}) and 537 nm ($\text{RD}_{\text{F}_2\text{D}_4}$). Inset: Solutions in the photographs correspond, from left to right, to RD_{F_2} and $\text{RD}_{\text{F}_2\text{D}_4}$ at 2 μM (absorbance) or 0.2 μM (emission). Absorbance and emission scans are averages ($n = 3$). All measurements were taken at room temperature.

510 nm (pH = 1.9). The suitability of $\text{RD}_{\text{F}_2\text{D}_4}$ as a fluorescent amplifier is, thus, limited by its inherent self-quenching.

Previous work has demonstrated aggregates tend to diminish upon temperature elevation due to changes in the dynamic equilibrium, and thus resulting in an increase of fluorescence intensity.^[45–47] Conversely, non-radiative rate constants and collisional quenching also tend to be amplified upon heating, leading to a decrease of fluorescence.^[48] In order to evaluate which of the two effects predominate in our dendritic fluorophores, the fluorescence of these molecules was measured at varying temperature values between 25 °C and 65 °C, as shown in Figure 4. In the event, the fluorescein-based dendrons **FD2** and **FD4** exhibited comparable fluorescence decay behavior. **FD8**, meanwhile, showed a diminished change in fluorescence intensity upon heating compared with **FD2** and **FD4**. This behavior could be indicative of a reconversion of aggregates to monomers in solution. For $\text{RD}_{\text{F}_2\text{D}_4}$, a less pronounced decay of fluorescence is shown in comparison to its fluorescein analogue **FD4**, indicating that aggregation might occur at a lesser extent for the former compound at higher temperatures. Overall, it is apparent that non-radiative processes and collisional quenching prevail for all fluorophores upon increase of temperature, leading to a general decay in their fluorescence intensity.

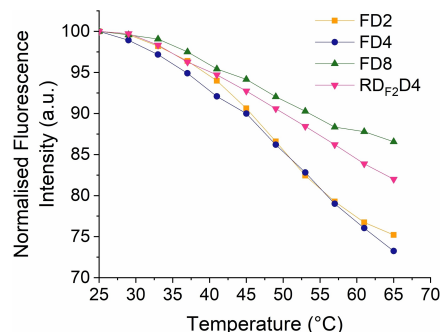


Figure 4. Effect of temperature on the fluorescence intensity of the synthesized dendritic fluorophores.

Conclusion

The improvement and development of new dyes is of utmost importance for fluorescence-based diagnostic advancements. In cell proliferation assays, high signal-to-noise ratios allow reliable detection of smaller number of proliferating cells. To achieve these requirements, fluorophores with enhanced fluorescent properties must be identified, synthesized, and introduced into biomolecules without jeopardizing their biological activity.

In this work, the successful development of a direct, divergent pathway for the synthesis of *ready-to-click* rhodamine

dyes afforded three fluorophores, namely, RD_{H_2} , RD_m and RD_{F_2} , showing remarkable photophysical properties, low pH-dependence, and high potential as fluorescent probes in EdU cell proliferation assays. The development of this new synthetic pathway, therefore, proves as a promising strategy for the rapid development of new click chemistry-conjugable fluorophores.

To further increase the fluorescence signal of our fluorophores, a family of three bis-MPA dendritic scaffolds containing 2, 4 and 8 alkyne functionalities were decorated via click chemistry. In this case, **fluorescein azide** was used as a standard fluorophore to afford **FD2**, **FD4**, and **FD8**, respectively. As for the photophysical properties, which were found to be highly pH-dependent, an increase of the maximum extinction coefficient along with the number of dye units was observed. In contrast, the fluorophores showed a decrease of quantum yield together with the increasing number of dye moieties which, in turn, caused a decay of the fluorescence intensity. We decided then to use our model rhodamine dye RD_{F_2} to prepare $RD_{F_2}D_4$. This latter molecule showed lower values of both extinction coefficient and quantum yield in comparison to RD_{F_2} and, thus, a decay of the fluorescence intensity. Ultimately, the effect of temperature on fluorescence intensity of the dendritic fluorophores was evaluated, leading to a general decay of fluorescence. This behavior suggests that collisional quenching prevails over aggregate dissociation upon temperature increase.

Albeit the observed self-quenching of fluorescence was not favorable in this study, comprehensive insights of the behavior of these dye-functionalized dendrons were acquired. It is apparent that the development of these dendritic structures remains challenging^[9,21,22] and further optimization must be carried out. Relatively high lipophilicity of the employed fluorophores appears to be the main reason for the observed self-quenching. Introduction of water-soluble functionalities into the dye moieties would reduce closeness between them, elude aggregation and possibly enable amplification of the fluorescent signal. Nevertheless, the strongly absorbing and nonfluorescent properties of these dendrons could serve in other applications as quenchers for Förster resonance energy transfer (FRET) experiments.^[49]

Experimental Section

Materials and methods for chemical synthesis and full characterization of all new compounds are found in the Supporting Information.

UV-vis and fluorescence spectroscopy: Samples for spectroscopy were prepared as stock solutions in DMSO and diluted such that the DMSO concentration did not exceed 1% (v/v). Absorption spectra were recorded on an Agilent Cary 50 spectrometer. Fluorescence spectra were recorded on a Shimadzu RF-5301PC fluorescence spectrometer. All measurements were performed at ambient temperature using 1 cm path length, 3.5 mL quartz cuvettes from Hellma Analytics. Absorbance/extinction coefficient and emission scans are averages ($n=3$).

Maximum extinction coefficient determination: All reported maximum extinction coefficients (ϵ_{max}) were calculated by a linear

regression analysis obeying the Beer-Lambert law. Measurements were carried out using moderately concentrated samples ($A < 0.8$) to ensure linearity between absorbance and concentration. All absorbance values are averages ($n=3$). Plots are found in the Supporting Information.

Quantum yield determination: All reported fluorescence quantum yield values (φ) were determined using the comparative method.^[50] Fluorescein ($\varphi=0.91$ in 0.1 M aqueous NaOH)^[36] and rhodamine 6G ($\varphi=0.95$ in EtOH)^[28] were used as references for fluorescein- and rhodamine-based fluorophores, respectively. Reported refractive index values were taken for the aqueous solutions and buffers^[51,52] ($n=1.33$) and EtOH^[53] ($n=1.36$). Measurements were carried out using dilute samples ($A < 0.1$) to minimize inner filter effects.^[54] All absorbance and integrated fluorescence intensity (fluorescence area) values are averages ($n=3$). The slopes of the plots of fluorescence area vs. absorbance were used in the comparative method by means of the following equation:

$$\phi_s = \phi_r \cdot \frac{m_s}{m_r} \cdot \left(\frac{n_s}{n_r}\right)^2$$

in which φ =fluorescence quantum yield, m =slope of the plot of fluorescence area vs. absorbance, n =refractive index and r and s subscripts refer to the reference and unknown fluorophore, respectively. Plots are found in the Supporting Information.

EdU cell proliferation assay: The EdU Cell Proliferation Kit for imaging EdU-Click 555 (baseclick GmbH) was used following the manufacturer's instruction with minor modifications. HEK-293T cells were seeded on No. 1 glass coverslips and grown in DMEM containing 10% FBS for 24 h before being pulsed for 2 h with 10 μ M EdU in the same growth medium. After washing with PBS, the cells were fixed with 4% formaldehyde in PBS for 15 min, permeabilized for 15 min with 0.1% saponin in PBS containing 1% BSA and incubated for 30 min in a cocktail containing 2 μ M dye-azide (either RD_{F_2} or the 5-TAMRA-PEG3-Azide provided with the kit), 1x Reaction buffer, 1x Buffer additive and Catalyst solution. Coverslips were then washed 3 times for 5 min with PBS containing 0.1% saponin and 1% BSA with inclusion of DAPI (1:15 dilution of NucBlue Fixed Cell ReadyProbes Reagent, Life Technologies) in the first wash. Finally, the coverslips were mounted with Fluoroshield mounting medium (Sigma) on glass slides and imaged using an EVOS FL II fluorescent microscope equipped with an oil immersion 100x Plan Fluorite objective and EVOS LED Cubes RFP (531/40 nm excitation, 593/40 nm emission) and DAPI (357/44 excitation, 447/60 nm; all from Life Technologies). Identical illumination intensity and exposure time were used for imaging samples treated with the two dye-azides. Images were processed using the ImageJ software.

Acknowledgements

This project has received funding from the European Union's Horizon 2020 Research and Innovation Programme under the Marie Skłodowska-Curie grant agreement No765266 and by the Deutsche Forschungsgemeinschaft (DFG, German Research Foundation), Project-ID 201269156-SFB 1032 (A05). We would like to express our gratitude to Dynamic Biosensors GmbH for providing the required instrumentation for the UV-vis and fluorescence spectroscopy. We would also like to thank Dr. Tim Schröder, Julian Bauer and Prof. Tinnefeld (Department of

Chemistry, LMU Munich) for their invaluable help with experiments on the effect of temperature and photobleaching.

Conflict of Interest

The authors declare no conflict of interest.

Data Availability Statement

The data that support the findings of this study are available from the corresponding author upon reasonable request.

Keywords: click chemistry · dendrons · ethynyldeoxyuridines · fluorescein · rhodamines

- [1] N. Nath, B. Godat, M. Urh, *J. Visualization* **2016**, *2016*, 54545.
- [2] R. W. Dirks, H. J. Tanke, *BioTechniques* **2006**, *40*, 489–496.
- [3] O. Roger, S. Collicie-Jouault, J. Ratiskol, C. Sinquin, J. Guezennec, A. M. Fischer, L. Chevolot, *Carbohydr. Polym.* **2002**, *50*, 273–278.
- [4] C. Schultz, A. B. Neef, T. W. Gadella, J. Goedhart, *Cold Spring Harb. Protoc.* **2010**, *5*, 10.1101/pdb.prot5459.
- [5] D. Maity, J. Jiang, M. Ehlers, J. Wu, C. Schmuck, *Chem. Commun.* **2016**, *52*, 6134–6137.
- [6] A. Nagy, E. Vitásková, L. Černíková, V. Křivda, H. Jiřincová, K. Sedlák, J. Horníčková, M. Havlíčková, *Sci. Rep.* **2017**, *7*, 1–10.
- [7] Y. Huang, D. Kong, Y. Yang, R. Niu, H. Shen, H. Mi, *Biotechnol. Lett.* **2004**, *26*, 891–895.
- [8] B. Oberleitner, A. Manetto, T. Frischmuth, *BIOSpektrum* **2014**, *20*, 188–190.
- [9] C. Wängler, G. Moldenhauer, R. Saffrich, E. M. Knapp, B. Beijer, M. Schnölzer, B. Wängler, M. Eisenhut, U. Haberkorn, W. Mier, *Chem. Eur. J.* **2008**, *14*, 8116–8130.
- [10] S. Nik-Zainal, P. Van Loo, D. C. Wedge, L. B. Alexandrov, C. D. Greenman, K. W. Lau, K. Raine, D. Jones, J. Marshall, M. Ramakrishna, A. Shlien, S. L. Cooke, J. Hinton, A. Menzies, L. A. Stebbings, C. Leroy, M. Jia, R. Rance, L. J. Mudie, S. J. Gamble, P. J. Stephens, S. McLaren, P. S. Tarpey, E. Papaemmanuil, H. R. Davies, I. Varela, D. J. McBride, G. R. Bignell, K. Leung, A. P. Butler, J. W. Teague, S. Martin, G. Jönsson, O. Mariani, S. Boyault, P. Miron, A. Fatima, A. Langerod, S. A. J. R. Aparicio, A. Tutt, A. M. Sieuwerts, Å. Borg, G. Thomas, A. V. Salomon, A. L. Richardson, A. L. Borresen-Dale, P. A. Futreal, M. R. Stratton, P. J. Campbell, *Cell* **2012**, *149*, 994–1007.
- [11] S. Vira, E. Mekhedov, G. Humphrey, P. S. Blank, *Anal. Biochem.* **2010**, *402*, 146–150.
- [12] C. P. Toseland, *J. Chem. Biol.* **2013**, *6*, 85–95.
- [13] J. B. Grimm, L. D. Lavis, *Nat. Methods* **2021**, *19*, 149–158.
- [14] A. Salic, T. J. Mitchison, *Proc. Nat. Acad. Sci.* **2008**, *105*, 2415–2420.
- [15] J. Gierlich, G. A. Burley, P. M. E. Gramlich, D. M. Hammond, T. Carell, *Org. Lett.* **2006**, *8*, 3639–3642.
- [16] G. M. Solius, D. I. Maltsev, V. V. Belousov, O. V. Podgorny, *J. Biol. Chem.* **2021**, *297*, 101345.
- [17] A. Carlmark, E. Malmström, M. Malkoch, *Chem. Soc. Rev.* **2013**, *42*, 5858–5879.
- [18] S. S. Santos, R. V. Gonzaga, J. V. Silva, D. F. Savino, D. Prieto, J. M. Shikay, R. S. Silva, L. H. A. Paulo, E. I. Ferreira, J. Giarolla, *Can. J. Chem.* **2017**, *95*, 907–916.
- [19] X. Yan, Y. Yang, Y. Sun, *J. Phys. Conf. Ser.* **2021**, *1948*, 012205.
- [20] S. K. Prajapati, S. D. Maurya, M. K. Das, V. K. Tilak, K. K. Verma, R. C. Dhakar, *J. Drug Deliv. Ther.* **2016**, *6*, 67–92.
- [21] J. Manono, C. A. Dougherty, K. Jones, J. DeMuth, M. M. B. Holl, S. DiMaggio, *Mater. Today Commun.* **2015**, *4*, 86–92.
- [22] C. A. Dougherty, S. Vaidyanathan, B. G. Orr, M. M. Banaszak Holl, *Bioconjugate Chem.* **2015**, *26*, 304–315.
- [23] Á. Martín-Serrano Ortiz, P. Stenström, P. Mesa Antunez, O. C. J. Andrén, M. J. Torres, M. I. Montañez, M. Malkoch, *J. Polym. Sci. Part A* **2018**, *56*, 1609–1616.
- [24] N. Raddaoui, S. Stazzoni, L. Möckl, B. Viverge, F. Geiger, H. Engelke, C. Bräuchle, T. Carell, *ChemBioChem* **2017**, *18*, 1716–1720.
- [25] M. Ceresole, Verfahren Zur Darstellung von Farbstoffen Aus Der Gruppe Des Meta-Amidophenolphthaleins. German Patent 44002, **1887**.
- [26] M. Beija, C. A. M. Afonso, J. M. G. Martinho, *Chem. Soc. Rev.* **2009**, *38*, 2410–2433.
- [27] L. D. Lavis, R. T. Raines, *ACS Chem. Biol.* **2008**, *3*, 142–155.
- [28] J. B. Grimm, A. K. Muthusamy, Y. Liang, T. A. Brown, W. C. Lemon, R. Patel, R. Lu, J. J. Macklin, P. J. Keller, N. Ji, L. D. Lavis, *Nat. Methods* **2017**, *14*, 987–994.
- [29] L. D. Lavis, R. T. Raines, *ACS Chem. Biol.* **2014**, *9*, 855–866.
- [30] J. B. Grimm, L. D. Lavis, *Org. Lett.* **2011**, *13*, 6354–6357.
- [31] J. B. Grimm, B. P. English, J. Chen, J. P. Slaughter, Z. Zhang, A. Revyakin, R. Patel, J. J. Macklin, D. Normanno, R. H. Singer, T. Lionnet, L. D. Lavis, *Nat. Methods* **2015**, *12*, 244–250.
- [32] T. Peng, D. Yang, *Org. Lett.* **2010**, *12*, 496–499.
- [33] D. Magde, R. Wong, P. G. Seybold, *Photochem. Photobiol.* **2002**, *75*, 327–334.
- [34] L. Wu, K. Burgess, *J. Org. Chem.* **2008**, *73*, 8711–8718.
- [35] T. G. Hwang, G. R. Han, J. M. Lee, J. W. Lee, H. M. Kim, D. Hwang, S. K. Kim, J. P. Kim, *J. Phys. Chem. C* **2019**, *123*, 24263–24274.
- [36] L. Porrès, A. Holland, L. O. Pålsson, A. P. Monkman, C. Kemp, A. Beeby, *J. Fluoresc.* **2006**, *16*, 267–273.
- [37] R. Sjöback, J. Nygren, M. Kubista, *Spectrochim. Acta Part A* **1995**, *51*, L7–L21.
- [38] J. R. Lakowicz, *Principles of Fluorescence Spectroscopy*, Springer, **2006**.
- [39] U. Mahmood, R. Weissleder, *Mol. Cancer Ther.* **2003**, *2*, 489–496.
- [40] A. Eisfeld, J. S. Briggs, *Chem. Phys.* **2006**, *324*, 376–384.
- [41] N. J. Hestand, F. C. Spano, *Chem. Rev.* **2018**, *118*, 7069–7163.
- [42] I. L. Arbeloa, *J. Chem. Soc. Faraday Trans. 2 Mol. Chem. Phys.* **1981**, *77*, 1725–1733.
- [43] M. Ogawa, N. Kosaka, P. L. Choyke, H. Kobayashi, *ACS Chem. Biol.* **2009**, *4*, 535–546.
- [44] M. Sun, K. Müllen, M. Yin, *Chem. Soc. Rev.* **2016**, *45*, 1513–1528.
- [45] A. Hassanzadeh, A. Zeini-Isfahani, M. H. Habibi, *Spectrochim. Acta Part A* **2006**, *64*, 464–476.
- [46] “ATTO-TEC GmbH – Dye-Aggregation,” can be found under <https://www.atto-tec.com/fluorescence/dye-aggregation/?language=en>, **2021**.
- [47] W. C. Lai, N. S. Dixit, R. A. Mackay, *J. Phys. Chem.* **1984**, *88*, 5364–5368.
- [48] H. R. Deepa, J. Thippudrappa, H. M. S. Kumar, *J. Phys. Conf. Ser.* **2020**, *1473*, 012046.
- [49] L. Wu, C. Huang, B. P. Emery, A. C. Sedgwick, S. D. Bull, X. P. He, H. Tian, J. Yoon, J. L. Sessler, T. D. James, *Chem. Soc. Rev.* **2020**, *49*, 5110–5139.
- [50] K. Lawson-Wood, S. Upstone, E. Kieran, *Fluoresc. Spectrosc.* **2018**, *4*, 1–5.
- [51] Z. C. Yang, M. Wang, A. M. Yong, S. Y. Wong, X. H. Zhang, H. Tan, A. Y. Chang, X. Li, J. Wang, *Chem. Commun.* **2011**, *47*, 11615–11617.
- [52] M. M. Koerner, L. A. Palacio, J. W. Wright, K. S. Schweitzer, B. D. Ray, H. I. Petrache, *Biophys. J.* **2011**, *101*, 362–369.
- [53] J. Rheims, J. Köser, T. Wriedt, *Meas. Sci. Technol.* **1997**, *8*, 601.
- [54] S. Dhama, A. J. D. Mello, G. Rumbles, S. M. Bishop, D. Phillips, A. Beeby, *Photochem. Photobiol.* **1995**, *61*, 341–346.

Manuscript received: August 23, 2022
Accepted manuscript online: November 1, 2022
Version of record online: December 7, 2022

4 UNPUBLISHED WORK

4.1 Synthesis and Validation of Clickable Multimeric Mannose Ligands for Dendritic Cell Targeting

4.1.1 Prolog: Targeted Delivery of Nucleic Acid Therapeutics

Specific drug delivery remains as the main hindrance for most therapeutic developments. The selective delivery of nucleic-acid-based drugs to cells and tissues of interest is, therefore, a sought-after attribute to enhance efficacy and limit side effects of these medicines. State-of-the-art advances in nucleic-acid-based therapies show exceptional potential, as diverse cutting-edge RNA-based medications start to gain approval or advance to phase III clinical trials. Current research and clinical efforts include a wide range of applications, such as protein replacement therapies, gene expression regulation, cell therapies, vaccination against cancer and infectious diseases and gene editing. Most emerging nucleic-acid-based drugs, however, present issues associated to fast degradation by nucleases, suboptimal cell penetration and immunogenicity that must be surmounted to fully exhibit their therapeutic properties.^[143,144]

For this purpose, various delivery platforms, including polymer- and lipid-based nanoparticles^[145–147] and ligand-conjugated systems,^[148–151] have been developed. The utilization of ligands able to induce uptake by receptor-mediated endocytosis emerges as a promising strategy to accomplish accumulation of therapeutic RNAs in desired cells and tissues. Peptides,^[152,153] antibodies,^[154–156] aptamers^[157] and biologically-active small molecules^[158,159] have been employed for the targeting of different tissues.^[160] Hitherto, one of the most significant advancements in RNA-based drug delivery comprises the recently reported hepatocyte-targeting ligand found on the carbohydrate-conjugated RNA drugs Givosiran (Alnylam), Lumasiran (Alnylam) and Inclisiran (Novartis). These triantennary *N*-acetylgalactosamine (GalNAc)-siRNA conjugates (**Figure 9**), currently on the market,^[101–103] are used to treat liver-related illnesses. The rationale behind the delivery and accumulation of these siRNAs into the liver is based on the specific binding of the GalNAc-based ligand to asialoglycoprotein receptors (ASGPR) of hepatocytes.^[161] Notwithstanding the considerable amount of potential ligands for specific cell-targeting, achieving favorable *in vivo* delivery to extrahepatic tissues persists as a main hurdle and additional research is essential.^[162]

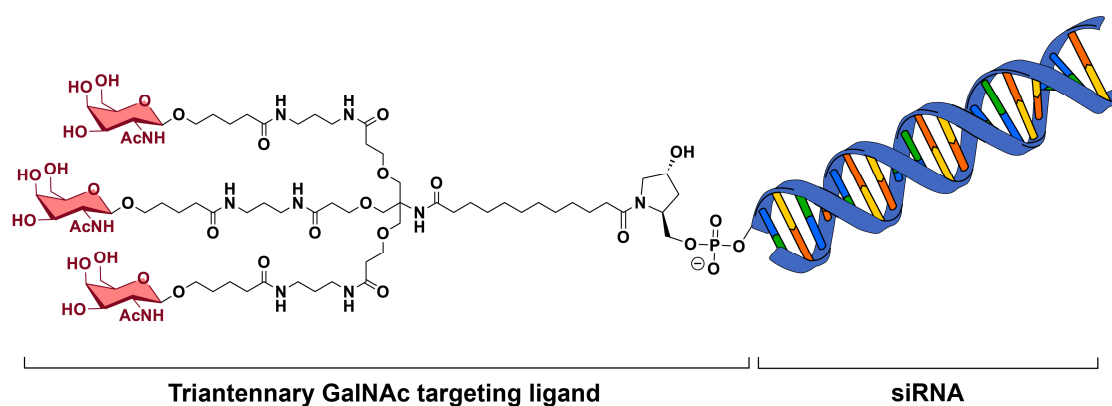


Figure 9. General structure of the commercially available triantennary GalNAc-siRNA conjugates.

In the context of cancer immunotherapy^[163] and vaccination,^[164] aiming at professional antigen-presenting cells (APCs), like dendritic cells (DCs) and macrophages (Mφs), is of prime concern to activate the immune system. APCs internalize and process cellular debris, cancer cells, and pathogens and present the generated antigens on their surface through MHC proteins to adaptive immune system cells.^[165,166] Several extensively expressed C-type lectins (CTLs) are present in DCs and Mφs. These CTLs bind to a number of carbohydrate structures, which are generally situated on pathogen surfaces and play a pivotal role in endocytic processes (**Figure 10**).^[167–169]

An established methodology to produce synthetic CTL-targeting ligands relies on functionalization of polymeric constructs with various units of monosaccharides.^[170,171] In this

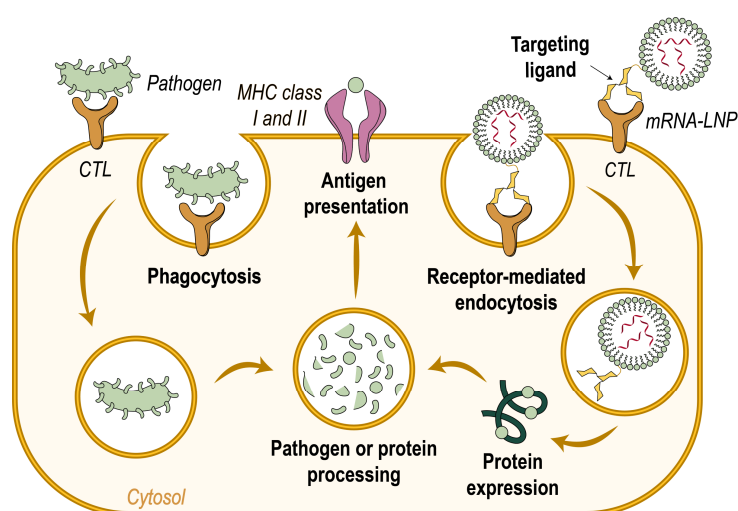
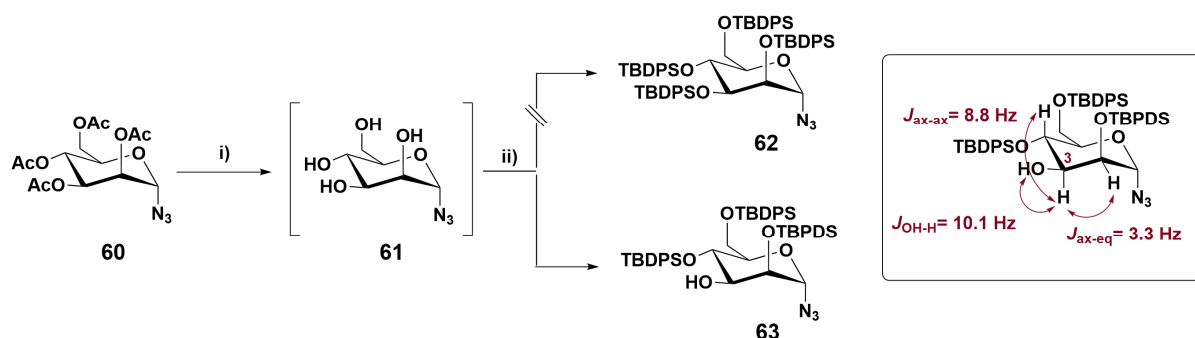


Figure 10. Endocytosis in DCs and Mφs of pathogens (left) and potential targeted delivery of RNA-based drugs, such as mRNA-LNPs, containing targeting ligands (right). The activation of the adaptive immune system is induced by antigen presentation on these cells. LNP = lipid nanoparticle.

thesis chapter, consequently, we aim to synthesize APC-targeting molecules and to evaluate their targeting properties for potential therapeutic applications in the field of vaccination and cancer immunotherapy.

4.1.2 Results and Discussion

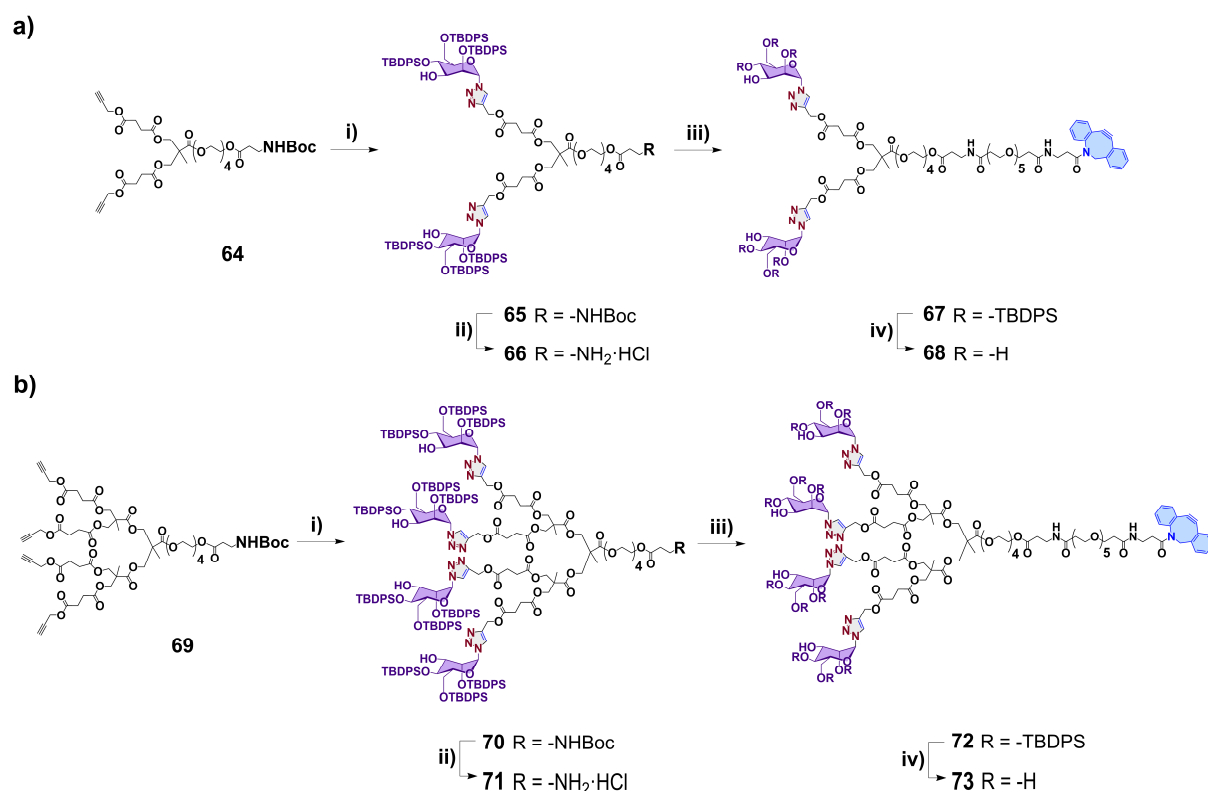
Several relevant CTLs, including Dectin-2, mannose receptor (MR) and dendritic cell-specific intercellular adhesion molecule-3-grabbing nonintegrin (DC-SIGN) play an essential role in endocytic processes upon binding to high-mannose structures.^[168] We envisioned, therefore, the synthesis of diantennary and tetraantennary mannose-presenting targeting ligands. With this in mind, we decided to use alkyne-functionalized 2,2-bis(methylol)propionic acid (bis-MPA) polyester dendrons as our structural scaffold. The selection of these polyester-based constructs relied on their biodegradable, functional and low-cytotoxic properties together with their facile click chemistry-functionalization.^[172] Considering the polyester nature of the utilized bis-MPA dendrons, we anticipated a protecting group exchange in our azide-presenting mannose precursor — 2,3,4,6-tetra-O-acetyl- α -D-mannopyranosyl azide (**60**) — where esters were replaced by silyl ether protecting groups (**Scheme 7**). In this manner, we ensured functional group orthogonality in the following synthetic steps and, due to the size increment of the products, purification by size exclusion chromatography was remarkably facilitated. Following our approach, mannose derivative **60** was subjected to deprotection by using NaOMe in MeOH to afford α -D-mannopyranosyl azide (**61**). Further treatment of compound **61** with *tert*-butyldiphenylsilyl chloride (TBDPSCl) along with imidazole in DMF gave rise to compound **63** in very good yields (83%) after two steps. The expected fully protected product **62**, nonetheless, was not produced. This probably occurred as a result of the steric hindrance



Scheme 7. Protecting group exchange of azide-presenting mannose precursor **60**. i) NaOMe, MeOH, RT, 3 h. ii) TBDPSCl, imidazole, DMF, RT, overnight, 83 % after 2 steps. TBDPS = *tert*-butyldiphenylsilyl. DMF = *N,N*-dimethylformamide.

related to the bulky silyl ethers formed via protection of the other three hydroxyl groups. The free hydroxyl group position in **63** was elucidated in accordance with the coupling constant values of the geminal proton relative to the hydroxyl group (**H-3**). The values of $J = 10.1$, 8.8 and 3.3 Hz are in agreement with the coupling between **H-3** and the hydroxyl group proton, vicinal axial proton, and vicinal equatorial proton, respectively.

The synthesis of diantennary targeting ligand **68** (**Scheme 8**) commenced with the mannose-functionalization of dendron **64** via CuAAC with mannose derivative **63** to afford compound **65** in good yields (70%). In order to perform a selective cleavage of the *tert*-butyloxycarbonyl (Boc) group of **65** in the presence of *tert*-butyldiphenylsilyl ether groups, we followed the deprotection methodology developed by Cavalier and Enjalbal.^[173] To this end, compound **65** was subjected to HCl 1.0 M in ethyl acetate to afford, in quantitative yield, the deprotected product **66**. Subsequent coupling between **66** and a DBCO-containing *N*-hydroxysuccinimide (NHS) ester gave rise to compound **67** in very good yield (84%). To conclude the synthesis,

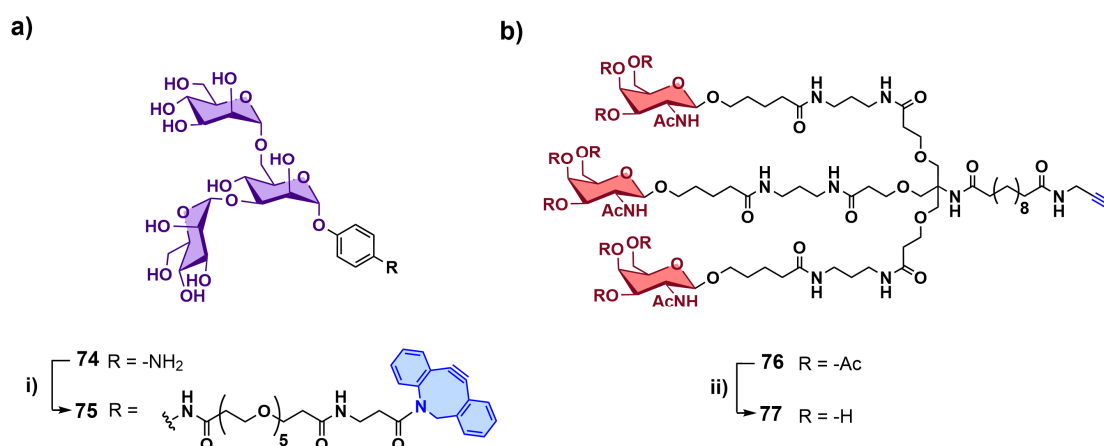


Scheme 8. Synthesis of mannose-based diantennary (**68**) and tetraantennary targeting ligands (**73**). i) **63**, CuBr, PMDTA, DMF, 45 °C, overnight, 70 % (**65**), 69 % (**70**). ii) HCl 1 M in EtOAc, RT, 2 h, 95 % (**63**), 98 % (**71**). iii) DBCO-PEG5-NHS, Et₃N, DMF, RT, 1h, 84 % (**67**), 93 % (**72**). iv) Et₃N·3HF, Et₃N, THF, 60 °C, 24 h, 93 % (**68**), 91 % (**73**). DBCO-PEG5-NHS = Dibenzoazacyclooctyne-penta(ethylene glycol)-propanoic acid succinimidyl ester. DMF = *N,N*-dimethylformamide. TBDPs = *tert*-butyldiphenylsilyl. PMDTA = pentamethyldiethylenetriamine. THF = tetrahydrofuran.

an alkaline buffered solution of $\text{Et}_3\text{N}\cdot 3\text{HF}$ and Et_3N in THF was employed to achieve the global deprotection of the carbohydrate moieties. A buffered basic medium was crucial in this step due to the relative acid-sensitivity of the DBCO group. After this last synthetic step, dendritic targeting ligand **68** was successfully obtained in excellent yield (93%).

Owing to the structural similarities, synthesis of tetraantennary targeting ligand **73** (Scheme 8) was accomplished analogously to that of targeting ligand **68**. In this respect, the introduction of silylated mannose **63** into dendritic scaffold **69**, by means of CuAAC, provided **70** in a 69% yield. Selective acidic deprotection of the *N*-Boc group (98% yield) and subsequent coupling between **71** and DBCO-presenting NHS ester delivered **72** in excellent yield (93%). As for the final basic deprotection of silyl groups, treatment of **72** with a buffered solution of $\text{Et}_3\text{N}\cdot 3\text{HF}$ and Et_3N yielded tetraantennary targeting ligand **73** (91%).

Dendritic cell immunoreceptor (DCIR), another significant CTL receptor, is reported by Bloem et al.^[174] to bind mannan structures. Taking this into consideration, we synthesized a *clickable* mannanose-based ligand (Scheme 9) in an uncomplicated manner by means of an aniline mannanose derivative (**74**) and a DBCO-functionalized NHS ester linker. The resulting mannanose targeting ligand **75** was afforded in 34% yield after RP-HPLC purification.



Scheme 9. Synthesis of mannanose- (a) and triantennary GalNAc-based (b) targeting ligands. i) DBCO-PEG5-NHS, Et_3N , DMF, RT, 1 h, 34%. ii) $\text{NH}_3(\text{aq})$, EtOH, 55 °C, 5 h, quantitative yield.

Moreover, and for cellular uptake comparative purposes, we generated a *clickable* version of the already successful triantennary GalNAc ligand, which is recognized by the macrophage galactose/*N*-acetylgalactosamine specific C-type lectin (MGL)^[175] in addition to ASGPR. Similarly to DCIR, Dectin-2, DC-SIGN and MR, MGL is expressed in subsets of DCs and

Mφs. For such purpose, peracetylated compound **76** was subjected to deprotection with aqueous ammonia and ethanol at 55°C for 5 h to quantitatively provide traintennary GalNAc targeting ligand **77** (Scheme 9).

In order to perform the subsequent cellular internalization assessment, mannose-based targeting ligands **68**, **73** and **75** as well as triantennary GalNAc ligand **77** were clicked to fluorescein azide **78** (Figure 11).

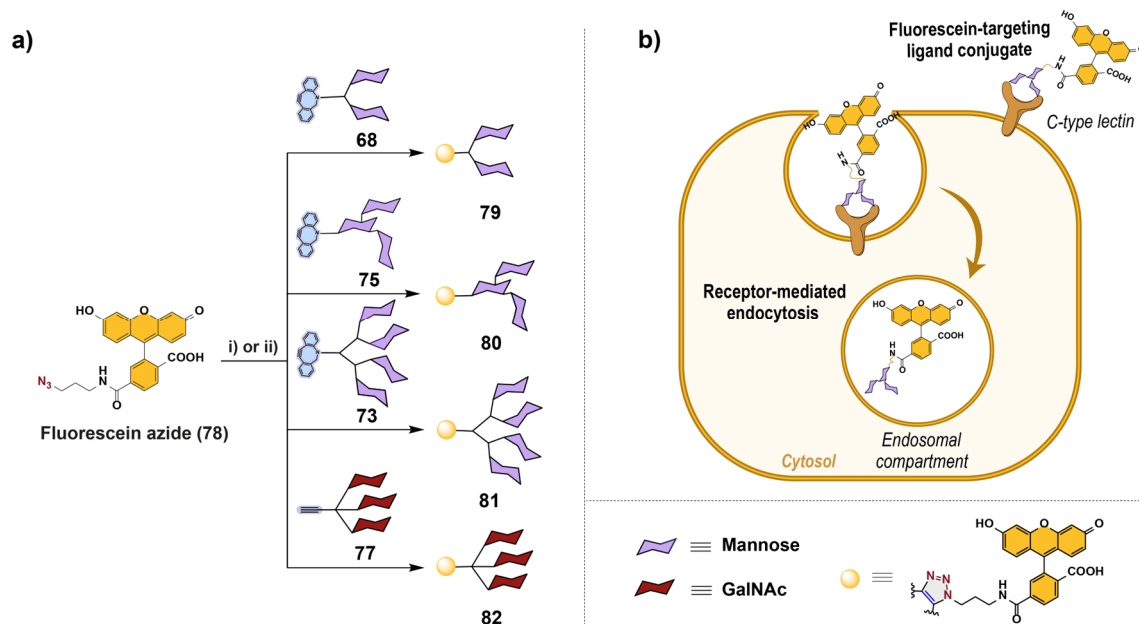


Figure 11. a) Conjugation of targeting ligands **68**, **72**, **75** and **77** with fluorescein azide **78**. b) Schematic representation of the postulated receptor-mediated endocytosis of **79-82** into DCs. i) **68**, **73** or **75**, DMSO, RT, overnight, quantitative yield. ii) **70**, Cu⁰ pellets, TBTA, DMSO, 600 rpm, 45 °C, 2h, quantitative yield. DMSO = dimethyl sulfoxide. TBTA = tris[(1-benzyl-1*H*-1,2,3-triazol-4-yl)methyl]amine.

Given that these click reactions were conducted at a micromolar level, the resulting yields were evaluated using HPLC chromatography. Both fluorescein azide (**78**) and targeting ligands **68**, **73**, **75** and **77** were added in equimolar amounts in each reaction. The yields were determined, therefore, by the presence or absence of the peak corresponding to fluorescein azide (**78**). **Figure 12** illustrates that no peak matching the free fluorophore was detected in the HPL chromatograms for conjugates **79-82**, and less than 5% of free fluorescein was observed in the HPL chromatogram of GalNAc-containing conjugate **82**. Thereby, we concluded that the reactions afforded the expected click products in nearly quantitative yields.

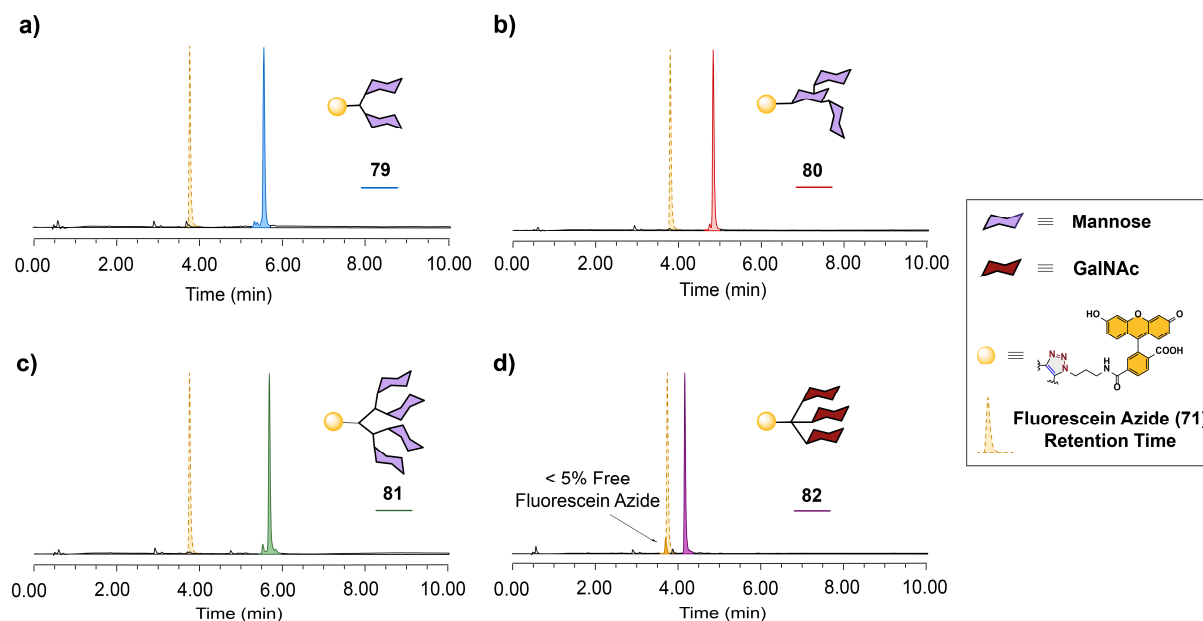


Figure 12. HPL chromatograms of a) diantennary mannose-fluorescein conjugate **79**, b) mannotriose-fluorescein conjugate **80**, c) tetraantennary mannose-fluorescein conjugate **81**, d) triantennary GalNAc-fluorescein conjugate **82**. $\lambda_{\text{abs}} = 497$ nm. Conditions: 1.5 mL/min, 40 °C, buffer B 0-30% v/v 0 \rightarrow 4 min, then 30-85% v/v 4 \rightarrow 10 min. The dotted, yellow peak represents the retention time of free fluorescein azide (**71**).

These conjugates were added to cultures of THP-1 monocytic leukemia cell line, previously exposed to growth factors IL-4 and GM-CSF for five days. Under the applied conditions, THP-1 cells undergo differentiation into immature DCs, which exhibit typical expression of C-type lectin receptors, including MR,^[176] and effectively internalize antigens by receptor-mediated endocytosis and macropinocytosis. Besides these conjugates, non-conjugated fluorescein azide **78** and FITC-labeled high molecular weight dextran, a genuine ligand for MR,^[177] were also employed as controls for cellular uptake evaluation (**Figure 13** and **Figure 14**).

As expected for receptor-mediated endocytosis, FITC-labeled dextran was internalized in a highly compartmentalized pattern.^[177] In contrast, fluorophore **78** showed a diffused cytoplasmic signal in the majority of cells, consistent with macropinocytosis. Among the synthesized fluorescent conjugates (**79-82**), diantennary mannose conjugate **79** exhibited a mostly diffuse cytoplasmic uptake distribution with some discrete compartments. As for mannotriose conjugate **80** and tetraantennary mannose conjugate **81**, these ligands displayed a progressively increased degree of compartmentalization upon higher branching degree and number of mannose units. Ultimately, triantennary GalNAc conjugate **82** showed a comparable proportion of cells with diffuse *versus* compartmentalized fluorescent signal to that of mannotriose conjugate **80**.

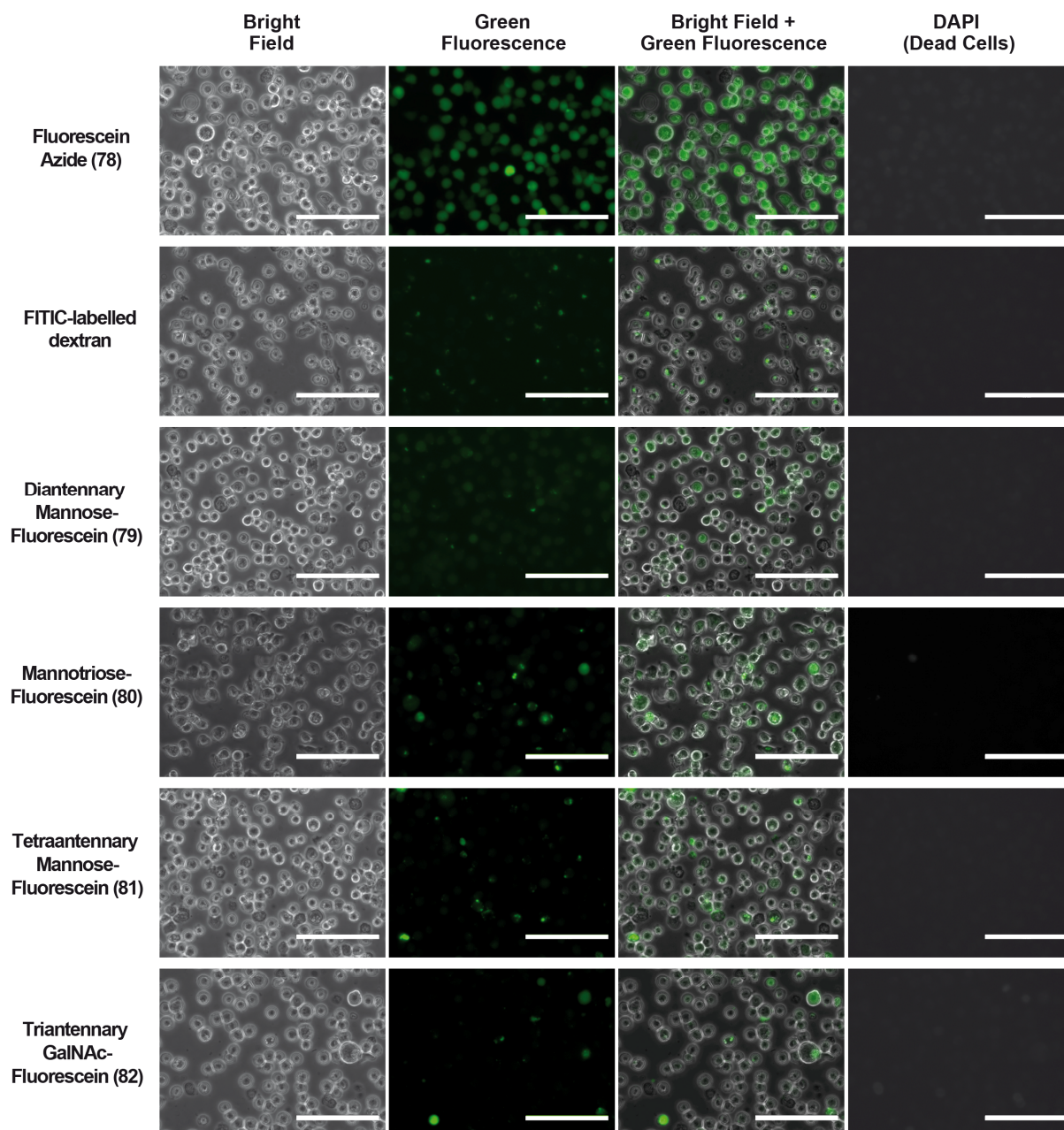


Figure 13. Fluorescent ligand uptake assays in THP-1 derived DCs. The indicated compounds and DAPI were added to the culture medium, and cells were imaged live after washing. Green signals show the distribution of fluorescein/FITC-labeled compound/conjugates as indicated. DAPI staining was used to assay cell viability (living cells are not permeable to DAPI and remain unstained). Scale bars represent 100 μm .

Despite the similar uptake results between **80** and **82**, additional studies with triantennary GalNAc ligand were discouraged due to its known major uptake by hepatocytes.^[161] From a perspective of binding affinity, the majority of CTLs possess various monosaccharide binding domains (CTLDs), where each of these domains bind to a single sugar unit. Not all CTLDs, however, exhibit monosaccharide binding activity. For instance, MR displays 8 CTLDs, of which only two domains (CTLD4 and CTLD5) bind mannose, GalNAc or fucose, the others

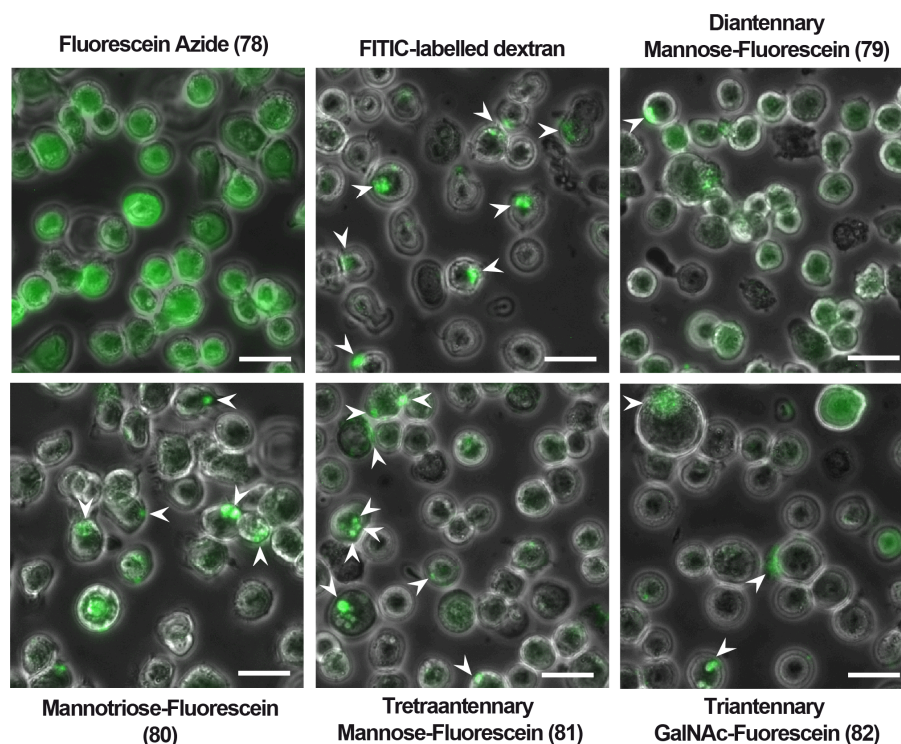


Figure 14. Magnified insets of merged green fluorescence and bright field images. Arrowheads point to signals confined to discrete compartments. Scale bars represent 20 μm .

seem to have other functions, and CTLD5 shows weak sugar binding. Based on topological effects, MR dimerization is only known to occur in non-immune cell types and even impairs monosaccharide binding in favor of other functions.^[178] We, thereby, tentatively hypothesize that fluorescent tetraantennary conjugate **81** is internalized more efficiently than fluorescent diantennary conjugate **79** as a result of a bridging effect, arising from the farther apart branches of the former between CTLDs. We also speculate that a diantennary ligand may not provide significant advantages over a monomeric one because of its short ‘span’, whereas a higher branching degree may potentially provide better binding. For other CTLs, this may vary depending on the adjacency of the monosaccharide-binding CTLDs.

To conclude, this study demonstrates efficient internalization into immature DCs prompted by the use of our synthesized high mannose branched structures. In line with previous work,^[179,180] our findings qualitatively indicate a positive correlation between the number of mannose units and endocytic internalization, presumably via receptor-mediated uptake. Interestingly, the comparable proclivity of tetraantennary and mannotriose ligands for higher compartmentalized uptake than the diantennary ligand implies that the structural arrangement of mannose units may influence their internalization modality in CTL-rich immature DCs.

Building upon our findings, this thesis chapter has served as a steppingstone towards the realization of cell-targeted therapeutics. The insights gained from this research contribute to expanding the field of click chemistry and paves the way for future investigations into the development of cutting-edge cell-specific drug delivery systems. In light of the success achieved in this chapter, aligned with the aims of the thesis, the next objective entails the application of these targeting ligands to a nucleic acid payload.

4.2 Application of Multimeric Mannose Targeting Ligands in an mRNA-Based SARS-CoV-2 Vaccine Candidate

4.2.1 Prolog: The COVID-19 Pandemic

The coronavirus disease 2019 (COVID-19) is caused by a viral infection with the severe acute respiratory syndrome coronavirus 2 (SARS-CoV-2).^[181] SARS-CoV-2 was first identified in December 2019 after clusters of pneumonia of unknown cause were reported in Wuhan (China).^[182] The rapid and global spread of the virus led the World Health Organization (WHO) to declare the outbreak of COVID-19 as a pandemic on March 11, 2020.^[183] COVID-19 symptoms range from asymptomatic or mild disease, such as fever, cough, dyspnea, smell- and loss of taste to eventually severe pneumonia and acute respiratory distress syndrome (ARDS), leading to multiorgan failure and death.^[184,185] As of December 27, 2022, the pandemic has globally caused over 651 million COVID-19 cases and more than 6.6 million deaths.^[186] Consequently, the COVID-19 pandemic has developed into an unparalleled challenge to worldwide healthcare and food systems, economies and humankind.^[181,187]

SARS-CoV-2 is an enveloped, positive-sense, single stranded RNA virus, sharing over 70% of its sequence with the severe acute respiratory syndrome coronavirus (SARS-CoV-1), and circa 50% with the Middle East respiratory syndrome-related coronavirus (MERS-CoV).^[188] Each

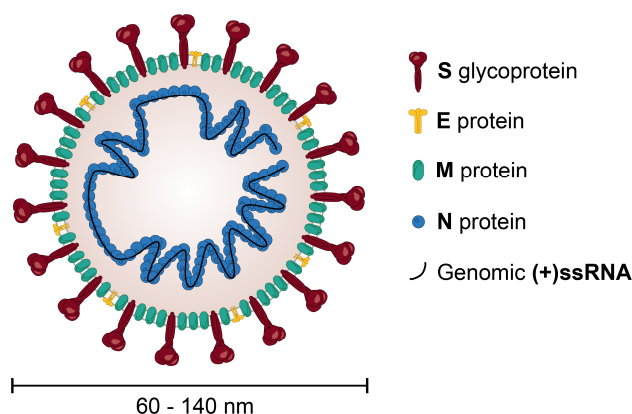


Figure 15. Structural proteins of SARS-CoV-2. S glycoprotein is responsible for enabling the virus to enter the host cell by attaching and fusing with the cell membrane.^[189] E protein is a multifunctional protein with structural, viral assembly and pathogenesis roles, among others.^[190-192] M protein assembles the virus through protein-protein interactions.^[193] N protein is believed to have multiple functions, such as forming a helical ribonucleoprotein (RNP) complex to pack and protect the RNA genome, protein-protein interactions and manipulating the cell cycle of the host cell.^[194-196]

viral unit is 60-140 nm in diameter^[197,198] and, like other coronaviruses, SARS-CoV-2 has 4 structural proteins, namely the spike (S), envelope (E), membrane (M) and nucleocapsid (N) proteins (**Figure 15**).

To prevent the spread of this virus and control the pandemic, numerous vaccine candidates have been developed since 2020.^[199,200] Vaccines are used to safely induce an immune response that confers protection against a specific pathogen. To achieve this, vaccines contain or express antigens that represent such a pathogen, which are usually proteins that induce immune responses.^[201] After vaccination or first pathogen exposure, a primary immune response occurs via proliferation and activation of pathogen-specific B and T cells (or lymphocytes). B cells are responsible for antibody production (humoral response) whereas T cells eliminate infected cells and activate more B and T lymphocytes (cell-mediated response). Once the pathogen or antigen is eradicated, B and T cell populations produced during the first immune response decline and long-term immunity is acquired by the presence of memory B and T cells in the body. Upon pathogen re-exposure, a more rapid and robust immune response is mounted

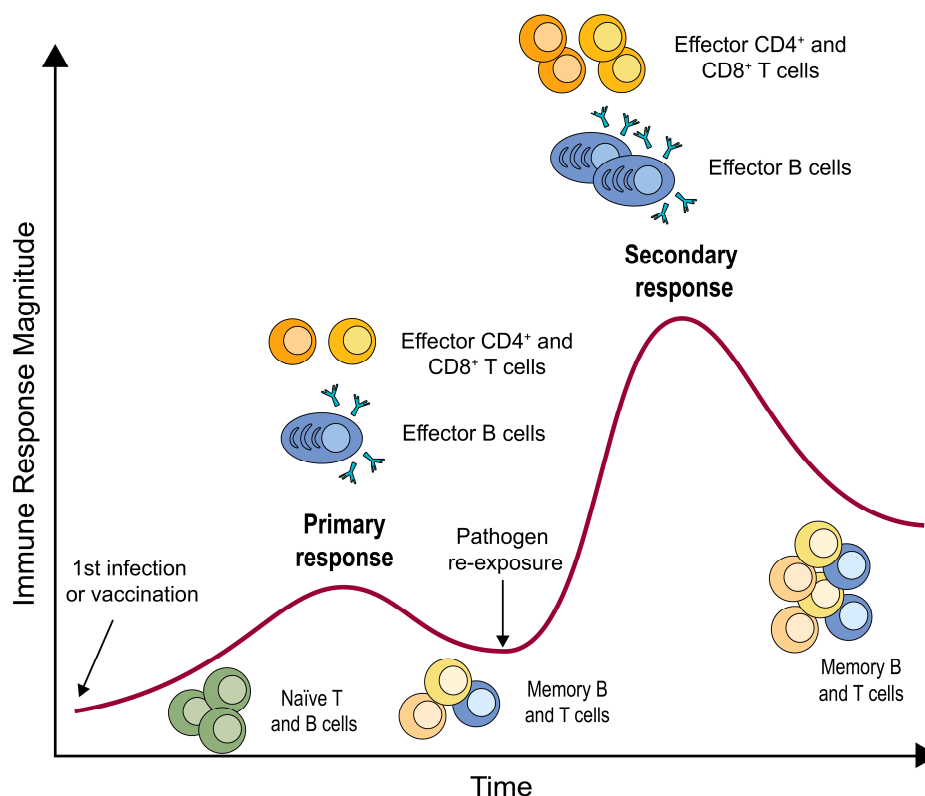


Figure 16. Schematic representation of primary and secondary immune responses. In the primary immune response, naïve B- and T cells differentiate into effector B- and T cells after antigen or pathogen exposure. During the secondary immune response, previously formed memory B- and T- cells differentiate into effector B- and T cells more rapidly and efficiently than their naïve counterparts, leading to a magnified immune response.

through these memory B and T cells, leading to mild or asymptomatic reinfection and generation of more memory cells after pathogen clearance (**Figure 16**). This secondary immune response after vaccination or pathogen infection is due to the so-called *immune memory*, which constitutes the rationale of vaccination.^[201,202]

As of December 2022, 11 different vaccine products, based on four distinct platforms, have been approved by the WHO for global use^[200] (**Table 1**). Most of these vaccines express the S protein as an antigen since its use in vaccine development against viruses of the same family has shown successful B and T cell responses as well as immune memory.^[203]

Due to the emergency situation caused by the COVID-19 pandemic, baseclick GmbH committed in early 2020 to the development of a novel mRNA-based SARS-CoV-2 vaccine candidate. For such purpose, and encouraged by the results in dendritic cell uptake in the previous chapter, we envisaged the use of our branched mannose-based ligands and baseclick's technology^[204] to form a mannose-mRNA conjugate.

Table 1. COVID-19 vaccines granted with emergency approval by the WHO as of December 2022.

Platform	Manufacturer	Vaccine Name	Approvals^[a]
Inactivated virus	Sinopharm	Covilo (BBIP-CorV)	93
	Sinovac	CoronaVac (PiCoVacc)	56
	Bharat Biotech	Covaxin (BBV-152)	14
mRNA	Pfizer/BioNTech	Comirnaty (BNT162b2)	149
	Moderna	Spikevax (mRNA-1273)	88
Viral vector	Oxford/AstraZeneca	Vaxzevria (ChAdOx1)	149
	Janssen (Johnson & Johnson)	JCovden (Ad26.COVS.S)	113
	Serum Institute of India	Covishield (ChAdOx1)	49
	CanSino	Convidecia (AD5-nCOV)	10
Protein subunit	Novavax	Nuvaxovid (NVX-CoV2373)	40
	Serum Institute of India	Covovax (NVX-CoV2373)	6

[a] Number of countries that have approved each vaccine.

4.2.2 Results and Discussion

Baseclick's vaccine candidate, named BCV-193N, is based on an *in vitro* transcribed mRNA encoding for the SARS-CoV-2 N protein and linked to mannan targeting ligand **68** via click chemistry (**Figure 17**). In contrast to the mRNA-based vaccines Comirnaty (Pfizer/Biontech) and Spikevax (Moderna), which express the S protein, BCV-193N was designed to induce translation of the N protein as the antigen due to its ostensibly lower incidence of non-synonymous mutations, large quantity of expressed protein during infection, and high relative immunogenicity.^[205,206] Moreover, BCV-193N avoids the use of lipid nanoparticles (LNPs), which have been associated with innate inflammatory side effects;^[207] instead replacing them by a mannose-based targeting ligand for specific delivery in dendritic cells (DCs).

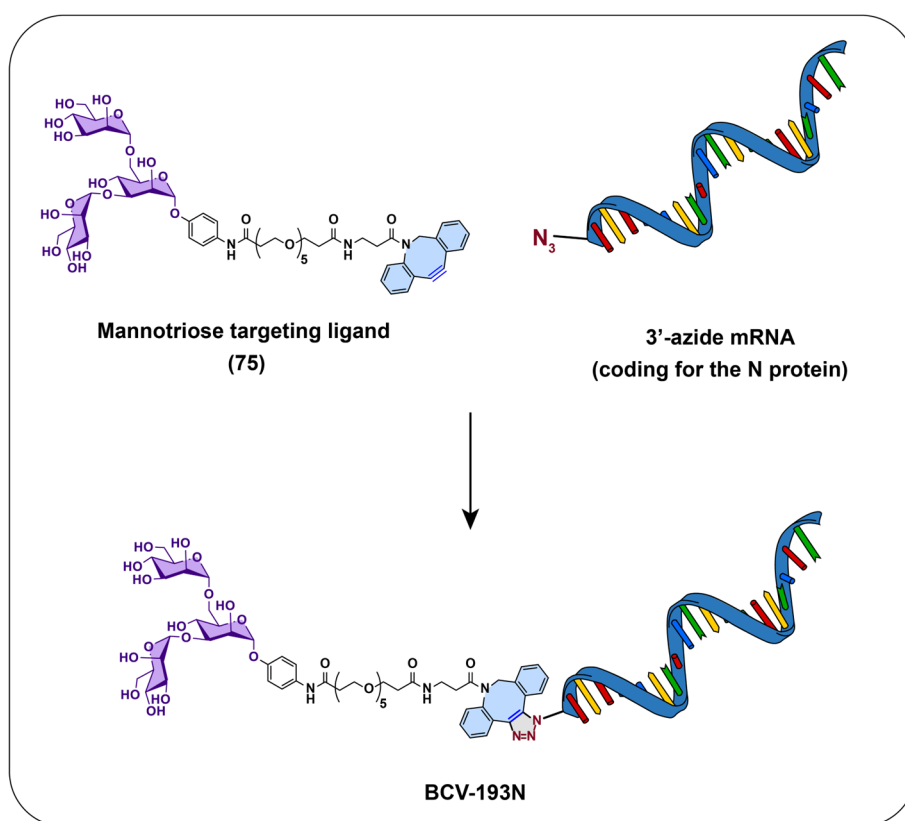


Figure 17. Synthesis of BCV-193N. The two constitutive units of the vaccine candidate (the targeting ligand and the 3'-azide mRNA) are straightforwardly conjugated via SPAAC to yield BCV-193N.

As shown in **Figure 18**, BCV-193N is hypothesized to interact with DCs through its targeting moiety, which should induce receptor-mediated endocytosis after interacting with C-type lectins (CTLs). Once the cell machinery has transcribed the mRNA coding sequence, N protein

units can be synthesized, processed, and presented on the surface of DCs, inducing strong cellular and humoral immune responses. This antigen presentation produces a primary immune response which, in turn, leads to the development of immune memory.

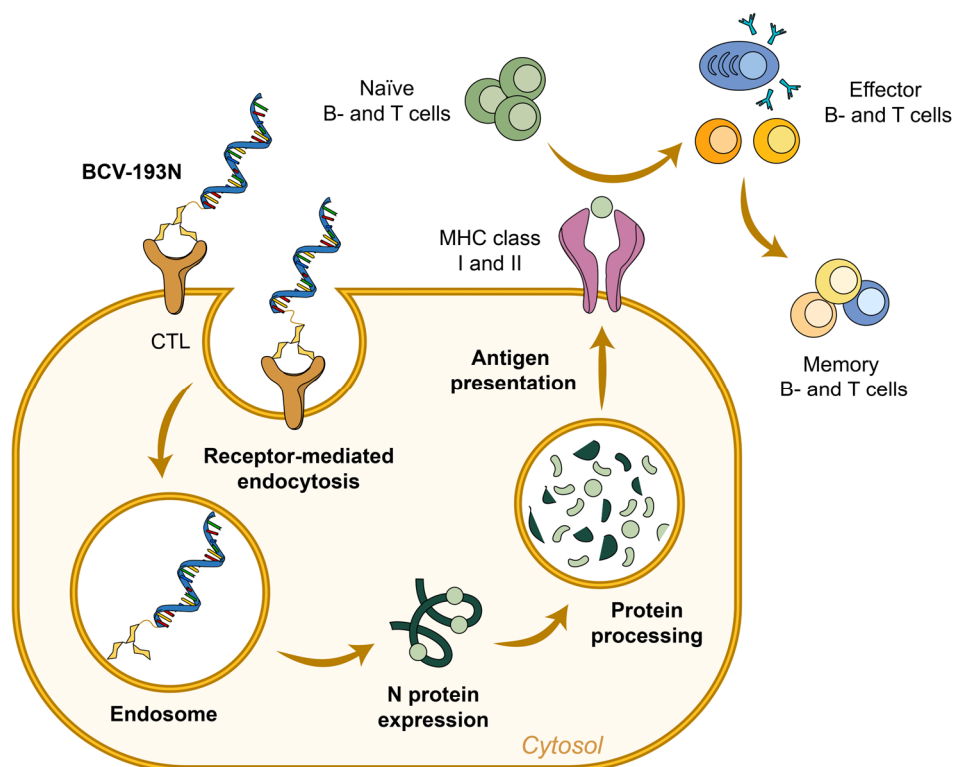
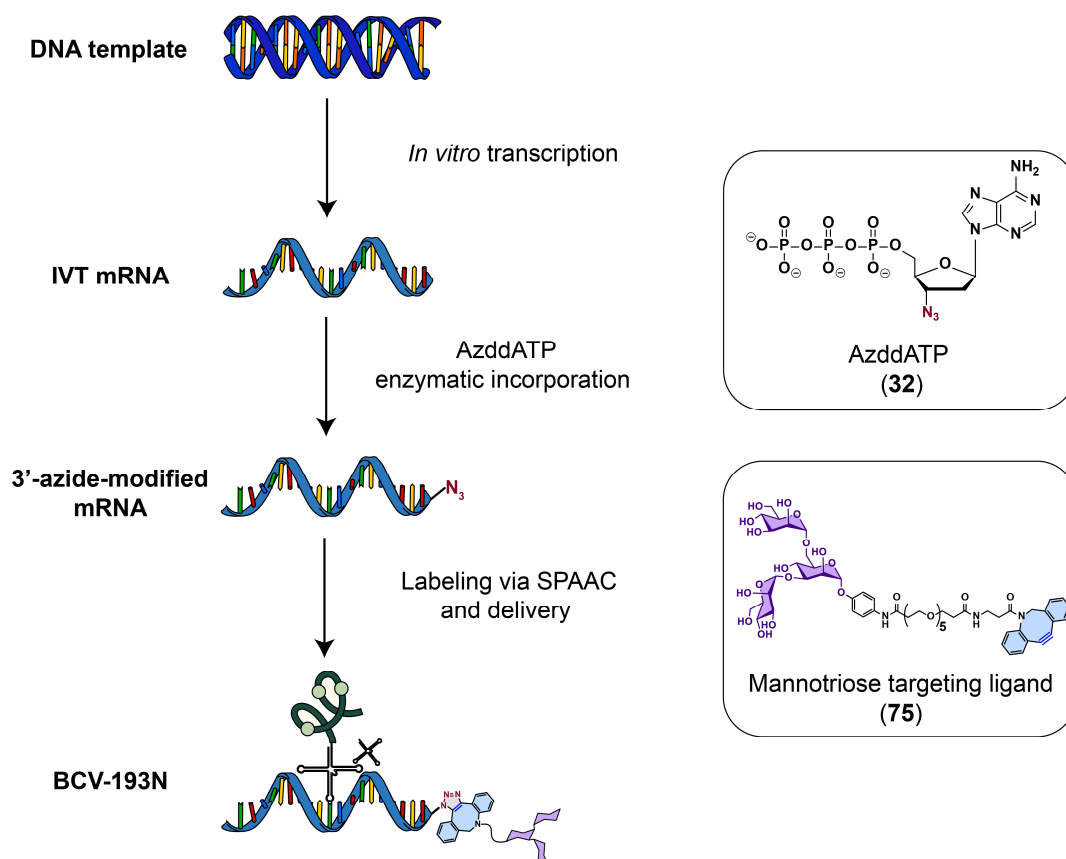


Figure 18. Postulated BCV-193N mechanism of action for immune response induction.

4.2.2.1 Synthesis of BCV-193N

BCV-193N synthesis (**Scheme 10**) begins with the linearization of a plasmid DNA (pDNA) template via BspQ1 restriction enzyme. This pDNA contains the coding sequence for the nucleocapsid protein (N) of SARS-CoV-2 virus and a poly(A) tail coding sequence. Thereafter, T7 RNA polymerase along with the corresponding nucleoside triphosphates (NTPs): ATP, CTP, GTP, UTP and Ψ TP (pseudouridine triphosphate), were employed for the *in vitro* transcription of mRNA. Ψ TP was used in order to enhance mRNA translation while reducing immunogenicity.^[208] In addition, a 5'-cap structure was co-transcriptionally introduced by T7 RNA polymerase using an Anti-Reverse Cap Analog (ARCA) to enhance mRNA stability and translation efficiency.^[209] Therefore, the transcription resulted in a stable mRNA including a 5'-cap structure and a poly(A) tail, ready for efficient expression in eukaryotic cells (refer **Experimental Section's Scheme 11** for more details). After digestion of the DNA template, the synthesis continued through the introduction of an azide modification at the end of the

poly(A) tail. To this aim, 3'-azido-2',3'-dideoxyadenosine triphosphate (AzddATP, **32**) and yeast poly(A) polymerase were used to incorporate such modification at the 3'-end of the *in vitro* transcribed (IVT) mRNA. Ultimately, the 3'-azide-modified mRNA was conjugated to mannatriose targeting ligand **75** via Cu-free click chemistry to yield BCV-193N as our SAR-CoV-2 vaccine candidate.



Scheme 10. *In vitro* synthesis of 3'-end-modified mRNA coding for the N protein and subsequent conjugation to the targeting ligand to yield BCV-193N.

Prior to conjugating our azide-containing IVT mRNA with mannatriose targeting ligand **75**, we assessed the efficiency of the SPAAC reaction using a model system. For this evaluation, we utilized a short RNA oligonucleotide (31-mer) containing a 3'-azide. The RNA 31-mer (1 nmol) and mannatriose targeting ligand **75** (10 nmol, 10 eq) were combined in a total reaction volume of 20 μ L (H_2O) and incubated at room temperature for 2 h. Subsequently, the reaction mixture was analyzed by HPLC, as depicted in **Figure 19**. The conversion of the 3'-azide-containing oligonucleotide into the clicked product was determined to be over 90% at the time of analysis. Therefore, to ensure complete conversion when employing our 3'-azide-containing IVT mRNA substrate, we performed the reaction using a 100-fold excess

of mannitriose targeting ligand **75** in a total reaction volume of 20 μL (H_2O) and incubated at room temperature for 2 h.

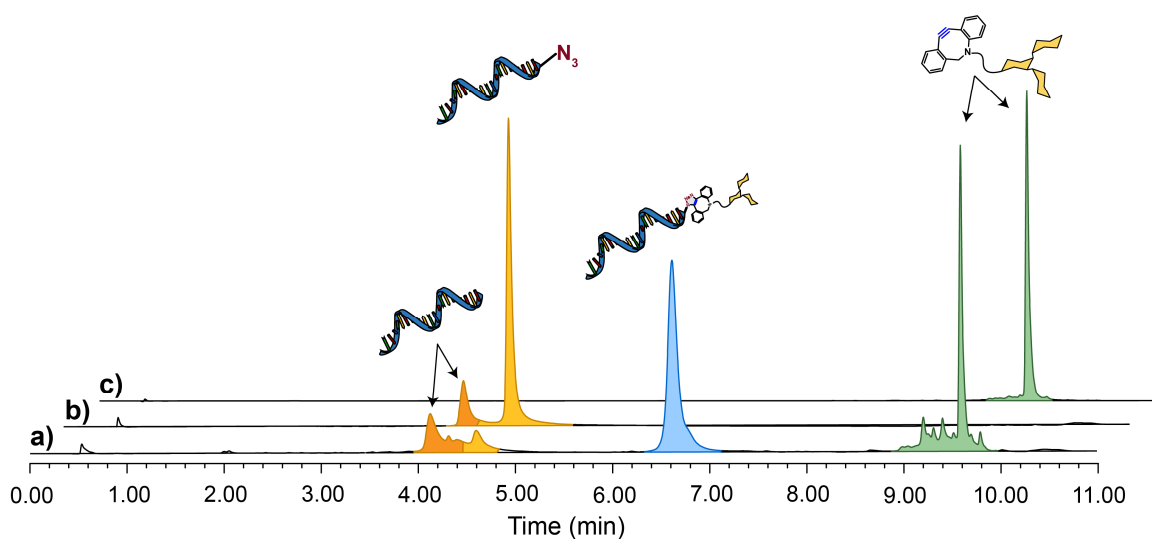


Figure 19. HPL chromatograms of a) click product after incubation at room temperature for 2 h ($\lambda_{\text{abs}} = 260$ nm), > 90% conversion; b) azide-modified mRNA ($\lambda_{\text{abs}} = 260$ nm), < 5% of unmodified mRNA is also present; and c) mannitriose targeting ligand **75** ($\lambda_{\text{abs}} = 290$ nm).

4.2.2.2 BCV-193N *In Vitro* Studies

A series of *in vitro* investigations, carried out in collaboration with Mikrogen GmbH, were performed to ensure efficient expression of BCV-193N in eukaryotic cells as well as recognition of the N protein by the human immune system. To such an end, HEK293T cells were transfected with our vaccine candidate, and the expression of the N protein was successfully determined by western blotting (**Figure 20**).

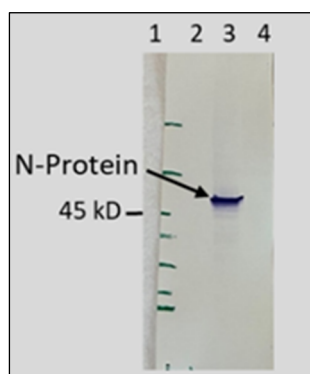


Figure 20. Western blot of HEK293T cell lysate transfected with BCV-193N. Lane 1: size standard (45 kD marker indicated). Lane 2: empty lane. Lane 3: cell lysate of cells transfected with BCV-193N. Lane 4: cell lysate of non-transfected cells. Detection with mouse monoclonal antibody from Mikrogen GmbH (Germany, Neuried). N-Protein (46.02 kD) is indicated.

To verify that the N protein is recognized by the human immune system, cell lysates of transfected and non-transfected HEK293T cells were subjected to western blotting and incubated with serum from healthy probands and recovered COVID-19 patients. In all COVID-19 recovered patients' sera, regardless of the disease severity, antibodies against the N protein were detected indicating a general immune response (**Figure 21**). This data supports the selection of the N protein as a suitable antigen to activate the human immune system against COVID-19.

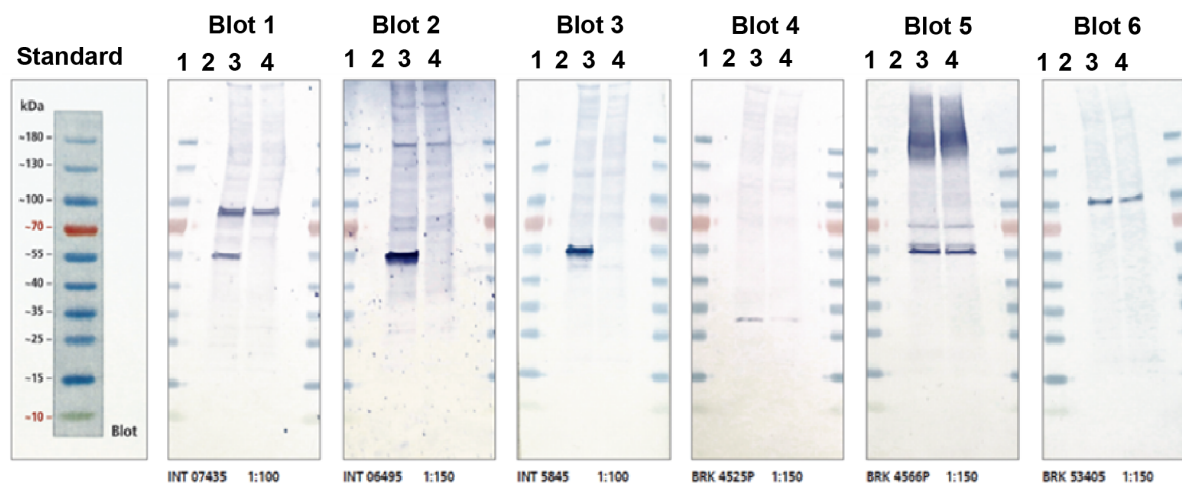


Figure 21. Western blot of HEK293T cell lysates transfected with BCV-193N. The lysates were incubated with serum of symptomatic COVID-19 patients. Left blot shows the molecular size standard. Blots 1-3 are incubated with serum of symptomatic COVID-19 patients. Blots 4-6 are incubated with serum of healthy probands. Lane 1: size standard. Lane 2: empty lane. Lane 3: cell lysate of (BCV-193N)-transfected cells. Lane 4: Cell lysate of non-transfected cells. Cell lysates were analyzed on 8% SDS-PAGE, blotted, and treated with a secondary antibody according to manufacturer's recommendation (Bio-Rad).

Although the comprehensive investigation of the pharmacokinetics and pharmacodynamics of our mRNA vaccine candidate is currently underway, it is important to acknowledge the limitations of the current stage and the absence of additional data at this time. These data would entail *in vivo* pre-clinical studies in mice — involving toxicity evaluation, assessment of mRNA immunogenicity, evaluation of cellular and humoral immune responses and investigation into the vaccine's biodistribution — followed by first-in-human studies. Nevertheless, the ultimate goal of this doctoral work, which is to apply the synthesized targeting ligands to a nucleic acid payload, has been accomplished, and promising initial *in vitro* results instill optimism about the vaccine uptake into DCs.

5 CONCLUSIONS AND OUTLOOK

Divergent Synthesis of Ultrabright and Dendritic Xanthenes for Enhanced Click-Chemistry-Based Bioimaging

In dye-based 5-ethynyl-2'-deoxyuridine (EdU) cell proliferation assays, high signal-to-noise ratios of labeled DNA allow reliable detection of a lower count of proliferating cells, entailing an overall enhancement in the sensitivity and quality of the method. In this thesis' published work, we report the successful development of a straightforward, divergent pathway for the synthesis of *ready-to-click* rhodamine dyes. The afforded fluorophores — **RD_{H2}**, **RD_m** and **RD_{F2}** — showed excellent photophysical properties, low pH-dependence, and remarkable potential as fluorescent probes for imaging experiments. Remarkably, the new 3,3-difluoroazetidone rhodamine azide (**RD_{F2}**) proved to be a superior alternative in EdU cell proliferation assays in comparison to commercially available 5-TAMRA-azide.

Additionally, with the aim to synthesize brighter fluorescent probes, we envisaged the synthesis of dendritic structures carrying multiple dye units. To such an end, a set of three bis-MPA dendrons — each containing 2, 4, and 8 alkyne functionalities — were functionalized via CuAAC with fluorescein azide as the standard fluorophore. The photophysical properties of the resulting dendritic dyes — **FD2**, **FD4** and **FD8** — were found to be highly pH-dependent. Furthermore, we observed an extinction coefficient increase with the number of dye units but, in contrast, we also observed a decrease in the quantum yield as the number of fluorescein moieties increased. This behavior led to an overall decay in fluorescence intensity. We decided then to use our model rhodamine dye **RD_{F2}** to afford **RD_{F2}D4**. This rhodamine-based multivalent dendron exhibited lower values of both extinction coefficient and quantum yield when compared to **RD_{F2}**, leading to a decay of the fluorescence intensity. Ultimately, we evaluated the impact of temperature on the fluorescence intensity of the dendritic fluorophores, which resulted in fluorescence decrease upon temperature rise. This observation implied that, as the temperature increases, collisional quenching prevails over aggregate dissociation.

Although the observed fluorescence self-quenching was not sought-after in this study, it provided valuable insights into the behavior of dye-functionalized dendrons. Further optimization, however, is necessary for the development of highly bright dendritic fluorophores. An effective approach to consider beyond the scope of this doctoral thesis would involve incorporating water-soluble functionalities into the chromophore units. This

would result in decreased proximity between the units, preventing their aggregation and potentially enhancing the intensity of the fluorescent signal. Nonetheless, the strongly absorbing and nonfluorescent properties of these dendrons could be useful in other applications, such as quenchers for FRET experiments.^[210]

Synthesis and Validation of Clickable Multimeric Mannose Ligands for Dendritic Cell Targeting

Targeted delivery of drugs to specific cells and tissues has the potential to enhance their effectiveness while minimizing their adverse effects. In this chapter, we aimed to develop immunocompetent cell-targeting ligands for potential therapeutic applications in the field of vaccination and cancer immunotherapies. Thereby, we directed our attention towards the development of a family of *clickable* carbohydrate-based ligands. These sugar-based structures were aimed to target CTLs found on the surface of DCs for receptor-mediated uptake. To this end, three distinct multimeric mannose-functionalized constructs — containing up to 4 mannose units — were synthesized and further functionalized with a DBCO group to enable their conjugation to the cargo of interest through Cu-free click chemistry. The synthesis of dianntenary (**75**) and tetraantenary (**80**) targeting ligands was successfully accomplished by branching click chemistry (CuAAC) of bis-MPA dendron scaffolds containing 2 and 4 alkyne groups, respectively. The utilization of silylated mannose derivatives played a pivotal role in ensuring the orthogonality of functional groups and facilitating the purification of subsequent reaction steps. As for the synthesis of the mannotriose targeting ligand (**75**), a straightforward approach was adopted through the application of NHS chemistry. Moreover, and for cellular uptake comparative purposes, we generated a *clickable* version of a triantennary GalNAc ligand (**77**).

We qualitatively confirmed the uptake of these carbohydrate-containing ligands utilizing a dendritic cell model and observed — by fluorescence microscopy — compartmentalized internalization that highly resembles endocytosis of well-established surface receptor ligands. In order to perform such assessment, fluorescent conjugates **79-82** were prepared via click chemistry. Fluorescein-diantennary mannose conjugate **79** exhibited a cytoplasmic distribution that was diffused with some discrete compartments. As for fluorescein-mannotriose conjugate **80** and fluorescein-tetraantennary mannose conjugate **81**, these ligands displayed an increased degree of compartmentalization with increasing number of mannose units. Lastly,

fluorescein-triantennary GalNAc conjugate **82** showed similar uptake results in comparison to fluorescein-mannotriose conjugate **80**. Further studies with **82**, however, were discouraged due to potential off-targeted delivery into the liver.

The results of this study indicate, therefore, that there is a qualitative direct relationship between the degree of branching in mannose-based ligands and their uptake into DCs via the endocytic pathway. These findings, consequently, support the application of click chemistry in the synthesis and conjugation of promising ligands for the delivery of drug and vaccine delivery.

Application of Multimeric Mannose Targeting Ligands in an mRNA-Based SARS-CoV-2 Vaccine Candidate

The COVID-19 pandemic prompted baseclick GmbH to take the commitment of developing a SARS-CoV-2 vaccine candidate, following an innovative approach based on click chemistry conjugation. For such purpose, and encouraged by the previous results in DC uptake, we envisioned the utilization of our mannose-based branched targeting ligands and baseclick's mRNA labeling technology^[204] to form a mannose-mRNA conjugate. In comparison to other mRNA-based vaccines, our candidate BCV-193N does not rely on LNPs as delivery carrier, expresses the N protein — a less-prone-to-mutate SARS-CoV-2 protein — and contains a targeting ligand for preferential delivery to DCs.

In the course of the project, *in vitro* synthesis of N-coding mRNA and subsequent 3'-end azide modification were achieved. This chemical modification enabled mRNA bioconjugation with mannose targeting ligand **75** to give rise to BCV-193N. Efficient *in vitro* expression of N protein in HEK293T cells transfected with BCV-193N was achieved. Furthermore, when incubating lysates of the transfected cells with sera from recovered COVID-19 patients, antibodies against this protein were detected, indicating that the N protein is a suitable antigen for immune system activation.

The initial findings presented in this study highlight the potential of click chemistry as a potent synthetic tool for advancing the development of nucleic acid therapeutics that specifically target cells. While the extensive investigation of the pharmacokinetics and pharmacodynamics of our mRNA vaccine candidate is currently ongoing, it is essential to acknowledge the limitations of the current stage and the absence of additional data at this time. Nonetheless, the encouraging results observed in the preliminary *in vitro* assessments inspire confidence in the

potential effectiveness of the vaccine. Looking ahead, aligned with the overarching aim of this doctoral thesis, we anticipate that our findings will yield valuable insights and serve as a foundation for future investigations in the field of cell-targeted nucleic acid therapeutics, leveraging the application of click-chemistry-based targeting ligands.

6 EXPERIMENTAL SECTION FOR UNPUBLISHED WORK

6.1 General Experimental Methods and Materials

Materials and Methods. Chemicals for organic synthesis and salts for buffers were purchased from Sigma-Aldrich, TCI, Fluka, ABCR, Acros Organics, Alfa Aesar, VWR, Polymer Factory, Synthose, Click Chemistry Tools, Sapala Organics, Carl Roth or baseclick GmbH and were used without further purification. Solvents were acquired in septum-sealed bottles stored under an inert atmosphere. All reactions were magnetically stirred under a positive pressure of Argon (Ar) unless otherwise stated. Reactions and chromatography fractions were monitored by qualitative thin-layer chromatography (TLC) on silica gel F254 TLC plates from Merck KGaA, visualized by UV illumination or developed with ninhydrin, ceric ammonium molybdate or KMnO_4 stains. Flash column chromatography was performed using silica gel (40-63 μm) from Merck KGaA. Size exclusion chromatography was performed using Sephadex® G-10 (40-120 μm), Sephadex® G-15 (40-120 μm) or Sephadex® LH-20 (18-111 μm) from Merck KGaA. Chemicals for the synthesis of IVT mRNA were acquired as follows: Anti-reverse cap analogue (ARCA), pseudouridine 5'-triphosphate (ΨUTP), EUTP, EATP, AzddATP and all unmodified nucleotides were provided by baseclick GmbH. T7 RNA polymerase, yeast poly(A) polymerase and DNase I were obtained from Thermo Fischer Scientific. E. coli poly(A) polymerase and BspQI were purchased from NEB. RNase free water (Ultra pure distilled water, DNase & RNase free) was purchased from Invitrogen. Qiaquick PCR purification and plasmid plus midi purification kits were ordered from Qiagen.

Nuclear Magnetic Resonance (NMR). NMR spectra were recorded on a *Bruker Avance III HD 400* (400 MHz), *Varian NMR-System 600* (600 MHz) and *Bruker Avance III HD with Cryo-Kopf 800* (800 MHz) spectrometers. ^1H chemical shifts were internally calibrated to the residual protons of the deuterated solvent: CHCl_3 (7.26 ppm), DMSO-d_5 (2.50 ppm), CD_2HOD (3.31 ppm) and HDO (4.79 ppm). ^{13}C NMR shifts were internally calibrated to the solvent signals: CDCl_3 (77.16 ppm), DMSO-d_6 (39.52 ppm), CD_3OD (49.00 ppm). Data for ^1H NMR spectra are reported as follows: chemical shift (δ ppm), multiplicity (s = singlet, d = doublet, t = triplet, q = quartet, p = pentuplet, dd = doublet of doublets, ddd = doublet of doublets of doublets, m = multiplet, br = broad), coupling constant (Hz), integration. Data for

proton-decoupled ^{13}C spectra are reported by chemical shift (δ ppm). All NMR spectra were analyzed using the software MestreNova 14.1.1 from Mestrelab Research S. L.

Infrared (IR) Spectroscopy. IR spectra were recorded on a PerkinElmer Spectrum BX II FT-IR system. All substances were directly applied as solids or on the ATR unit.

Mass Spectrometry (MS). High resolution mass spectra (ESI-MS) were recorded by the analytical section of the Department of Chemistry of the Ludwigs-Maximilians-Universität München on a spectrometer MAT 90 (ESI) from Thermo Finnigan GmbH. Matrix-assisted laser desorption/ionization-time-of-flight (MALDI-TOF) mass spectra were recorded on a Bruker Autoflex II. The instrument was calibrated using SpheriCal™ calibrants. Samples were prepared by mixing 5 μL of 1 mg/mL analyte solution in EtOAc or MeOH, 5 μL of a 1 mg/mL counterion solution of sodium trifluoroacetate (NaTFA) in tetrahydrofuran (THF) and 20 μL of a 10 mg/mL matrix solution. *trans*-2-[3-(4-*tert*-butylphenyl)-2-methyl-2-propenylidene]-malononitrile (DCTB) and 2,5-dihydroxybenzoic acid (DHB) in THF were used as matrices for non-polar and polar compounds, respectively. 1 μL of the final mixture was applied to a stainless-steel sample plate using the dried droplet method. The obtained spectra were analyzed with FlexAnalysis version 2.2 from Bruker Daltonics.

Analytical and preparative HPLC. Analytical RP-HPLC was performed on a Waters Alliance (e2695 Separation Module, 2998 Photodiode Array Detector) instrument equipped with an XBridge™ OST C18 column (2.5 μm , 4.6 mm x 50 mm) using a flow of 1.5 mL/min at 40° column temperature. A linear gradient of buffer B 0-30% v/v from 0 \rightarrow 4 min and then 30-85% v/v from 4 \rightarrow 10 min was applied. Buffer A: 0.1 M triethylammonium acetate in H_2O . Buffer B: 0.1 M triethylammonium acetate in MeCN/ H_2O 8:2 v/v. Preparative RP-HPLC was performed on a Waters Breeze (2487 Dual λ Array Detector, 1525 Binary HPLC Pump) instrument equipped with the column VP 250/32 C18 from Macherey Nagel using a flow of 5 mL/min at room temperature. Compounds were detected at the wavelength of maximum absorption (λ_{max}) of the corresponding molecule. The employed gradients for the subsequent purifications are specified in the Synthetic Procedures section.

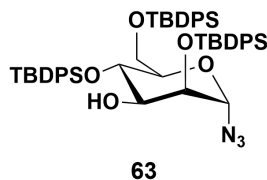
Fluorescent Conjugates Uptake Assays. THP-1 monocytic leukaemia cells were maintained in DMEM/F12 (Sigma) supplemented with 10% FBS (Life Technologies) and differentiated into immature DCs as previously described^[176] with minor modifications. Briefly, THP-1 cells were cultured in the same medium as above additionally supplemented with recombinant human IL-4 and GM-CSF (both from PeproTech) at 3000 and 1500 IU/ml, respectively, for

5-6 days before assaying ligand uptake. For the latter, cultures were supplemented with either 500 kDa FITC-Dextran (1 mg/ml; Sigma), Fluorescein-conjugated branched sugar constructs or fluorescein azide (baseclick GmbH; 80 μ M) and DAPI (1:15 dilution of NucBlue Fixed Cell ReadyProbes Reagent, Life Technologies) in culture medium and incubated for 1 h at 37°C in 5% CO₂. After washing twice with culture medium, cells were resuspended in Hank's balanced salt solution without Ca²⁺, Mg²⁺ and phenol-red (Sigma) and imaged with an EVOS FL II microscope equipped with a 40x achromat objective (Life Technologies). Images were processed with ImageJ v.1.4.3.67.

Agarose gel electrophoresis: 1.5 % agarose gels (10 x 15 cm) were prepared in 0.5 x TAE buffer (10 mM TRIS, 5 mM acetic acid, 0.25 mM EDTA, pH 8.5). 1.12 g agarose (CARL ROTH GmbH, Roti®agarose) was dissolved in 75 g 0.5x TAE buffer in a 250 mL Erlenmeyer flask by alternating microwave heating and manual mixing. Loss of water during heating was controlled by weighing and replaced, if necessary, with dH₂O. The warm mixture was poured into a planned gel cast equipped with either a 15 or 20 sample comb. Samples were prepared with 20 % purple loading dye (NEB), 1 kb Plus DNA Ladder (NEB N3200S) and ssRNA Ladder (NEB N0362S). Gels were run in 0.5x TAE buffer applying constant power (10 W, max. 500 V, max. 100 mA) for 60 min. Then, gels were incubated in a freshly prepared 1:10000 ethidium bromide dilution for 15 min and then destained in dH₂O for 15 min. For visualization a Gel Doc EZ Imager (BIO RAD) was used.

6.2 Chemical Synthesis

6.2.1 Synthesis of TBDPS-Protected Mannose Derivative (63)



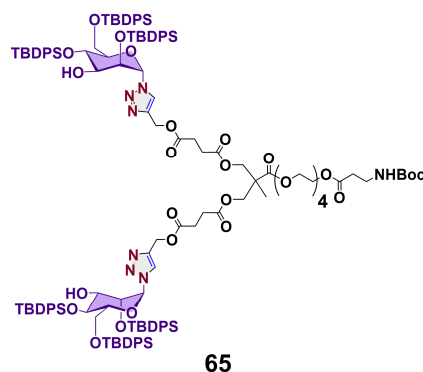
Chemical Formula: $C_{54}H_{65}N_3O_5Si_3$
Molecular Weight: 920.39

Compound 63. A magnetically stirred solution containing 2,3,4,6-tetra-O-acetyl- α -D-mannopyranosyl azide (**60**) (1.00 g, 2.68 mmol, 1 eq) in MeOH (25 mL) was treated with NaOMe (25 wt% in MeOH, 110 μ L, 0.480 mmol). The reaction mixture was stirred at room temperature for 3 h, neutralized with Amberlite® CG50 (Type I) hydrogen form ion-exchange resin, filtered and concentrated *in vacuo*. The crude product was dissolved in anhydrous DMF (7 mL) followed by addition of imidazole (3.28 g, 48.2 mmol, 18 eq) and tert-butyl(chloro)diphenylsilane (TBDPSCl) (6.3 mL, 24 mmol, 9 eq) and the resulting mixture was stirred at room temperature overnight. After addition of water (50 mL) to the crude product, the mixture was extracted with ether (3 x 50 mL). The combined organic extracts were dried over $MgSO_4$, filtered, and concentrated *in vacuo*. Purification by silica gel flash chromatography (isohexane/diethyl ether, 9:1) afforded compound **63** (2.05 g, 2.23 mmol, 83%) as a white solid.

R_f (SiO₂; ¹Hex/Et₂O, 9:1): 0.6. **¹H NMR** (800 MHz, CDCl₃) δ 7.79 – 7.71 (m, 6H, Ar), 7.70 – 7.66 (m, 2H, Ar), 7.64 – 7.61 (m, 2H, Ar), 7.55 – 7.50 (m, 2H, Ar), 7.46 – 7.27 (m, 18H, Ar), 4.98 (d, $J = 1.9$ Hz, 1H, **H-1**), 4.12 (d, $J = 8.9$ Hz, 1H, **H-6**), 4.04 (t, $J = 9.0$ Hz, 1H, **H-4**), 3.94 – 3.91 (m, 2H, **H-6'** and **H-5**), 3.69 (ddd, $J = 10.1, 8.8, 3.3$ Hz, 1H, **H-3**), 3.66 (dd, $J = 3.4, 1.9$ Hz, 1H, **H-2**), 1.42 (d, $J = 10.2$ Hz, 1H, **OH**), 1.08 (s, 9H, C(CH₃)₃), 0.92 (s, 9H, C(CH₃)₃), 0.82 (s, 9H, C(CH₃)₃). **¹³C NMR** (201 MHz, CDCl₃) δ 136.1, 136.0 ($\times 2$), 135.9, 135.8, 135.6, 134.3, 133.8 ($\times 2$), 133.5 ($\times 2$), 131.6, 130.3, 130.1, 129.8, 129.7, 129.6, 128.1, 127.9 ($\times 2$), 127.8 ($\times 2$), 127.7 ($\times 2$) (24 \times Ar), 89.2 (**C-1**), 76.3 (**C-5**), 72.8 (**C-2**), 71.8 (**C-3**), 70.2 (**C-4**), 63.5 (**C-6**), 27.1, 27.0, 26.9 (3 \times (CH₃)₃C), 19.9, 19.4 ($\times 2$) (3 \times (CH₃)₃C). **IR** (ATR): $\tilde{\nu}$ (cm⁻¹) = 3570 (w), 3071 (w), 3042 (w), 2928 (m), 2855 (m), 2109 (s), 1589 (m), 1471 (m), 1462 (m), 1426 (s), 1391 (m), 1361 (m), 1239 (m), 1104 (vs), 998 (m), 935 (s), 873 (s), 821 (s), 787 (w), 757

(w), 737 (s), 699 (vs). **HRMS** (ESI): m/z calcd for $C_{54}H_{67}N_3O_6Si_3^+$ $[M+H_2O]^+$: 937.4338, found: 937.4562. m/z calcd for $C_{54}H_{64}N_3O_5Si_3$ $[M-H]^-$: 918.4159, found: 918.4164.

6.2.2 Synthesis of Diantennary-Mannose Targeting Ligand (68)



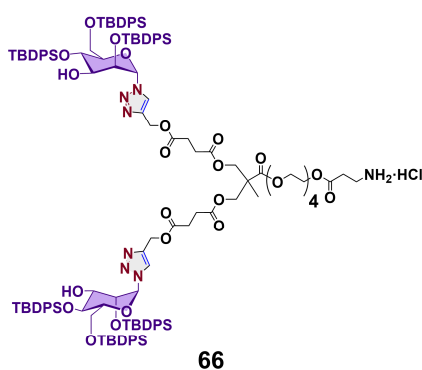
Chemical Formula: $C_{143}H_{181}N_7O_{27}Si_6$

Molecular Weight: 2598.55

Compound 65. A Schlenk tube was charged with bis-MPA Acetylene Dendron, Generation 1 (**64**) (150 mg, 0.198 mmol, 1 eq), silylated mannose azide **63** (547 mg, 0.594 mmol, 3 eq), anhydrous DMF (2 mL) and *N,N,N',N'',N'''*-pentamethyldiethylenetriamine (PMDTA) (165 μ L, 0.792 mmol, 4 eq). After three cycles of freeze-pump-thaw, CuBr (114 mg, 0.792 mmol, 4 eq) was added and the mixture was stirred overnight under a positive pressure of Ar at 45°C. Water (20 mL) was added to the reaction mixture and the crude product was extracted with EtOAc (3 x 20 mL). The combined organic extracts were dried over $MgSO_4$, filtered, and concentrated *in vacuo*. The crude product was dissolved in DMF (1.5 mL) and purified by size exclusion chromatography (Sephadex G-15, DMF). After solvent removal, the crude was further washed with isohexane to afford compound **65** (358 mg, 0.138 mmol, 70%) as a white solid.

R_f (19:1 $CH_2Cl_2/MeOH$) = 0.6. 1H NMR (800 MHz, $CDCl_3$) δ 7.84 – 7.20 (m, 58H), 7.18 (t, J = 7.6 Hz, 2H), 7.03 (t, J = 7.5 Hz, 2H), 5.97 (dd, J = 9.2, 2.0 Hz, 1H), 5.66 (d, J = 4.3 Hz, 1H), 5.27 (d, J = 3.7 Hz, 2H), 5.13 (d, J = 2.3 Hz, 2H), 5.12 – 5.10 (m, 1H), 4.75 (t, J = 3.8 Hz, 1H), 4.45 – 4.39 (m, 1H), 4.39 – 4.36 (m, 1H), 4.29 – 4.19 (m, 8H), 4.15 – 3.98 (m, 3H), 3.94 – 3.77 (m, 3H), 3.72 – 3.58 (m, 14H), 3.41 – 3.36 (m, 2H), 3.08 (dd, J = 11.8, 3.5 Hz, 1H), 2.68 – 2.57 (m, 8H), 2.54 (t, J = 6.2 Hz, 2H), 1.90 (d, J = 7.2 Hz, 1H), 1.43 (s, 9H), 1.24 (s, 3H), 0.99 (s, 9H), 0.96 (s, 9H), 0.92 (s, 18H), 0.87 (s, 9H), 0.82 (s, 9H). ^{13}C NMR (201 MHz, $CDCl_3$) δ 172.7, 172.5, 172.0 ($\times 2$), 171.7 ($\times 2$), 155.9, 142.8, 142.6, 136.2 ($\times 2$), 136.0, 135.9, 135.8 ($\times 2$), 135.7 ($\times 4$), 135.6 ($\times 2$), 133.4 ($\times 2$), 133.3 ($\times 2$), 133.2, 133.1, 132.9, 132.7 ($\times 2$), 132.1 ($\times 2$),

132.0, 130.4, 130.2 ($\times 2$), 130.1 ($\times 2$), 130.0, 129.9, 129.8 ($\times 2$), 129.7, 128.1, 128.0, 127.9, 127.8 ($\times 3$), 122.9, 122.6, 85.1, 82.7 ($\times 2$), 82.4, 79.4, 78.4, 73.5, 72.3, 71.2, 70.7 ($\times 2$), 70.6, 70.2, 69.1, 69.0, 68.8, 68.7, 65.6, 64.3, 63.8, 62.9, 61.3 ($\times 2$), 58.0, 57.8, 46.4, 36.2, 34.8, 29.0, 28.9, 28.5, 27.1 ($\times 2$), 27.0, 26.9 ($\times 2$), 26.8, 19.6 ($\times 2$), 19.3 ($\times 3$), 19.2, 19.1, 18.9, 17.9. **IR** (ATR): $\tilde{\nu}$ (cm^{-1}) = 2930 (m), 2855 (m), 2112 (w), 1737 (s), 1589 (w), 1471 (m), 1426 (s), 1390 (m), 1362 (m), 1245 (m), 1144 (s), 1111 (vs), 998 (m), 939 (m), 872 (w), 822 (s), 740 (s), 700 (vs). **MS (MALDI-ToF)**: m/z calcd for $\text{C}_{143}\text{H}_{181}\text{N}_7\text{NaO}_{27}\text{Si}_6^+$ $[\text{M}+\text{Na}]^+$: 2619.1513 (monoisotopic mass), 2621.5428 (molecular weight), found: 2619.5.

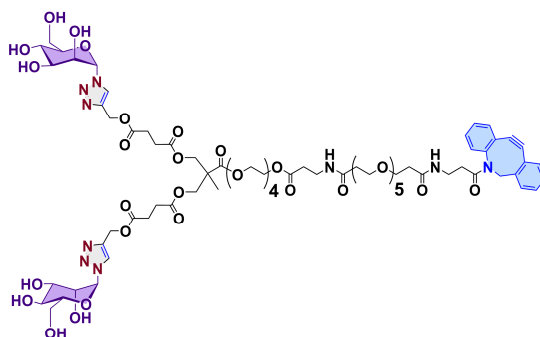


Chemical Formula: $\text{C}_{138}\text{H}_{174}\text{ClN}_7\text{O}_{27}\text{Si}_6$
Molecular Weight: 2534.89

Compound 66. Compound **65** (274 mg, 0.105 mmol, 1 eq) was suspended in 3 mL HCl, 1 M solution in EtOAc and the resulting mixture was maintained at room temperature for 2 h with vigorous stirring. The solvent was removed *in vacuo* to afford compound **66** (253 mg, 0.0998 mmol, 95%) as a white solid.

$R_f = 0.3$ (19:1 $\text{CH}_2\text{Cl}_2/\text{MeOH}$). **^1H NMR** (800 MHz, CDCl_3) δ 7.80 – 7.12 (m, 60H), 7.02 (t, $J = 7.4$ Hz, 2H), 5.98 (d, $J = 9.1$ Hz, 1H), 5.67 (d, $J = 4.2$ Hz, 1H), 5.27 (s, 2H), 5.13 (s, 2H), 4.80 – 4.71 (m, 1H), 4.52 – 4.40 (m, 1H), 4.40 – 4.37 (m, 1H), 4.35 – 4.19 (m, 8H), 4.15 – 3.97 (m, 3H), 3.94 – 3.79 (m, 3H), 3.79 – 3.56 (m, 14H), 3.35 – 3.32 (m, 2H), 3.09 – 3.02 (m, 1H), 2.63 (m, 10H), 1.26 (s, 3H), 0.99 (s, 9H), 0.96 (s, 9H), 0.92 (s, 9H), 0.91 (s, 9H), 0.86 (s, 9H), 0.82 (s, 9H). **^{13}C NMR** (201 MHz, CDCl_3) δ 172.9, 172.1, 172.0, 171.8, 136.2, 136.0 ($\times 2$), 135.9, 135.8, 135.7, 135.6 ($\times 2$), 135.3, 134.9, 134.1, 133.6, 133.4, 133.3, 133.2, 133.1, 132.8, 132.7, 132.6, 132.1, 132.0, 130.4, 130.3, 130.1 ($\times 3$), 130.0, 129.9 ($\times 2$), 129.8 ($\times 3$), 129.7 ($\times 2$), 129.6, 128.1, 128.0, 127.9, 127.8 ($\times 2$), 127.7, 123.0, 85.1, 82.9, 82.4, 78.5, 73.6, 72.3, 71.1, 70.6, 70.2, 68.7, 65.8, 65.7, 63.8, 62.9, 61.3, 58.1, 58.0, 46.5, 32.1, 29.1, 29.0, 27.1, 27.0, 26.9 ($\times 2$), 26.8 ($\times 2$), 26.6, 19.6, 19.3 ($\times 2$), 19.1 ($\times 2$), 18.0. **IR** (ATR): $\tilde{\nu}$ (cm^{-1}) = 3073 (w), 3044

$C_{170}H_{211}N_9NaO_{33}Si_6^+$ $[M+Na]^+$: 3097.3617 (monoisotopic mass), 3100.0878 (molecular weight), found: 3096.8. m/z calcd for $C_{170}H_{215}N_9NaO_{35}Si_6^+$ $[M+2H_2O+Na]^+$: 3133.3828 (monoisotopic mass), 3136.1178 (molecular weight), found: 3133.3.



68

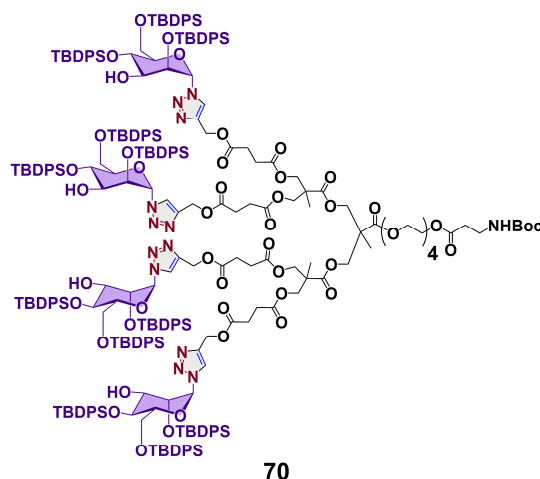
Chemical Formula: $C_{74}H_{103}N_9O_{33}$
Molecular Weight: 1646.67

Compound 68. A plastic container was charged with triethylamine trihydrofluoride (32 μ L, 0.20 mmol), anhydrous THF (200 μ L) and triethylamine (59 μ L, 0.42 mmol). The mixture was added to a Falcon tube containing compound **67** (20 mg, 6.5 μ mol, 1 eq). The resulting reaction mixture was magnetically stirred at 55 $^{\circ}$ C for 24 h. After this time, the reaction crude was quenched by dropwise addition of methoxytrimethylsilane (160 μ L) and stirred at room temperature for 1 h. The crude was concentrated *in vacuo*, DMF (2 mL) was added, and the dissolved fraction was purified by size exclusion chromatography (Sephadex G-10, DMF) to afford dianntenary-mannose targeting ligand **68** (10 mg, 6.1 μ mol, 93%) as a pale, brown solid.

R_t = 6.74 (Analytical RP-HPLC; 1.5 mL/min, 40 $^{\circ}$, buffer B 0-30% v/v 0 \rightarrow 4 min, then 30-85% v/v 4 \rightarrow 10 min). 1H NMR (800 MHz, CD_3OD) δ 8.20 (s, 2H), 7.67 (d, J = 7.5 Hz, 1H), 7.52 – 7.48 (m, 1H), 7.48 – 7.44 (m, 3H), 7.40 – 7.36 (m, 1H), 7.36 – 7.32 (m, 1H), 7.27 (dd, J = 7.5, 1.4 Hz, 1H), 6.03 (d, J = 2.8 Hz, 2H), 5.27 – 5.20 (m, 4H), 5.15 (d, J = 14.2 Hz, 1H), 4.67 (t, J = 3.1 Hz, 2H), 4.27 – 4.19 (m, 8H), 4.07 (dd, J = 8.4, 3.5 Hz, 2H), 3.84 – 3.47 (m, 39H), 3.44 (t, J = 6.7 Hz, 2H), 3.33 (overlapped by solvent, 1H), 3.26 (overlapped by solvent, 2H), 3.18 – 3.12 (m, 1H), 2.64 (s, 8H), 2.55 (t, J = 6.7 Hz, 2H), 2.52 (dt, J = 16.0, 6.5 Hz, 1H), 2.42 (t, J = 6.2 Hz, 2H), 2.31 – 2.26 (m, 2H), 2.06 (dt, J = 16.0, 6.5 Hz, 1H), 1.23 (s, 3H). ^{13}C NMR (201 MHz, CD_3OD) δ 174.2, 174.1, 173.9, 173.6, 173.4, 173.3, 173.2, 152.6, 149.5, 144.3, 133.5, 130.6, 130.0, 129.7, 129.3, 129.0, 128.2, 126.6, 125.9, 124.4, 123.7, 115.6, 108.9, 88.4, 78.7, 72.6, 71.6, 71.6 – 71.5 (multiple peaks), 71.4 (\times 3), 71.3, 70.1 (\times 2), 69.9, 68.6, 68.2, 68.1, 66.7, 65.5, 64.8, 62.5, 58.5, 56.6, 47.6, 37.6, 37.5, 36.7, 36.5, 36.3, 35.5, 34.9, 29.8 (\times 2),

18.2. **IR** (ATR): $\tilde{\nu}$ (cm⁻¹) = 3343 (br), 2925 (s), 2876 (s), 1735 (vs), 1656 (s), 1555 (m), 1454 (m), 1400 (s), 1357 (m), 1248 (s), 1150 (vs), 1113 (vs), 1044 (s), 827 (w), 706 (m). **MS** (**MALDI-ToF**): m/z calcd for C₇₄H₁₀₃N₉NaO₃₃⁺ [M+Na]⁺: 1668.6556 (monoisotopic mass), 1669.6578 (molecular weight), found: 1668.9.

6.2.3 Synthesis of Tetraantennary-Mannose Targeting Ligand (**73**)

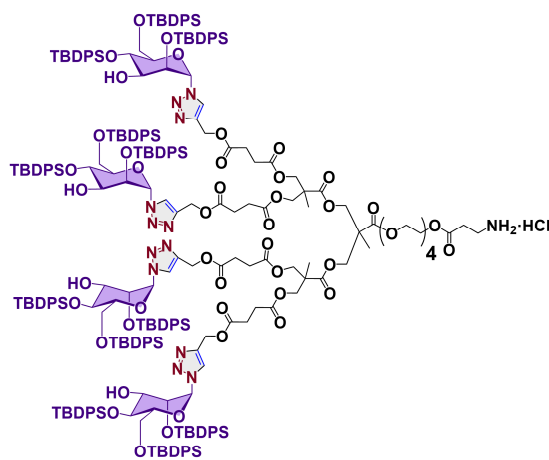


Chemical Formula: C₂₇₅H₃₃₉N₁₃O₄₉Si₁₂
Molecular Weight: 4947.80

Compound 70. A Schlenk tube was charged with bis-MPA Acetylene Dendron, Generation 2 (**69**) (130 mg, 0.115 mmol, 1 eq), silylated mannose azide **63** (633 mg, 0.688 mmol, 6 eq), anhydrous DMF (2.5 mL) and *N,N,N',N'',N'''*-pentamethyldiethylenetriamine (PMDTA) (192 μ L, 0.919 mmol, 8 eq). After three cycles of freeze-pump-thaw, CuBr (132 mg, 0.920 mmol, 8 eq) was added and the mixture was stirred overnight under a positive pressure of Ar at 45°C. Water (20 mL) was added to the reaction mixture and the crude was extracted with EtOAc (3 x 20 mL). The combined organic extracts were dried over MgSO₄, filtered, and concentrated *in vacuo*. The crude product was dissolved in 1.5 mL DMF and purified by size exclusion chromatography (Sephadex LH-20, DMF) to afford compound **70** (383 mg, 79.5 μ mol, 69%) as an off-white solid.

R_f (CH₂Cl₂/MeOH, 19:1): 0.2. **¹H NMR** (800 MHz, CDCl₃) δ 7.82 (d, J = 2.4 Hz, 2H), 7.63 (d, J = 7.4 Hz, 4H), 7.61 – 7.57 (m, 8H), 7.57 – 7.55 (m, 8H), 7.52 – 7.46 (m, 8H), 7.46 – 7.19 (m, 86H), 7.17 (t, J = 7.6 Hz, 4H), 7.02 (t, J = 7.5 Hz, 4H), 5.96 (d, J = 9.1 Hz, 2H), 5.65 (d, J = 4.2 Hz, 2H), 5.25 (d, J = 5.1 Hz, 4H), 5.12 (t, J = 1.9 Hz, 4H), 5.10 (br, 1H), 4.74 (t, J = 3.8 Hz, 2H), 4.45 – 4.40 (m, 2H), 4.40 – 4.35 (m, 2H), 4.30 – 4.18 (m, 16H), 4.11 – 4.06 (m, 2H),

4.06 – 4.01 (m, 4H), 3.90 – 3.83 (m, 4H), 3.83 – 3.79 (m, 2H), 3.71 – 3.58 (m, 16H), 3.40 – 3.35 (m, 2H), 3.07 (dd, $J = 11.9, 3.4$ Hz, 2H), 2.68 – 2.62 (m, 8H), 2.63 – 2.57 (m, 8H), 2.53 (t, $J = 6.0$ Hz, 2H), 1.90 (d, $J = 7.3$ Hz, 2H), 1.42 (s, 9H), 1.26 (s, 3H), 1.22 (s, 6H), 0.99 (s, 18H), 0.95 (s, 18H), 0.91 (s, 36H), 0.86 (s, 18H), 0.81 (d, $J = 1.9$ Hz, 18H). ^{13}C NMR (201 MHz, CDCl_3) δ 172.5, 172.2, 172.1 ($\times 2$), 172.0 ($\times 2$), 171.8, 155.9, 142.8, 142.6, 136.2, 136.0, 135.9, 135.8 ($\times 3$), 135.7 ($\times 3$), 133.6 ($\times 2$), 133.4 ($\times 2$), 133.3 ($\times 2$), 133.2, 133.1, 132.9, 132.8, 132.7, 132.1 ($\times 2$), 132.0, 130.4, 130.2 ($\times 2$), 130.1 ($\times 3$), 130.0, 129.9 ($\times 2$), 129.8 ($\times 2$), 129.7, 128.1, 128.0, 127.9 ($\times 2$), 127.8 ($\times 3$), 122.9, 122.6, 85.1, 82.7 ($\times 2$), 82.4, 79.4, 78.4, 73.6, 73.5, 72.3, 71.2, 70.7, 70.6 ($\times 2$), 70.2, 69.1, 68.9, 68.7 ($\times 2$), 65.9, 65.5, 64.5, 63.8, 62.9, 61.3, 58.0, 57.8, 46.8, 46.5, 36.2, 34.8, 29.0, 28.9 ($\times 3$), 28.8 ($\times 2$), 28.6, 27.1 ($\times 2$), 27.0, 26.9 ($\times 2$), 26.8, 19.6, 19.3 ($\times 3$), 19.2, 19.1, 17.9 ($\times 2$), 17.7. IR (ATR): $\tilde{\nu}$ (cm^{-1}) = 2954 (w), 2928 (w), 2889 (w), 2853 (w), 1736 (s), 1589 (w), 1472 (w), 1426 (m), 1391 (w), 1361 (w), 1241 (w), 1104 (s), 997 (m), 937 (m), 821 (s), 739 (s), 700 (vs). MS (MALDI-ToF): m/z calcd for $\text{C}_{275}\text{H}_{339}\text{N}_{13}\text{NaO}_{49}\text{Si}_{12}^+$ $[\text{M}+\text{Na}]^+$: 4966.1564 (monoisotopic mass), 4970.7888 (molecular weight), found: 4966.0.



71

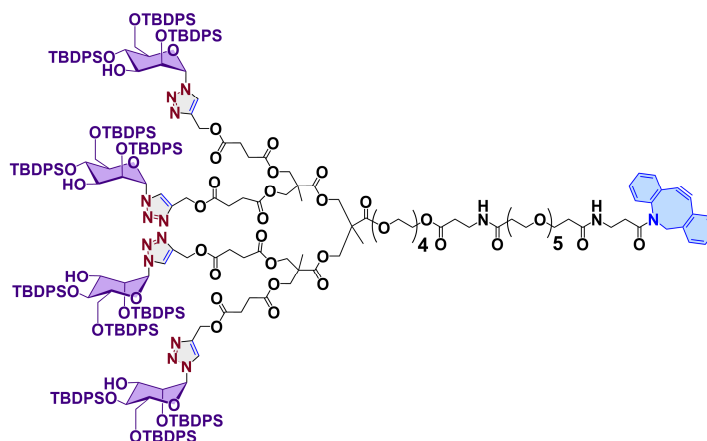
Chemical Formula: $\text{C}_{270}\text{H}_{332}\text{ClN}_{13}\text{O}_{47}\text{Si}_{12}$

Molecular Weight: 4884.14

Compound 71. Compound **70** (100 mg, 20.2 μmol , 1 eq) was suspended in 1.5 mL HCl, 1 M solution in EtOAc and the resulting mixture was maintained at room temperature for 2 h with vigorous stirring. The solvent was removed *in vacuo* to afford compound **71** (97 mg, 20 μmol , 98%) as a white solid.

R_f ($\text{CH}_2\text{Cl}_2/\text{MeOH}$, 9:1): 0.5. ^1H NMR (800 MHz, CDCl_3) δ 7.89 – 7.14 (m, 120H), 7.01 (t, $J = 7.4$ Hz, 4H), 5.97 (d, $J = 7.4$ Hz, 2H), 5.66 (d, $J = 3.8$ Hz, 2H), 5.28 – 5.24 (m, 4H), 5.18 –

5.05 (m, 4H), 4.74 (d, $J = 4.2$ Hz, 2H), 4.47 – 4.16 (m, 20H), 4.12 – 4.06 (m, 2H), 4.02 (m, 4H), 3.90 – 3.78 (m, 6H), 3.76 – 3.54 (m, 16H), 3.45 – 3.23 (m, 2H), 3.12 – 2.97 (m, 2H), 2.78 – 2.50 (m, 18H), 1.91 (br, 2H), 1.26 (s, 3H), 1.22 (s, 6H), 0.99 (s, 18H), 0.96 (s, 18H), 0.91 (s, 18H), 0.90 (s, 18H), 0.87 (s, 18H), 0.81 (s, 18H). ^{13}C NMR (201 MHz, CDCl_3) δ 172.5, 172.1, 172.0, 171.8, 142.7, 142.6, 136.3, 136.0, 135.9, 135.8, 135.8, 135.7, 135.7, 135.6, 135.3, 134.9, 133.6, 133.4, 133.4, 133.3, 133.2, 132.9, 132.8, 132.6, 132.2, 132.0, 130.4 ($\times 2$), 130.3, 130.2, 130.1 ($\times 2$), 130.0, 129.9, 129.8 ($\times 3$), 128.1 ($\times 2$), 128.0 ($\times 2$), 127.9 ($\times 2$), 127.8 ($\times 2$), 123.0, 122.9, 85.1, 83.0, 82.4 ($\times 2$), 78.4, 73.6, 72.3, 71.2, 70.7, 70.6, 70.2, 68.6, 65.6, 65.4, 62.9, 61.4, 58.0, 57.9, 46.8, 46.6, 38.9, 37.2, 32.1, 29.1, 28.9, 28.8 ($\times 2$), 27.1, 27.0 ($\times 2$), 26.9, 26.8, 26.6, 19.6, 19.3 ($\times 2$), 19.2, 19.1, 18.0, 17.9. IR (ATR): $\tilde{\nu}$ (cm^{-1}) = 3072 (w), 3048 (w), 2958 (m), 2929 (m), 2895 (m), 2857 (m), 1738 (s), 1590 (w), 1472 (m), 1462 (m), 1428 (m), 1391 (w), 1362 (w), 1261 (m), 1104 (vs), 939 (m), 873 (w), 821 (s), 802 (s), 739 (s), 700 (vs). MS (MALDI-ToF): m/z calcd for $\text{C}_{270}\text{H}_{331}\text{N}_{13}\text{NaO}_{47}\text{Si}_{12}^+$ $[\text{M}-\text{HCl}+\text{Na}]^+$: 4866.1039 (monoisotopic mass), 4870.6718 (molecular weight), found: 4865.6.



72

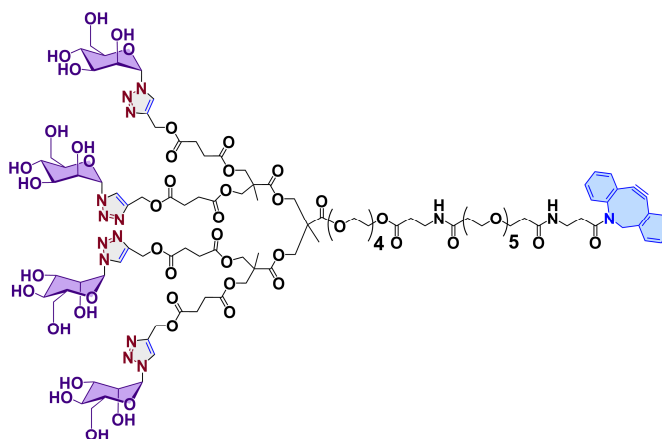
Chemical Formula: $\text{C}_{302}\text{H}_{369}\text{N}_{15}\text{O}_{55}\text{Si}_{12}$

Molecular Weight: 5426.24

Compound 72. A magnetically stirred solution containing compound **71** (63 mg, 13 μmol , 1 eq) in 0.25 mL DMF was treated with DBCO-PEG5-NHS (18 mg, 26 μmol , 2 eq) and triethylamine (5.4 μL , 39 μmol , 3 eq), and the resulting mixture was maintained at room temperature for 2h. After this time, the solvent was removed *in vacuo*, the reaction crude redissolved in the minimum amount of DMF and purified by size exclusion chromatography (Sephadex LH-20, DMF) to afford compound **72** (65 mg, 12 μmol , 93%) as a pale, brown solid.

R_f ($\text{CH}_2\text{Cl}_2/\text{MeOH}$, 19:1): 0.2. ^1H NMR (800 MHz, CDCl_3) δ 7.84 – 7.79 (m, 2H), 7.75 – 7.12 (m, 126H), 7.01 (t, $J = 7.4$ Hz, 4H), 5.96 (d, $J = 8.8$ Hz, 2H), 5.65 (d, $J = 4.2$ Hz, 2H), 5.29 –

5.20 (m, 4H), 5.15 – 5.10 (m, 5H), 5.09 (br, 1H), 4.74 (t, $J = 3.7$ Hz, 2H), 4.51 – 4.40 (m, 2H), 4.41 – 4.34 (m, 2H), 4.29 – 4.16 (m, 16H), 4.14 – 4.06 (m, 2H), 4.06 – 4.00 (m, 4H), 3.89 – 3.84 (m, 4H), 3.83 – 3.79 (m, 2H), 3.75 – 3.42 (m, 41H), 3.07 (d, $J = 12.9$ Hz, 2H), 2.71 – 2.40 (m, 24H), 1.90 (d, $J = 7.1$ Hz, 2H), 1.26 (s, 3H), 1.22 (s, 6H), 0.99 (s, 18H), 0.95 (s, 18H), 0.91 (s, 36H), 0.86 (s, 18H), 0.81 (s, 18H). ^{13}C NMR (201 MHz, CDCl_3) δ 172.5, 172.2, 172.1 ($\times 2$), 172.0 ($\times 2$), 171.8, 142.8, 142.6, 136.2, 136.0, 135.9, 135.8 ($\times 3$), 135.7 ($\times 3$), 135.6, 133.6, 133.4 ($\times 2$), 133.3 ($\times 2$), 133.2, 133.1, 132.9, 132.8, 132.7, 132.1, 132.0, 130.4, 130.3, 130.2, 130.1 ($\times 2$), 130.0, 129.9, 129.8 ($\times 2$), 129.7, 128.1, 128.0, 127.9 ($\times 2$), 127.8 ($\times 3$), 127.2, 123.7, 122.9, 122.6, 121.8, 121.6, 121.1, 119.8, 109.4, 91.4, 85.1, 82.8, 82.4, 78.4, 73.6, 72.3, 71.2, 70.7 – 70.3 (multiple peaks), 70.2, 69.1, 68.9, 68.7, 67.5, 67.3, 65.9, 65.5, 64.5, 63.8, 62.9, 61.3, 58.0, 57.8, 48.6 ($\times 2$), 46.5, 37.0, 36.9, 35.1, 35.0, 34.3, 34.1, 32.1, 29.0, 28.9, 28.8 ($\times 2$), 27.1 ($\times 2$), 27.0, 26.9 ($\times 2$), 26.8, 19.6, 19.3 ($\times 3$), 19.2, 19.1, 17.9, 17.7. IR (ATR): $\tilde{\nu}$ (cm^{-1}) = 3073 (w), 3050 (w), 2954 (m), 2928 (m), 2892 (m), 2857 (m), 2350 (m), 1738 (s), 1659 (m), 1590 (w), 1471 (m), 1427 (s), 1391 (m), 1360 (m), 1240 (m), 1111 (vs), 998 (s), 938 (m), 875 (w), 822 (s), 740 (s), 701 (vs). MS (MALDI-ToF): m/z calcd for $\text{C}_{302}\text{H}_{369}\text{N}_{15}\text{NaO}_{55}\text{Si}_{12}^+$ $[\text{M}+\text{Na}]^+$: 5444.3667 (monoisotopic mass), 5449.3338 (molecular weight), found: 5447.2.



73

Chemical Formula: $\text{C}_{101}\text{H}_{153}\text{N}_{15}\text{O}_{55}$

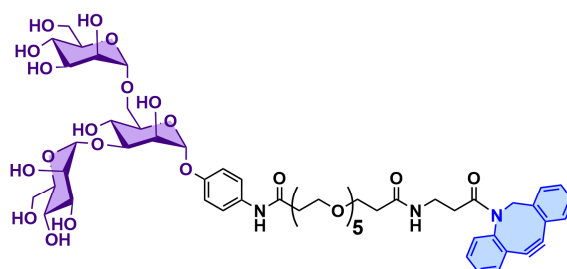
Molecular Weight: 2565.48

Compound 73. A plastic container was charged with triethylamine trihydrofluoride (54 μL , 330 μmol), anhydrous THF (1.8 mL) and triethylamine (100 μL , 717 μmol). This mixture was added to a Falcon tube containing compound 72 (30 mg, 5.5 μmol , 1 eq). The resulting reaction mixture was magnetically stirred at 55°C for 24 h. After this time, the reaction crude was quenched by dropwise addition of methoxytrimethylsilane (480 μL) and stirred at room temperature for 1 h. The crude was concentrated *in vacuo*, DMF (2 mL) was added, and the

dissolved fraction was purified by size exclusion chromatography (Sephadex G-10, DMF) to afford tetraantennary-mannose targeting ligand **73** (13 mg, 5.1 μmol , 91%) as a pale, brown solid.

R_t = 6.34 min (Analytical RP-HPLC; 1.5 mL/min, 40°, buffer B 0-30% v/v 0 \rightarrow 4 min, then 30-85% v/v 4 \rightarrow 10 min). $^1\text{H NMR}$ (800 MHz, CD_3OD) δ 8.20 (s, 4H), 7.67 (d, J = 7.6 Hz, 1H), 7.51 – 7.49 (m, 1H), 7.48 – 7.44 (m, 3H), 7.41 – 7.36 (m, 1H), 7.36 – 7.32 (m, 1H), 7.27 (dd, J = 7.5, 1.4 Hz, 1H), 6.04 (d, J = 2.8 Hz, 4H), 5.27 – 5.20 (m, 8H), 5.15 (d, J = 14.2 Hz, 1H), 4.67 (t, J = 3.1 Hz, 4H), 4.34 – 4.18 (m, 16H), 4.07 (dd, J = 8.5, 3.5 Hz, 4H), 3.87 – 3.47 (m, 45H), 3.44 (t, J = 6.7 Hz, 2H), 3.33 (overlapped by solvent, 4H), 3.28 (overlapped by solvent, 1H), 3.18 – 3.12 (m, 1H), 2.65 (s, 16H), 2.55 (t, J = 6.7 Hz, 2H), 2.52 (dt, J = 16.1, 6.5 Hz, 1H), 2.42 (t, J = 6.2 Hz, 2H), 2.31 – 2.27 (m, 2H), 2.06 (dt, J = 16.1, 6.5 Hz, 1H), 1.29 (s, 3H), 1.23 (s, 6H). $^{13}\text{C NMR}$ (201 MHz, CD_3OD) δ 174.1, 174.0, 173.9, 173.6 ($\times 2$), 173.4, 173.3, 173.2, 152.6, 149.5, 144.3, 133.5, 130.6, 130.1, 129.7, 129.3, 129.0, 128.2, 126.6, 125.9, 124.4, 123.7, 115.7, 108.9, 88.4, 78.7, 72.6, 71.6 – 71.5 (multiple peaks), 71.4 ($\times 3$), 71.3, 70.1 ($\times 2$), 69.9, 68.6, 68.2, 68.1, 66.9, 66.8, 65.7, 64.8, 62.5, 58.5, 56.6, 47.9, 47.8, 40.4, 37.6, 37.5, 36.7, 36.5, 36.3, 35.5, 34.9, 33.1, 29.9, 29.8, 18.2, 18.1. **IR** (ATR): $\tilde{\nu}$ (cm^{-1}) = 3348 (br), 2957 (s), 2922 (vs), 2870 (s), 2854 (s), 1732 (vs), 1652 (s), 1556 (m), 1458 (s), 1404 (m), 1378 (m), 1260 (m), 1073 (vs), 1044 (vs), 818 (m), 755 (w), 704 (w). **MS (MALDI-ToF)**: m/z calcd for $\text{C}_{110}\text{H}_{153}\text{N}_{15}\text{NaO}_{55}^+ [\text{M}+\text{Na}]^+$: 2586.9529 (monoisotopic mass), 2588.4491 (molecular weight), found: 2588.1.

6.2.4 Synthesis of Mannotriose Targeting Ligand (**75**)



75

Chemical Formula: $\text{C}_{56}\text{H}_{75}\text{N}_3\text{O}_{24}$

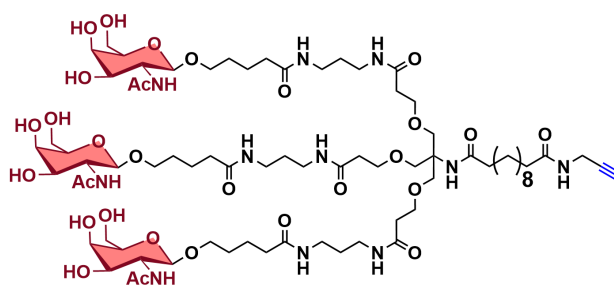
Molecular Weight: 1174.21

Compound 75. A magnetically stirred solution containing 4-aminophenyl-3,6-di-O-(α -D-mannopyranosyl)- α -D-mannopyranoside (**74**) (15 mg, 25 μmol , 1 eq) in DMF (150 μL) was treated with DBCO-PEG5-NHS (35 mg, 50 μmol , 2 eq) and triethylamine (10.5 μL , 75.6 μmol ,

3 eq) and the resulting mixture was maintained at room temperature for 1 h. Purification by RP-HPLC (30-50% v/v buffer B in 45 min, 5 mL/min, room temperature) and consequent lyophilization afforded mannotriose targeting ligand **75** (10 mg, 8.5 μmol , 34%) as a pale, yellow solid.

R_t = 9.52 min (Analytical RP-HPLC; 1.5 mL/min, 40°, buffer B 0-30% v/v 0 \rightarrow 8 min, then 30-85% v/v 8 \rightarrow 10 min). $^1\text{H NMR}$ (400 MHz, D_2O) δ 7.57 (d, J = 7.4 Hz, 1H), 7.51 – 7.25 (m, 8H), 7.26 – 7.18 (m, 1H), 7.00 (d, J = 8.2 Hz, 2H), 5.43 (d, J = 1.9 Hz, 1H), 5.11 (s, 1H), 4.94 (d, J = 14.3 Hz, 1H), 4.66 (t, J = 1.7 Hz, 1H), 4.28 – 4.12 (m, 1H), 4.09 – 4.01 (m, 2H), 3.93 – 3.42 (m, 36H), 3.14 – 3.05 (m, 1H), 3.06 – 2.97 (m, 1H), 2.59 (t, J = 5.9 Hz, 2H), 2.36 – 2.26 (m, 1H), 2.25 (t, J = 6.4 Hz, 2H), 2.11 (ddd, J = 15.2, 8.6, 6.1 Hz, 1H). $^{13}\text{C NMR}$ (151 MHz, D_2O) δ 173.6, 173.5, 172.5, 152.3, 150.5, 131.9, 131.8, 129.1, 129.0, 128.9, 128.5, 128.1, 127.1, 125.8, 123.2, 122.3, 121.5, 117.3, 114.2, 113.4, 107.8, 102.4, 98.8, 97.9, 78.1, 73.3, 72.5, 71.3, 70.5, 70.3, 70.0, 69.8, 69.6-69.4 (multiple peaks), 66.7-66.5 (multiple peaks), 65.8, 65.0 ($\times 2$), 60.9 ($\times 2$), 55.3, 36.6, 35.8, 35.7, 33.6. **IR** (ATR): $\tilde{\nu}$ (cm^{-1}) = 3303 (br), 2916 (m), 1648 (s), 1547 (s), 1508 (s), 1404 (s), 1348 (m), 1218 (s), 1065 (vs), 1022 (vs), 980 (s), 881 (w), 836 (m), 755 (m). **MS (MALDI-ToF)**: m/z calcd for $\text{C}_{56}\text{H}_{75}\text{N}_3\text{NaO}_{24}^+$ $[\text{M}+\text{Na}]^+$: 1196.4633 (monoisotopic mass), 1197.2028 (molecular weight), found: 1197.1 $[\text{M}+\text{Na}]^+$.

6.2.5 Synthesis of Triantennary-GalNAc Targeting Ligand (77)



77

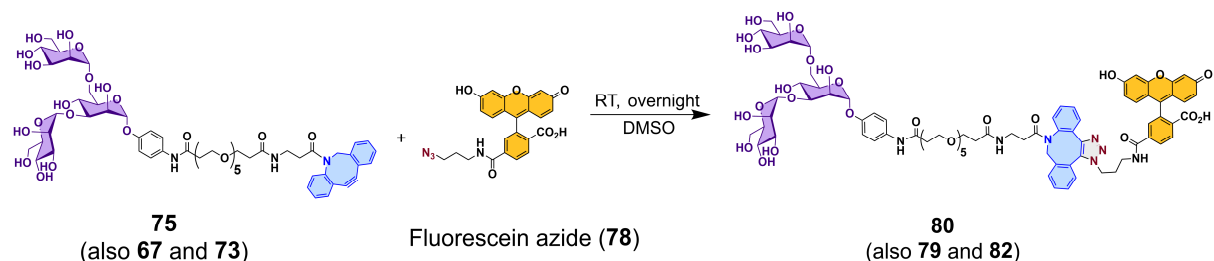
Chemical Formula: $\text{C}_{76}\text{H}_{133}\text{N}_{11}\text{O}_{29}$

Molecular Weight: 1664.95

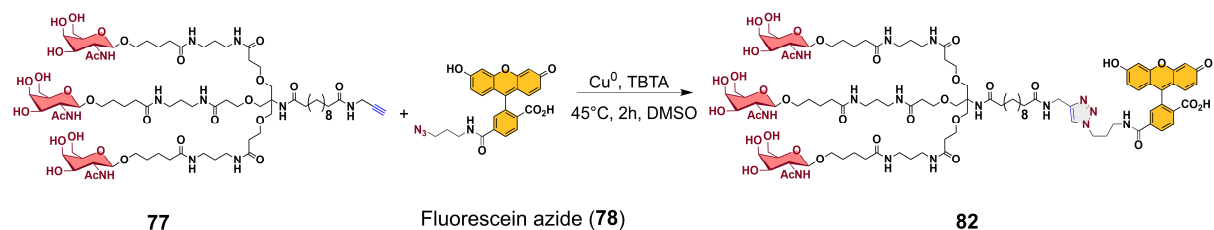
Compound 77. A magnetically stirred solution containing peracetylated Trebler GalNAc alkyne (**76**) (10 mg, 4.9 μmol , 1 eq) in 2.5 mL of $\text{NH}_3(\text{aq})/\text{EtOH}$ (3:1, v/v solution) was heated at 55 $^\circ\text{C}$ for 5 h. After this time, solvents were evaporated *in vacuo* to afford triantennary-GalNAc targeting ligand **77** (8 mg, 4.9 μmol , quantitative yield) as a white solid.

R_f(MeOH): 0.4. **¹H NMR** (800 MHz, CD₃OD) δ 4.36 (d, *J* = 8.4 Hz, 3H), 3.95 – 3.89 (m, 6H), 3.84 (dd, *J* = 3.3, 1.1 Hz, 3H), 3.79 – 3.72 (m, 6H), 3.68 – 3.66 (m, 12H), 3.59 (dd, *J* = 10.7, 3.3 Hz, 3H), 3.53 – 3.47 (m, 6H), 3.25 – 3.17 (m, 12H), 2.58 (t, *J* = 2.5 Hz, 1H), 2.43 (t, *J* = 6.1 Hz, 6H), 2.24 – 2.15 (m, 10H), 1.99 (s, 9H), 1.74 – 1.53 (m, 24H), 1.31 (br, 12H). **¹³C NMR** (201 MHz, CD₃OD) δ 176.4, 176.1, 175.9, 174.1, 174.0, 103.1, 80.8, 76.7, 73.3, 72.1, 70.1, 69.7, 68.7, 62.6, 61.4, 54.3, 37.9, 37.8, 37.7 (×2), 36.8, 36.7, 30.6, 30.5, 30.4 (×2), 30.3, 30.2, 30.0, 29.4, 27.1, 26.9, 23.9, 23.2. **IR** (ATR): $\tilde{\nu}$ (cm⁻¹) = 3287 (br), 3091 (m), 2927 (m), 2859 (m), 1634 (vs), 1547 (vs), 1434 (s), 1372 (s), 1266 (s), 1100 (vs), 1051 (vs), 981 (m), 893 (w), 730 (vs), 699 (vs). **MS (MALDI-ToF)**: *m/z* calcd for C₇₆H₁₃₃N₁₁NaO₂₉⁺ [M+Na]⁺: 1686.9163 (monoisotopic mass), 1687.9153 (molecular weight), found: 1688.1.

6.2.6 General Procedure for Click-Chemistry-Conjugation of Targeting Ligands with Fluorescein Azide



General procedure for Cu-free click ligation (SPAAC). In a 2 mL Eppendorf, 32 μL of a 1 mM solution of targeting ligand **68**, **73** and **75** (32 nmol, 1 eq) in DMSO were mixed with 3.2 μL of a 10 mM solution of fluorescein azide (32 nmol, 1 eq) in DMSO. The reaction mixture was allowed to stand overnight. After this time, the reaction crude was diluted in H_2O (1 mL) and lyophilized to obtain fluorescein conjugates **79**, **80** and **82** as a yellow solid in quantitative yields.



General procedure for Cu-catalyzed click ligation (CuAAC). In a 2 mL Eppendorf, 2 copper pellets were added together with 3.2 μL of a 10 mM solution of targeting agent **77** (32 nmol, 1 eq) in DMSO, 3.2 μL of a 10 mM solution of fluorescein azide (32 nmol, 1 eq) in DMSO, 7 μL of an 8 mM solution of tris[(1-benzyl-1*H*-1,2,3-triazol-4-yl)methyl]amine (TBTA) in DMSO and 21.6 μL DMSO. The reaction mixture was then stirred in the thermomixer at 600 rpm at 45 $^\circ\text{C}$ for 2 h. After this time, the reaction crude was diluted with DI H_2O (1 mL) and extracted with ethyl acetate (3 x 500 μL). The aqueous fraction was then lyophilized to obtain fluorescein conjugate **82** as a yellow solid in quantitative yields.

6.3 Minimum Energy Geometry Optimization of Fluorescent Conjugates

Optimized minimum energy geometry calculations (MM2 force field) were carried out for compounds **72**, **73** and **74** utilizing the software package Chem3D 21.0.0, and with the default parameters enabled. As shown in **Figure 22**, the carbohydrate moieties are distant from, and thus unincumbered by the DBCO and fluorescein substituents. The effects on CTL-carbohydrate interactions should thus be minimal.

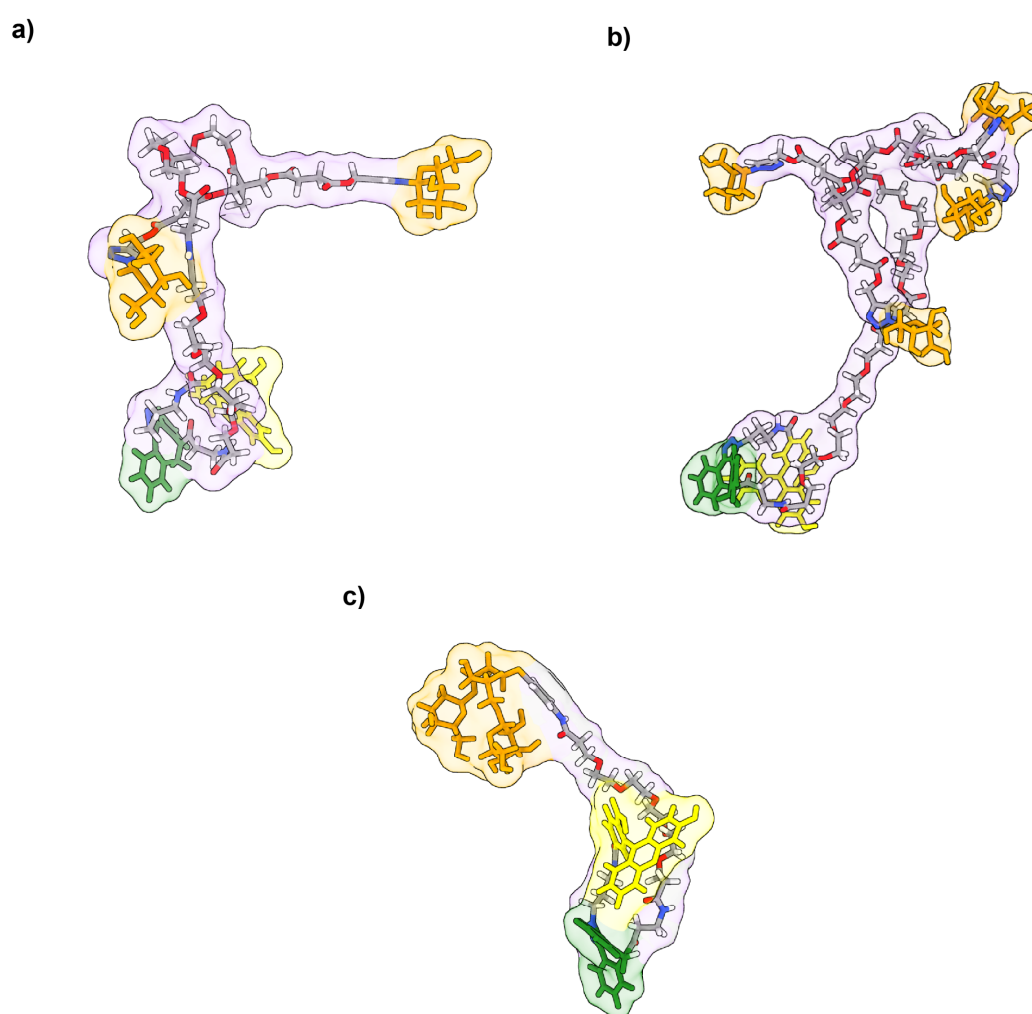


Figure 22. Optimized minimum energy geometries of fluorescein conjugates a) **72**, b) **73**, and c) **74**. Color coding: Orange: mannose; Green: DBCO group; Yellow: fluorescein. Images were obtained using the molecular visualization software UCSF ChimeraX.^[211] We have assumed that the geometries at gas and condensed phase are significantly similar.

6.4 Solution Stability Study of Fluorescent Conjugates

Chemical stability is an essential factor that determines the *in vivo* fate of a prospective therapeutic agent. To address this issue, the following solution stability study was conducted on conjugates **79-82**. Solutions at a concentration of 0.3 mM were prepared in a standard cell culture medium buffered with a carbonate system to maintain close-to-neutral pH at 5% CO₂. The pCO₂ level in cell culture incubators was set to mimic typical conditions in peripheral tissues. Following sample preparation and HPLC measurements, the samples were immediately stored at a temperature of -20 °C for 1 year. After this period, samples were measured and allowed to stand under ambient conditions for 7 days, at room temperature and shielded from light, after which they were measured again. **Figure 23** shows that all conjugates are in optimal conditions immediately after sample preparation. After 1 year at -20 °C, the polyester-based samples (**79-82**) exhibited significant signs of degradation. In contrast, mannotriose-fluorescein conjugate (**80**) and triantennary GalNAc-fluorescein conjugate (**82**) showed no decomposition, either after 1 year at -20 °C or further 7 days at room temperature. Upon handling the samples in atmospheric conditions (pCO₂ ~0.04%), the culture medium became mildly alkaline, which exposed the conjugates to such conditions. It is evident that the polyester scaffolds, being more sensitive to basic conditions, underwent decomposition through cleavage of the different ester groups. Overall, samples were stable after being freshly prepared and were used immediately for cell experiments.

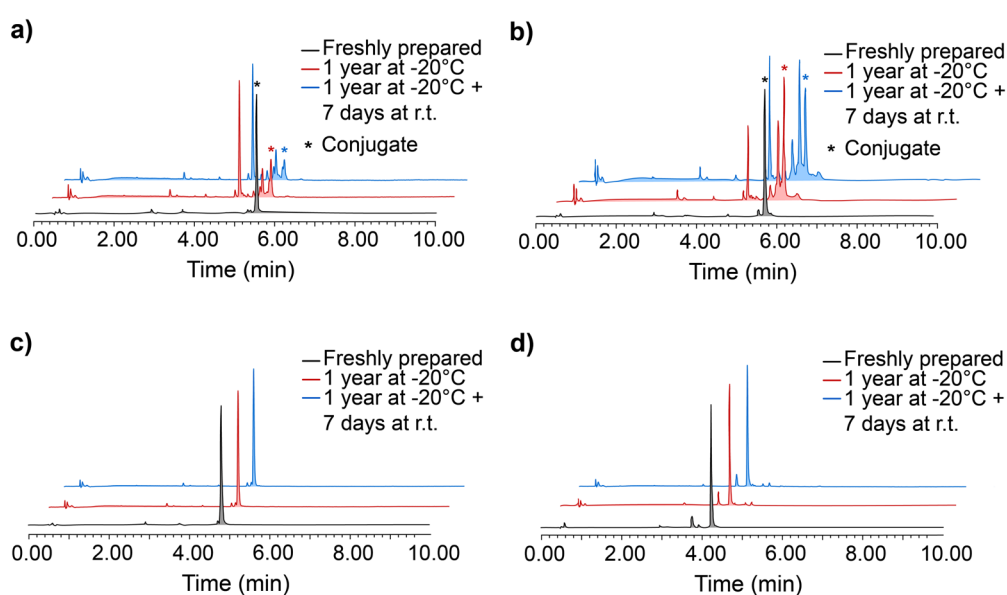


Figure 23. Solution stability of a) diantennary mannose-fluorescein conjugate **79**, b) tetraantennary mannose-fluorescein conjugate **81**, c) mannotriose-fluorescein conjugate **80** and d) triantennary GalNAc-fluorescein conjugate **82**. HPLC run conditions: 1.5 mL/min, 40 °C, buffer B 0-30 % v/v 0 → 4 min, then 30-85% v/v 4 → 10 min.

6.5 Synthesis of IVT mRNA

Plasmid description and preparation. The plasmid used for the mRNA production, pSTI-A120-N2, contains an expression cassette composed by 5 differentiated parts (**Scheme 11** and **Figure 24**): i) T7 RNA polymerase promoter, ii) 5' UTR consisting of a ribosome binding site (RBS), iii) nucleocapsid open reading frame from SARS-CoV-2 (*NCBI GenBank: MN908947.3, Severe acute respiratory syndrome coronavirus 2 isolate Wuhan-Hu-1, complete genome* <https://www.ncbi.nlm.nih.gov/nuccore/MN908947>), iv) 3' UTR consisting of two repetitive sequences of the human β -globulin 3'UTR and v) a Poly(A) tail. The plasmid is propagated in NEB 5-alpha *E. coli* cells (a derivative of DH5 α), grown in standard LB medium containing 50 μ g/mL Kanamycin for selection, and isolated using the Plasmid Plus Midi Kit (Qiagen) according to manufacturer's instructions.

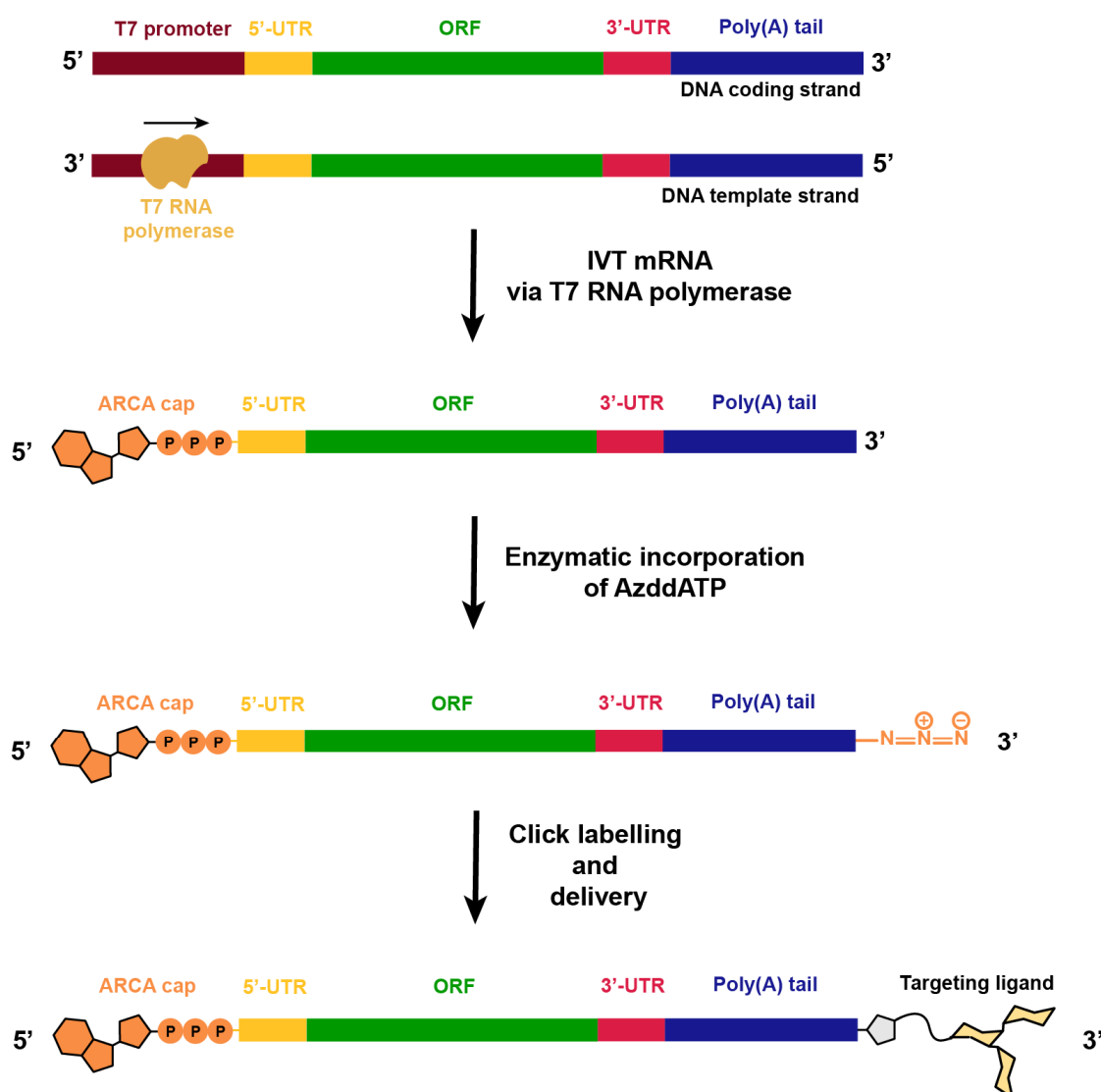
Plasmid linearization. 10 μ g of plasmid are linearized by incubating with 20 U of BspQ1 restriction enzyme in NEBuffer 3.1 at 50°C for 2 hours. This results in a linear DNA template with the 3'-end relative to the sense strand of the ORF located directly after the poly(A) tail sequence. The extent of digestion is assessed by gel electrophoresis on a 1.5% agarose gel in 0.5x Tris-Acetate-EDTA (TAE) buffer. The linearized plasmid is then purified using a silica-based spin column kit (QIAquick PCR Purification Kit) and purity as well as concentration are assessed by nanophotometer measurement.

In vitro transcription and plasmid digestion. 50 μ L reactions each containing 1 μ g of linear template DNA, 20 units of T7 RNA polymerase and several nucleotides (ARCA, 4.00 mM; ATP, 1.50 mM; CTP, 1.25 mM; GTP, 1.00 mM; UTP, 1.25 mM; Ψ TP, 1.25 mM) are combined in transcription buffer (40 mM Tris-HCl, pH 7.9, 6 mM MgCl₂, 4 mM spermidine, 10 mM DTT) and incubated at 37°C for 2 hours. After this time, 2 U of RNase-free DNase I are added to each 50 μ l reaction aliquot and incubation is continued for 15 minutes at 37°C. The transcript is then purified with the QIAquick PCR Purification Kit using one column for each IVT reaction aliquot. Columns are eluted with 32 μ l of water and eluates (~30 μ l/column) are pooled. The transcript concentration is measured by fluorometry (Qubit assay) and its integrity is assessed by electrophoresis on a 1.5% agarose/0.5x TAE gel (**Figure 25**).

3'-end azide labeling. 25 μ L reactions each containing up to 10 μ g of mRNA, 0.5 mM 3'-Azido-2',3'-ddATP and 600 units of yeast poly(A) polymerase are combined in reaction buffer (20 mM Tris-HCl, pH 7.0, 0.6 mM MnCl₂, 20 μ M EDTA, 200 μ M DTT, 10 μ g/mL

acetylated BSA, 10 % glycerol) and incubated for 2 h at 37 °C. The mRNA is purified (up to 7 µg RNA/column) and measured by fluorometry (Qubit assay). The integrity of the mRNA is assessed by agarose gel electrophoresis.

mRNA bioconjugation via SPAAC. 10 µg (~18 pmol) of purified azide-labeled mRNA and 2 nmol of mannitriose targeting ligand **75** are combined in a total reaction volume of 30 µL. The reaction mixture is incubated at room temperature for 3 h and the material is then purified by loading onto two columns of the QIAquick PCR Purification Kit. The integrity of the mRNA is assessed by agarose gel electrophoresis.



Scheme 11. *In vitro* synthesis scheme of 3'-end-conjugated mRNA coding for SARS-CoV-2 N protein. UTR = untranslated region; ORF = open reading frame.

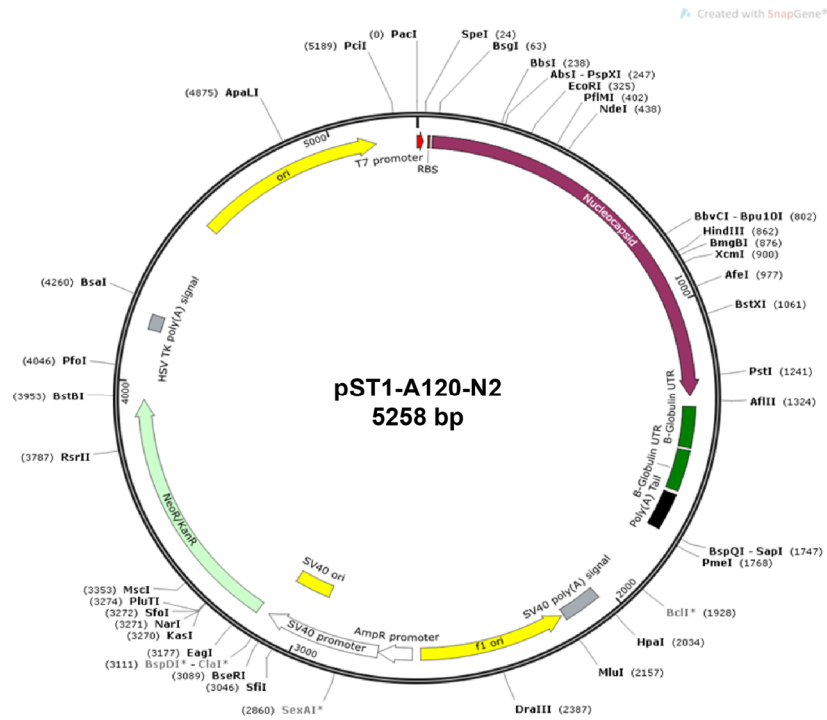


Figure 24: Map of the pSTI-A120-N2 plasmid used to produce mRNA coding for the N protein of SARS-CoV-2. Expression cassette: T7 RNA polymerase promoter (RBS, red), 5' UTR (orange), N ORF (violet), 3' UTR (dark green) and Poly(A) tail (black). Plasmid map was obtained using the SnapGene® software (from Dotmatics; available at snappgene.com).

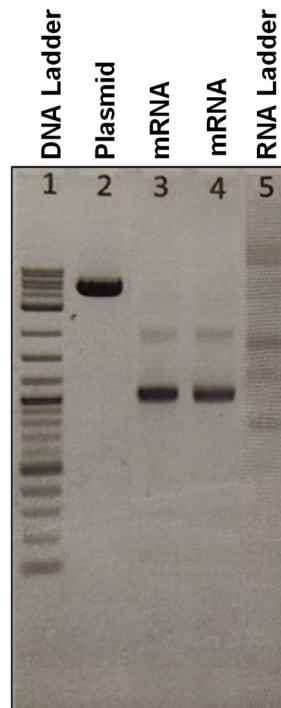


Figure 25. Agarose gel electrophoresis (1.5% agarose/0.5x TAE gel) for the analysis of linearized pSTI-A120-N2 plasmid and its respective mRNA generated by *in vitro* transcription.

7 REFERENCES

Citation Convention: *Angew. Chem. Int. Ed.*

- [1] H. C. Kolb, M. G. Finn, K. B. Sharpless, *Angew. Chemie Int. Ed.* **2001**, *40*, 2004–2021.
- [2] N. Jung, S. Bräse, in *Kirk-Othmer Encycl. Chem. Technol.*, **2013**, pp. 1–43.
- [3] M. Breugst, H.-U. Reissig, *Angew. Chemie Int. Ed.* **2020**, *59*, 12293–12307.
- [4] A. Michael, *J. für Prakt. Chemie* **1893**, *48*, 94–95.
- [5] R. Huisgen, *Angew. Chemie Int. Ed. English* **1963**, *2*, 633–645.
- [6] R. Huisgen, *Proc. Chem. Soc.* **1961**, 357–396.
- [7] R. Huisgen, *Angew. Chemie Int. Ed. English* **1963**, *2*, 565–598.
- [8] R. Ramapanicker, P. Chauhan, in *Click React. Org. Synth.*, **2016**, pp. 1–24.
- [9] C. W. Tornøe, C. Christensen, M. Meldal, *J. Org. Chem.* **2002**, *67*, 3057–3064.
- [10] V. V Rostovtsev, L. G. Green, V. V Fokin, K. B. Sharpless, *Angew. Chemie Int. Ed.* **2002**, *41*, 2596–2599.
- [11] R. Berg, B. F. Straub, *Beilstein J. Org. Chem.* **2013**, *9*, 2715–2750.
- [12] B. T. Worrell, J. A. Malik, V. V Fokin, *Science (80-.)*. **2013**, *340*, 457–460.
- [13] M. Meldal, C. W. Tornøe, *Chem. Rev.* **2008**, *108*, 2952–3015.
- [14] V. O. Rodionov, S. I. Presolski, D. Díaz Díaz, V. V Fokin, M. G. Finn, *J. Am. Chem. Soc.* **2007**, *129*, 12705–12712.
- [15] C. J. Pickens, S. N. Johnson, M. M. Pressnall, M. A. Leon, C. J. Berkland, *Bioconjug. Chem.* **2018**, *29*, 686–701.
- [16] D. Astruc, L. Liang, A. Rapakousiou, J. Ruiz, *Acc. Chem. Res.* **2012**, *45*, 630–640.
- [17] K. Kempe, A. Krieg, C. R. Becer, U. S. Schubert, *Chem. Soc. Rev.* **2012**, *41*, 176–191.
- [18] K. D. Hänni, D. A. Leigh, *Chem. Soc. Rev.* **2010**, *39*, 1240–1251.
- [19] V. Ganesh, V. S. Sudhir, T. Kundu, S. Chandrasekaran, *Chem. – An Asian J.* **2011**, *6*, 2670–2694.

-
- [20] R. P. Johnson, J. V John, I. Kim, *Eur. Polym. J.* **2013**, *49*, 2925–2948.
- [21] E. Lallana, F. Fernandez-Trillo, A. Sousa-Herves, R. Riguera, E. Fernandez-Megia, *Pharm. Res.* **2012**, *29*, 902–921.
- [22] P. Thirumurugan, D. Matosiuk, K. Jozwiak, *Chem. Rev.* **2013**, *113*, 4905–4979.
- [23] F. Himo, T. Lovell, R. Hilgraf, V. V Rostovtsev, L. Noodleman, K. B. Sharpless, V. V Fokin, *J. Am. Chem. Soc.* **2005**, *127*, 210–216.
- [24] L. Jin, D. R. Tolentino, M. Melaimi, G. Bertrand, *Sci. Adv.* **2015**, *1*, e1500304.
- [25] V. D. Bock, H. Hiemstra, J. H. van Maarseveen, *European J. Org. Chem.* **2006**, *2006*, 51–68.
- [26] L.-H. Qin, W. Hu, Y.-Q. Long, *Tetrahedron Lett.* **2018**, *59*, 2214–2228.
- [27] J. A. Prescher, C. R. Bertozzi, *Nat. Chem. Biol.* **2005**, *1*, 13–21.
- [28] S. Díez-González, *Catal. Sci. Technol.* **2011**, *1*, 166–178.
- [29] L. Li, Z. Zhang, *Molecules* **2016**, *21*, DOI 10.3390/molecules21101393.
- [30] C. Besanceney-Webler, H. Jiang, T. Zheng, L. Feng, D. Soriano del Amo, W. Wang, L. M. Klivansky, F. L. Marlow, Y. Liu, P. Wu, *Angew. Chemie Int. Ed.* **2011**, *50*, 8051–8056.
- [31] S. I. Presolski, V. Hong, S.-H. Cho, M. G. Finn, *J. Am. Chem. Soc.* **2010**, *132*, 14570–14576.
- [32] Q. Wang, T. R. Chan, R. Hilgraf, V. V Fokin, K. B. Sharpless, M. G. Finn, *J. Am. Chem. Soc.* **2003**, *125*, 3192–3193.
- [33] V. Hong, S. I. Presolski, C. Ma, M. G. Finn, *Angew. Chem. Int. Ed. Engl.* **2009**, *48*, 9879–9883.
- [34] D. Soriano Del Amo, W. Wang, H. Jiang, C. Besanceney, A. C. Yan, M. Levy, Y. Liu, F. L. Marlow, P. Wu, *J. Am. Chem. Soc.* **2010**, *132*, 16893–16899.
- [35] Z. Zhou, C. J. Fahrni, *J. Am. Chem. Soc.* **2004**, *126*, 8862–8863.
- [36] M. Yang, A. S. Jalloh, W. Wei, J. Zhao, P. Wu, P. R. Chen, *Nat. Commun.* **2014**, *5*, 4981.
-

- [37] W. Wang, S. Hong, A. Tran, H. Jiang, R. Triano, Y. Liu, X. Chen, P. Wu, *Chem. – An Asian J.* **2011**, *6*, 2796–2802.
- [38] V. O. Rodionov, S. I. Presolski, S. Gardinier, Y.-H. Lim, M. G. Finn, *J. Am. Chem. Soc.* **2007**, *129*, 12696–12704.
- [39] W. G. Lewis, F. G. Magallon, V. V Fokin, M. G. Finn, *J. Am. Chem. Soc.* **2004**, *126*, 9152–9153.
- [40] S. Ozçubukçu, E. Ozkal, C. Jimeno, M. A. Pericàs, *Org. Lett.* **2009**, *11*, 4680–4683.
- [41] D. C. Kennedy, C. S. McKay, M. C. B. Legault, D. C. Danielson, J. A. Blake, A. F. Pegoraro, A. Stolow, Z. Mester, J. P. Pezacki, *J. Am. Chem. Soc.* **2011**, *133*, 17993–18001.
- [42] L. S. Campbell-Verduyn, L. Mirfeizi, R. A. Dierckx, P. H. Elsinga, B. L. Feringa, *Chem. Commun. (Camb)*. **2009**, 2139–2141.
- [43] N. J. Agard, J. A. Prescher, C. R. Bertozzi, *J. Am. Chem. Soc.* **2004**, *126*, 15046–15047.
- [44] J. Dommerholt, O. van Rooijen, A. Borrmann, C. F. Guerra, F. M. Bickelhaupt, F. L. van Delft, *Nat. Commun.* **2014**, *5*, 5378.
- [45] M. Yang, J. Li, P. R. Chen, *Chem. Soc. Rev.* **2014**, *43*, 6511–6526.
- [46] K. Lang, J. W. Chin, *ACS Chem. Biol.* **2014**, *9*, 16–20.
- [47] D. M. Patterson, L. A. Nazarova, J. A. Prescher, *ACS Chem. Biol.* **2014**, *9*, 592–605.
- [48] M. King, A. Wagner, *Bioconjug. Chem.* **2014**, *25*, 825–839.
- [49] M. F. Debets, J. C. M. van Hest, F. P. J. T. Rutjes, *Org. Biomol. Chem.* **2013**, *11*, 6439–6455.
- [50] C. Gröst, T. Berg, *Org. Biomol. Chem.* **2015**, *13*, 3866–3870.
- [51] “The Nobel Prize in Chemistry 2022,” can be found under <https://www.nobelprize.org/prizes/chemistry/2022/summary/>, **2022**.
- [52] J. Berg, J. Tymoczko, L. Stryer, *Biochemistry*, W. H. Freeman Publishing, New York, **2002**.
- [53] N. Z. Fantoni, A. H. El-Sagheer, T. Brown, *Chem. Rev.* **2021**, *121*, 7122–7154.

- [54] D. Graham, J. A. Parkinson, T. Brown, *J. Chem. Soc. {,} Perkin Trans. 1* **1998**, 1131–1138.
- [55] P. Ding, D. Wunnicke, H.-J. Steinhoff, F. Seela, *Chemistry* **2010**, *16*, 14385–14396.
- [56] P. M. E. Gramlich, S. Warncke, J. Gierlich, T. Carell, *Angew. Chem. Int. Ed. Engl.* **2008**, *47*, 3442–3444.
- [57] F. Seela, X. Ming, *Helv. Chim. Acta* **2008**, *91*, 1181–1200.
- [58] F. Seela, V. R. Sirivolu, P. Chittepu, *Bioconjug. Chem.* **2008**, *19*, 211–224.
- [59] M. C. Wamberg, R. Wieczorek, S. B. Brier, J. W. de Vries, M. Kwak, A. Herrmann, P.-A. Monnard, *Bioconjug. Chem.* **2014**, *25*, 1678–1688.
- [60] F. Seela, H. Xiong, P. Leonard, S. Budow, *Org. Biomol. Chem.* **2009**, *7*, 1374–1387.
- [61] J. Gierlich, K. Gutsmedl, P. M. E. Gramlich, A. Schmidt, G. A. Burley, T. Carell, *Chem. – A Eur. J.* **2007**, *13*, 9486–9494.
- [62] P. M. E. Gramlich, C. T. Wirges, J. Gierlich, T. Carell, *Org. Lett.* **2008**, *10*, 249–251.
- [63] H. Macíčková-Cahová, R. Pohl, M. Hocek, *Chembiochem* **2011**, *12*, 431–438.
- [64] X. Ren, A. H. El-Sagheer, T. Brown, *Analyst* **2015**, *140*, 2671–2678.
- [65] J. Balintová, J. Špaček, R. Pohl, M. Brázdová, L. Havran, M. Fojta, M. Hocek, *Chem. Sci.* **2015**, *6*, 575–587.
- [66] X. Ren, A. H. El-Sagheer, T. Brown, *Nucleic Acids Res.* **2016**, *44*, e79.
- [67] X. Ren, M. Gerowska, A. H. El-Sagheer, T. Brown, *Bioorg. Med. Chem.* **2014**, *22*, 4384–4390.
- [68] H. Staudinger, J. Meyer, *Helv. Chim. Acta* **1919**, *2*, 635–646.
- [69] A. H. El-Sagheer, T. Brown, *Curr. Protoc. Nucleic Acid Chem.* **2008**, *35*, 4.33.1–4.33.21.
- [70] S. A. Ingale, H. Mei, P. Leonard, F. Seela, *J. Org. Chem.* **2013**, *78*, 11271–11282.
- [71] J. Gierlich, G. A. Burley, P. M. E. Gramlich, D. M. Hammond, T. Carell, *Org. Lett.* **2006**, *8*, 3639–3642.
- [72] M. Slavíčková, M. Janoušková, A. Šimonová, H. Cahová, M. Kambová, H. Šanderová, L. Krásný, M. Hocek, *Chem. – A Eur. J.* **2018**, *24*, 8311–8314.

- [73] A. Salic, T. J. Mitchison, *Proc. Natl. Acad. Sci.* **2008**, *105*, 2415–2420.
- [74] A. B. Neef, L. Pernot, V. N. Schreier, L. Scapozza, N. W. Luedtke, *Angew. Chemie Int. Ed.* **2015**, *54*, 7911–7914.
- [75] A. B. Neef, N. W. Luedtke, *Proc. Natl. Acad. Sci.* **2011**, *108*, 20404–20409.
- [76] E. Paredes, S. R. Das, *ChemBioChem* **2011**, *12*, 125–131.
- [77] A. Samanta, A. Krause, A. Jäschke, *Chem. Commun.* **2014**, *50*, 1313–1316.
- [78] M.-L. Winz, A. Samanta, D. Benzinger, A. Jäschke, *Nucleic Acids Res.* **2012**, *40*, e78–e78.
- [79] C. M. Dojahn, M. Hesse, C. Arenz, *Chem. Commun.* **2013**, *49*, 3128–3130.
- [80] R. T. Ranasinghe, T. Brown, *Chem. Commun.* **2005**, 5487–5502.
- [81] R. T. Ranasinghe, T. Brown, *Chem. Commun.* **2011**, *47*, 3717–3735.
- [82] J. Shendure, R. D. Mitra, C. Varma, G. M. Church, *Nat. Rev. Genet.* **2004**, *5*, 335–344.
- [83] L. D. Lavis, R. T. Raines, *ACS Chem. Biol.* **2014**, *9*, 855–866.
- [84] I. K. Astakhova, J. Wengel, *Chem. – A Eur. J.* **2013**, *19*, 1112–1122.
- [85] A. Raulf, C. K. Spahn, P. J. M. Zessin, K. Finan, S. Bernhardt, A. Heckel, M. Heilemann, *RSC Adv.* **2014**, *4*, 30462–30466.
- [86] T. Ishizuka, H. S. Liu, K. Ito, Y. Xu, *Sci. Rep.* **2016**, *6*, 33217.
- [87] S. Serdjukow, F. Kink, B. Steigenberger, M. Tomás-Gamasa, T. Carell, *Chem. Commun.* **2014**, *50*, 1861–1863.
- [88] E. Doe, H. L. Hayth, R. Brumett, E. F. Khisamutdinov, *Int. J. Mol. Sci.* **2023**, *24*, DOI 10.3390/ijms24054797.
- [89] V. N. Schreier, M. O. Loehr, T. Deng, E. Lattmann, A. Hajnal, S. C. F. Neuhauss, N. W. Luedtke, *ACS Chem. Biol.* **2020**, *15*, 2996–3003.
- [90] S. Berndl, N. Herzig, P. Kele, D. Lachmann, X. Li, O. S. Wolfbeis, H.-A. Wagenknecht, *Bioconjug. Chem.* **2009**, *20*, 558–564.
- [91] C. Wängler, G. Moldenhauer, R. Saffrich, E. M. Knapp, B. Beijer, M. Schnölzer, B. Wängler, M. Eisenhut, U. Haberkorn, W. Mier, *Chem. – A Eur. J.* **2008**, *14*, 8116–8130.

-
- [92] J. Manono, C. A. Dougherty, K. Jones, J. DeMuth, M. M. B. Holl, S. DiMaggio, *Mater. Today Commun.* **2015**, *4*, 86–92.
- [93] C. A. Dougherty, S. Vaidyanathan, B. G. Orr, M. M. Banaszak Holl, *Bioconjug. Chem.* **2015**, *26*, 304–315.
- [94] Á. Martín-Serrano Ortiz, P. Stenström, P. Mesa Antunez, O. C. J. Andrén, M. J. Torres, M. I. Montañez, M. Malkoch, *J. Polym. Sci. Part A Polym. Chem.* **2018**, *56*, 1609–1616.
- [95] N. Raddaoui, S. Stazzoni, L. Möckl, B. Viverge, F. Geiger, H. Engelke, C. Bräuchle, T. Carell, *ChemBioChem* **2017**, *18*, 1716–1720.
- [96] N. Raddaoui, S. Stazzoni, L. Möckl, B. Viverge, F. Geiger, H. Engelke, C. Bräuchle, T. Carell, *ChemBioChem* **2017**, *18*, 1716–1720.
- [97] T. Yamada, C. G. Peng, S. Matsuda, H. Addepalli, K. N. Jayaprakash, M. R. Alam, K. Mills, M. A. Maier, K. Charisse, M. Sekine, M. Manoharan, K. G. Rajeev, *J. Org. Chem.* **2011**, *76*, 1198–1211.
- [98] M. Manoharan, *Antisense Nucleic Acid Drug Dev.* **2002**, *12*, 103–128.
- [99] X. Ming, B. Laing, *Adv. Drug Deliv. Rev.* **2015**, *87*, 81–89.
- [100] J. Willibald, J. Harder, K. Sparrer, K.-K. Conzelmann, T. Carell, *J. Am. Chem. Soc.* **2012**, *134*, 12330–12333.
- [101] L. J. Scott, *Drugs* **2020**, *80*, 335–339.
- [102] L. J. Scott, S. J. Keam, *Drugs* **2021**, *81*, 277–282.
- [103] Y. N. Lamb, *Drugs* **2021**, *81*, 389–395.
- [104] V. M. Farzan, E. A. Ulashchik, Y. V Martynenko-Makaev, M. V Kvach, I. O. Aparin, V. A. Brylev, T. A. Prikazchikova, S. Y. Maklakova, A. G. Majouga, A. V Ustinov, G. A. Shipulin, V. V Shmanai, V. A. Korshun, T. S. Zatsepin, *Bioconjug. Chem.* **2017**, *28*, 2599–2607.
- [105] E. B. Glass, S. Masjedi, S. O. Dudzinski, A. J. Wilson, C. L. Duvall, F. E. Yull, T. D. Giorgio, *ACS Omega* **2019**, *4*, 16756–16767.
- [106] S. S. Yu, C. M. Lau, W. J. Barham, H. M. Onishko, C. E. Nelson, H. Li, C. A. Smith, F. E. Yull, C. L. Duvall, T. D. Giorgio, *Mol. Pharm.* **2013**, *10*, 975–987.
-

- [107] H. G. Gratzner, *Science (80-.)*. **1982**, *218*, 474–475.
- [108] F. M. Waldman, K. Chew, B. M. Ljung, W. Goodson, J. Hom, L. A. Duarte, H. S. Smith, B. Mayall, *Mod. Pathol. an Off. J. United States Can. Acad. Pathol. Inc* **1991**, *4*, 718–722.
- [109] M. Uddin, G. G. Altmann, C. P. Leblond, *J. Cell Biol.* **1984**, *98*, 1619–1629.
- [110] D. Cmarko, P. J. Verschure, T. E. Martin, M. E. Dahmus, S. Krause, X.-D. Fu, R. van Driel, S. Fakan, *Mol. Biol. Cell* **1999**, *10*, 211–223.
- [111] S. Meneni, I. Ott, C. D. Sergeant, A. Sniady, R. Gust, R. Dembinski, *Bioorg. Med. Chem.* **2007**, *15*, 3082–3088.
- [112] A. B. Neef, N. W. Luedtke, *ChemBioChem* **2014**, *15*, 789–793.
- [113] C. Y. Jao, A. Salic, *Proc. Natl. Acad. Sci.* **2008**, *105*, 15779–15784.
- [114] D. Curanovic, M. Cohen, I. Singh, C. E. Slagle, C. S. Leslie, S. R. Jaffrey, *Nat. Chem. Biol.* **2013**, *9*, 671–673.
- [115] M. Grammel, H. Hang, N. K. Conrad, *ChemBioChem* **2012**, *13*, 1112–1115.
- [116] S. Nainar, S. Beasley, M. Fazio, M. Kubota, N. Dai, I. R. Corrêa Jr., R. C. Spitale, *ChemBioChem* **2016**, *17*, 2149–2152.
- [117] Y. Motorin, J. Burhenne, R. Teimer, K. Koynov, S. Willnow, E. Weinhold, M. Helm, *Nucleic Acids Res.* **2011**, *39*, 1943–1952.
- [118] K. Hartstock, B. S. Nilges, A. Ovcharenko, N. V Cornelissen, N. Püllen, A.-M. Lawrence-Dörner, S. A. Leidel, A. Rentmeister, *Angew. Chemie Int. Ed.* **2018**, *57*, 6342–6346.
- [119] J. M. Holstein, D. Schulz, A. Rentmeister, *Chem. Commun.* **2014**, *50*, 4478–4481.
- [120] D. Schulz, J. M. Holstein, A. Rentmeister, *Angew. Chemie Int. Ed.* **2013**, *52*, 7874–7878.
- [121] S. Ma, I. Saaem, J. Tian, *Trends Biotechnol.* **2012**, *30*, 147–154.
- [122] A. H. El-Sagheer, T. Brown, *J. Am. Chem. Soc.* **2009**, *131*, 3958–3964.
- [123] A. H. El-Sagheer, T. Brown, *Chem. Commun.* **2011**, *47*, 12057–12058.
- [124] A. H. El-Sagheer, A. P. Sanzone, R. Gao, A. Tavassoli, T. Brown, *Proc. Natl. Acad. Sci.*

- 2011**, *108*, 11338–11343.
- [125] A. H. El-Sagheer, T. Brown, *Chem. Commun.* **2017**, *53*, 10700–10702.
- [126] Y. N. Teo, X.-J. Chen, T. Khurana, *Methods for Chemical Ligation of Nucleic Acids*, **2018**, U.S. Patent Application No. 15/788,483.
- [127] M. Kollaschinski, J. Sobotta, A. Schalk, T. Frischmuth, B. Graf, S. Serdjukow, *Bioconjug. Chem.* **2020**, *31*, 507–512.
- [128] E. S. Schönegger, A. Crisp, M. Müller, J. Fertl, S. Serdjukow, S. Croce, M. Kollaschinski, T. Carell, T. Frischmuth, *Bioconjug. Chem.* **2022**, *33*, 1789–1795.
- [129] A. H. El-Sagheer, T. Brown, *Chem. Sci.* **2014**, *5*, 253–259.
- [130] P. Kumar, A. H. El-Sagheer, L. Truong, T. Brown, *Chem. Commun.* **2017**, *53*, 8910–8913.
- [131] P. Kumar, L. Truong, Y. R. Baker, A. H. El-Sagheer, T. Brown, *ACS Omega* **2018**, *3*, 6976–6987.
- [132] V. K. Sharma, S. K. Singh, P. M. Krishnamurthy, J. F. Alterman, R. A. Haraszti, A. Khvorova, A. K. Prasad, J. K. Watts, *Chem. Commun.* **2017**, *53*, 8906–8909.
- [133] K. He, E. T. Chou, S. Begay, E. M. Anderson, A. van Brabant Smith, *ChemBioChem* **2016**, *17*, 1809–1812.
- [134] L. Taemaitree, A. Shivalingam, A. H. El-Sagheer, T. Brown, *Nat. Commun.* **2019**, *10*, 1610.
- [135] E. P. Lundberg, A. H. El-Sagheer, P. Kocalka, L. M. Wilhelmsson, T. Brown, B. Nordén, *Chem. Commun.* **2010**, *46*, 3714–3716.
- [136] M. F. Jacobsen, J. B. Ravnsbæk, K. V. Gothelf, *Org. Biomol. Chem.* **2010**, *8*, 50–52.
- [137] Y. Xu, Y. Suzuki, M. Komiyama, *Angew. Chemie Int. Ed.* **2009**, *48*, 3281–3284.
- [138] P. Nordell, F. Westerlund, A. Reymer, A. H. El-Sagheer, T. Brown, B. Nordén, P. Lincoln, *J. Am. Chem. Soc.* **2008**, *130*, 14651–14658.
- [139] A. H. El-Sagheer, T. Brown, *Int. J. Pept. Res. Ther.* **2008**, *14*, 367–372.
- [140] M. Nakane, S. Ichikawa, A. Matsuda, *J. Org. Chem.* **2008**, *73*, 1842–1851.

- [141] C. R. Dialer, S. Stazzoni, D. J. Drexler, F. M. Müller, S. Veth, A. Pichler, H. Okamura, G. Witte, K.-P. Hopfner, T. Carell, *Chem. – A Eur. J.* **2019**, *25*, 2089–2095.
- [142] R. Kumar, A. El-Sagheer, J. Tumpane, P. Lincoln, L. M. Wilhelmsson, T. Brown, *J. Am. Chem. Soc.* **2007**, *129*, 6859–6864.
- [143] T. C. Roberts, R. Langer, M. J. A. Wood, *Nat. Rev. Drug Discov. 2020 1910* **2020**, *19*, 673–694.
- [144] P. S. Kowalski, A. Rudra, L. Miao, D. G. Anderson, *Mol. Ther.* **2019**, *27*, 710–728.
- [145] M. Zhao, M. Li, Z. Zhang, T. Gong, X. Sun, *Drug Deliv.* **2016**, *23*, 2596–2607.
- [146] A. V. Kristen, S. Ajroud-Driss, I. Conceição, P. Gorevic, T. Kyriakides, L. Obici, *Neurodegener. Dis. Manag.* **2019**, *9*, 5–23.
- [147] J. A. Kulkarni, D. Witzigmann, S. Chen, P. R. Cullis, R. Van Der Meel, *Acc. Chem. Res.* **2019**, *52*, 2435–2444.
- [148] C. Lorenz, P. Hadwiger, M. John, H. P. Vornlocher, C. Unverzagt, *Bioorg. Med. Chem. Lett.* **2004**, *14*, 4975–4977.
- [149] K. Nishina, T. Unno, Y. Uno, T. Kubodera, T. Kanouchi, H. Mizusawa, T. Yokota, *Mol. Ther.* **2008**, *16*, 734–740.
- [150] C. F. Xia, R. J. Boado, W. M. Pardridge, *Mol. Pharm.* **2009**, *6*, 747–751.
- [151] S. A. Moschos, S. W. Jones, M. M. Perry, A. E. Williams, J. S. Erjefalt, J. J. Turner, P. J. Barnes, B. S. Sproat, M. J. Gait, M. A. Lindsay, *Bioconjug. Chem.* **2007**, *18*, 1450–1459.
- [152] C. Zhang, Z. Gu, L. Shen, X. Liu, H. Lin, *Curr. Pharm. Biotechnol.* **2018**, *19*, 1124–1131.
- [153] A. F. Klein, M. A. Varela, L. Arandel, A. Holland, N. Naouar, A. Arzumanov, D. Seoane, L. Revillod, G. Bassez, A. Ferry, D. Jauvin, G. Gourdon, J. Puymirat, M. J. Gait, D. Furling, M. J. A. Wood, *J. Clin. Invest.* **2019**, *129*, 4739–4744.
- [154] S. Weinstein, I. A. Toker, R. Emmanuel, S. Ramishetti, I. Hazan-Halevy, D. Rosenblum, M. Goldsmith, A. Abraham, O. Benjamini, O. Bairey, P. Raanani, A. Nagler, J. Lieberman, D. Peer, *Proc. Natl. Acad. Sci. U. S. A.* **2016**, *113*, E16–E22.

-
- [155] J. Tushir-Singh, *Expert Opin. Biol. Ther.* **2017**, *17*, 325–338.
- [156] T. Sugo, M. Terada, T. Oikawa, K. Miyata, S. Nishimura, E. Kenjo, M. Ogasawara-Shimizu, Y. Makita, S. Imaichi, S. Murata, K. Otake, K. Kikuchi, M. Teratani, Y. Masuda, T. Kamei, S. Takagahara, S. Ikeda, T. Ohtaki, H. Matsumoto, *J. Control. Release* **2016**, *237*, 1–13.
- [157] J. O. McNamara, E. R. Andreckek, Y. Wang, K. D. Viles, R. E. Rempel, E. Gilboa, B. A. Sullenger, P. H. Giangrande, *Nat. Biotechnol.* **2006**, *24*, 1005–1015.
- [158] D. Wang, H. Li, W. Chen, H. Yang, Y. Liu, B. You, X. Zhang, *Mater. Sci. Eng. C* **2021**, *119*, DOI 10.1016/j.msec.2020.111583.
- [159] H. Jung, G. Yu, H. Mok, *Appl. Biol. Chem.* **2016**, *59*, 759–763.
- [160] K. Paunovska, D. Loughrey, J. E. Dahlman, *Nat. Rev. Genet.* **2022**, *23*, 265–280.
- [161] J. K. Nair, J. L. S. Willoughby, A. Chan, K. Charisse, M. R. Alam, Q. Wang, M. Hoekstra, P. Kandasamy, A. V. Kelin, S. Milstein, N. Taneja, J. Oshea, S. Shaikh, L. Zhang, R. J. Van Der Sluis, M. E. Jung, A. Akinc, R. Hutabarat, S. Kuchimanchi, K. Fitzgerald, T. Zimmermann, T. J. C. Van Berkel, M. A. Maier, K. G. Rajeev, M. Manoharan, *J. Am. Chem. Soc.* **2014**, *136*, 16958–16961.
- [162] Y. Yan, X. Y. Liu, A. Lu, X. Y. Wang, L. X. Jiang, J. C. Wang, *J. Control. Release* **2022**, *342*, 241–279.
- [163] J. Liu, M. Fu, M. Wang, D. Wan, Y. Wei, X. Wei, *J. Hematol. Oncol.* **2022**, *15*, 1–26.
- [164] N. Pardi, M. J. Hogan, F. W. Porter, D. Weissman, *Nat. Rev. Drug Discov.* **2018**, *17*, 261–279.
- [165] L. Song, G. Dong, L. Guo, D. T. Graves, *Mol. Oral Microbiol.* **2018**, *33*, 13–21.
- [166] D. K. Flaherty, in *Immunol. Pharm.*, Elsevier Inc, St. Louis, Missouri, **2012**, pp. 37–44.
- [167] D. Sancho, C. Reis e Sousa, *Annu. Rev. Immunol.* **2012**, *30*, 491–529.
- [168] A. J. Foster, J. H. Bird, M. S. M. Timmer, B. L. Stocker, in *C-Type Lectin Recept. Immun.*, Nature Publishing Group, **2016**, pp. 191–215.
- [169] G. D. Brown, J. A. Willment, L. Whitehead, *Nat. Rev. Immunol.* **2018**, *18*, 374–389.
- [170] Y. Kim, J. Y. Hyun, I. Shin, *Chem. Soc. Rev.* **2021**, *50*, 10567–10593.
-

- [171] M. Hartweg, Y. Jiang, G. Yilmaz, C. M. Jarvis, H. V.-T. Nguyen, G. A. Primo, A. Monaco, V. P. Beyer, K. K. Chen, S. Mohapatra, S. Axelrod, R. Gómez-Bombarelli, L. L. Kiessling, C. R. Becer, J. A. Johnson, *JACS Au* **2021**, *1*, 1621–1630.
- [172] A. Carlmark, E. Malmström, M. Malkoch, *Chem. Soc. Rev.* **2013**, *42*, 5858–5879.
- [173] F. Cavelier, C. Enjalbal, *Tetrahedron Lett.* **1996**, *37*, 5131–5134.
- [174] K. Bloem, I. M. Vuist, M. van den Berk, E. J. Klaver, I. van Die, L. M. J. Knippels, J. Garsen, J. J. García-Vallejo, S. J. van Vliet, Y. Van Kooyk, *Immunol. Lett.* **2014**, *158*, 33–41.
- [175] N. Higashi, K. Fujioka, K. Denda-Nagai, S. I. Hashimoto, S. Nagai, T. Sato, Y. Fujita, A. Morikawa, M. Tsuiji, M. Miyata-Takeuchi, Y. Sano, N. Suzuki, K. Yamamoto, K. Matsushima, T. Irimura, *J. Biol. Chem.* **2002**, *277*, 20686–20693.
- [176] C. Berges, C. Naujokat, S. Tinapp, H. Wiczorek, A. Höh, M. Sadeghi, G. Opelz, V. Daniel, *Biochem. Biophys. Res. Commun.* **2005**, *333*, 896–907.
- [177] F. Sallusto, M. Cella, C. Danieli, A. Lanzavecchia, *J. Exp. Med.* **1995**, *182*, 389–400.
- [178] L. East, C. M. Isacke, *Biochim. Biophys. Acta* **2002**, *1572*, 364–386.
- [179] M. Glaffig, N. Stergiou, S. Hartmann, E. Schmitt, H. Kunz, *ChemMedChem* **2018**, *13*, 25–29.
- [180] K. Uehara, T. Harumoto, A. Makino, Y. Koda, J. Iwano, Y. Suzuki, M. Tanigawa, H. Iwai, K. Asano, K. Kurihara, A. Hamaguchi, H. Kodaira, T. Atsumi, Y. Yamada, K. Tomizuka, *Nucleic Acids Res.* **2022**, *50*, 4840–4859.
- [181] H. Onyeaka, C. K. Anumudu, Z. T. Al-Sharify, E. Egele-Godswill, P. Mbaegbu, *Sci. Prog.* **2021**, *104*, 1–18.
- [182] “Pneumonia of unknown cause – China,” can be found under <https://www.who.int/emergencies/disease-outbreak-news/item/2020-DON229>, **2020**.
- [183] D. Cucinotta, M. Vanelli, *Acta Biomed.* **2020**, *91*, 157–160.
- [184] Y. Jin, H. Yang, W. Ji, W. Wu, S. Chen, W. Zhang, G. Duan, *Viruses* **2020**, *12*, 372.
- [185] A. A. Agyeman, K. L. Chin, C. B. Landersdorfer, D. Liew, R. Ofori-Asenso, *Mayo Clin. Proc.* **2020**, *95*, 1621–1631.

-
- [186] “WHO Coronavirus Disease (COVID-19) Dashboard With Vaccination Data,” can be found under <https://covid19.who.int/>, **2021**.
- [187] K. Chriscaden, “Impact of COVID-19 on people’s livelihoods, their health and our food systems,” **2020**.
- [188] R. Lu, X. Zhao, J. Li, P. Niu, B. Yang, H. Wu, W. Wang, H. Song, B. Huang, N. Zhu, Y. Bi, X. Ma, F. Zhan, L. Wang, T. Hu, H. Zhou, Z. Hu, W. Zhou, L. Zhao, J. Chen, Y. Meng, J. Wang, Y. Lin, J. Yuan, Z. Xie, J. Ma, W. J. Liu, D. Wang, W. Xu, E. C. Holmes, G. F. Gao, G. Wu, W. Chen, W. Shi, W. Tan, *Lancet* **2020**, *395*, 565–574.
- [189] X. Fan, D. Cao, L. Kong, X. Zhang, *Nat. Commun.* **2020**, *11*, 1–10.
- [190] V. S. Mandala, M. J. McKay, A. A. Shcherbakov, A. J. Dregni, A. Kolocouris, M. Hong, *Nat. Struct. Mol. Biol.* **2020**, *27*, 1202–1208.
- [191] D. Schoeman, B. C. Fielding, *Virol. J.* **2019**, *16*, 69.
- [192] D. X. Liu, Q. Yuan, Y. Liao, *Cell. Mol. Life Sci.* **2007**, *64*, 2043–2048.
- [193] A. L. Arndt, B. J. Larson, B. G. Hogue, *J. Virol.* **2010**, *84*, 11418–11428.
- [194] R. McBride, M. Van Zyl, B. C. Fielding, *Viruses* **2014**, *6*, 2991–3018.
- [195] C. Chang, M.-H. Hou, C.-F. Chang, C.-D. Hsiao, T. Huang, *Antiviral Res.* **2014**, *103*, 39–50.
- [196] M. Su, Y. Chen, S. Qi, D. Shi, L. Feng, D. Sun, *Front. Vet. Sci.* **2020**, *7*, 586826.
- [197] N. Zhu, D. Zhang, W. Wang, X. Li, B. Yang, J. Song, X. Zhao, B. Huang, W. Shi, R. Lu, P. Niu, F. Zhan, X. Ma, D. Wang, W. Xu, G. Wu, G. F. Gao, W. Tan, C. N. C. I. and R. Team, *N. Engl. J. Med.* **2020**, *382*, 727–733.
- [198] N. Chen, M. Zhou, X. Dong, J. Qu, F. Gong, Y. Han, Y. Qiu, J. Wang, Y. Liu, Y. Wei, J. Xia, T. Yu, X. Zhang, L. Zhang, *Lancet* **2020**, *395*, 507–513.
- [199] D. H. Barouch, *N. Engl. J. Med.* **2022**, *387*, 1011–1020.
- [200] “WHO – COVID19 Vaccine Tracker,” can be found under <https://covid19.trackvaccines.org/agency/who/>, **2022**.
- [201] A. J. Pollard, E. M. Bijker, *Nat. Rev. Immunol.* **2021**, *21*, 83–100.
-

- [202] K. Murphy, C. Weaver, in *Janeway's Immunobiol.*, Garland Science, **2017**, pp. 473–475.
- [203] L. Du, Y. He, Y. Zhou, S. Liu, B. J. Zheng, S. Jiang, *Nat. Rev. Microbiol.* **2009**, *7*, 226–236.
- [204] S. Croce, S. Serdjukow, T. Carell, T. Frischmuth, *ChemBioChem* **2020**, *21*, 1641–1646.
- [205] S. Thakur, S. Sasi, S. G. Pillai, A. Nag, D. Shukla, R. Singhal, S. Phalke, G. S. K. Velu, *Front. Med.* **2022**, *9*.
- [206] D. Li, J. Li, *J. Clin. Microbiol.* **2021**, *59*, e02160-20.
- [207] S. M. Moghimi, D. Simberg, *Mol. Ther.* **2022**, *30*, 2109–2110.
- [208] Y. V Svitkin, Y. M. Cheng, T. Chakraborty, V. Presnyak, M. John, N. Sonenberg, *Nucleic Acids Res.* **2017**, *45*, 6023–6036.
- [209] D. R. Gallie, *Genes Dev.* **1991**, *5*, 2108–2116.
- [210] L. Wu, C. Huang, B. P. Emery, A. C. Sedgwick, S. D. Bull, X. P. He, H. Tian, J. Yoon, J. L. Sessler, T. D. James, *Chem. Soc. Rev.* **2020**, *49*, 5110–5139.
- [211] E. F. Pettersen, T. D. Goddard, C. C. Huang, E. C. Meng, G. S. Couch, T. I. Croll, J. H. Morris, T. E. Ferrin, *Protein Sci.* **2021**, *30*, 70–82.

8 APPENDICES

8.1 Supporting Information for Published Work

Chemistry–A European Journal

Supporting Information

Divergent Synthesis of Ultrabright and Dendritic Xanthenes for Enhanced Click-Chemistry-Based Bioimaging

Luis Montiel, Fabio Spada, Antony Crisp, Sascha Serdjukow, Thomas Carell, and
Thomas Frischmuth*

Table of Contents

1. General Experimental Methods	2
2. Synthetic Procedures	5
3. Photophysical Properties of the Synthesised Fluorophores	16
4. Photostability Studies of RD _{H2} , RD _m and RD _{F2}	25
5. pK _a Values Calculation of RD _{H2} , RD _m and RD _{F2}	27
6. Solution Stability Studies	29
7. Mass Spectra of the Synthesised Compounds	30
8. NMR Spectra of the Synthesised Compounds	33
9. References	45
10. Author Contributions	45

1. General Experimental Methods

Materials and methods. Chemicals were purchased from Sigma-Aldrich, TCI, Fluka, ABCR, Acros Organics, VWR, Polymer Factory or Sapala Organics and were used without further purification. Solvents were purchased in septum-sealed bottles stored under an inert atmosphere. All reactions were magnetically stirred under a positive pressure of Argon (Ar) unless otherwise stated. Reactions and chromatography fractions were monitored by qualitative thin-layer chromatography (TLC) on silica gel F254 TLC plates from Merck KGaA, visualised by UV illumination or developed with ninhydrin, ceric ammonium molybdate or KMnO₄ stains. Flash column chromatography was performed using silica gel (40-63 μm) or basic alumina (~150 mesh) from Merck KGaA. Size exclusion chromatography was performed on Sephadex® LH-20 (18-111 μm) from Merck KGaA. Dialysis membranes Spectra/Por® 6 MWCO 1 KDa (18 mm flat width) and Spectra/Por® 6 MWCO 3.5 KDa (18 mm flat width) were purchased from Repligen and used as received.

Nuclear Magnetic Resonance (NMR). Spectra were recorded on a *Bruker Avance III HD 400* (400 MHz), *Varian NMR-System 600* (600 MHz) and *Bruker Avance III HD with Cryo-Kopf 800* (800 MHz) spectrometers. ¹H chemical shifts were internally calibrated to the residual protons of the deuterated solvent: DMSO-d₅ (2.50 ppm) and CD₂HOD (3.31 ppm). ¹³C NMR shifts were calibrated to the residual solvent: DMSO-d₆ (39.52 ppm), CD₃OD (49.00 ppm). ¹⁹F chemical shifts (δ) were referenced to an external reference: CFCI₃ (0.00 ppm) or CF₃COOH (-76.55 ppm). Data for ¹H NMR spectra are reported as follows: chemical shift (δ ppm), multiplicity (s = singlet, d = doublet, t = triplet, q = quartet, p = pentuplet, dd = doublet of doublets, m = multiplet, br = broad), coupling constant (Hz), integration. Data for proton-decoupled ¹³C and ¹⁹F NMR spectra are reported by chemical shift (δ ppm) and, where necessary, multiplicity (s = singlet, t = triplet, q = quartet). All NMR spectra were analysed using the software MestreNova 14.1.1 from Mestrelab Research S. L. Broadening of aromatic signals was observed in the ¹H and ¹³C NMR spectra of the synthesised dendritic dyes, most likely due to strong π - π stacking between the dye moieties, as previously reported by Parenti *et al.*^[1]

IR spectroscopy. IR spectra were recorded on a PerkinElmer Spectrum BX II FT-IR system. All substances were directly applied as solids or on the ATR unit.

Mass Spectrometry (MS). High resolution mass spectra (ESI-MS) were recorded by the analytical section of the Department of Chemistry of the Ludwig-Maximilians-Universität München on a spectrometer MAT 90 (ESI) from Thermo Finnigan GmbH. Raw data was extracted using OpenChrome Lablicate Edition version 1.5.0, and spectra were processed in Origin 2018. Theoretical spectra were calculated using the Isotope Distributor Calculator and Mass Spec Plotter by Adaptas Solutions (<https://www.sisweb.com/mstools/isotope.htm>) and processed in Origin 2018. Matrix-assisted laser

desorption/ionization-time-of-flight (MALDI-TOF) mass spectra were recorded on a Bruker Autoflex II. The instrument was calibrated using SpheriCal™ calibrants. Samples were prepared by mixing 5 μ L of 1 mg/mL analyte solution in EtOAc or MeOH, 5 μ L of a 1 mg/mL counterion solution of sodium trifluoroacetate (NaTFA) in tetrahydrofuran (THF) and 20 μ L of a 10 mg/mL trans-2-[3-(4-tert-butylphenyl)-2-methyl-2-propenylidene]-malononitrile (DCTB) solution in THF. 1 μ L of the final mixture was applied to a stainless-steel sample plate using the dried droplet method. The obtained spectra were analysed with FlexAnalysis version 2.2 from Bruker Daltonics and processed in Origin 2018.

Analytical and preparative HPLC. Analytical RP-HPLC was performed on a Waters Alliance (e2695 Separation Module, 2998 Photodiode Array Detector) instrument equipped with an XBridge™ OST C18 column (2.5 μ m, 4.6mm x 50mm) using a flow of 1.5 mL/min at 40 °C column temperature. A linear gradient of buffer B 0-30 % v/v from 0 \rightarrow 4 min and then 30-85 % v/v from 4 \rightarrow 10 min was applied. Buffer A: 0.1 M triethylammonium acetate in H₂O. Buffer B: 0.1 M triethylammonium acetate in MeCN/H₂O 8:2 v/v. Preparative RP-HPLC was performed on a Waters Breeze (2487 Dual λ Array Detector, 1525 Binary HPLC Pump) instrument equipped with the column VP 250/32 C18 from Macherey Nagel using a flow of 5 mL/min at room temperature. Compounds were detected at the wavelength of maximum absorption (λ_{max}) of the corresponding dyes. The employed gradients for the subsequent purifications are specified in the Synthetic Procedures section.

Purification of dendrons by dialysis. High molecular weight dendrons were unsuitable for conventional flash chromatography and were instead purified according to the following procedure. A solution containing a particular dendron and other reaction components in DMSO (1 mL) was transferred to a dialysis membrane (ca. 10 cm of tubing) and carefully sealed at each end with a conventional clamp. The filled membrane was subsequently placed a beaker containing 1.0 L of DMSO and gently stirred for the reported time. The outer dialysate was replaced with fresh DMSO 2-3 times throughout the specified time course. The dialysis bag was then placed in a beaker containing 1.0 L H₂O for the specified time to remove the majority DMSO from the inner compartment by diffusion.

Visualisation of spectroscopic data in Origin. Absorption spectra, emission spectra, calibration curves, and their regression line equations were plotted and calculated using the software package Origin 2018 according to the developers' instructions.

Photostability measurements. A VFL-P-532 and a VFL-P-560 lasers from MPB communications were utilised to irradiate the samples at 532 nm and 560 nm, respectively. An iBEAM SMART 488 laser from TOPTICA was utilised to irradiate the samples at 488 nm.

SUPPORTING INFORMATION

The relationship between relative fluorescence intensity and irradiation time satisfies **Equation 1**:

$$\ln \left(\frac{I}{I_0} \right) = -k \cdot t \quad (\text{Equation 1})$$

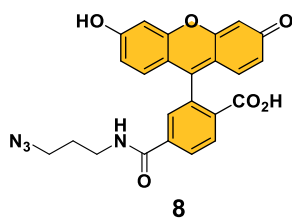
Where I = fluorescence intensity at a time t , I_0 = initial fluorescence intensity, k = photobleaching rate constant and t = irradiation time. The slope's absolute value of the linear fitting between $\ln \left(\frac{I}{I_0} \right)$ and t corresponds to the photobleaching rate constant (k). The fluorescence half-life time ($t_{1/2}$), therefore, was obtained following **Equation 2**:

$$t_{1/2} = \frac{\ln 2}{k} \quad (\text{Equation 2})$$

Calculation of pK_a values with Marvin. The software package Marvin (version 21.17.0, ChemAxon) was used for calculating the pK_a values of **RD_{H2}**, **RD_m** and **RD_{F2}** (<https://www.chemaxon.com>).

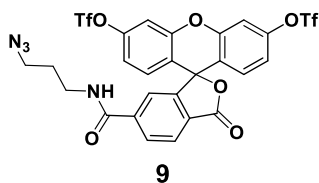
Nomenclature of synthesised fluorophores. Rhodamine dyes are named following the structure **RD_X**, where **RD** stands for rhodamine dye and **X** the substituent of the azetidine moiety (e.g. **RD_{F2}** corresponds to the rhodamine dye containing 4,4-difluoroazetidine groups). Fluorescein-based dendrons are abbreviated as **FD_n**, being **FD** fluorescein dendron and n the number of fluorescein substituents present in the dendritic scaffold (e.g. **FD4** corresponds to the dendron containing 4 fluorescein units). Rhodamine-based dendrons are named following the structure **(RD_X)D_n**, where **RD_X** is the type of rhodamine dye found in the scaffold, **D** stands for dendron, and n is the number of dye copies (e.g. **RD_{F2}D4** corresponds to the dendron containing 4 units of **RD_{F2}**).

2. Synthetic Procedures

**8****Chemical Formula:** C₂₄H₁₈N₄O₆**Molecular Weight:** 458.43

Fluorescein azide (8). A magnetically-stirred solution containing 6-carboxyfluorescein (**1**) (200 mg, 0.53 mmol, 1 eq) and *N,N'*-disuccinimidyl carbonate (DSC) (300 mg, 1.17 mmol, 2.2 eq) in DMF (8 mL) was treated with triethylamine (0.45 mL, 3.19 mmol, 6 eq) and then 4-dimethylaminopyridine (DMAP) (6.49 mg, 0.053 mmol, 0.1 eq), and the resulting mixture was maintained at room temperature for 1 h while shielded from light. After this time, 3-azidopropan-1-amine (133 mg, 1.33 mmol, 2.5 eq) was added and the reaction stirred an additional 2 h at room temperature. The crude product was subsequently concentrated *in vacuo*, dissolved in EtOAc (20 mL), and washed with aqueous KHSO₄ (1 M, 2 x 10 mL) and brine (10 mL). The combined organic extracts were dried over Na₂SO₄, filtered, and concentrated *in vacuo*. Purification by silica gel flash chromatography (9:1 CH₂Cl₂/MeOH v/v) afforded compound **8** (171 mg, 0.37 mmol, 70 %) as an orange solid.

R_f = 0.4 (SiO₂; CH₂Cl₂/MeOH, 9:1). **¹H NMR** (600 MHz, DMSO-*d*₆) δ 10.17 (br, 2H), 8.74 (t, *J* = 5.6 Hz, 1H), 8.17 (dd, *J* = 8.0, 1.4 Hz, 1H), 8.08 (d, *J* = 8.0 Hz, 1H), 7.67 (d, *J* = 1.3 Hz, 1H), 6.71 (d, *J* = 2.2 Hz, 2H), 6.59 (d, *J* = 8.7 Hz, 2H), 6.56 (dd, *J* = 8.7, 2.3 Hz, 2H), 3.35 (t, *J* = 6.7 Hz, 2H), 3.26 (app. q, *J* = 6.5 Hz, 2H), 1.72 (app. p, *J* = 6.8 Hz, 2H). **¹³C NMR** (151 MHz, DMSO-*d*₆) δ 168.2, 164.7, 159.8, 152.7, 151.9, 140.7, 129.5, 129.4, 128.3, 125.0, 122.3, 112.9, 109.2, 102.3, 83.6, 48.5, 36.9, 28.2. **IR** (ATR): $\tilde{\nu}$ (cm⁻¹) = 3326 (br), 3148 (br), 2100 (s), 1704 (vs), 1644 (m), 1631 (m), 1612 (s), 1588 (s), 1554 (s), 1505 (s), 1463 (s), 1363 (m), 1342 (m), 1318 (w), 1292 (w), 1273 (m), 1248 (vs), 1232 (vs), 1191 (vs), 1176 (s), 1149 (s), 1108 (s), 1014 (w), 998 (m), 977 (w), 950 (w), 925 (w), 852 (s), 838 (s), 797 (m), 753 (m), 717 (w), 691 (m), 672 (m). **HRMS** (ESI): *m/z* calcd for C₂₄H₁₉N₄O₆⁺ [M+H]⁺: 459.1305, found: 459.1299.

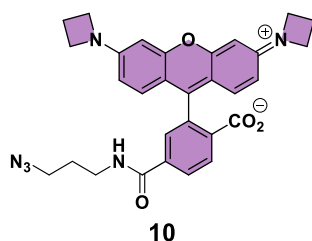


Chemical Formula: C₂₆H₁₆F₆N₄O₁₀S₂

Molecular Weight: 722.54

Fluorescein azide ditriflate (9). Fluorescein azide (**8**) (1.00 g, 2.18 mmol, 1 eq) was suspended in CH₂Cl₂ (12.5 mL) and cooled to 0 °C under a positive pressure of Ar. Pyridine (2.6 mL, 32.7 mmol, 15 eq) and trifluoromethanesulfonic anhydride (2.75 mL, 16.4 mmol, 7.5 eq) were added, the ice bath removed, and the reaction stirred at room temperature overnight. The crude mixture was subsequently diluted with H₂O (75 mL) and extracted with CH₂Cl₂ (3 x 75 mL). The combined organic extracts were washed with CuSO₄ (100 mL of a sat. aq. solution) and brine (100 mL), dried with MgSO₄, filtered, and concentrated *in vacuo*. Purification by silica gel flash chromatography (CH₂Cl₂:MeOH 197:3 → 195:5) afforded compound **9** (1.28 g, 1.77 mmol, 81 %) as a pale-yellow powder.

R_f = 0.4 (SiO₂; CH₂Cl₂/MeOH, 98:2). **¹H NMR** (400 MHz, CD₃OD) δ 8.16 (dd, *J* = 8.1, 1.4 Hz, 1H), 8.13 (d, *J* = 8.1 Hz, 1H), 7.67 (s, 1H), 7.52 (d, *J* = 2.5 Hz, 2H), 7.17 (dd, *J* = 8.9, 2.5 Hz, 2H), 7.10 (d, *J* = 8.8 Hz, 2H), 3.35 (t, *J* = 6.8 Hz, 2H), 3.30 (t, *J* = 5.7 Hz, 2H), 1.76 (app. p, *J* = 6.8 Hz, 2H). **¹³C NMR** (101 MHz, CD₃OD) δ 169.3, 168.0, 154.0, 152.7, 151.9, 143.0, 131.7, 131.2, 129.2, 126.8, 123.8, 120.4, 120.1 (q, ¹*J*_{CF} = 319.9 Hz), 119.1, 112.1, 81.7, 50.1, 38.6, 29.5. **¹⁹F NMR** (377 MHz, CD₃OD) δ -73.1 (s). **IR** (ATR): $\tilde{\nu}$ (cm⁻¹) = 3318 (br), 3076 (w), 2925 (w), 2095 (s), 1772 (s), 1645 (m), 1607 (m), 1539 (m), 1487 (m), 1419 (vs), 1207 (vs), 1136 (vs), 1104 (vs), 985 (vs), 939 (s), 851 (vs), 826 (s), 745 (w), 718 (m). **HRMS** (ESI): *m/z* calcd for C₂₆H₁₇F₆N₄O₁₀S₂⁺ [M+H]⁺: 723.0290, found: 723.0289.



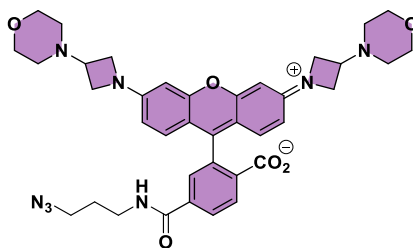
10

Chemical Formula: C₃₀H₂₈N₆O₄

Molecular Weight: 536.59

Rhodamine dye RD_{H2} (10). A heavy-walled sealable pressure tube was charged with fluorescein azide ditriflate (**9**) (100 mg, 0.138 mmol, 1 eq), azetidinium hydrochloride (130 mg, 1.39 mmol, 10 eq), Pd₂(dba)₃ (25 mg, 27.3 μmol, 0.2 eq), XPhos (40 mg, 84.0 μmol, 0.6 eq), and Cs₂CO₃ (902 mg, 2.77 mmol, 20 eq). The reaction vessel was sealed, evacuated, and backfilled with Ar (x3). Dioxane (3 mL) was added, and the reaction was magnetically stirred at 100 °C for 4 h. The crude mixture was subsequently filtered, and the residue washed with dioxane (20 mL). After concentration of the filtrate *in vacuo*, the crude product was precipitated *via* dissolution in the minimum volume of CH₂Cl₂, followed by dropwise addition of the mixture to hexane/MeOH (100 mL of a 95 % v/v solution) and storage at 4 °C overnight. The supernatant was removed by centrifugation, and the precipitate dried *in vacuo*. The crude material was subjected to further rounds of precipitation (x2) according to the same procedure, without storage at 4 °C. Purification of the solid by basic alumina flash chromatography (CH₂Cl₂/MeOH 1:0 → 93:7 v/v) afforded **RD_{H2} (10)** (31 mg, 0.058 mmol, 42 %) as a dark, purple solid. A small quantity of the chromatographed material (15 mg) was further subjected to RP-HPLC (30–80 % v/v MeCN/H₂O in 1 h, 5 mL/min, room temperature) to obtain an analytically pure sample for photophysical characterisation.

R_f = 0.4 (SiO₂; CH₂Cl₂/MeOH, 85:15). **¹H NMR** (800 MHz, CD₃OD) δ 8.11 (dd, *J* = 8.2, 0.5 Hz, 1H), 8.06 (dd, *J* = 8.1, 1.8 Hz, 1H), 7.67 (dd, *J* = 1.8, 0.5 Hz, 1H), 7.17 (d, *J* = 9.2 Hz, 2H), 6.56 (dd, *J* = 9.2, 2.2 Hz, 2H), 6.49 (d, *J* = 2.2 Hz, 2H), 4.27 (t, *J* = 7.5 Hz, 8H), 3.45 (t, *J* = 6.8 Hz, 2H), 3.40 (t, *J* = 6.7 Hz, 2H), 2.54 (p, *J* = 7.4 Hz, 4H), 1.86 (app. p, *J* = 6.7 Hz, 2H). **¹³C NMR** (201 MHz, CD₃OD) δ 172.5, 168.7, 161.8, 158.9, 158.0, 144.5, 136.3, 134.1, 132.9, 131.0, 129.6, 129.3, 115.0, 113.1, 95.0, 52.7, 50.2, 38.6, 29.7, 16.8. **IR** (ATR): $\tilde{\nu}$ (cm⁻¹) = 3260 (br), 2928 (s), 2857 (s), 2094 (s), 1751 (w), 1592 (vs), 1550 (s), 1532 (s), 1467 (s), 1408 (s), 1377 (vs), 1343 (s), 1296 (s), 1255 (vs), 1221 (s), 1181 (s), 1137 (s), 1113 (s), 1068 (s), 1029 (vs), 971 (w), 928 (w), 818 (s), 754 (w), 697 (w). **HRMS** (ESI): *m/z* calcd for C₃₀H₂₉N₆O₄⁺ [M+H]⁺: 537.2250, found: 537.2248.



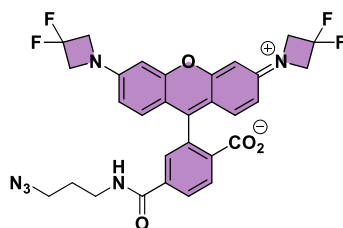
11

Chemical Formula: C₃₈H₄₂N₈O₆

Molecular Weight: 706.80

Rhodamine dye RD_m (11). A heavy-walled sealable pressure tube was charged with fluorescein ditriflate (**9**) (100 mg, 0.138 mmol, 1 eq), 4-(azetidin-3-yl)morpholine hydrochloride (247 mg, 1.38 mmol, 10 eq), Pd₂(dba)₃ (25 mg, 27.3 μmol, 0.2 eq), XPhos (40 mg, 84.0 μmol, 0.6 eq) and Cs₂CO₃ (902 mg, 2.77 mmol, 20 eq). The reaction vessel was sealed, evacuated, and backfilled with Ar (x3). Dioxane (3 mL) was added, and the reaction was then stirred at 100 °C for 4 h. The crude mixture was subsequently filtered, and the residue washed with dioxane (20 mL). After concentration of the filtrate *in vacuo*, the crude product was precipitated *via* dissolution in the minimum volume of CH₂Cl₂, followed by dropwise addition of the mixture to ¹hexane/MeOH (100 mL of a 95 % v/v solution) and storage at 4 °C overnight. The supernatant was removed by centrifugation, and the precipitate dried *in vacuo*. The crude material was subjected to further rounds of precipitation (x2) according to the same procedure, without storage at 4 °C. Purification of the solid by basic alumina flash chromatography (CH₂Cl₂:MeOH 1:0 → 9:1 v/v) afforded **RD_m (11)** (59 mg, 0.083 mmol, 60 %) as a purple solid. A small quantity of the chromatographed material (15 mg) was further subjected to RP-HPLC (0-80 % v/v MeCN/H₂O in 30 min, 5 mL/min, room temperature) to obtain an analytically pure sample for photophysical characterisation.

R_f = 0.4 (SiO₂; CH₂Cl₂/MeOH, 95:5). **¹H NMR** (800 MHz, CD₃OD) δ 8.13 (d, *J* = 8.2 Hz, 1H), 8.07 (dd, *J* = 8.2, 1.8 Hz, 1H), 7.67 (d, *J* = 1.8 Hz, 1H), 7.19 (d, *J* = 9.2 Hz, 2H), 6.62 (dd, *J* = 9.2, 2.2 Hz, 2H), 6.57 (d, *J* = 2.2 Hz, 2H), 4.34 – 4.24 (m, 4H), 4.15 – 4.08 (m, 4H), 3.46 (t, *J* = 6.8 Hz, 2H), 3.40 (t, *J* = 6.6 Hz, 2H), 2.50 (br, 8H), 1.87 (app. p, *J* = 6.7 Hz, 2H). **¹³C NMR** (201 MHz, CD₃OD) δ 172.3, 168.7, 159.5, 158.7, 157.8, 143.9, 136.6, 134.5, 133.0, 130.9, 129.4, 129.3, 115.1, 113.3, 95.6, 67.5, 56.1, 55.7, 51.1, 50.2, 38.6, 29.7. **IR** (ATR): $\tilde{\nu}$ (cm⁻¹) = 3304 (br), 2923 (s), 2851 (s), 2095 (s), 1754 (s), 1632 (w), 1594 (vs), 1552 (w), 1513 (w), 1481 (w), 1450 (w), 1428 (w), 1407 (w), 1377 (s), 1341 (w), 1320 (w), 1293 (s), 1270 (w), 1245 (w), 1215 (w), 1185 (s), 1139 (w), 1111 (vs), 1067 (w), 965 (w), 926 (w), 888 (w), 864 (w), 820 (s), 750 (w), 716 (w), 691 (w). **HRMS** (ESI): *m/z* calcd for C₃₈H₄₃N₈O₆⁺ [M+H]⁺: 707.3306, found: 707.3301.



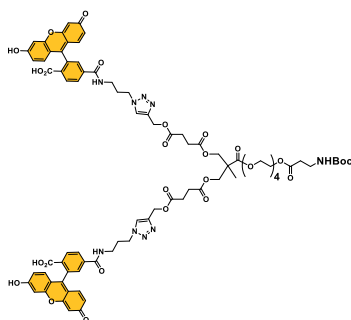
12

Chemical Formula: $C_{30}H_{24}F_4N_6O_4$

Molecular Weight: 608.55

Rhodamine dye RD_{F_2} (12). A heavy-walled sealable pressure tube was charged with fluorescein ditriflate (**9**) (100 mg, 0.138 mmol, 1 eq), 4,4-difluoroazetidinium hydrochloride (179 mg, 1.38 mmol, 10 eq), $Pd_2(dba)_3$ (25 mg, 0.027 mmol, 0.2 eq), XPhos (40 mg, 0.084 mmol, 0.6 eq) and Cs_2CO_3 (902 mg, 2.77 mmol, 20 eq). The reaction vessel was sealed, evacuated, and backfilled with Ar (x3). Dioxane (3 mL) was added, and the reaction was then stirred at 100 °C for 4 h. The crude mixture was subsequently filtered, and the residue washed with dioxane (20 mL). After concentration of the filtrate *in vacuo*, the crude product was precipitated *via* dissolution in the minimum volume of CH_2Cl_2 , followed by dropwise addition of the mixture to ¹hexane/MeOH (100 mL of a 95 % v/v solution) and storage at 4 °C overnight. The supernatant was removed by centrifugation, and the precipitate dried *in vacuo*. The crude material was subjected to further rounds of precipitation (x2) according to the same procedure, without storage at 4 °C, to afford RD_{F_2} (**12**) (62 mg, 0.10 mmol, 74 %) as a purple solid. A small quantity of the chromatographed material (15 mg) was further subjected to RP-HPLC (30–80 % v/v MeCN/ H_2O in 1 h, 5 mL/min, room temperature) to obtain an analytically pure sample for photophysical characterisation.

R_f = 0.5 (SiO₂; CH_2Cl_2 /MeOH, 8:2). **¹H NMR** (800 MHz, CD_3OD) δ 8.11 (dd, J = 8.1, 1.4 Hz, 1H), 8.08 (d, J = 8.1 Hz, 1H), 7.59 (d, J = 1.7 Hz, 1H), 6.71 (d, J = 8.6 Hz, 2H), 6.46 (d, J = 2.4 Hz, 2H), 6.36 (dd, J = 8.7, 2.4 Hz, 2H), 4.31 (t, J = 11.5 Hz, 8H), 3.38 (t, J = 6.8 Hz, 2H), 3.34 (t, J = 6.6 Hz, 2H), 1.80 (app. p, J = 6.8 Hz, 2H). **¹³C NMR** (201 MHz, CD_3OD) δ 170.8, 168.3, 154.5, 153.9, 152.2, 141.5, 132.2, 130.5, 130.2, 126.8, 124.7, 117.3 (t, $^1J_{CF}$ = 272.7 Hz), 110.9, 110.7, 100.0, 96.8, 64.2 (t, $^2J_{CF}$ = 26.6 Hz), 50.2, 38.6, 29.6. **¹⁹F NMR** (377 MHz, CD_3OD) δ -100.1 (p, $^3J_{FH}$ = 11.8 Hz). **IR** (ATR): $\tilde{\nu}$ (cm^{-1}) = 3321 (br), 2928 (w), 2862 (w), 2095 (s), 1754 (s), 1632 (m), 1610 (s), 1553 (m), 1511 (s), 1462 (m), 1429 (s), 1370 (s), 1352 (m), 1318 (s), 1295 (m), 1270 (m), 1222 (vs), 1124 (s), 1086 (s), 960 (w), 906 (s), 857 (w), 821 (w), 810 (w), 750 (w), 725 (s), 664 (s), 664 (s). **HRMS** (ESI): m/z calcd for $C_{30}H_{25}F_4N_6O_4^+$ [M+H]⁺: 609.1873, found: 609.1877.



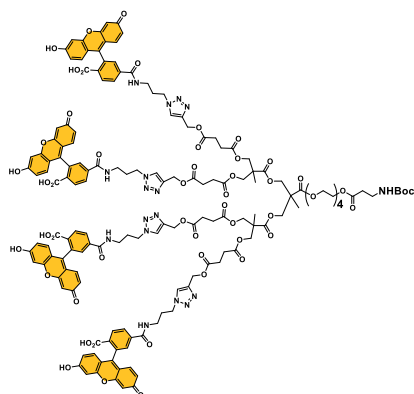
13

Chemical Formula: $C_{83}H_{87}N_9O_{29}$

Molecular Weight: 1674.64

Dendritic dye FD2 (13). A Schlenk tube was charged with bis-MPA Acetylene Dendron, NH-Boc Core, Generation 1 (50 mg, 0.066 mmol, 1 eq), fluorescein azide (**8**) (121 mg, 0.264 mmol, 4 eq), CuBr (9 mg, 0.06 mmol, 0.9 eq) and *N,N,N',N'',N'''*-pentamethyldiethylenetriamine (PMDTA) (27.8 μ L, 0.132 mmol, 2 eq) under a positive pressure of Ar. Anhydrous DMSO (0.5 mL) was added, and the reaction mixture was stirred for 2 h at 50 °C. After cooling to room temperature, the crude reaction mixture was subjected to dialysis (1 KDa MWCO) against DMSO for 72 h and then against DI H₂O for 24 h according to the procedure specified in the General Experimental Methods section. Concentration of the dialysed solution *in vacuo* afforded **FD2 (7)** (67 mg, 0.040 mmol, 61 %) as an orange solid.

R_t = 5.94 min (Analytical RP-HPLC; 1.5 mL/min, 40 °C, buffer B 0-30 % v/v 0 \rightarrow 4 min, then 30-85 % v/v 4 \rightarrow 10 min). **¹H NMR** (800 MHz, DMSO-*d*₆) δ 10.36 (br, 4H), 8.75 (s, 2H), 8.14 (br, 6H), 7.69 (br, 2H), 6.82 (t, J = 5.6 Hz, 1H), 6.77 – 6.17 (m, 12H), 5.08 (s, 4H), 4.37 (s, 4H), 4.21 – 4.06 (m, 8H), 3.60 – 3.55 (m, 4H), 3.52 – 3.47 (m, 8H), 3.23 (br, 4H), 3.14 (app. q, J = 6.5 Hz, 2H), 2.56 (s, 8H), 2.42 (t, J = 7.1 Hz, 2H), 2.03 (br, 4H), 1.35 (s, 9H), 1.13 (s, 3H). **¹³C NMR** (201 MHz, DMSO-*d*₆) δ 172.2, 171.7, 171.4, 171.2, 164.8, 155.4, 141.6, 129.2, 124.8, 111.6, 102.4, 77.7, 69.7, 68.2, 68.1, 65.1, 64.0, 63.2, 57.4, 47.4, 45.9, 36.7, 36.1, 34.1, 29.6, 28.5, 28.4, 28.2, 17.1. **IR (ATR):** $\tilde{\nu}$ (cm⁻¹) = 3279 (br), 2962 (w), 1737 (vs), 1640 (m), 1591 (s), 1506 (m), 1461 (s), 1385 (m), 1316 (m), 1250 (vs), 1209 (s), 1174 (vs), 1108 (vs), 1027 (m), 851 (s), 808 (s), 759 (w), 662 (w). **MS (MALDI-ToF):** m/z calcd for $C_{83}H_{87}N_9NaO_{29}^+$ [M+Na]⁺: 1696.5502 (monoisotopic mass), 1697.6322 (molecular weight), found: 1697.9.

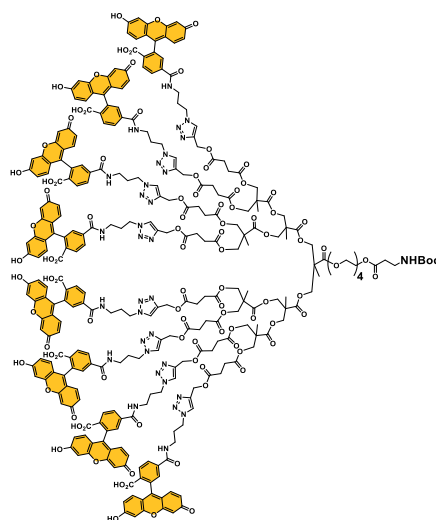


14

Chemical Formula: C₁₅₅H₁₅₁N₁₇O₅₃
Molecular Weight: 3099.98

Dendritic dye FD4 (14). A Schlenk tube was charged with bis-MPA Acetylene Dendron, NH-Boc Core, Generation 2 (50 mg, 0.040 mmol, 1 eq), fluorescein azide (**8**) (145 mg, 0.316 mmol, 8 eq), CuBr (11 mg, 0.077 mmol, 1.9 eq) and *N,N,N',N'',N'''*-pentamethyldiethylenetriamine (PMDTA) (33.0 μ L, 0.158 mmol, 4 eq) under a positive pressure of Ar. Anhydrous DMSO (0.5 mL) was added, and the reaction mixture was stirred for 2 h at 50 °C. After cooling to room temperature, the crude reaction mixture was subjected to dialysis (1 KDa MWCO) against DMSO for 72 h and then against DI H₂O for 24 h according to the procedure specified in the General Experimental Methods section. Concentration of the dialysed solution *in vacuo* afforded **FD4 (14)** (82 mg, 0.026 mmol, 67 %) as an orange solid.

R_t = 5.88 min (Analytical RP-HPLC; buffer B 0-30 % v/v 0 \rightarrow 4 min, then 30-85 % v/v 4 \rightarrow 10 min). **¹H NMR** (800 MHz, DMSO-*d*₆) δ 10.50 (s, 8H), 8.77 (s, 4H), 8.60 – 7.88 (m, 12H), 7.85 – 7.40 (m, 4H), 6.81 (t, *J* = 5.6 Hz, 1H), 6.78 – 6.27 (m, 24H), 5.07 (s, 8H), 4.36 (t, *J* = 6.9 Hz, 8H), 4.25 – 4.04 (m, 16H), 3.58 (t, *J* = 4.9 Hz, 2H), 3.56 (t, *J* = 4.8 Hz, 2H), 3.53 – 3.44 (m, 8H), 3.27 – 3.18 (m, 8H), 3.13 (q, *J* = 6.7 Hz, 2H), 2.54 (s, 16H), 2.41 (t, *J* = 7.0 Hz, 2H), 2.02 (app. p, *J* = 7.4 Hz, 8H), 1.34 (s, 9H), 1.18 (s, 3H), 1.11 (s, 6H). **¹³C NMR** (201 MHz, DMSO-*d*₆) δ 172.0, 171.7, 171.6, 171.4, 171.2, 164.9, 155.4, 152.5, 141.5, 139.6, 129.3 (br, x2), 124.8, 123.1, 114.1, 109.5, 102.4, 77.7, 69.7, 68.2, 68.0, 65.5, 65.1, 64.1, 63.2, 57.4, 47.4, 46.1, 46.0, 36.7, 36.1, 34.1, 29.6, 28.4, 28.3, 28.2, 17.0, 16.9. **IR** (ATR): $\tilde{\nu}$ (cm⁻¹) = 3289 (br), 2927 (w), 1737 (vs), 1639 (m), 1591 (vs), 1506 (s), 1462 (vs), 1383 (s), 1318 (s), 1248 (vs), 1208 (vs), 1157 (vs), 1108 (vs), 1053 (w), 1028 (w), 995 (w), 968 (w), 921 (w), 850 (s), 808 (w), 758 (m), 717 (w), 663 (w). **MS (MALDI-ToF)**: *m/z* calcd for C₁₅₅H₁₅₁N₁₇NaO₅₃⁺ [M+Na]⁺: 3120.9535 (monoisotopic mass), 3122.9682 (molecular weight), found: 3121.9.

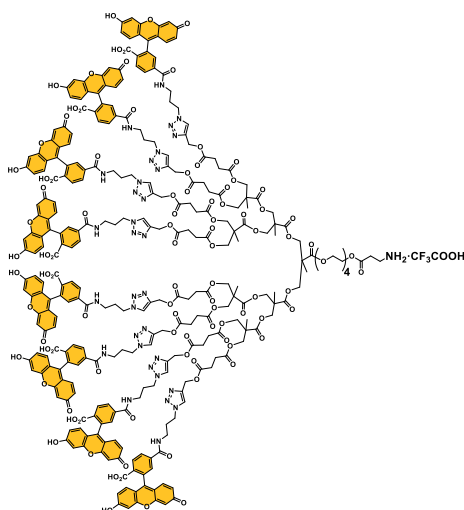


15

Chemical Formula: $C_{299}H_{279}N_{33}O_{101}$
Molecular Weight: 5950.65

Dendritic dye FD8 (15). A Schlenk tube was charged with bis-MPA Acetylene Dendron, NH-Boc Core, Generation 3 (47 mg, 0.021 mmol, 1 eq), fluorescein azide (**8**) (154 mg, 0.336 mmol, 16 eq), CuBr (12 mg, 0.084 mmol, 4 eq) and *N,N,N',N'',N'''*-pentamethyldiethylenetriamine (PMDTA) (34.2 μ L, 0.164 mmol, 8 eq) under a positive pressure of Ar. Anhydrous DMSO (0.5 mL) was added, and the reaction mixture was stirred for 2 h at 50 °C. After cooling to room temperature, the crude reaction mixture was subjected to dialysis (3.5 KDa MWCO) against DMSO for 24 h and then against DI H₂O for 24 h according to the procedure specified in the General Experimental Methods section. Concentration of the dialysed solution *in vacuo* afforded **FD8 (15)** (50 mg, 8.4 μ mol, 40 %) as a yellow solid.

R_f = 5.64 min (Analytical RP-HPLC; 1.5 mL/min, 40 °C, buffer B 0-30 % v/v 0 \rightarrow 4 min, then 30-85 % v/v 4 \rightarrow 10 min). **¹H NMR** (800 MHz, DMSO-*d*₆) δ 10.17 (s, 16H), 8.75 (t, *J* = 5.6 Hz, 8H), 8.15 (dd, *J* = 8.1, 1.4 Hz, 8H), 8.10 (s, 8H), 8.06 (d, *J* = 8.1 Hz, 8H), 7.67 (s, 8H), 6.77 (t, *J* = 5.7 Hz, 1H), 6.68 (d, *J* = 2.4 Hz, 16H), 6.58 (d, *J* = 8.6 Hz, 16H), 6.54 (dd, *J* = 8.7, 2.4 Hz, 16H), 5.05 (s, 16H), 4.34 (t, *J* = 7.1 Hz, 16H), 4.26 – 4.03 (m, 32H), 3.60 – 3.56 (m, 2H), 3.55 – 3.52 (m, 2H), 3.51 – 3.42 (m, 8H), 3.20 (app. q, *J* = 6.5 Hz, 16H), 3.12 (q, *J* = 6.7 Hz, 2H), 2.52 (s, 32H), 2.39 (t, *J* = 7.0 Hz, 2H), 2.00 (app. p, *J* = 7.0 Hz, 16H), 1.31 (s, 9H), 1.20 (s, 3H), 1.17 (s, 6H), 1.10 (s, 12H). **¹³C NMR** (201 MHz, DMSO-*d*₆) δ 171.9, 171.7, 171.6, 171.4, 171.2, 168.0, 164.7, 159.8, 155.4, 152.4, 151.9, 141.5, 140.5, 129.4, 129.3, 128.5, 124.9, 124.8, 122.3, 112.9, 109.2, 102.3, 77.7, 69.7, 69.6, 68.2, 68.0, 65.1, 65.0, 64.1, 63.2, 57.3, 47.4, 46.2, 46.1, 46.0, 36.8, 36.0, 34.1, 29.6, 28.3, 28.3, 28.1, 17.0, 16.9, 16.8. **IR** (ATR): $\tilde{\nu}$ (cm⁻¹) = 3260 (br), 2922 (s), 2852 (m), 1734 (vs), 1635 (m), 1610 (s), 1543 (m), 1506 (m), 1450 (s), 1368 (m), 1315 (m), 1239 (s), 1175 (vs), 1152 (vs), 1110 (vs), 994 (s), 949 (w), 847 (s), 822 (m), 752 (m), 688 (m). **MS (MALDI-ToF):** *m/z* calcd for $C_{299}H_{279}N_{33}NaO_{101}^+$ [M+Na]⁺: 5969.7602 (monoisotopic mass), 5973.6402 (molecular weight), found: 5970.0. *m/z* calcd for $C_{299}H_{278}N_{33}Na_2O_{101}^+$ [M-H+2Na]⁺: 5991.7427 (monoisotopic mass), 5995.6225 (molecular weight), found: 5991.5.



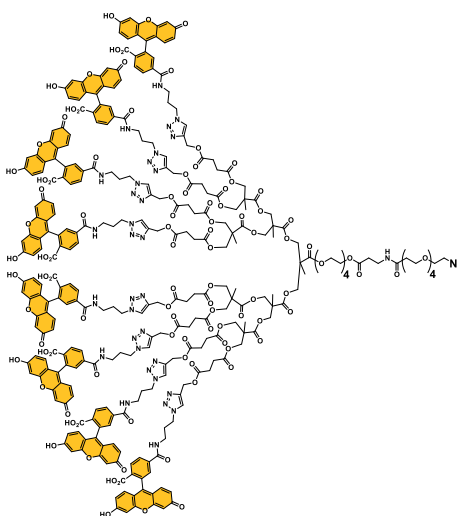
15b

Chemical Formula: C₂₉₆H₂₇₂F₃N₃₃O₁₀₁

Molecular Weight: 5964.56

Dendritic dye 15b. Dendritic dye **FD8 (15)** (15 mg, 2.5 μ mol) was suspended in *neat* trifluoroacetic acid (18 μ L) and the resulting mixture was maintained at room temperature for 2 h with vigorous stirring. After this time, the reaction mixture was subjected to successive strip cycles (x3) by addition and evaporation of methanol *in vacuo* to afford **15b** (15 mg, 2.5 μ mol, quant.) as a yellow solid.

R_t = 5.23 min (Analytical RP-HPLC; 1.5 mL/min, 40 °C, buffer B 0-30 % v/v 0 \rightarrow 4 min, then 30-85 % v/v 4 \rightarrow 10 min). $^1\text{H NMR}$ (800 MHz, DMSO-*d*₆) δ 10.16 (s, 16H), 8.75 (t, J = 5.5 Hz, 8H), 8.15 (dd, J = 8.1, 1.4 Hz, 8H), 8.11 (s, 8H), 8.06 (d, J = 8.2 Hz, 8H), 7.71 (br, 3H), 7.66 (s, 8H), 6.69 (d, J = 2.4 Hz, 16H), 6.58 (d, J = 8.7 Hz, 16H), 6.54 (dd, J = 8.7, 2.4 Hz, 16H), 5.05 (s, 16H), 4.34 (t, J = 7.1 Hz, 16H), 4.25 – 4.02 (m, 32H), 3.60 – 3.54 (m, 4H), 3.52 – 3.42 (m, 8H), 3.20 (app. q, J = 6.4 Hz, 16H), 3.02 (app. h, J = 6.3 Hz, 2H), 2.64 (t, J = 6.9 Hz, 2H), 2.54 – 2.51 (m, 32H), 2.00 (app. p, J = 7.0 Hz, 16H), 1.23 (s, 3H), 1.17 (d, J = 5.2 Hz, 6H), 1.10 (s, 12H). $^{13}\text{C NMR}$ (201 MHz, DMSO-*d*₆) δ 171.7, 171.6, 171.4, 170.4, 168.0, 164.7, 159.6, 157.9, 152.7, 151.8, 141.5, 140.6, 129.4, 129.3, 128.2, 124.8, 124.8, 122.3, 112.7, 109.1, 102.2, 83.3, 69.6, 68.1, 68.0, 65.1, 65.0, 63.8, 57.3, 47.4, 46.2, 46.1, 46.0, 36.8, 34.7, 31.3, 29.6, 28.3, 28.3, 17.0, 16.9, 16.8. **IR** (ATR): $\tilde{\nu}$ (cm⁻¹) = 3430 (br), 3186 (br), 2924 (s), 2850 (m), 2158 (w), 1731 (s), 1652 (s), 1606 (s), 1505 (w), 1453 (m), 1378 (w), 1314 (w), 1240 (m), 1177 (vs), 1128 (vs), 992 (m), 841 (m), 803 (m), 759 (w), 749 (w), 720 (m), 685 (w). **MS (MALDI-ToF)**: m/z calcd for C₂₉₄H₂₇₁N₃₃NaO₉₉⁺ [M-H+Na]⁺: 5869.7083 (monoisotopic mass), 5873.5238 (molecular weight), found: 5870.1. m/z calcd for C₂₉₄H₂₇₀N₃₃Na₂O₉₉⁺ [M-2H+2Na]⁺: 5891.6897 (monoisotopic mass), 5895.5050 (molecular weight), found: 5891.4.



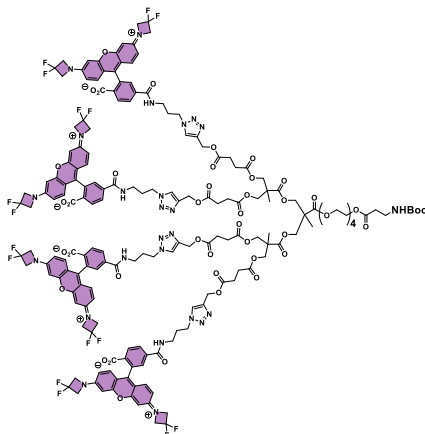
16

Chemical Formula: $C_{305}H_{290}N_{36}O_{104}$

Molecular Weight: 6123.82

Dendritic dye FD8-N₃ (16). Dendritic dye **15b** (10 mg, 1.7 μ mol, 1 eq) was dissolved in DMF (100 μ L). Triethylamine (1.2 μ L, 8.4 μ mmol, 5 eq) and azido-PEG4-NHS ester (1.3 mg, 3.4 μ mol, 2 eq) were added and the resulting mixture was maintained at room temperature for 1 h with vigorous stirring. After this time, the crude reaction mixture was concentrated *in vacuo*, dissolved in the minimum amount of DMSO and subjected to dialysis (3.5 KDa MWCO) against DI H₂O for 48 h according to the procedure specified in the General Experimental Methods section. Concentration of the dialysed solution *in vacuo* afforded **FD8-N₃ (16)** (7 mg, 1 μ mol, 67 %) as an orange solid.

R_t = 5.55 min (Analytical RP-HPLC; 1.5 mL/min, 40 °C, buffer B 0-30 % v/v 0 \rightarrow 4 min, then 30-85 % v/v 4 \rightarrow 10 min). **¹H NMR** (800 MHz, DMSO-*d*₆) δ 10.18 (s, 16H), 8.74 (t, J = 5.6 Hz, 8H), 8.14 (dd, J = 8.0, 1.4 Hz, 8H), 8.09 (s, 8H), 8.05 (d, J = 8.1 Hz, 8H), 7.88 (t, J = 5.7 Hz, 1H), 7.66 (s, 8H), 6.68 (d, J = 2.4 Hz, 16H), 6.58 (d, J = 8.6 Hz, 16H), 6.54 (dd, J = 8.6, 2.5 Hz, 16H), 5.04 (s, 16H), 4.33 (t, J = 6.8 Hz, 16H), 4.25 – 3.98 (m, 32H), 3.64 – 3.31 (m, 30H), 3.23 (app. q, J = 6.7 Hz, 2H), 3.20 (q, J = 6.5 Hz, 16H), 2.54 – 2.46 (m, 34H), 2.25 (t, J = 6.5 Hz, 2H), 2.00 (app. p, J = 7.0 Hz, 16H), 1.19 (s, 3H), 1.16 (s, 6H), 1.09 (s, 12H). **¹³C NMR** (201 MHz, DMSO-*d*₆) δ 171.8, 171.7, 171.5, 171.4, 170.3, 168.1, 164.8, 159.7, 152.7, 151.9, 141.6, 140.7, 129.7, 129.5, 129.3, 128.3, 124.9, 124.8, 122.3, 112.8, 109.2, 102.3, 83.4, 69.8 (x2), 69.8, 69.7 (x2), 69.6, 69.3, 68.2, 68.0, 66.8, 65.2, 65.0, 63.3, 57.4, 50.0, 47.4, 46.2 (x2), 46.1, 36.8, 29.6, 28.4 (x2), 17.1, 17.0, 16.9. **IR** (ATR): $\tilde{\nu}$ (cm⁻¹) = 3130 (br), 2923 (m), 2853 (w), 2357 (w), 2251 (w), 2110 (w), 1734 (vs), 1634 (m), 1610 (s), 1545 (m), 1507 (m), 1451 (s), 1368 (w), 1242 (s), 1177 (vs), 1150 (vs), 1110 (vs), 1084 (m), 1045 (m), 1023 (s), 993 (vs), 848 (m), 818 (s), 757 (m), 688 (w), 674 (w), 688 (w). **MS (MALDI-ToF)**: m/z calcd for $C_{305}H_{290}N_{36}NaO_{104}^+$ [M+Na]⁺: 6142.8403 (monoisotopic mass), 6146.8122 (molecular weight), found: 6145.6. m/z calcd for $C_{305}H_{289}N_{36}Na_2O_{104}^+$ [M-H+2Na]⁺: 6164.8222 (monoisotopic mass), 6148.7940 (molecular weight), found: 6167.1.



17

Chemical Formula: $C_{179}H_{175}F_{16}N_{25}O_{45}$

Molecular Weight: 3700.47

Dendritic dye $RD_{F_2}D_4$ (17). A vial was charged with bis-MPA Acetylene Dendron, Generation 2 (5 mg, 4 μ mol, 1 eq), dye RD_{F_2} (12) (14 mg, 23 μ mol, 5.8 eq), CuBr (1.1 mg, 7.9 μ mol, 2 eq) and *N,N,N',N'',N'''*-pentamethyldiethylenetriamine (PMDTA) (3.3 μ L, 15.8 μ mol, 4 eq) under Ar atmosphere. After dissolution with 300 μ L of anhydrous DMF, the reaction mixture was stirred for 2 h at 50 $^{\circ}$ C. The crude was then purified by size exclusion chromatography (Sephadex LH-20, DMF) to yield $RD_{F_2}D_4$ (17) (12 mg, 3.2 μ mol, 85 %) as a pink solid.

R_f = 0.6 (SiO₂; EtOAc/MeOH, 8:2). **1H NMR** (600 MHz, DMSO-*d*₆) δ 8.76 (s, 4H), 8.16 (d, J = 6.6 Hz, 4H), 8.11 (s, 4H), 8.08 (d, J = 8.1 Hz, 4H), 7.62 (s, 4H), 6.80 (s, 1H), 6.62 (dd, J = 8.6, 2.3 Hz, 8H), 6.46 (s, 8H), 6.31 (d, J = 8.6, 8H), 5.07 (s, 8H), 4.40 – 4.27 (m, 40H), 4.22 – 4.06 (m, 16H), 3.64 – 3.53 (m, 4H), 3.49 (t, J = 9.0 Hz, 8H), 3.23 – 3.20 (m, 8H), 3.16 – 3.11 (m, 2H), 2.54 (s, 16H), 2.42 (t, J = 7.0 Hz, 2H), 2.01 (t, J = 7.0 Hz, 8H), 1.34 (s, 9H), 1.18 (s, 3H), 1.12 (s, 6H). **^{13}C NMR** (151 MHz, DMSO-*d*₆) δ 172.0, 171.7, 171.6, 171.4, 171.2, 168.1, 164.7, 155.4, 152.7, 151.6, 141.5, 140.5, 128.9, 128.3, 124.9, 124.8, 122.2, 116.5 (t, $^1J_{CF}$ = 273.1 Hz), 109.6, 108.3, 99.2, 83.5, 77.7, 69.7, 68.2, 68.0, 65.1, 64.1, 63.2, 62.9 (t, $^2J_{CF}$ = 25.3 Hz), 57.3, 47.3, 46.1, 36.7, 36.0, 34.1, 29.6, 28.3, 28.2, 17.0, 16.9. **^{19}F NMR** (377 MHz, DMSO-*d*₆) δ -101.6 (p, $^3J_{FH}$ = 12.9 Hz). **IR** (ATR): $\tilde{\nu}$ (cm⁻¹) = 3353 (br), 2954 (s), 2921 (vs), 2851 (vs), 2364 (w), 1738 (s), 1634 (w), 1613 (s), 1514 (m), 1463 (s), 1429 (w), 1377 (s), 1320 (w), 1270 (m), 1230 (s), 1087 (w), 965 (w), 910 (m), 830 (w), 727 (m). **MS (MALDI-ToF)**: m/z calcd for $C_{179}H_{175}N_{25}O_{45}^+$ [M+H]⁺: 3699.1991 (monoisotopic mass), 3701.4809 (molecular weight), found: 3702.7; m/z calcd for $C_{179}H_{175}N_{25}NaO_{45}^+$ [M+Na]⁺: 3721.1811 (monoisotopic mass), 3723.4627 (molecular weight), found: 3724.7.

3. Photophysical Properties of the Synthesised Fluorophores

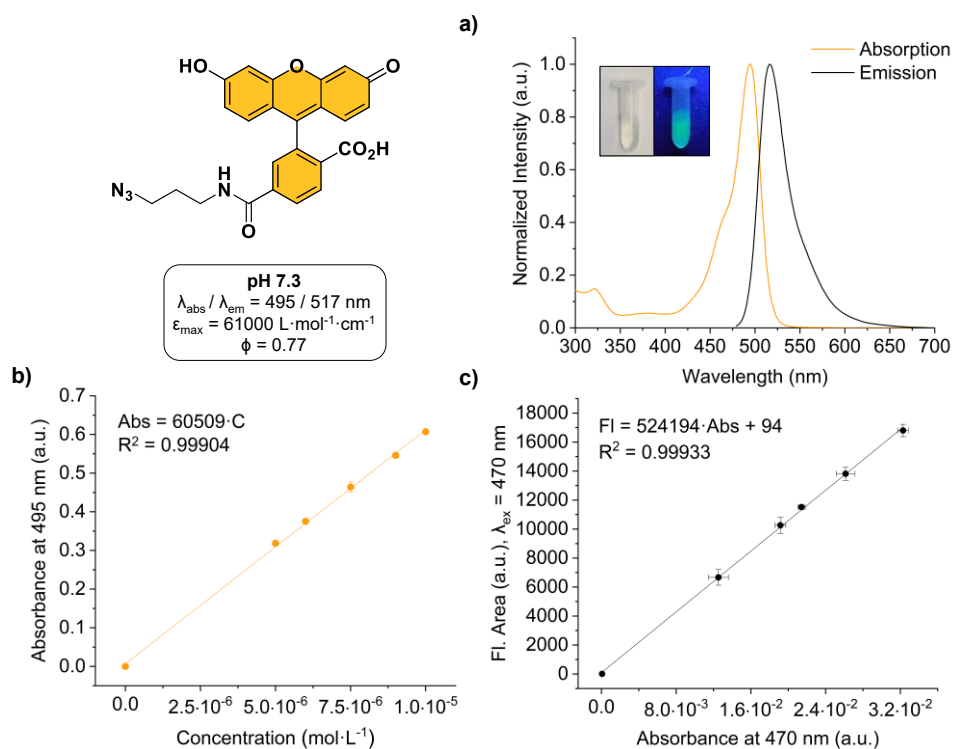


Figure S1. Photophysical properties of **fluorescein azide (8)** in 10 mM HEPES, pH 7.3 buffer at room temperature. a) Absorption and emission spectra. Solutions in the photographs correspond to **fluorescein azide** at 2 μM (absorbance; left) and 0.2 μM (emission; right). b) Linear regression analysis obeying the Beer-Lambert law. All absorbance values are averages ($n = 3$). c) Fluorescence area vs. absorbance plot for the quantum yield comparative method. All absorbance and fluorescence area values are averages ($n = 3$).

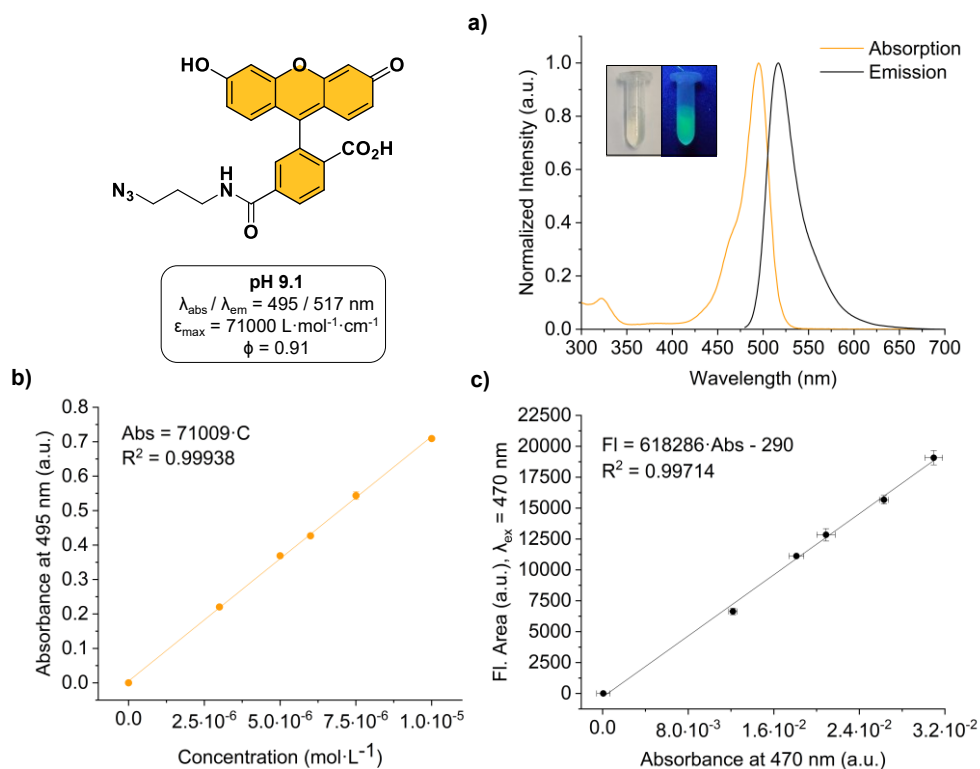


Figure S2. Photophysical properties of **fluorescein azide (8)** in 10 mM sodium borate, pH 9.1 buffer at room temperature. a) Absorption and emission spectra. Solutions in the photographs correspond to **fluorescein azide** at 2 μM (absorbance; left) and 0.2 μM (emission; right). b) Linear regression analysis obeying the Beer-Lambert law. All absorbance values are averages ($n = 3$). c) Fluorescence area vs. absorbance plot for the quantum yield comparative method. All absorbance and fluorescence area values are averages ($n = 3$).

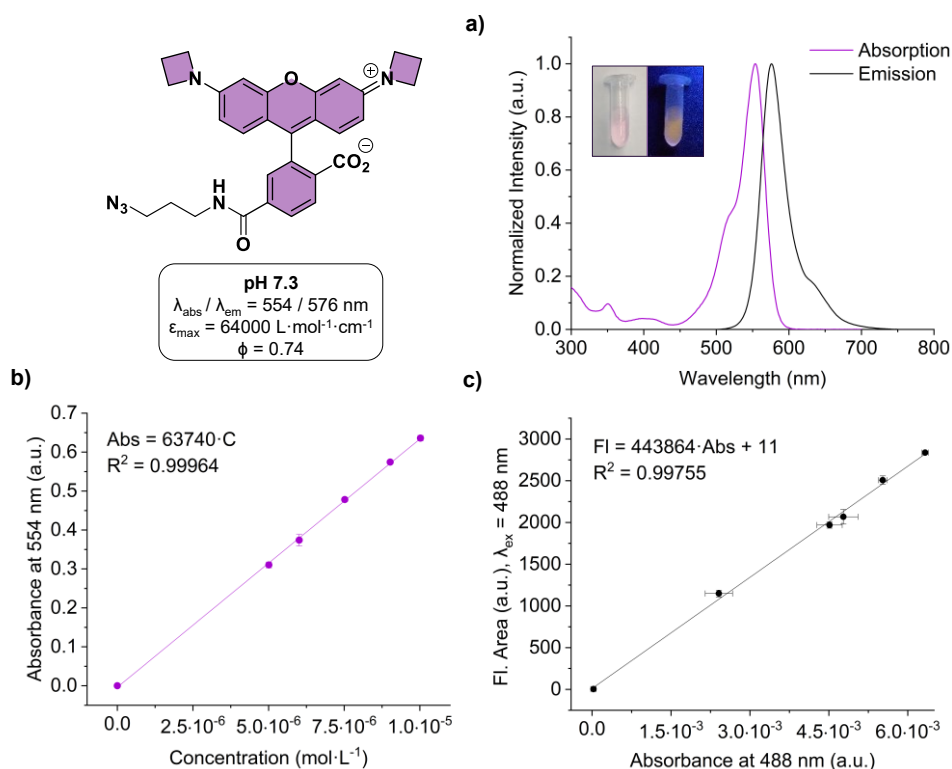


Figure S3. Photophysical properties of **RD_{H2}** (**10**) in 10 mM HEPES, pH 7.3 buffer at room temperature. a) Absorption and emission spectra. Solutions in the photographs correspond to **RD_{H2}** at 2 μ M (absorbance; left) and 0.2 μ M (emission; right). b) Linear regression analysis obeying the Beer-Lambert law. All absorbance values are averages ($n = 3$). c) Fluorescence area vs. absorbance plot for quantum yield comparative method. All absorbance and fluorescence area values are averages ($n = 3$).

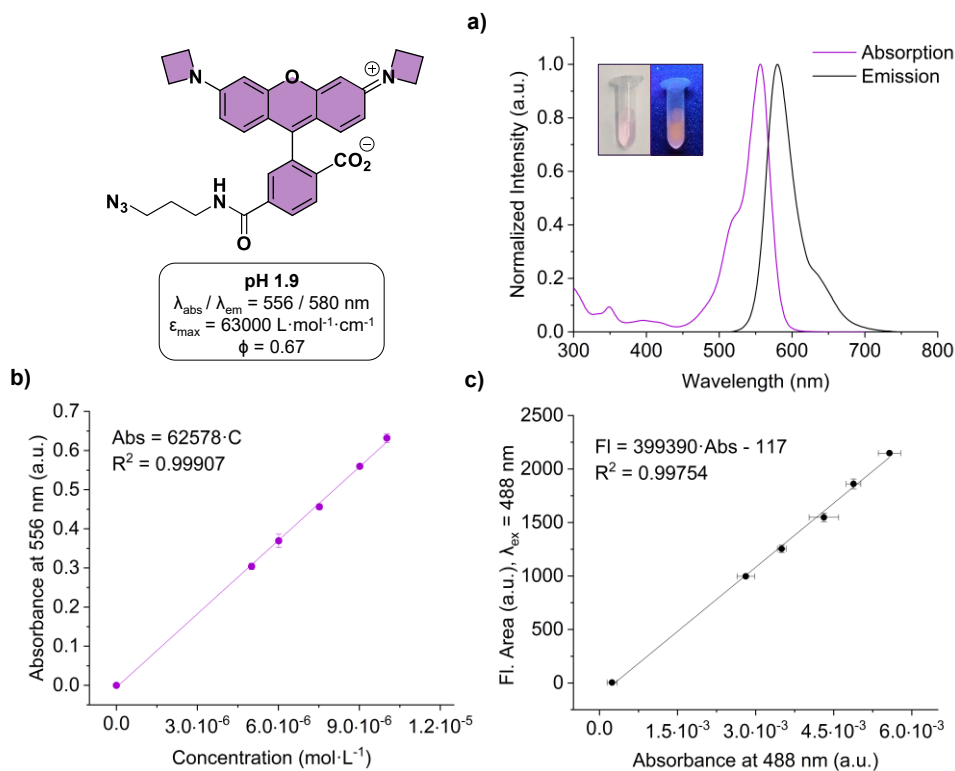


Figure S4. Photophysical properties of **RD_{H2}** (**10**) in aqueous TFA (0.1 % v/v) at room temperatures. a) Absorption and emission spectra. Solutions in the photographs correspond to **RD_{H2}** at 2 μ M (absorbance; left) and 0.2 μ M (emission; right). b) Linear regression analysis obeying the Beer-Lambert law. All absorbance values are averages ($n = 3$). c) Fluorescence area vs. absorbance plot for the quantum yield comparative method. All absorbance and fluorescence area values are averages ($n = 3$).

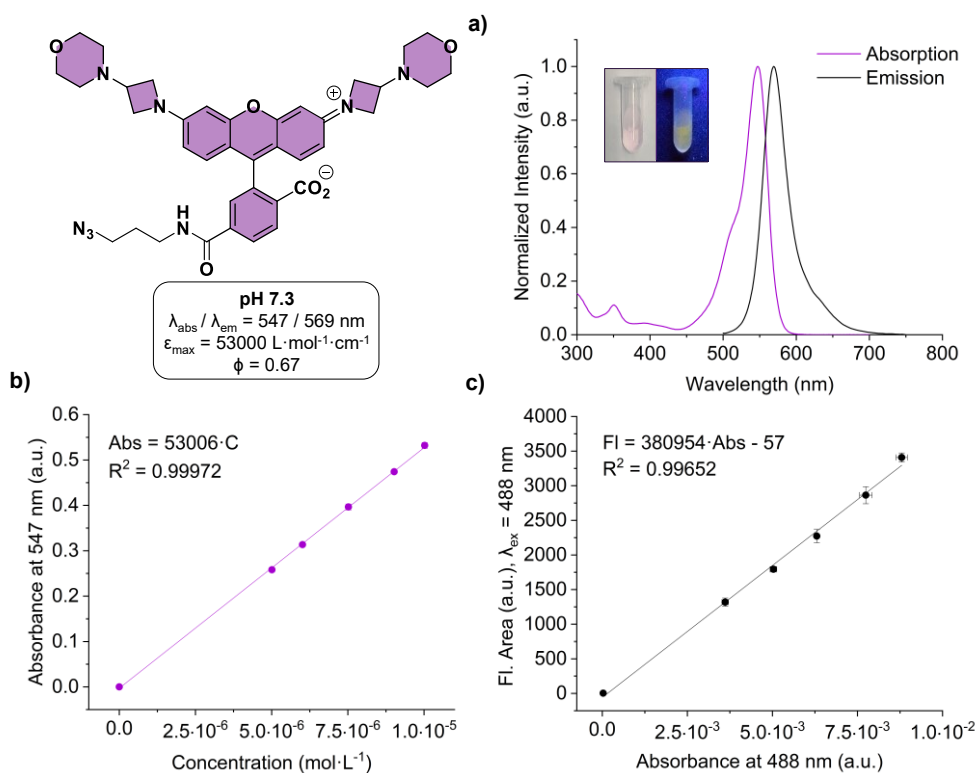


Figure S5. Photophysical properties of **RD_m** (**11**) in 10 mM HEPES, pH 7.3 buffer at room temperature. a) Absorption and emission spectra. Solutions in the photographs correspond to **RD_m** at 2 μM (absorbance; left) and 0.2 μM (emission; right). b) Linear regression analysis obeying the Beer-Lambert law. All absorbance values are averages (n = 3). c) Fluorescence area vs. absorbance plot for the quantum yield comparative method. All absorbance and fluorescence area values are averages (n = 3).

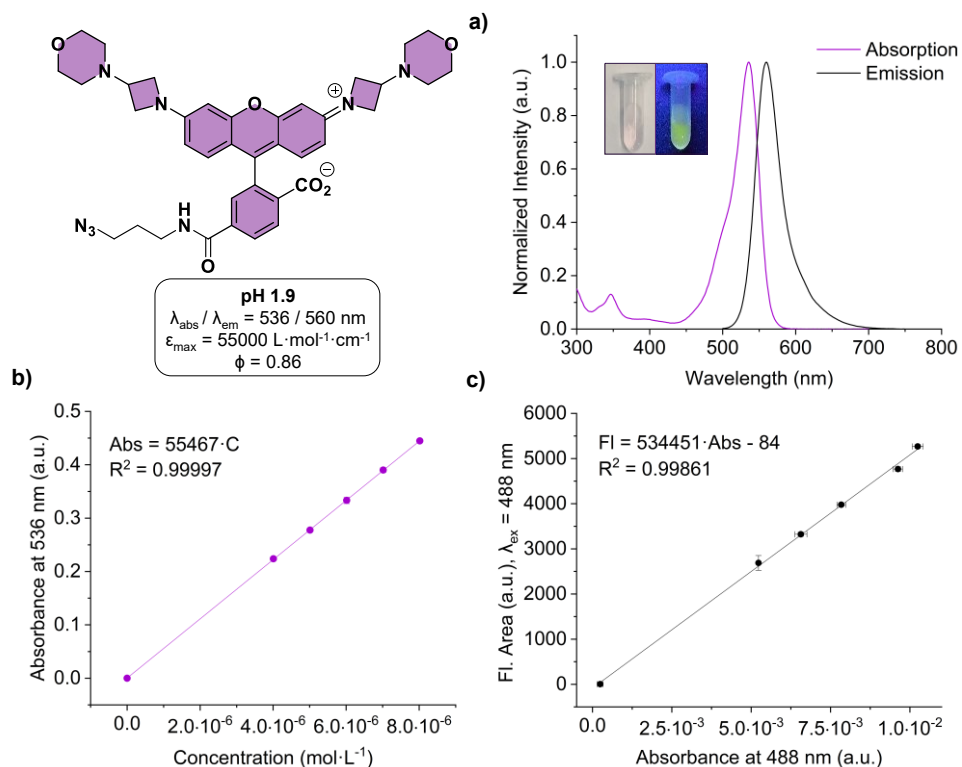


Figure S6. Photophysical properties of **RD_m** (**11**) in aqueous TFA (0.1 % v/v) at room temperature. a) Absorption and emission spectra. Solutions in the photographs correspond to **RD_m** at 2 μM (absorbance; left) and 0.2 μM (emission; right). b) Linear regression analysis obeying the Beer-Lambert law. All absorbance values are averages (n = 3). c) Fluorescence area vs. absorbance plot for the quantum yield comparative method. All absorbance and fluorescence area values are averages (n = 3).

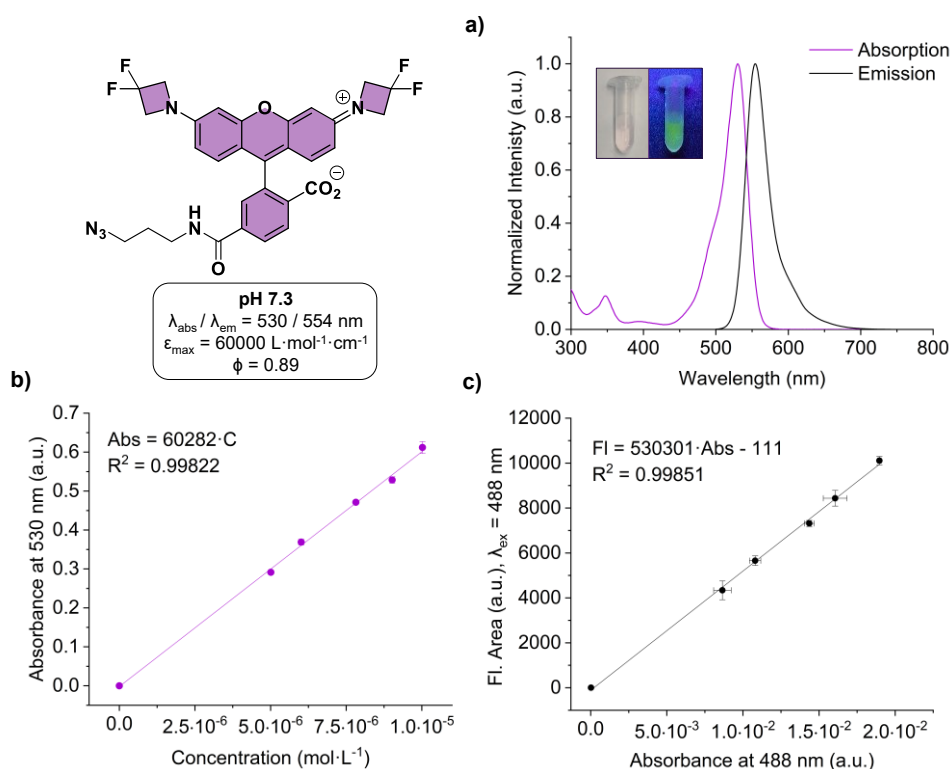


Figure S7. Photophysical properties of RD_{F_2} (**12**) in 10 mM HEPES, pH 7.3 buffer at room temperature. a) Absorption and emission spectra. Solutions in the photographs correspond to RD_{F_2} at 2 μM (absorbance; left) and 0.2 μM (emission; right). b) Linear regression analysis obeying the Beer-Lambert law. All absorbance values are averages ($n = 3$). c) Fluorescence area vs. absorbance plot for the quantum yield comparative method. All absorbance and fluorescence area values are averages ($n = 3$).

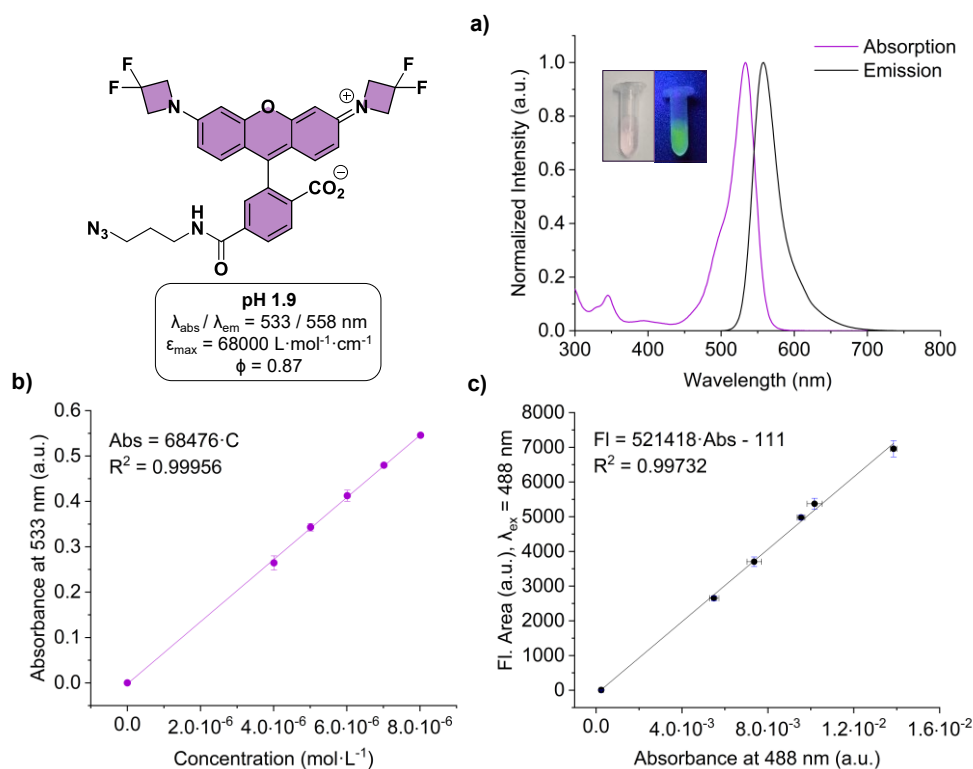


Figure S8. Photophysical properties of RD_{F_2} (**12**) in aqueous TFA (0.1 % v/v) at room temperature. a) Absorption and emission spectra. Solutions in the photographs correspond to RD_{F_2} at 2 μM (absorbance; left) and 0.2 μM (emission; right). b) Linear regression analysis obeying the Beer-Lambert law. All absorbance values are averages ($n = 3$). c) Fluorescence area vs. absorbance plot for the quantum yield comparative method. All absorbance and fluorescence area values are averages ($n = 3$).

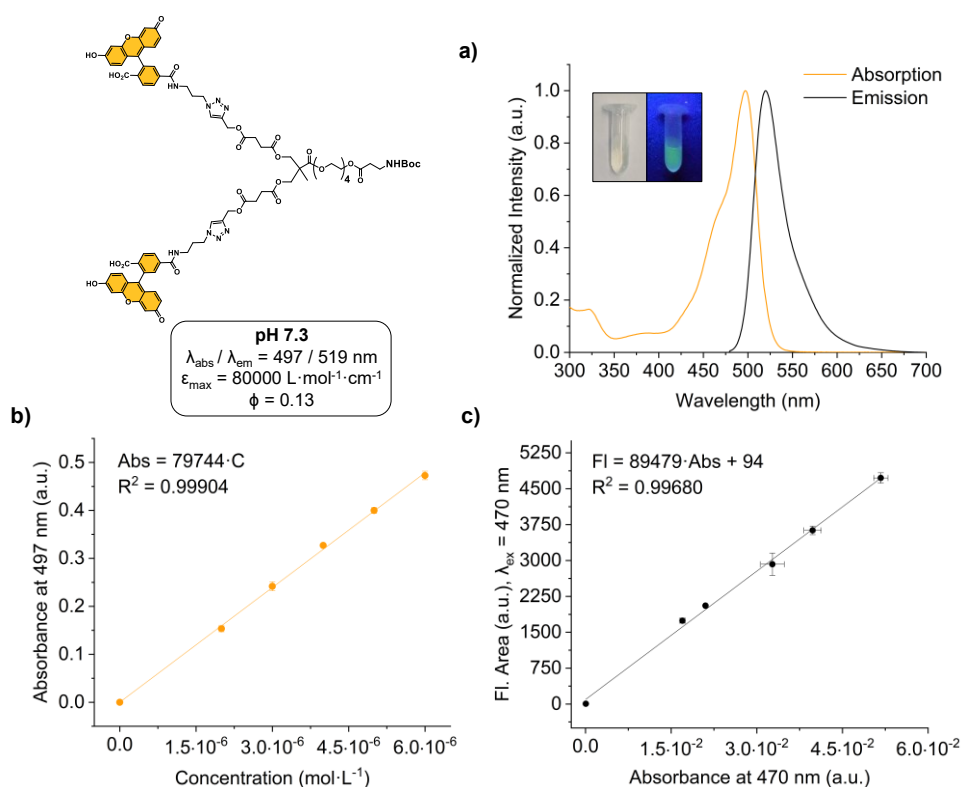


Figure S9. Photophysical properties of **FD2 (13)** in 10 mM HEPES, pH 7.3 buffer at room temperature. a) Absorption and emission spectra. Solutions in the photographs correspond to **FD2** at 2 μM (absorbance; left) and 0.2 μM (emission; right). b) Linear regression analysis obeying the Beer-Lambert law. All absorbance values are averages ($n = 3$). c) Fluorescence area vs. absorbance plot for the quantum yield comparative method. All absorbance and fluorescence area values are averages ($n = 3$).

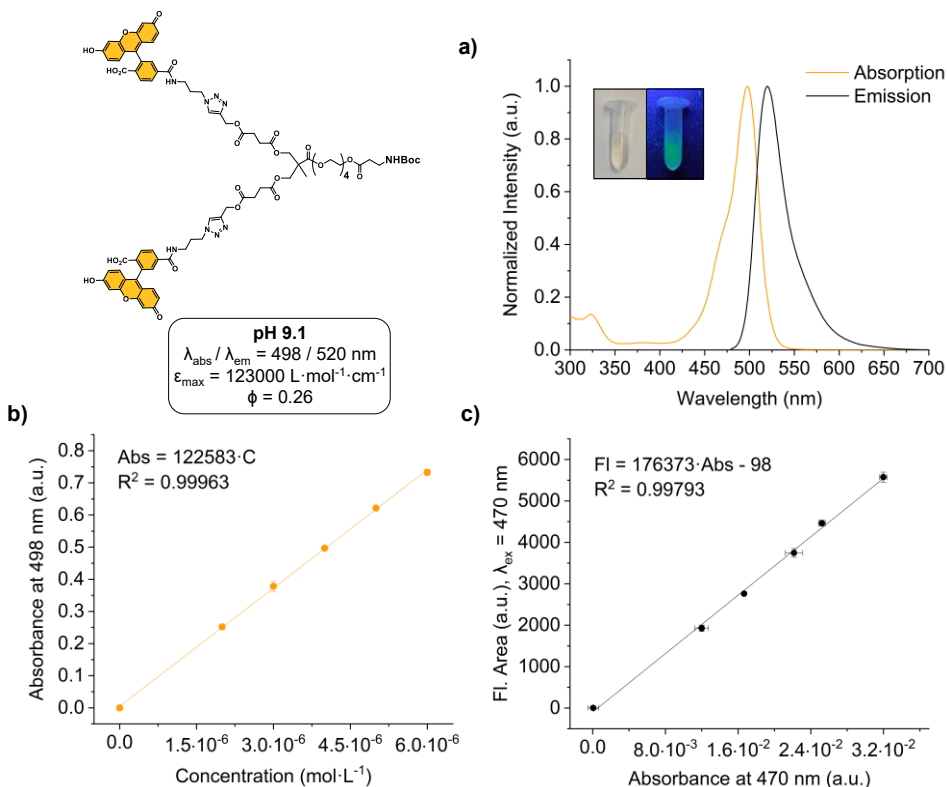


Figure S10. Photophysical properties of **FD2 (13)** in 10 mM sodium borate, pH 9.1 buffer at room temperature. a) Absorption and emission spectra. Solutions in the photographs correspond to **FD2** at 2 μM (absorbance; left) and 0.2 μM (emission; right). b) Linear regression analysis obeying the Beer-Lambert law. All absorbance values are averages ($n = 3$). c) Fluorescence area vs. absorbance plot for the quantum yield comparative method. All absorbance and fluorescence area values are averages ($n = 3$).

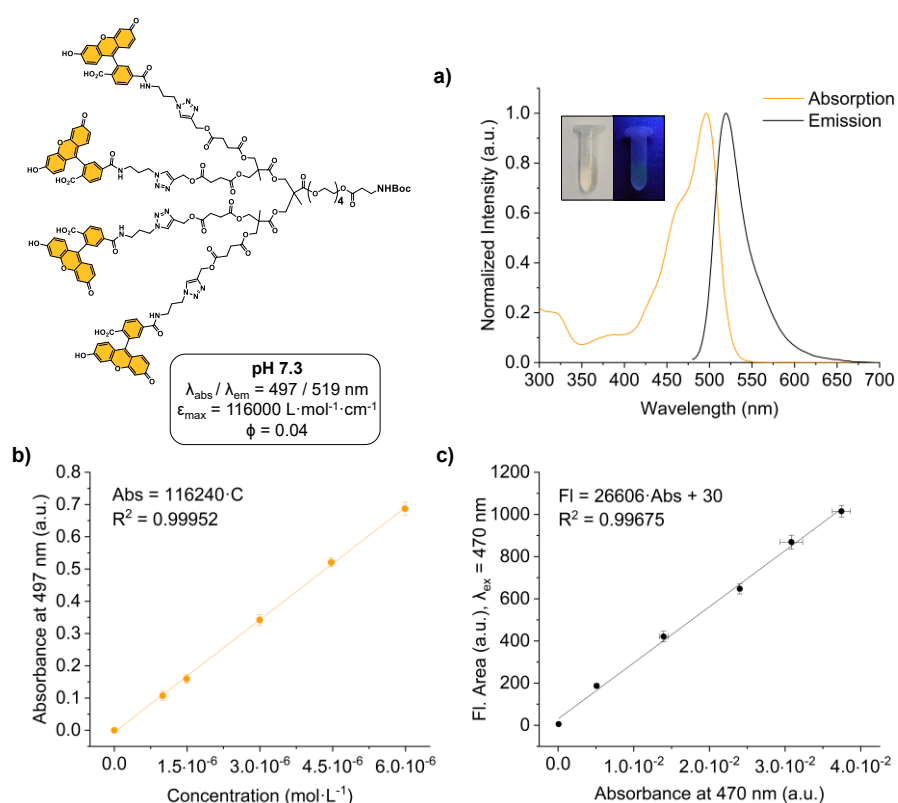


Figure S11. Photophysical properties of **FD4 (14)** in 10 mM HEPES, pH 7.3 buffer at room temperature. a) Absorption and emission spectra. Solutions in the photographs correspond to **FD4** at 2 μM (absorbance; left) and 0.2 μM (emission; right). b) Linear regression analysis obeying the Beer-Lambert law. All absorbance values are averages ($n = 3$). c) Fluorescence area vs. absorbance plot for the quantum yield comparative method. All absorbance and fluorescence area values are averages ($n = 3$).

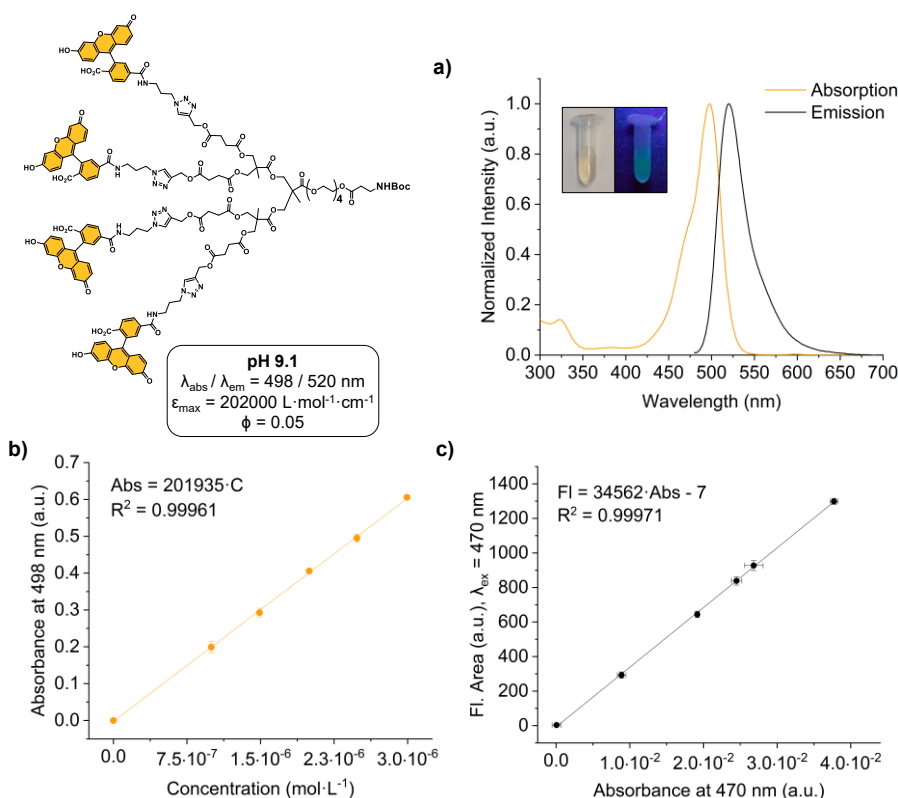


Figure S12. Photophysical properties of **FD4 (14)** in 10 mM sodium borate, pH 9.1 buffer at room temperature. a) Absorption and emission spectra. Solutions in the photographs correspond to **FD4** at 2 μM (absorbance; left) and 0.2 μM (emission; right). b) Linear regression analysis obeying the Beer-Lambert law. All absorbance values are averages ($n = 3$). c) Fluorescence area vs. absorbance plot for the quantum yield comparative method. All absorbance and fluorescence area values are averages ($n = 3$).

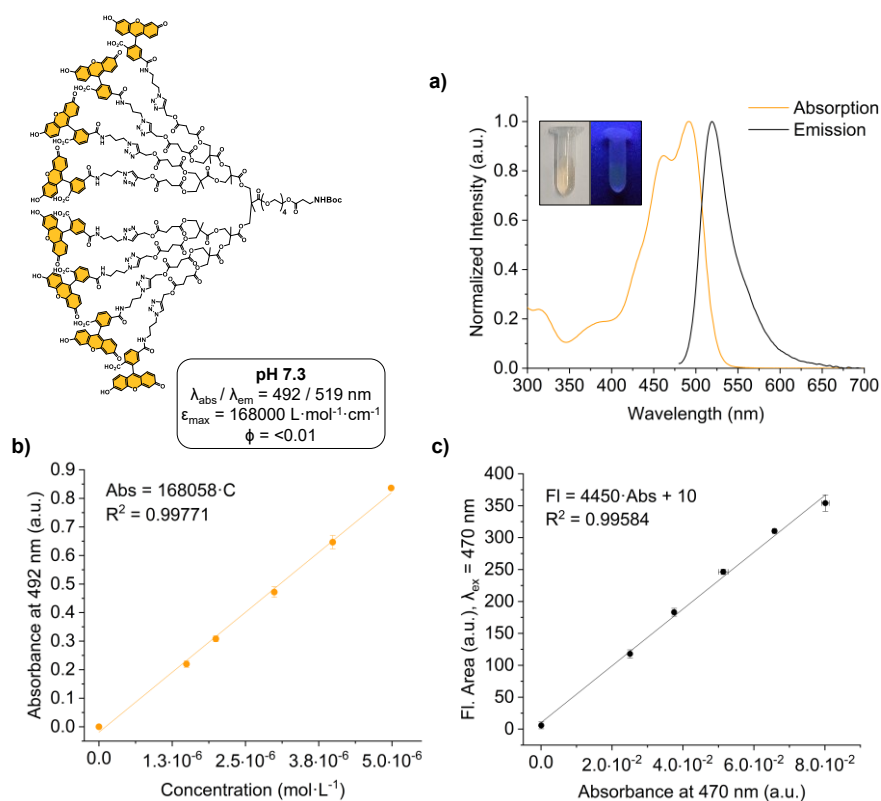


Figure S13. Photophysical properties of **FD8 (15)** in 10 mM HEPES, pH 7.3 buffer at room temperature. a) Absorption and emission spectra. Solutions in the photographs correspond to **FD8** at 2 μM (absorbance; left) and 0.2 μM (emission; right). b) Linear regression analysis obeying the Beer-Lambert law. All absorbance values are averages ($n = 3$). c) Fluorescence area vs. absorbance plot for the quantum yield comparative method. All absorbance and fluorescence area values are averages ($n = 3$).

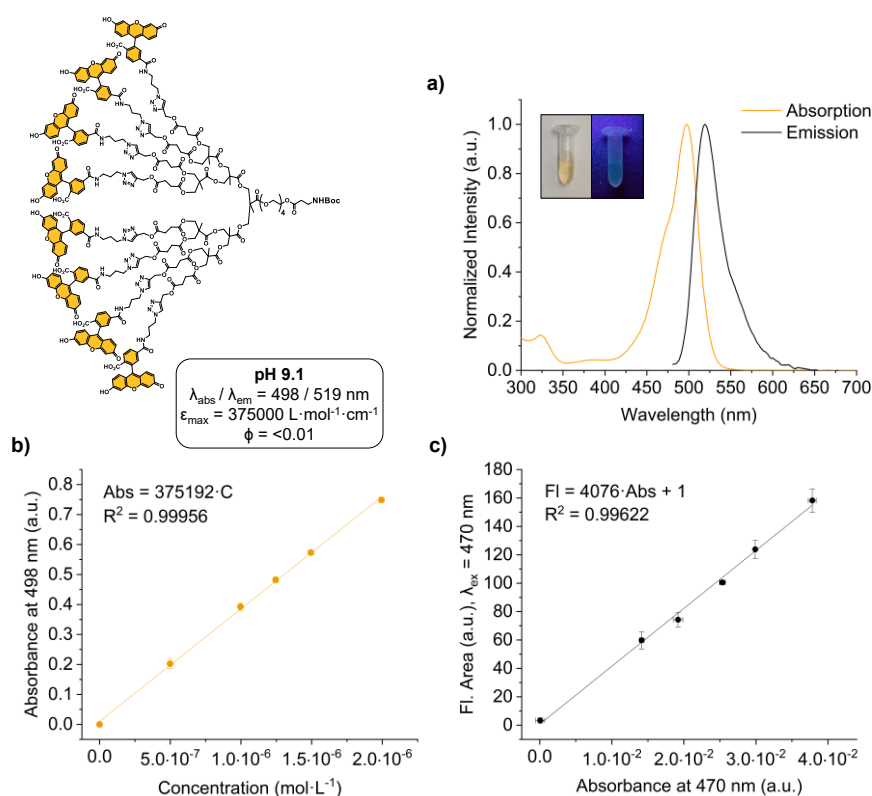


Figure S14. Photophysical properties of **FD8 (15)** in 10 mM sodium borate, pH 9.1 buffer at room temperature. a) Absorption and emission spectra. Solutions in the photographs correspond to **FD8** at 2 μM (absorbance; left) and 0.2 μM (emission; right). b) Linear regression analysis obeying the Beer-Lambert law. All absorbance values are averages ($n = 3$). c) Fluorescence area vs. absorbance plot for the quantum yield comparative method. All absorbance and fluorescence area values are averages ($n = 3$).

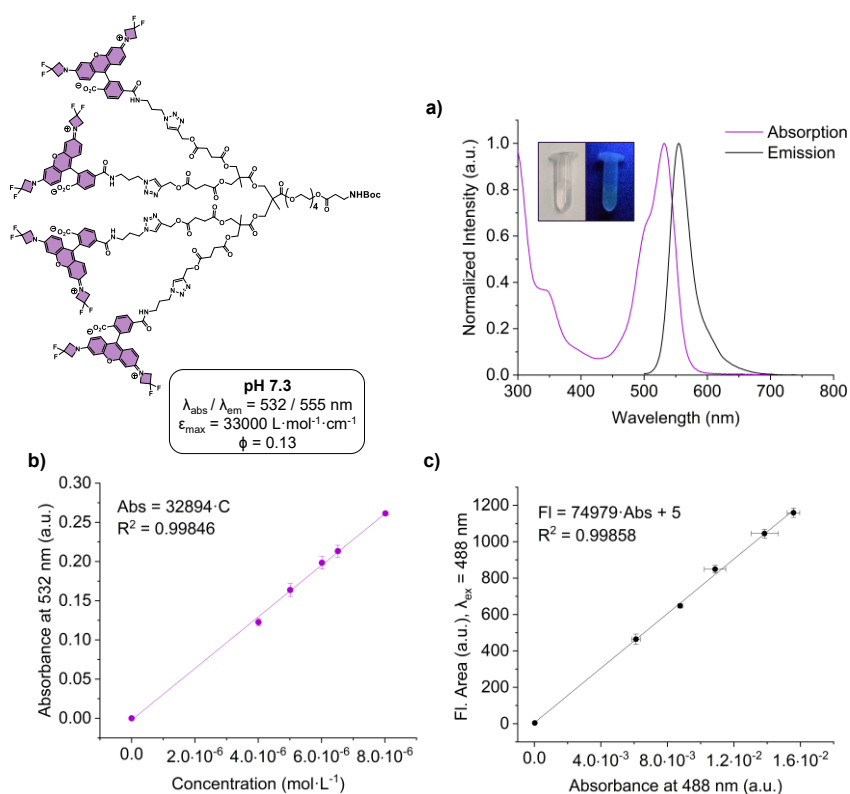


Figure S15. Photophysical properties of **RD₂D4 (17)** in 10 mM HEPES, pH 7.3 buffer at room temperature. a) Absorption and emission spectra. Solutions in the photographs correspond to **RD₂D4** at 2 μM (absorbance; left) and 0.2 μM (emission; right). b) Linear regression analysis obeying the Beer-Lambert law. All absorbance values are averages ($n = 3$). c) Fluorescence area vs. absorbance plot for the quantum yield comparative method. All absorbance and fluorescence area values are averages ($n = 3$).

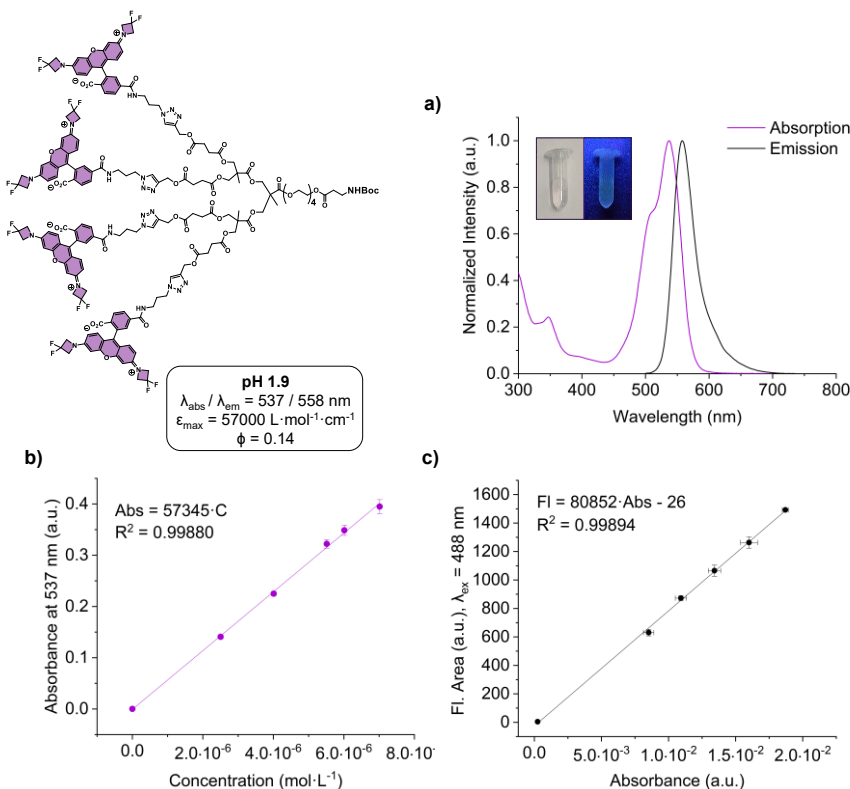


Figure S16. Photophysical properties of **RD₂D4 (17)** in aqueous TFA (0.1 % v/v) at room temperature. a) Absorption and emission spectra. Solutions in the photographs correspond to **RD₂D4** at 2 μM (absorbance; left) and 0.2 μM (emission; right). b) Linear regression analysis obeying the Beer-Lambert law. All absorbance values are averages ($n = 3$). c) Fluorescence area vs. absorbance plot for the quantum yield comparative method. All absorbance and fluorescence area values are averages ($n = 3$).

SUPPORTING INFORMATION

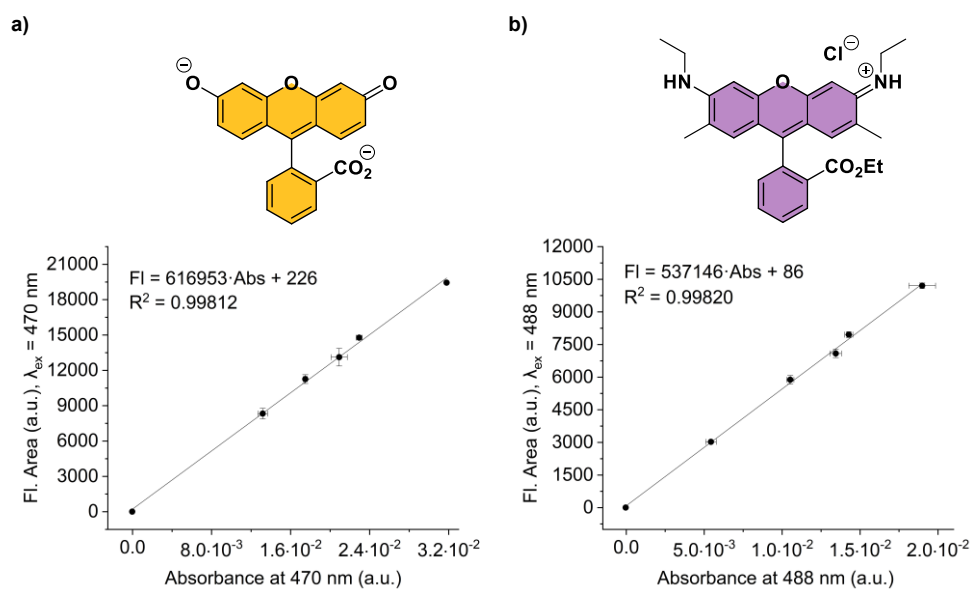


Figure S17. Fluorescence area vs. absorbance plots of the references used for the quantum yield comparative method. a) Fluorescein in aqueous 0.1 M NaOH. b) Rhodamine 6G in ethanol. All absorbance and fluorescence area values are averages ($n = 3$) and the measurements were taken at room temperature.

4. Photostability Studies of RD_{H2}, RD_m and RD_{F2}

The photobleaching rate constant values (k) and fluorescence half-life time values ($t_{1/2}$) of RD_{H2}, RD_m, and RD_{F2} were evaluated to characterise the photostability of these new dyes. As described in the General Experimental Methods section, $\ln\left(\frac{I}{I_0}\right)$ was plotted against the irradiation time (t) (**Equation 1**) to obtain the photobleaching constant rate as the absolute value of the slope's linear fitting (see **Table S1** and **Figure S18**). Fluorescence half-life time values were calculated, therefore, based on the photobleaching constant rates (**Equation 2**). The photostability of **TAMRA-PEG3-azide** and **fluorescein azide** was also evaluated for comparative reasons. As shown in **Table S1**, the newly synthesised rhodamine dyes exhibit similar fluorescence half-life times to that of **TAMRA-PEG3-azide**, demonstrating the photostability of the new dyes is comparable to that of a commercially available rhodamine dye. The half-life time of **fluorescein azide** was also calculated to show, as already reported,^[2,3] the exceptional photostability of rhodamine dyes in comparison to fluorescein.

Table S1. Photobleaching rate constants (k) and fluorescence half-life times ($t_{1/2}$) of RD_{H2}, RD_m, RD_{F2}, TAMRA-PEG3-azide and fluorescein azide.

Fluorophore	k (min ⁻¹)	$t_{1/2}$ (min)
RD _{H2} ^[a]	2.15×10^{-2}	32.3
RD _m ^[b]	4.89×10^{-2}	14.2
RD _{F2} ^[b]	2.75×10^{-2}	25.2
TAMRA-PEG3-azide ^[a]	2.39×10^{-2}	29.0
Fluorescein azide ^[c]	8.60×10^{-2}	8.1

[a] 0.2 μ M sample irradiated using a 560 nm laser at a power density of 550 mW/cm². [b] 0.2 μ M sample irradiated using a 531 nm laser at a power density of 550 mW/cm². [c] 0.2 μ M sample irradiated using a 488 nm laser at a power density of 13 mW/cm². TAMRA-PEG3-azide and fluorescein azide were used as references for comparison.

SUPPORTING INFORMATION

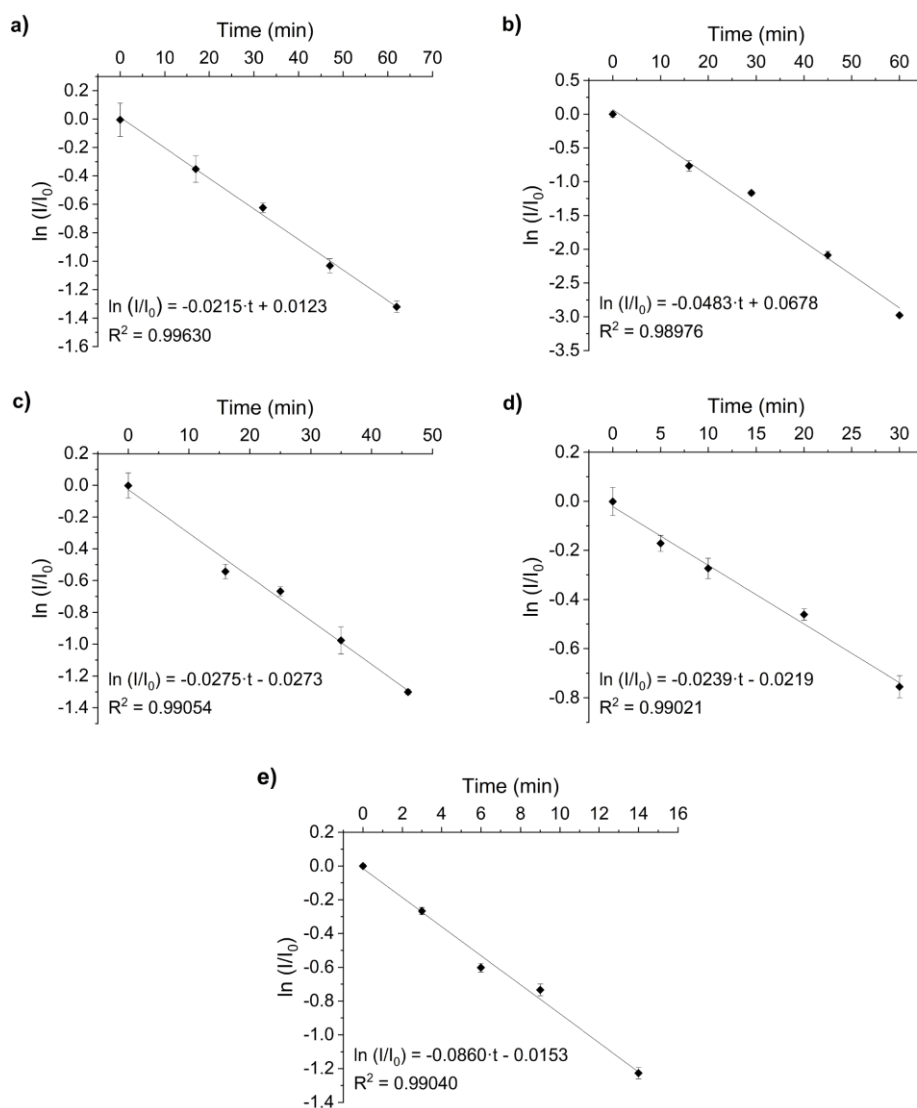


Figure S18. $\ln(I/I_0)$ plotted against irradiation time (t) of a) RD_{H2} , b) RD_m , c) RD_{F2} , d) TAMRA-PEG3-azide and e) fluorescein azide. The absolute value of the linear fitting's slope corresponds to the photobleaching rate constant (k). I_0 = initial intensity. I = intensity at time t. All $\ln(I/I_0)$ values are averages (n = 3).

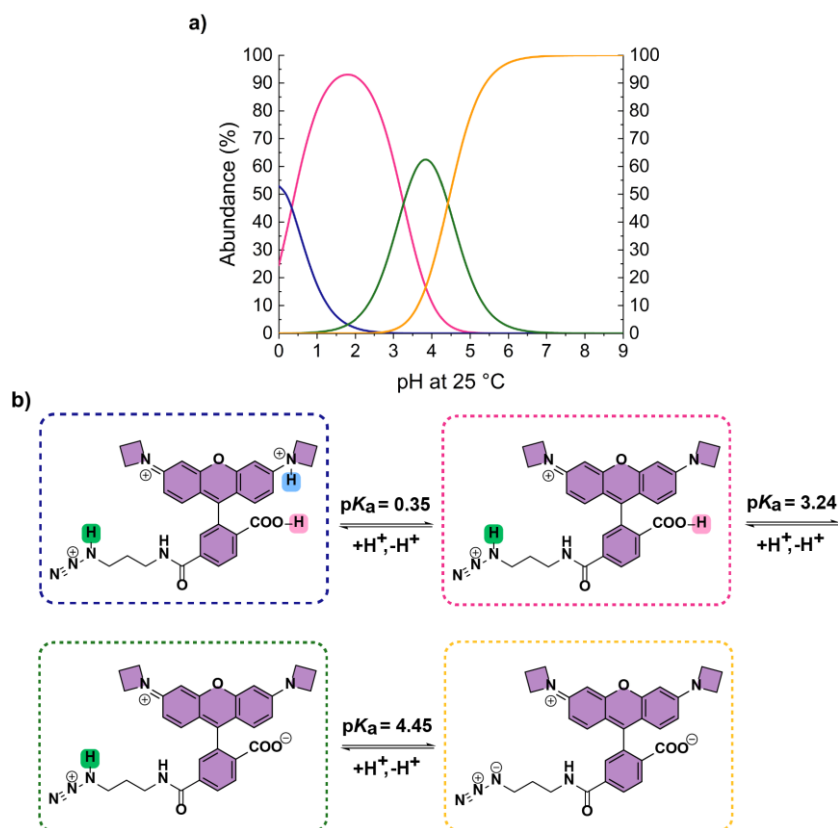
5. pK_a Values Calculation of RD_{H_2} , RD_m and RD_{F_2} 

Figure S19. Calculation of the different pK_a values of RD_{H_2} at 25 °C. a) Distribution of the different species in solution as a function of pH. b) Structure of the different protonated and unprotonated forms of RD_{H_2} . At pH 7.3 the main species found in solution is the deprotonated form of RD_{H_2} , whereas the doubly protonated form of RD_{H_2} is the prevailing one at pH 1.9.

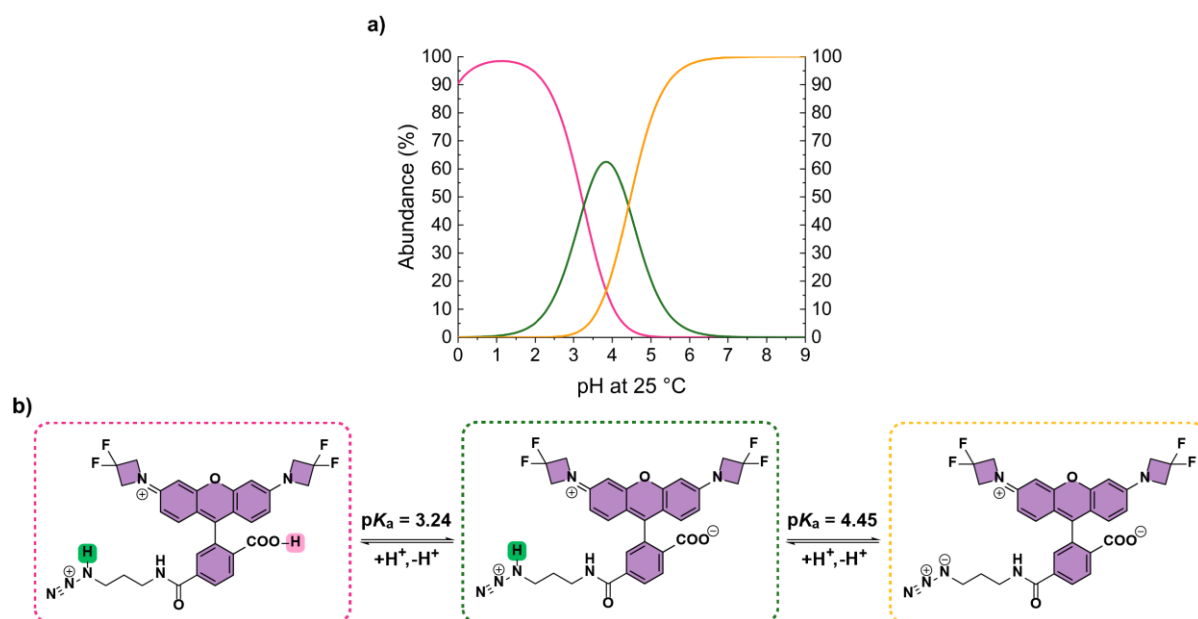


Figure S20. Calculation of the different pK_a values of RD_{F_2} at 25 °C. a) Distribution of the different species in solution as a function of pH. b) Structure of the different protonated and unprotonated forms of RD_{F_2} . At pH 7.3 the main species found in solution is unprotonated form of RD_{F_2} , whereas the doubly protonated form of RD_{F_2} is the prevailing one at pH 1.9.

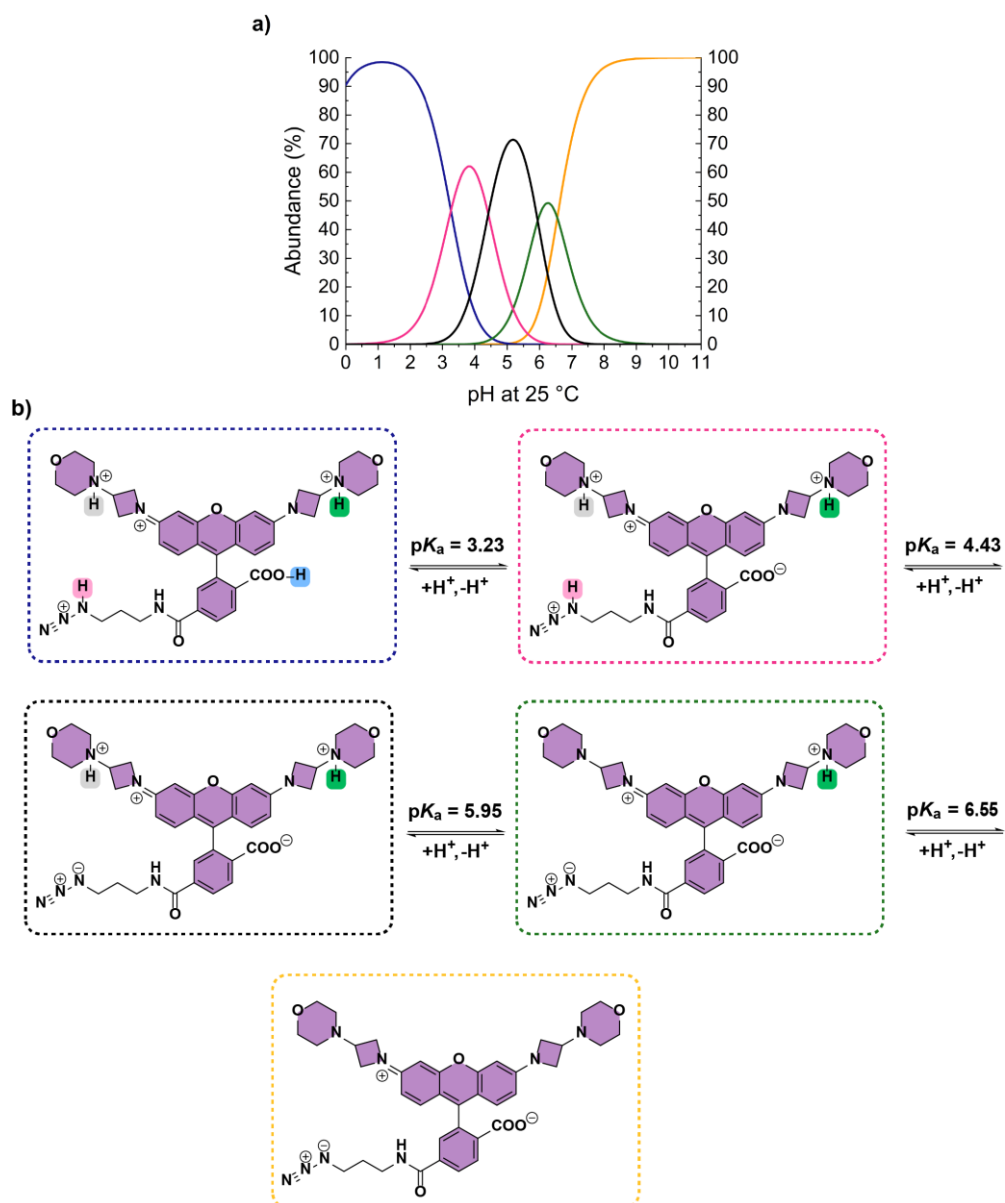


Figure S21. Calculation of the different $\text{p}K_a$ values of RD_m at 25 °C. a) Distribution of the different species in solution as a function of pH. b) Structure of the different protonated and unprotonated forms of RD_m . At pH 7.3 the main species found in solution are the unprotonated and monoprotoneated form of RD_m , whereas the tetraprotonated form of RD_m is the prevailing one at pH 1.9.

6. Solution Stability Studies

A solution stability study was performed for **fluorescein azide**, **FD2**, **FD4**, **FD8**, **RD_{H2}**, **RD_m**, **RD_{F2}** and **RD_{F2}D4**. In order to carry out this experiment, buffered pH 7.3 aqueous solutions (HEPES, 10 mM) of the fluorophores were prepared at a concentration of 2.0 μ M. The samples were allowed to stand under ambient conditions for 7 days, at room temperature and shielded from sunlight. Aliquots were taken and measured by HPLC at three time points, shown below. For solubility reasons, analyses of **RD_{F2}D4** by HPLC were not possible and, consequently, MALDI-ToF measurements were performed. Overall, all fluorophores are stable after 1 week in solution under these conditions.

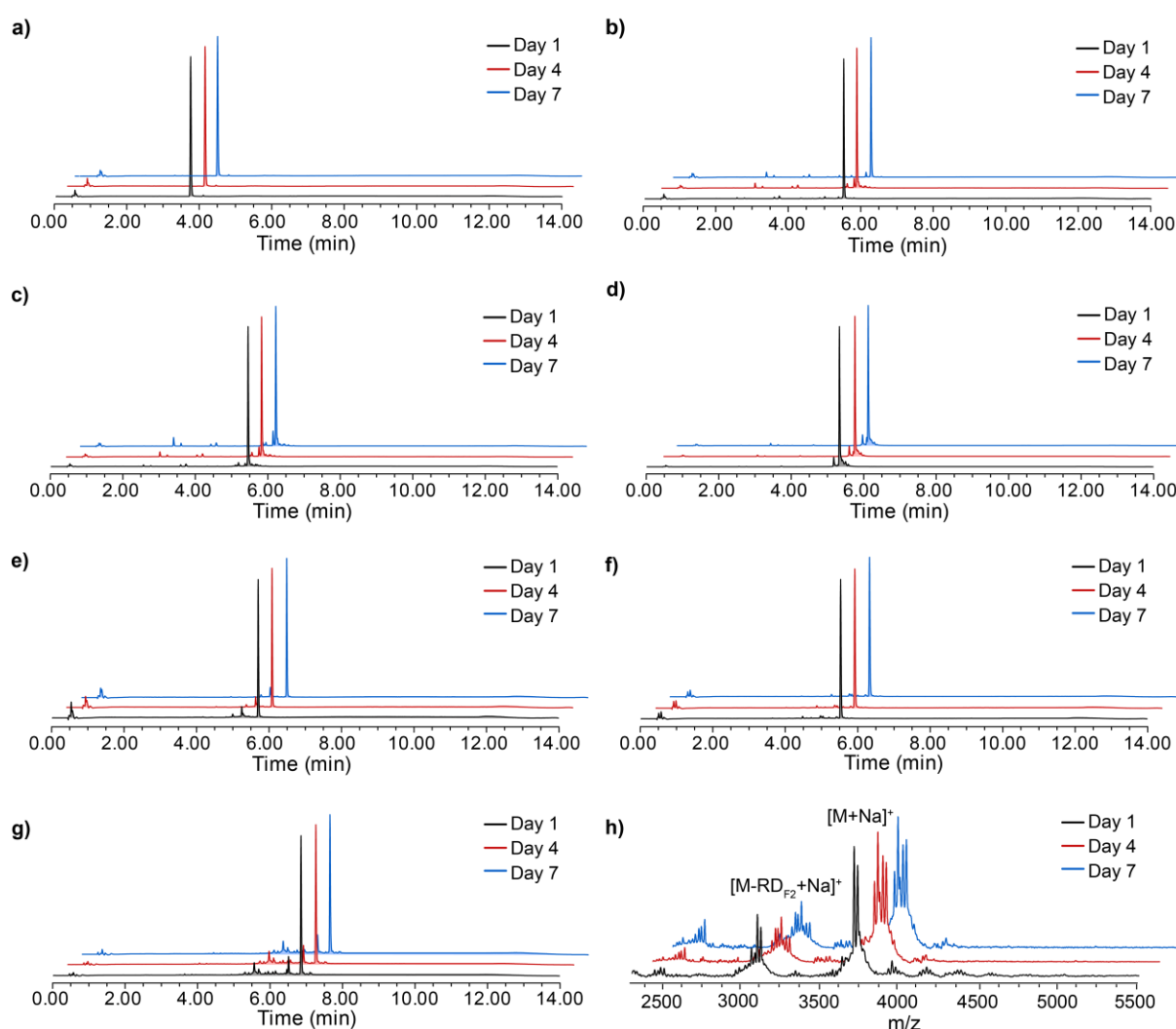


Figure S22. Solution stability study of a) fluorescein azide, b) FD2, c) FD4, d) FD8, e) RD_{H2}, f) RD_m, g) RD_{F2} and h) RD_{F2}D4. HPLC run conditions: a-f) 1.5 mL/min, 40 °C, buffer B 0-30 % v/v 0 → 4 min, then 30-85 % v/v 4 → 10 min. g) 1.5 mL/min, 40 °C, buffer B 0-30 % v/v 0 → 4 min and 85 % v/v 6 → 10 min. MALDI-ToF conditions: h) positive ionization mode, DCTB (matrix), NaTFA (cationization agent).

7. Mass Spectra of the Synthesised Compounds

7.1 ESI spectra

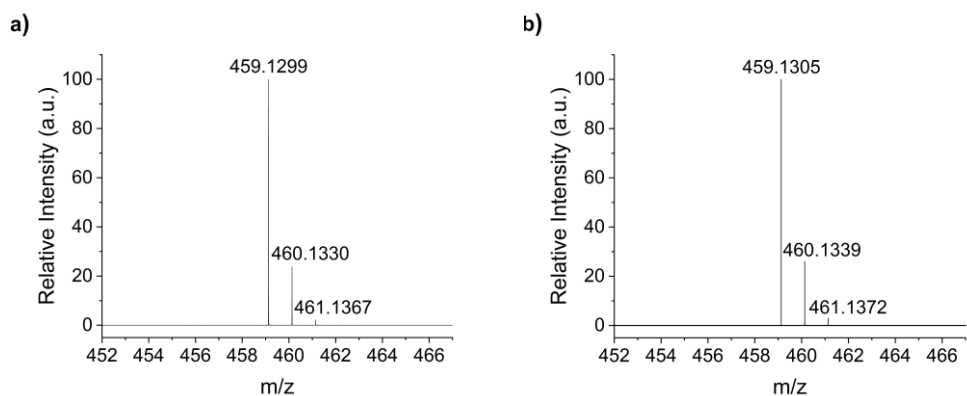


Figure S23. a) Experimental and b) theoretical isotopic distributions of $[M+H]^+$ for fluorescein azide.

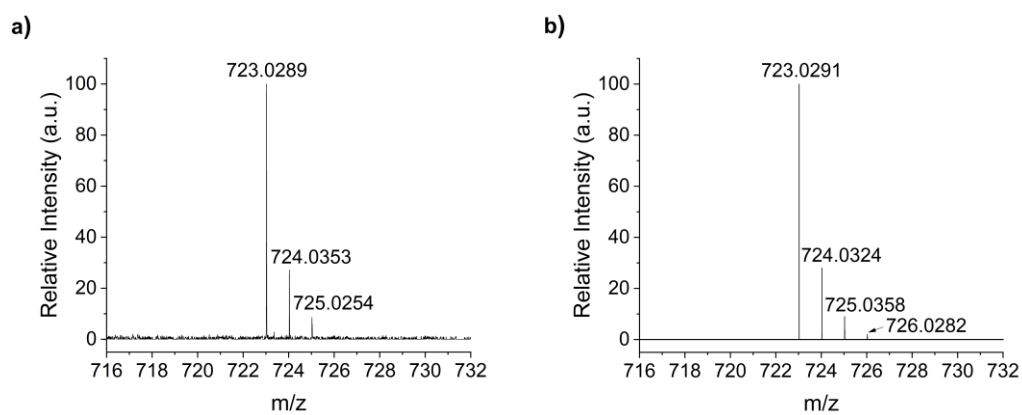


Figure S24. a) Experimental and b) theoretical isotopic distributions of $[M+H]^+$ for fluorescein dinitrate.

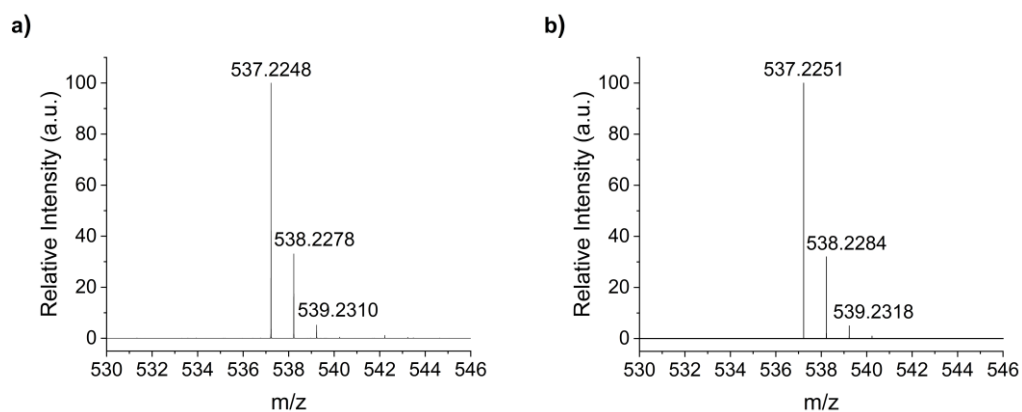


Figure S25. a) Experimental and b) theoretical isotopic distributions of $[M+H]^+$ for RD_{H2}.

SUPPORTING INFORMATION

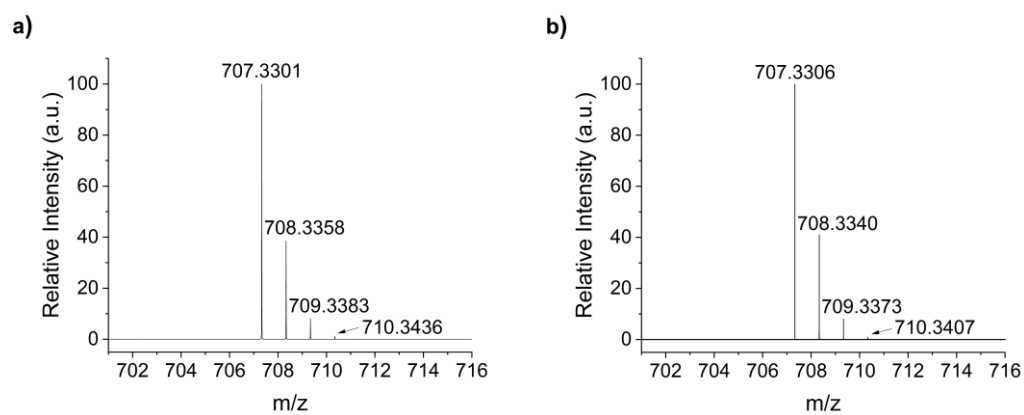


Figure S26. Experimental and b) theoretical isotopic distributions of $[M+H]^+$ for RD_m.

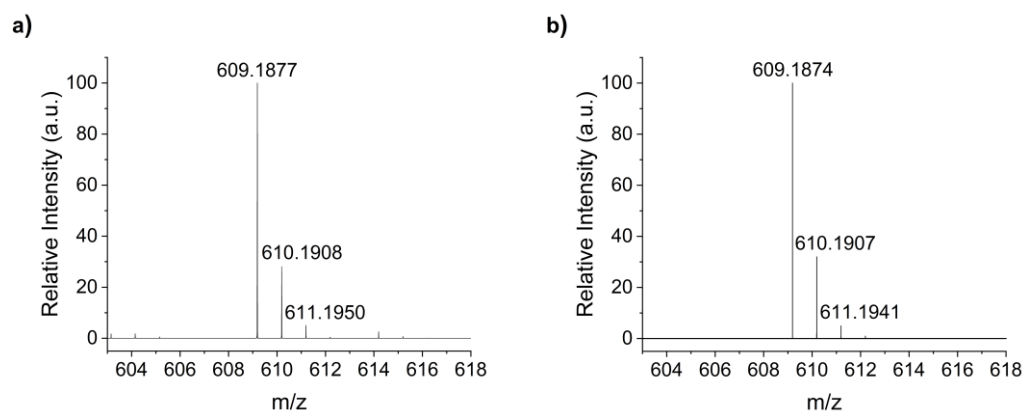


Figure S27. Experimental and b) theoretical isotopic distributions of $[M+H]^+$ for RD_{f2}.

7.2 MALDI-ToF spectra

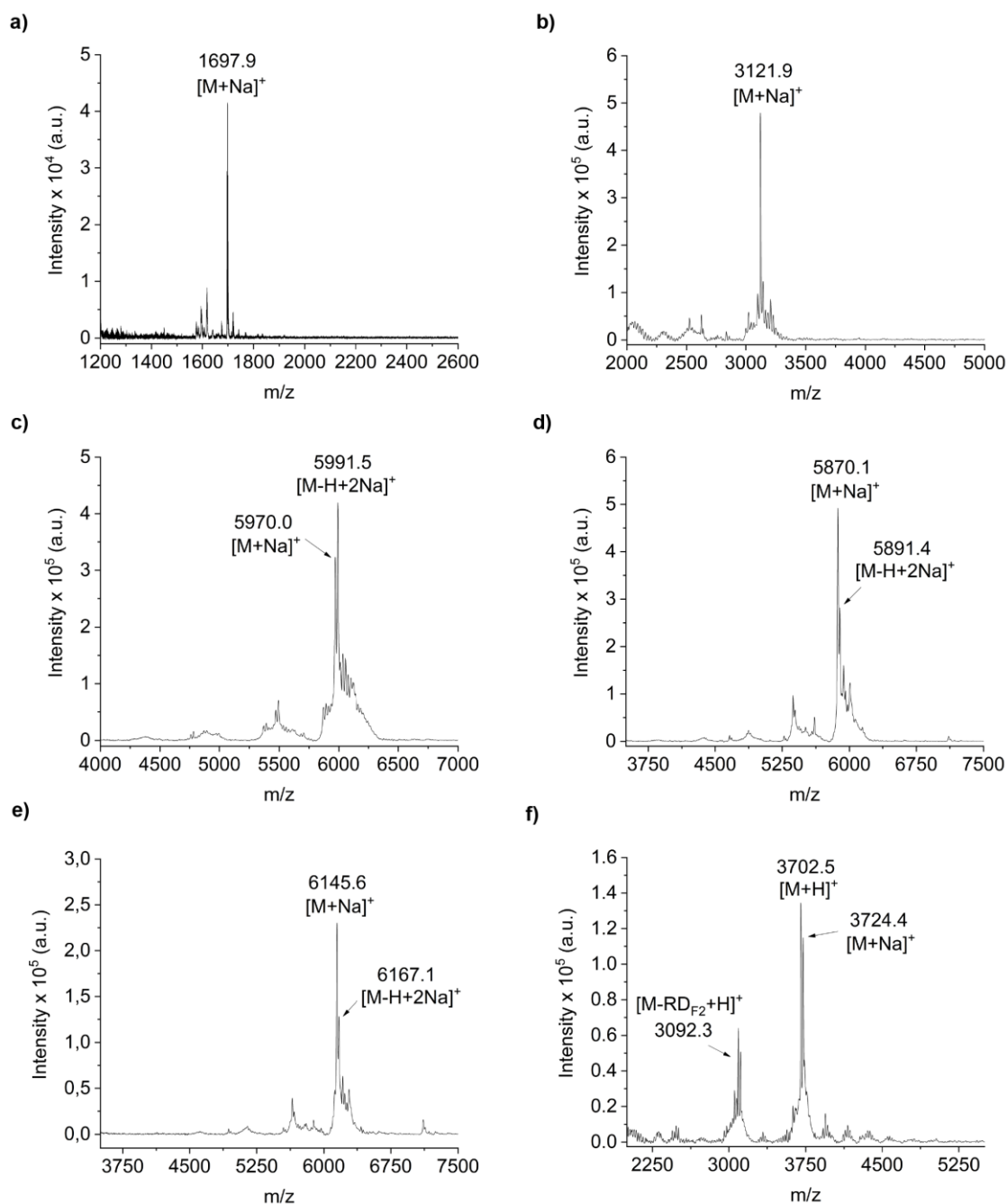
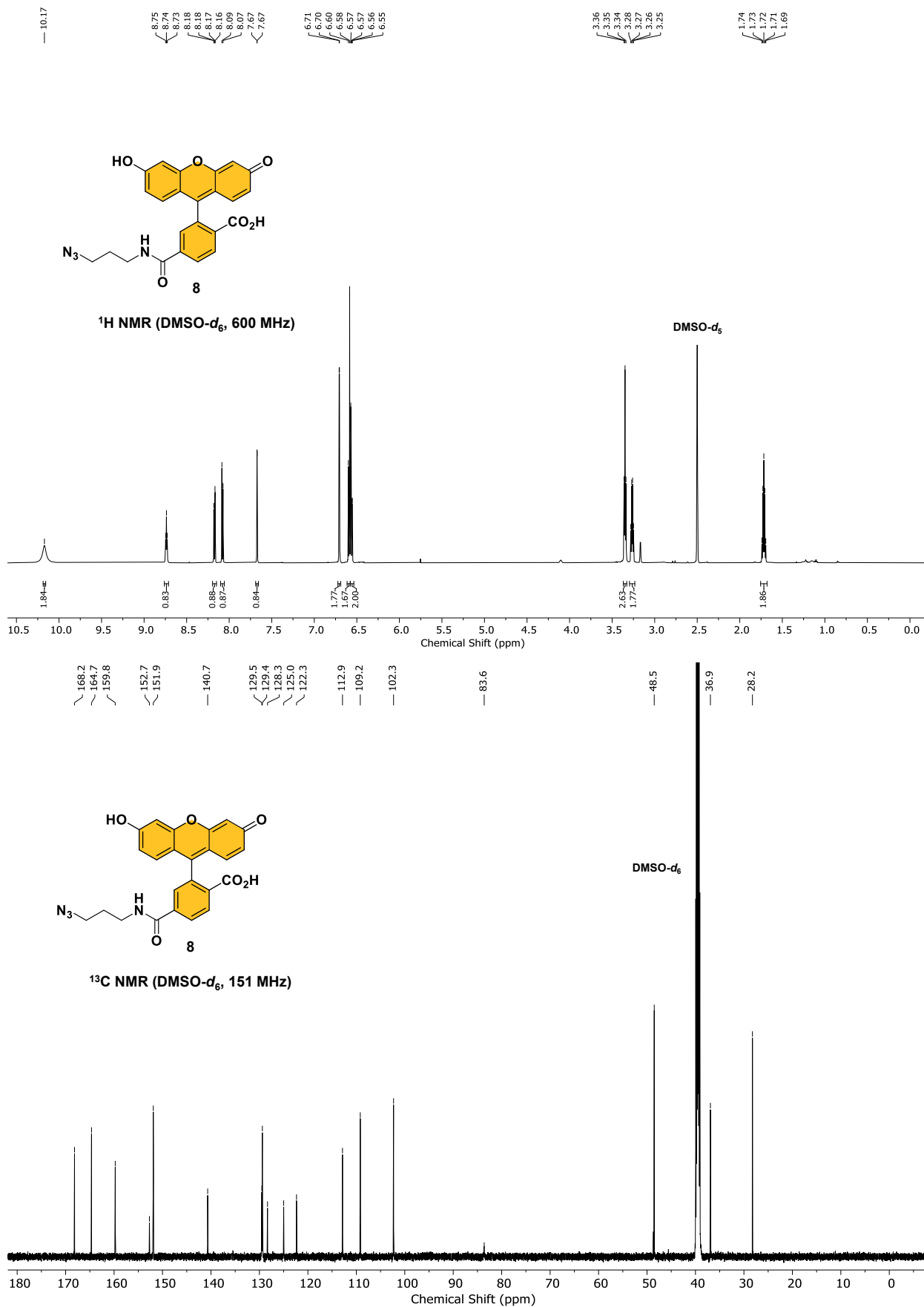
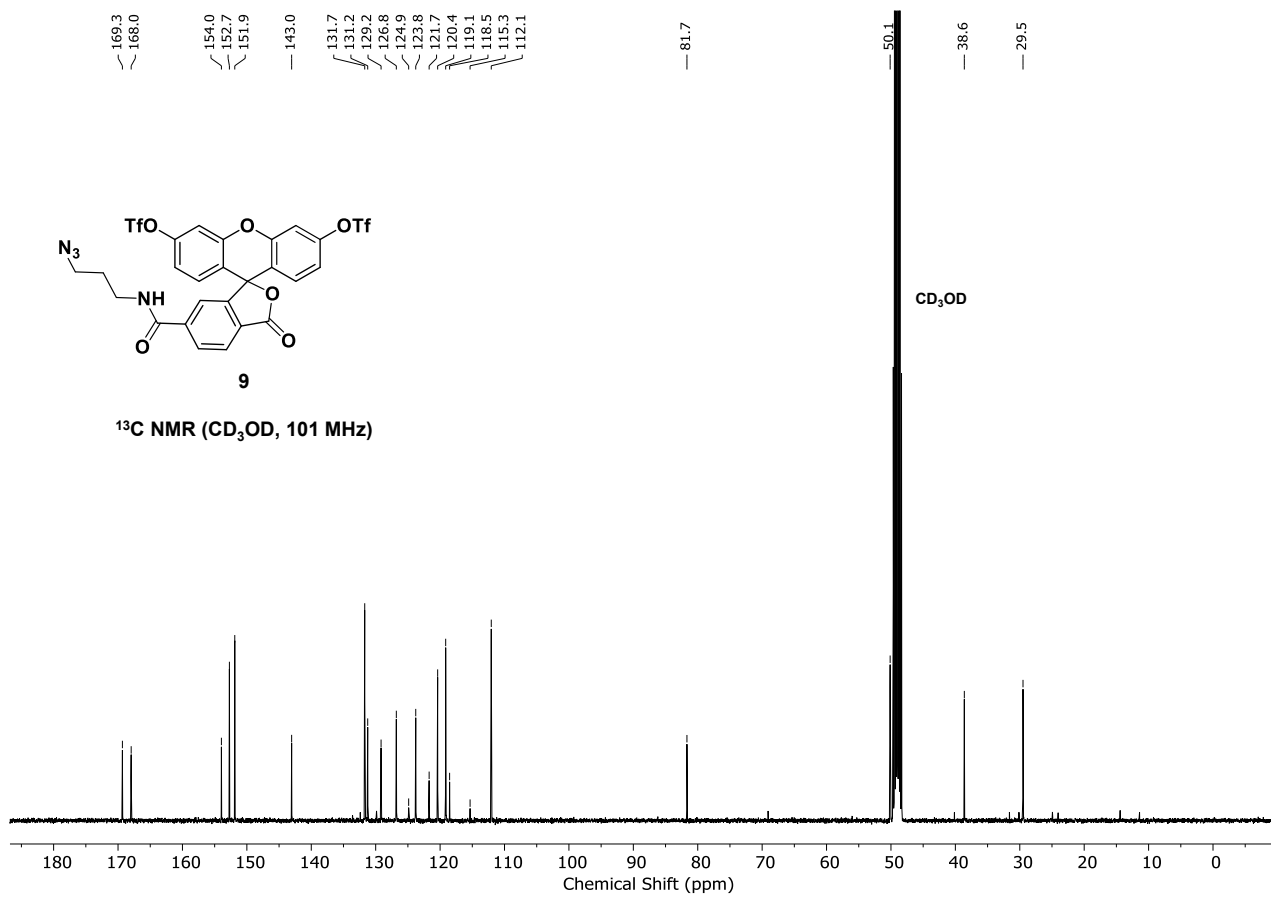
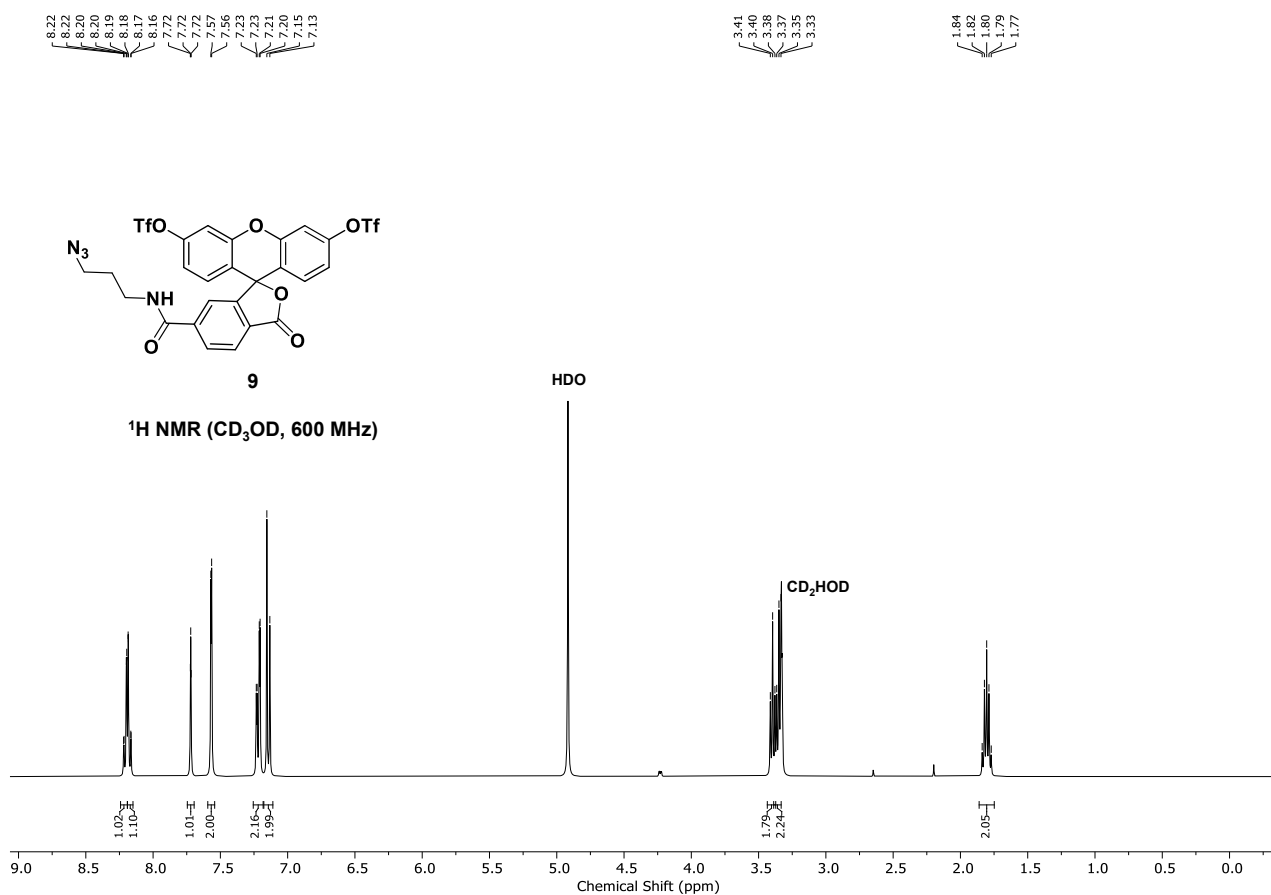


Figure S28. MALDI-ToF spectra of a) FD2, b) FD4, c) FD8, d) FD8-NH₃, e) FD8-N₃ and f) RD_{F2}D4.

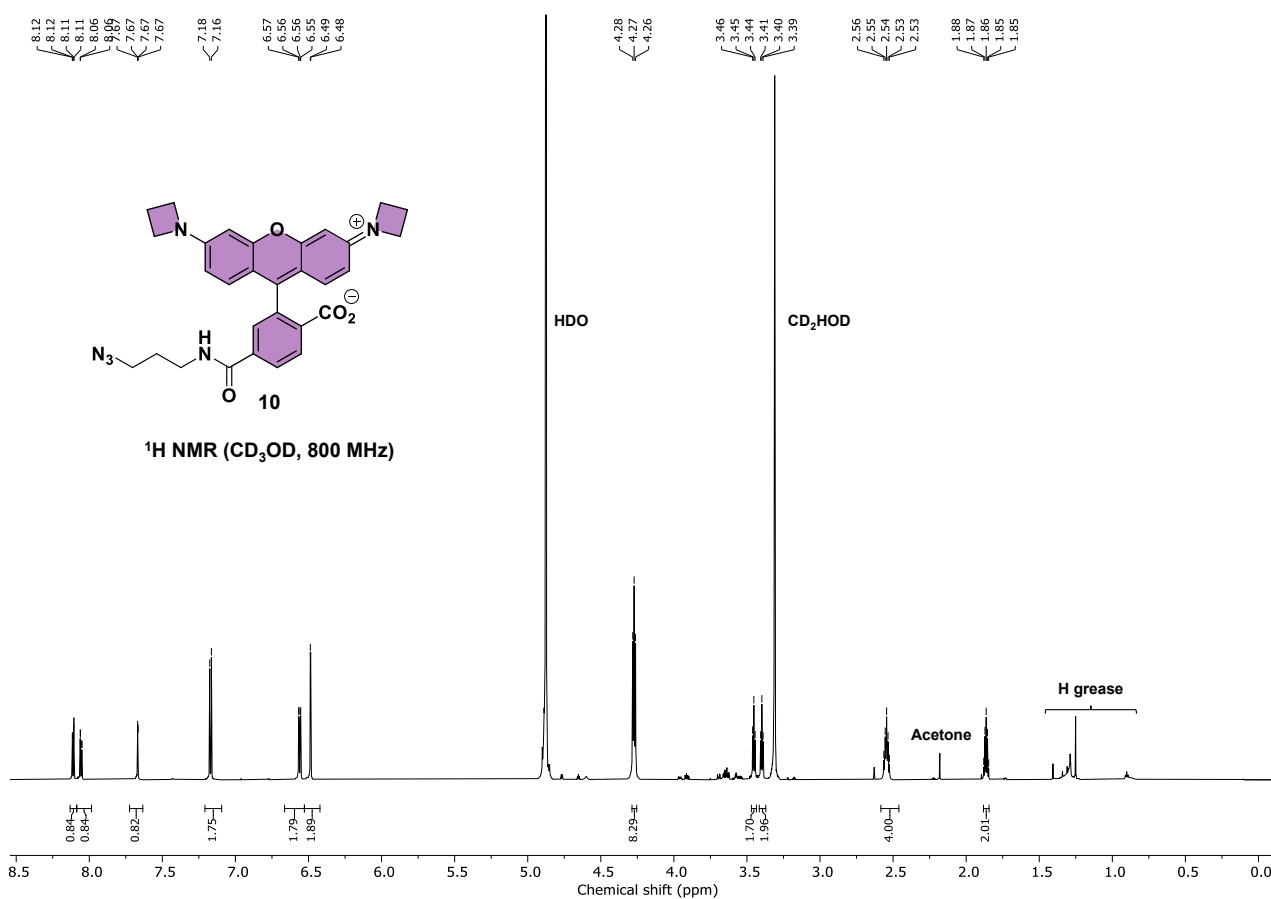
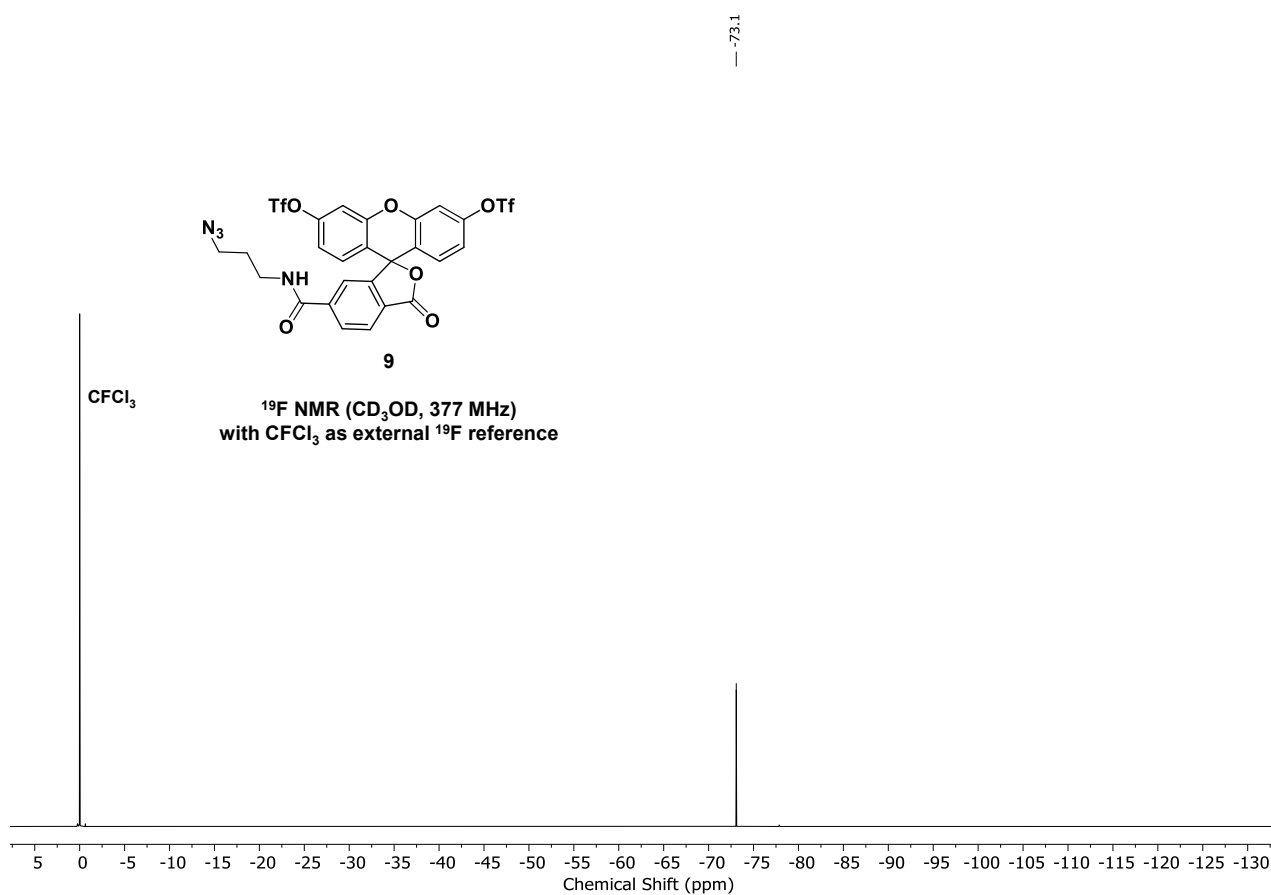
8. NMR Spectra of the Synthesised Compounds



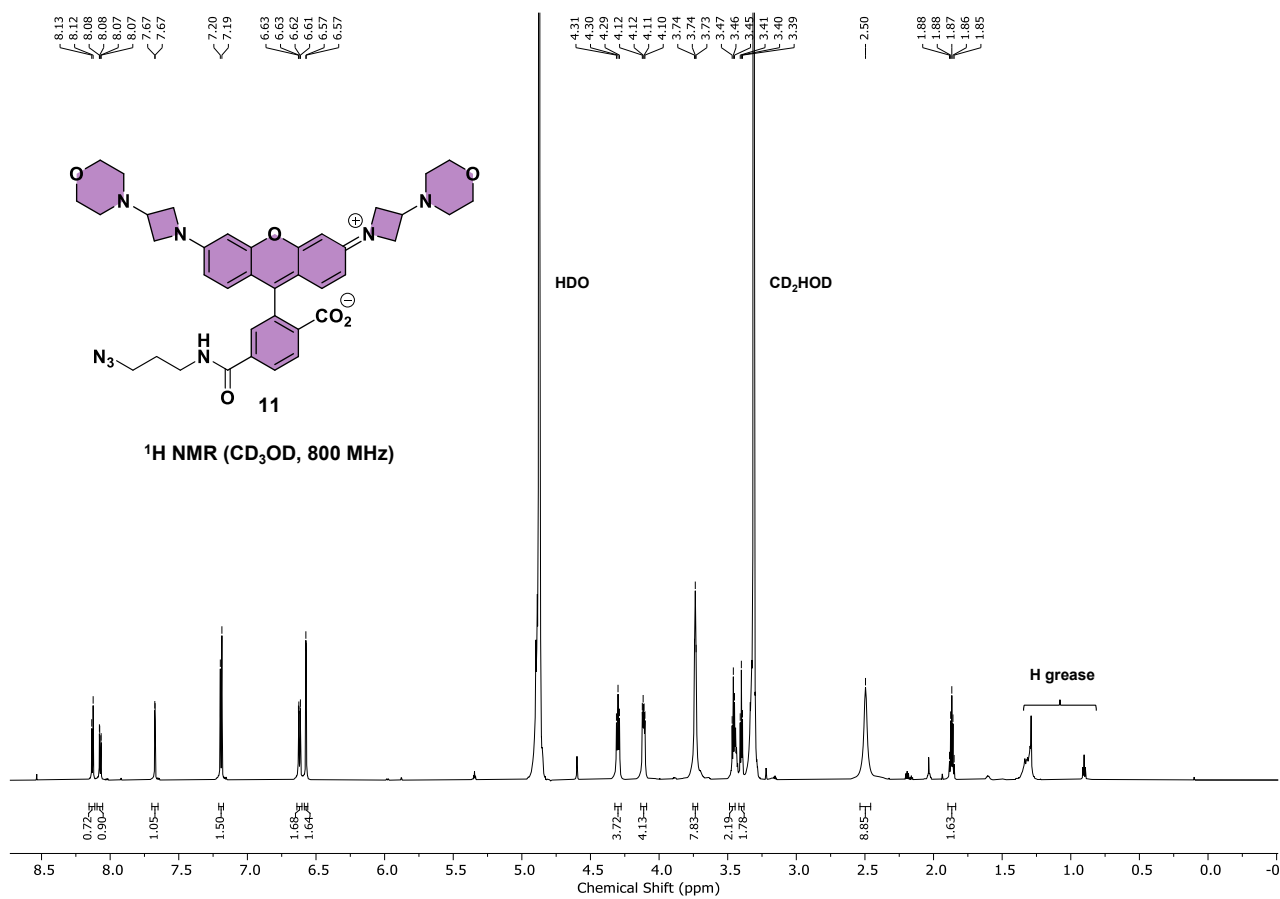
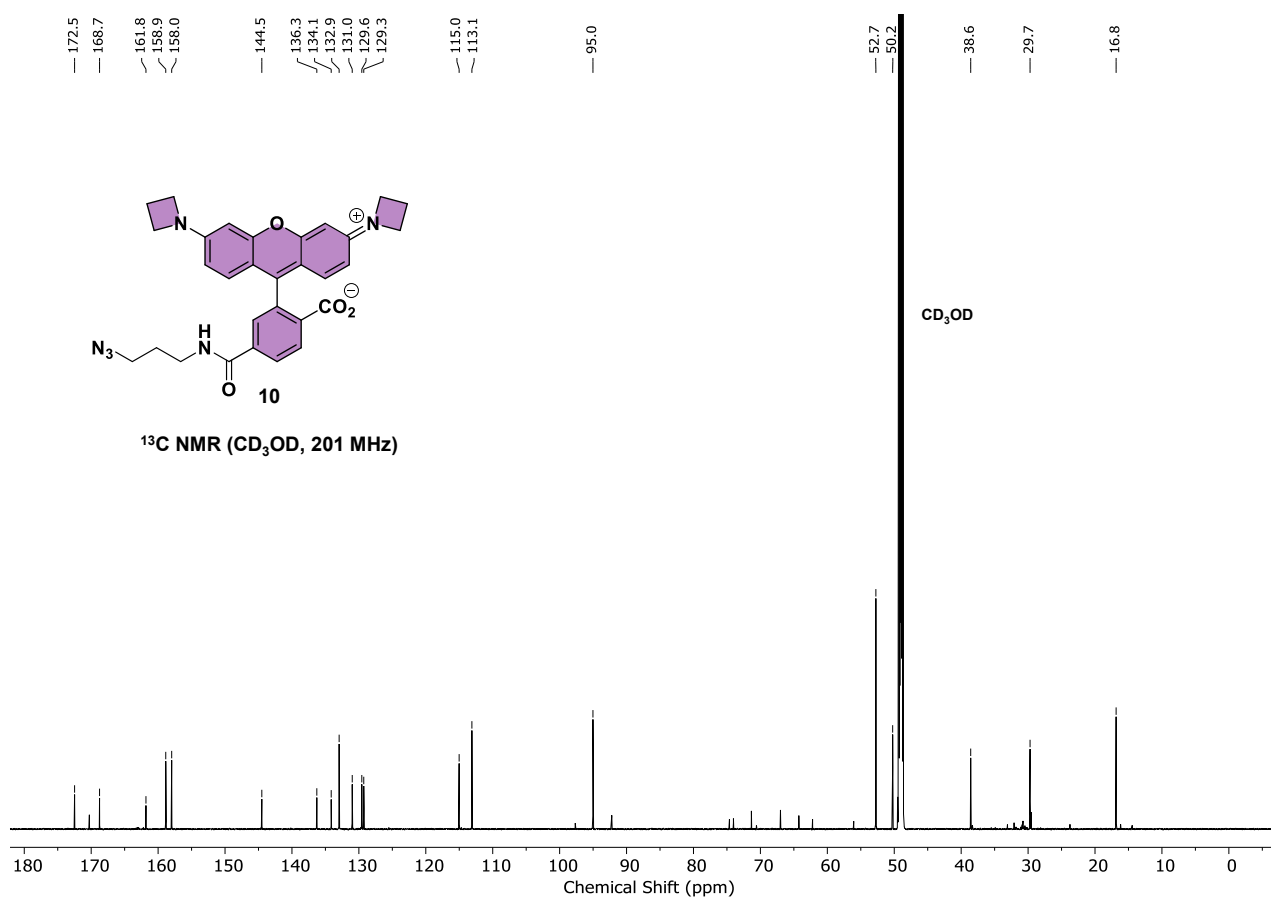
SUPPORTING INFORMATION



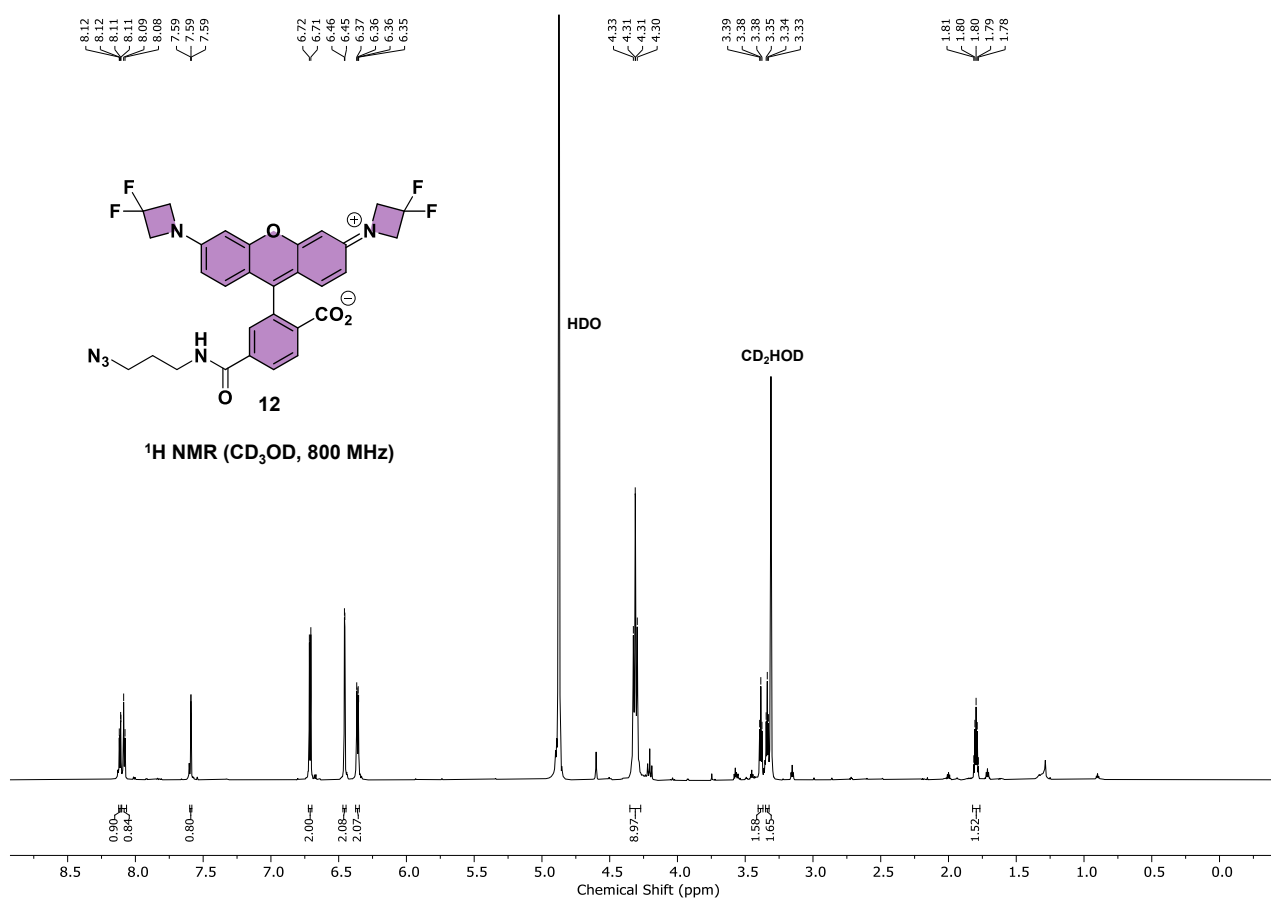
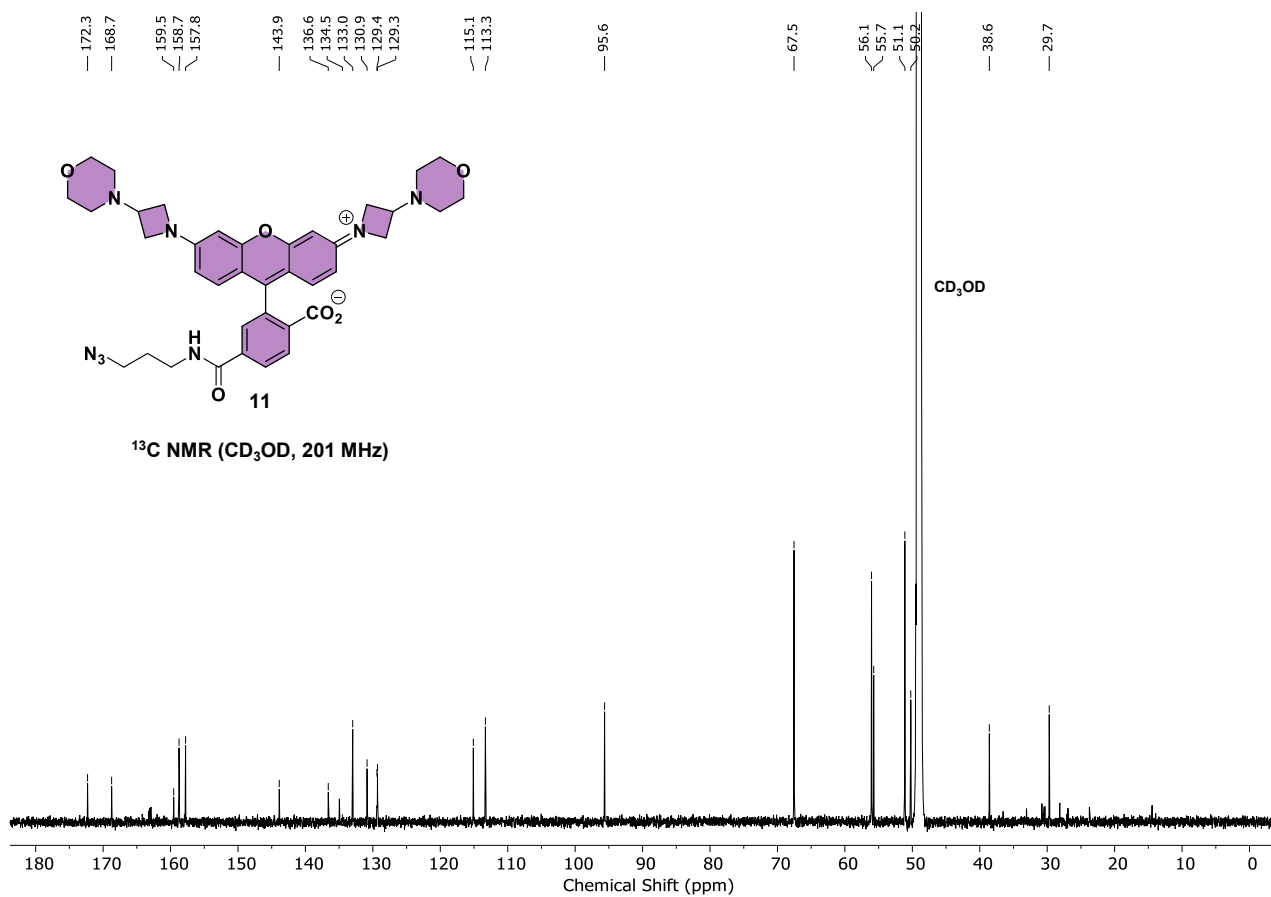
SUPPORTING INFORMATION



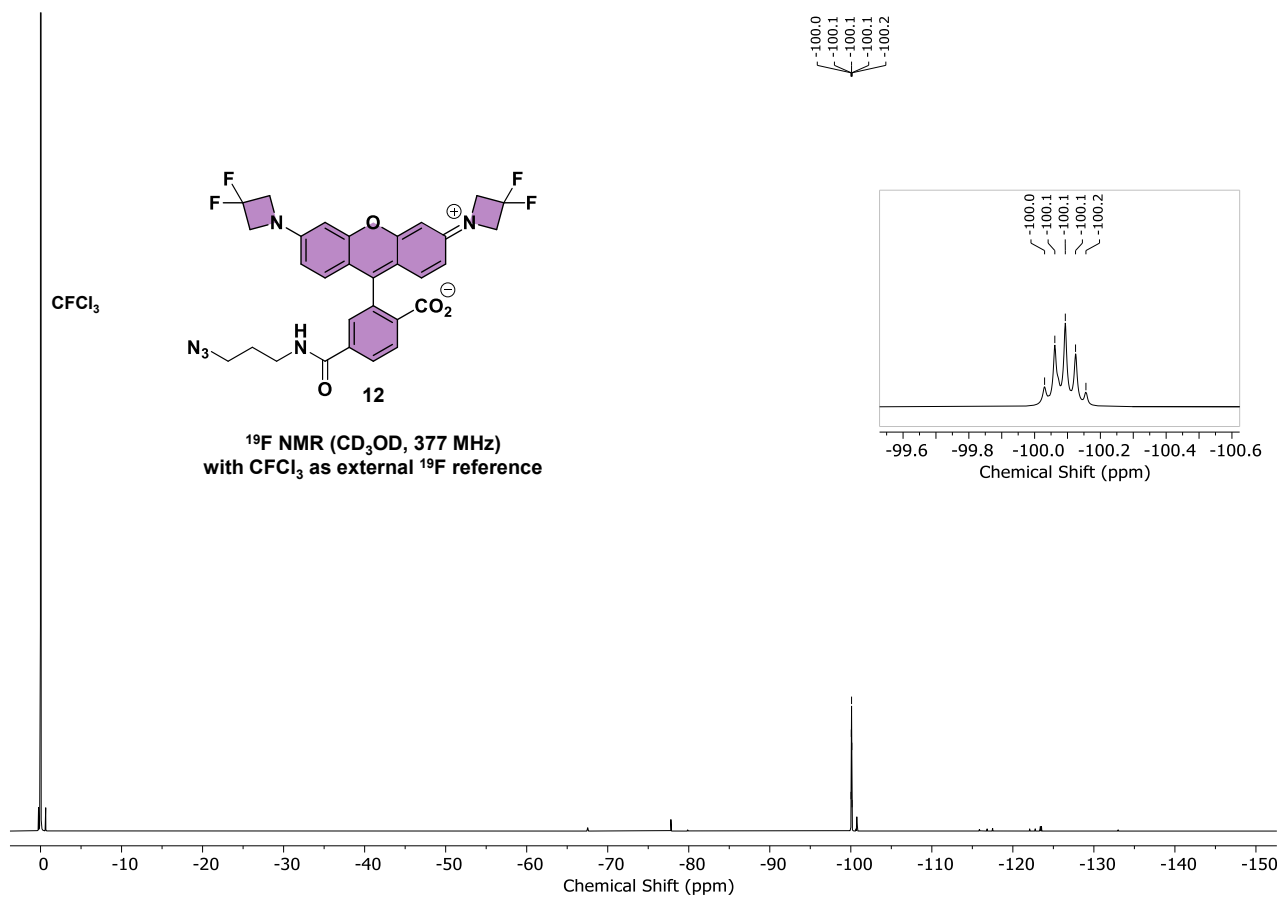
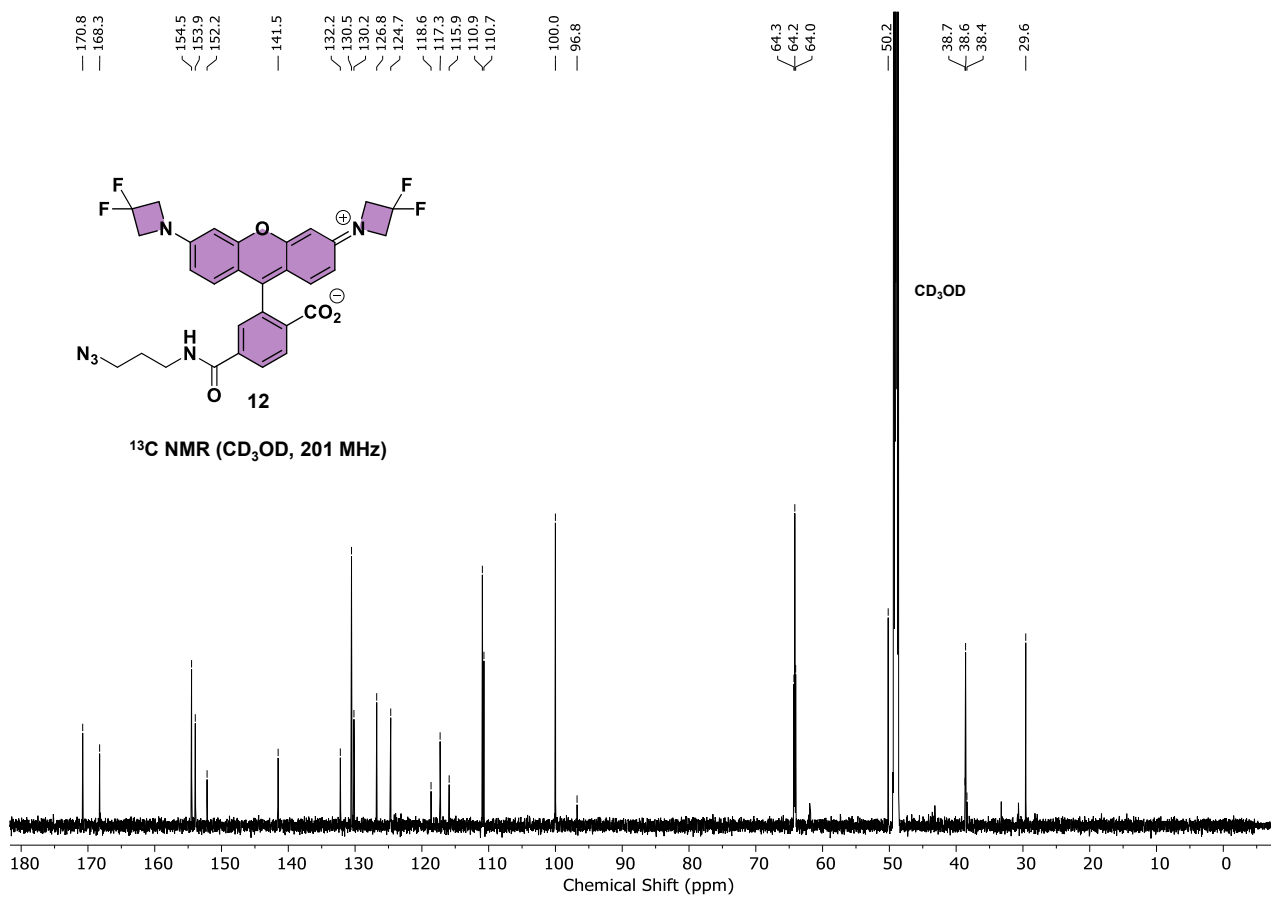
SUPPORTING INFORMATION



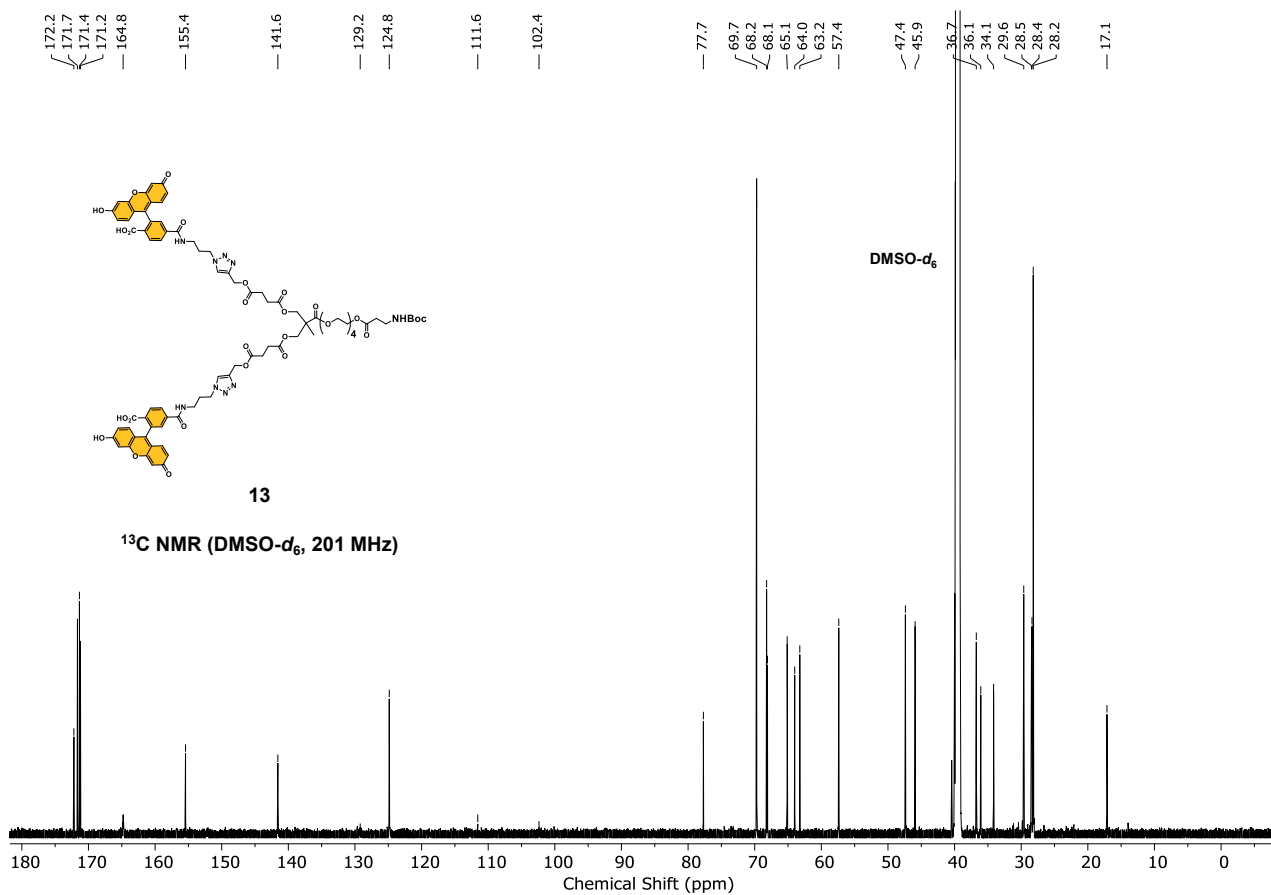
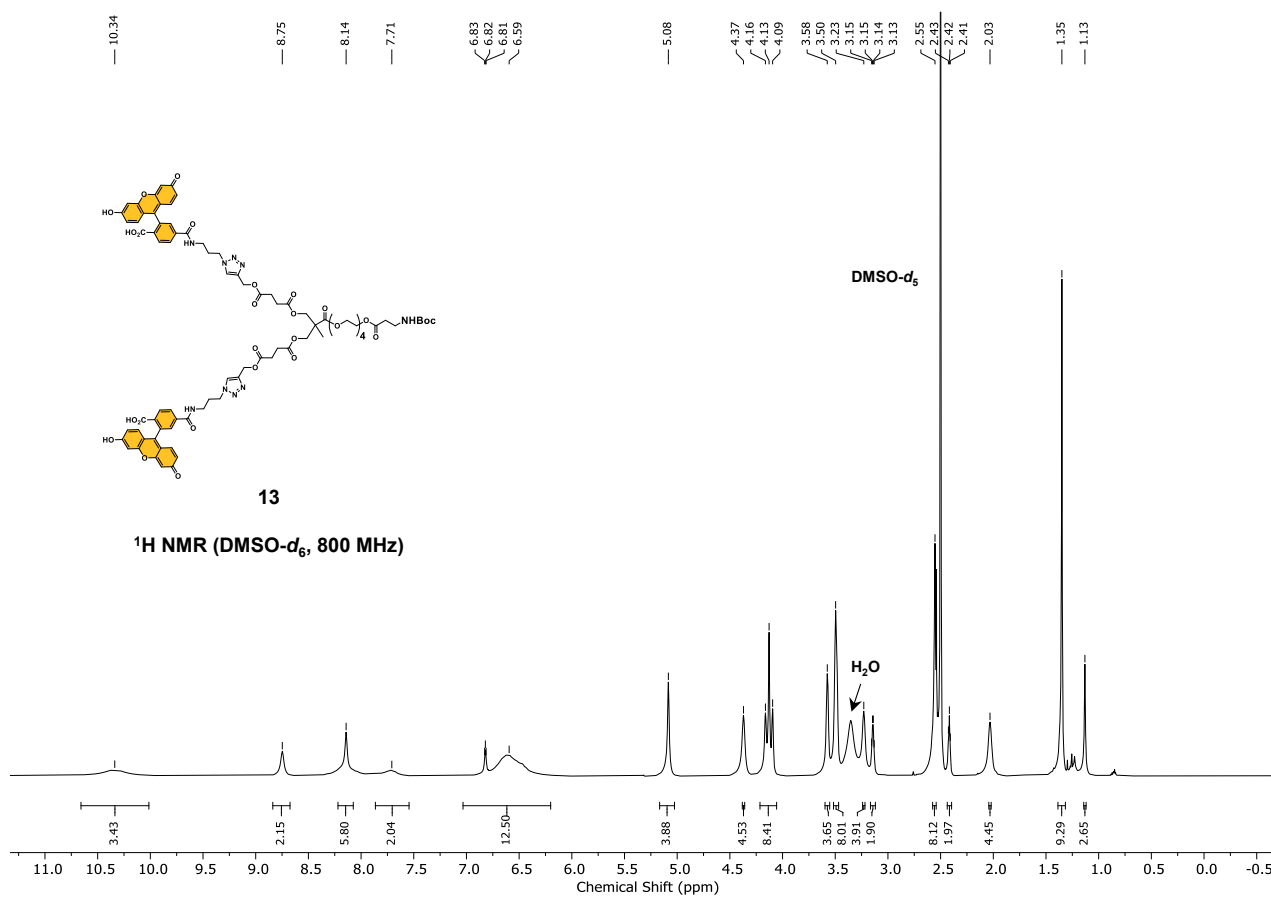
SUPPORTING INFORMATION



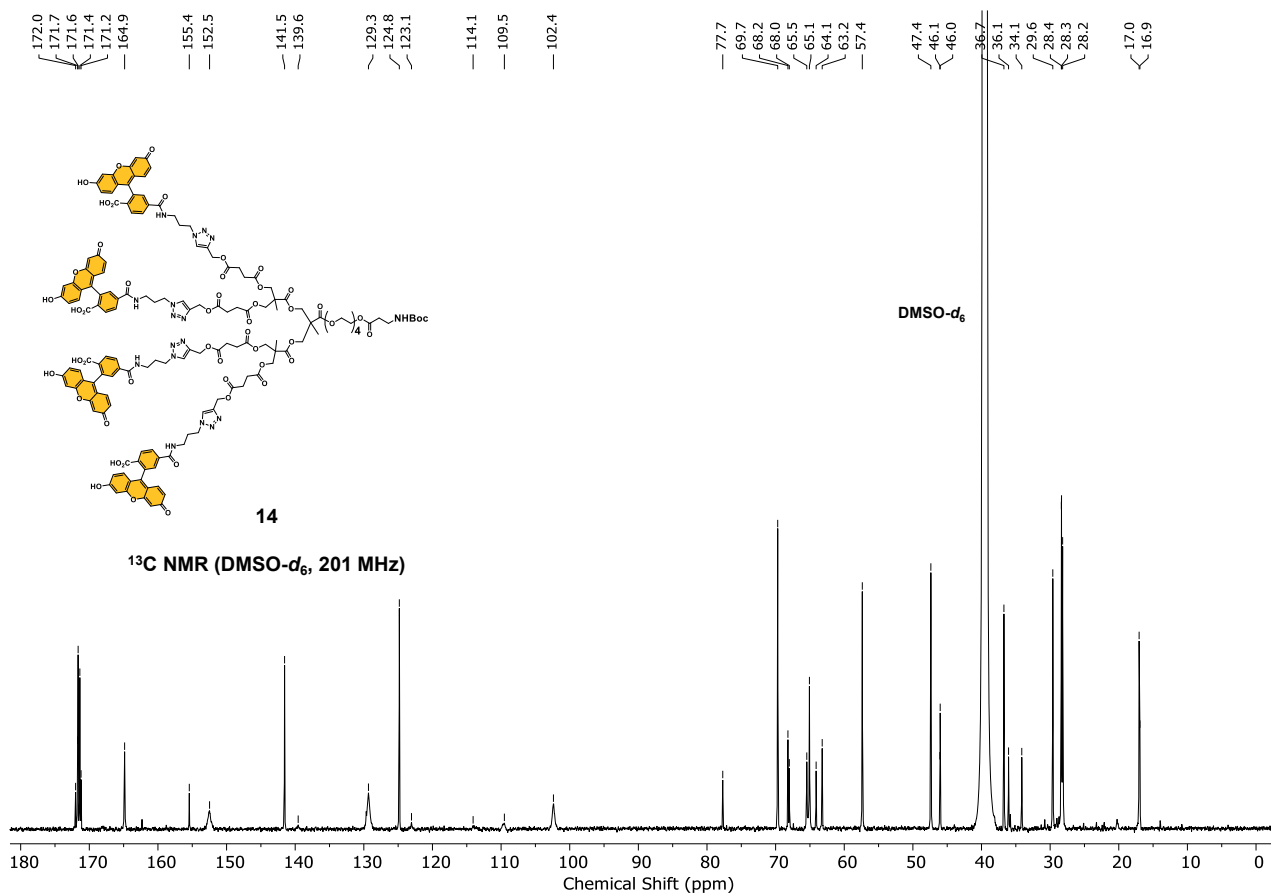
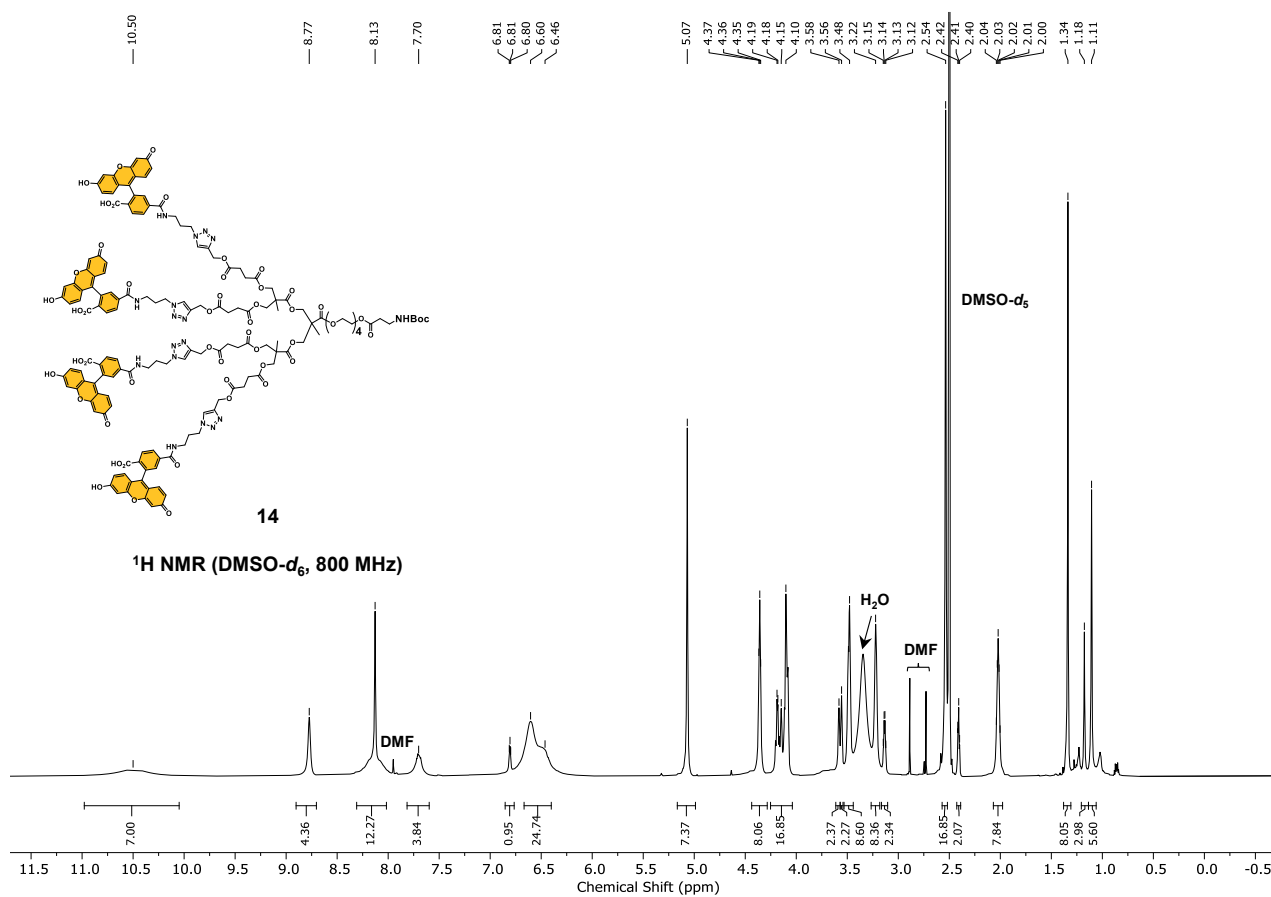
SUPPORTING INFORMATION



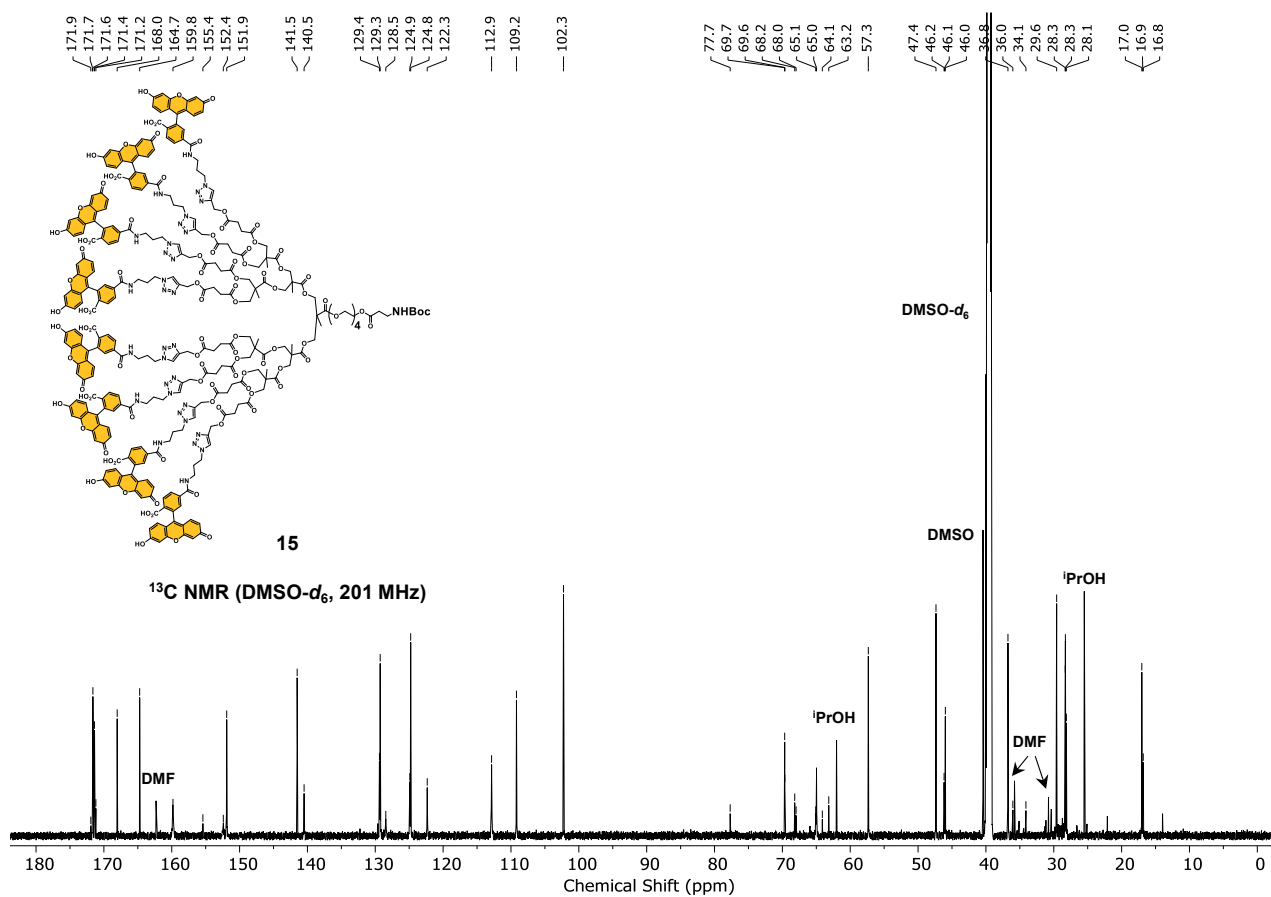
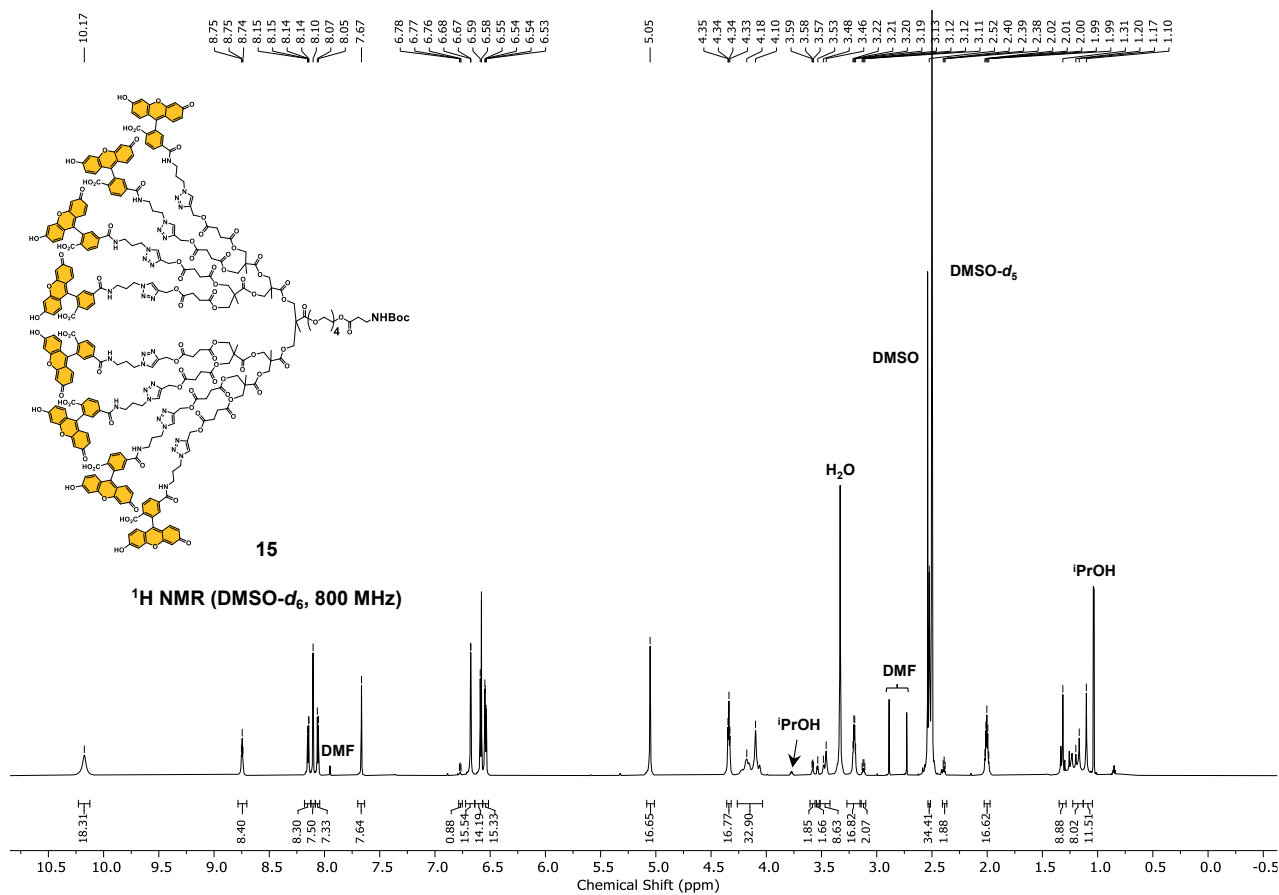
SUPPORTING INFORMATION



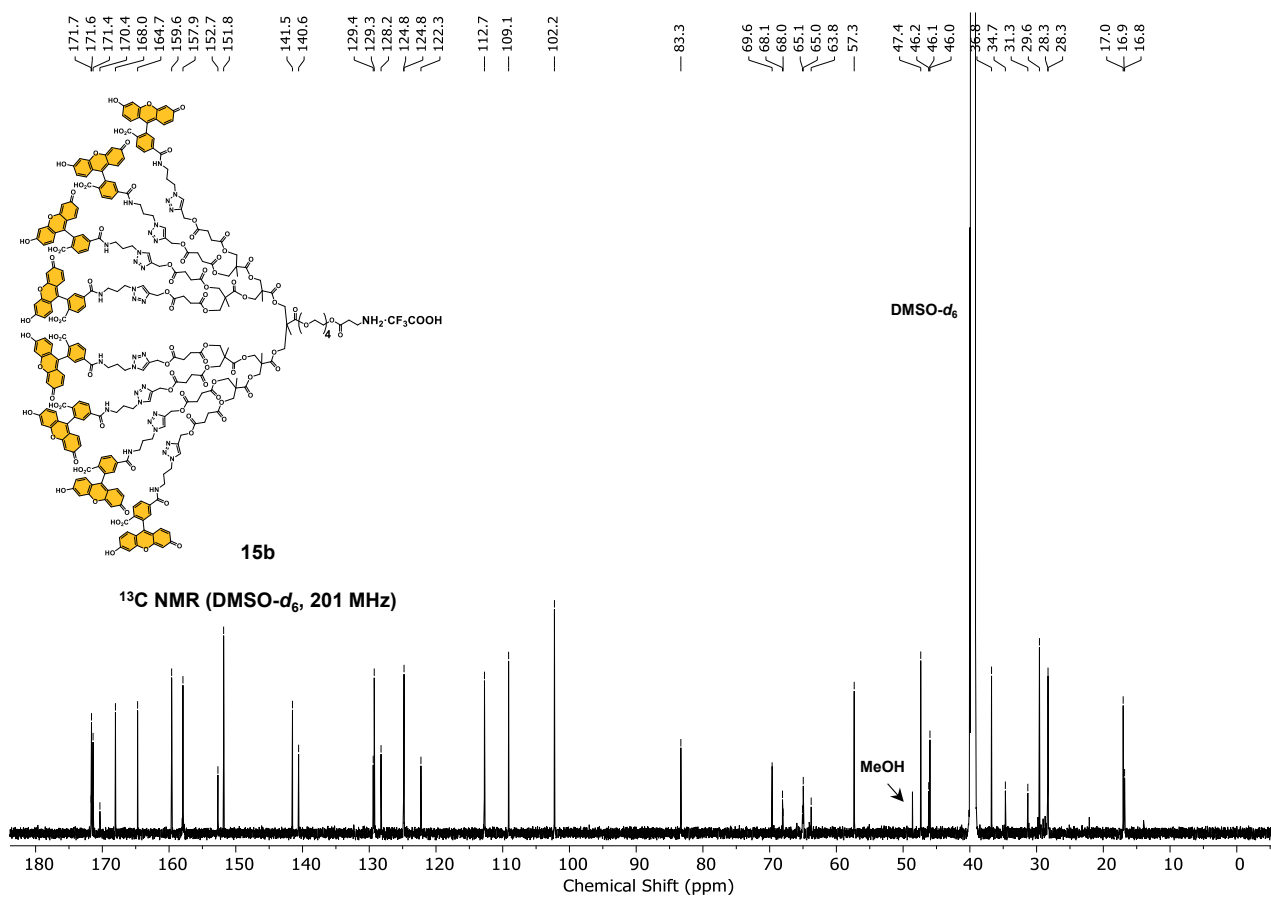
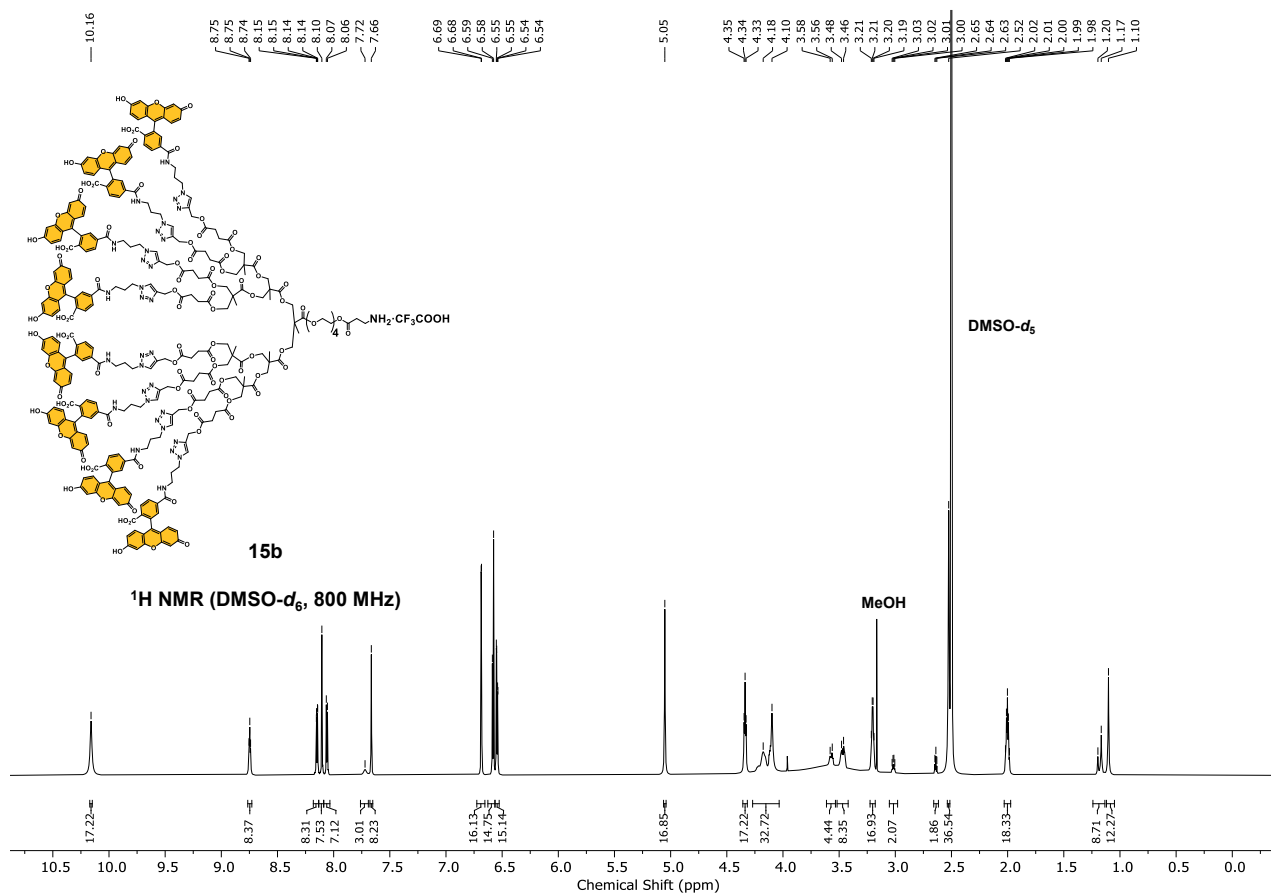
SUPPORTING INFORMATION



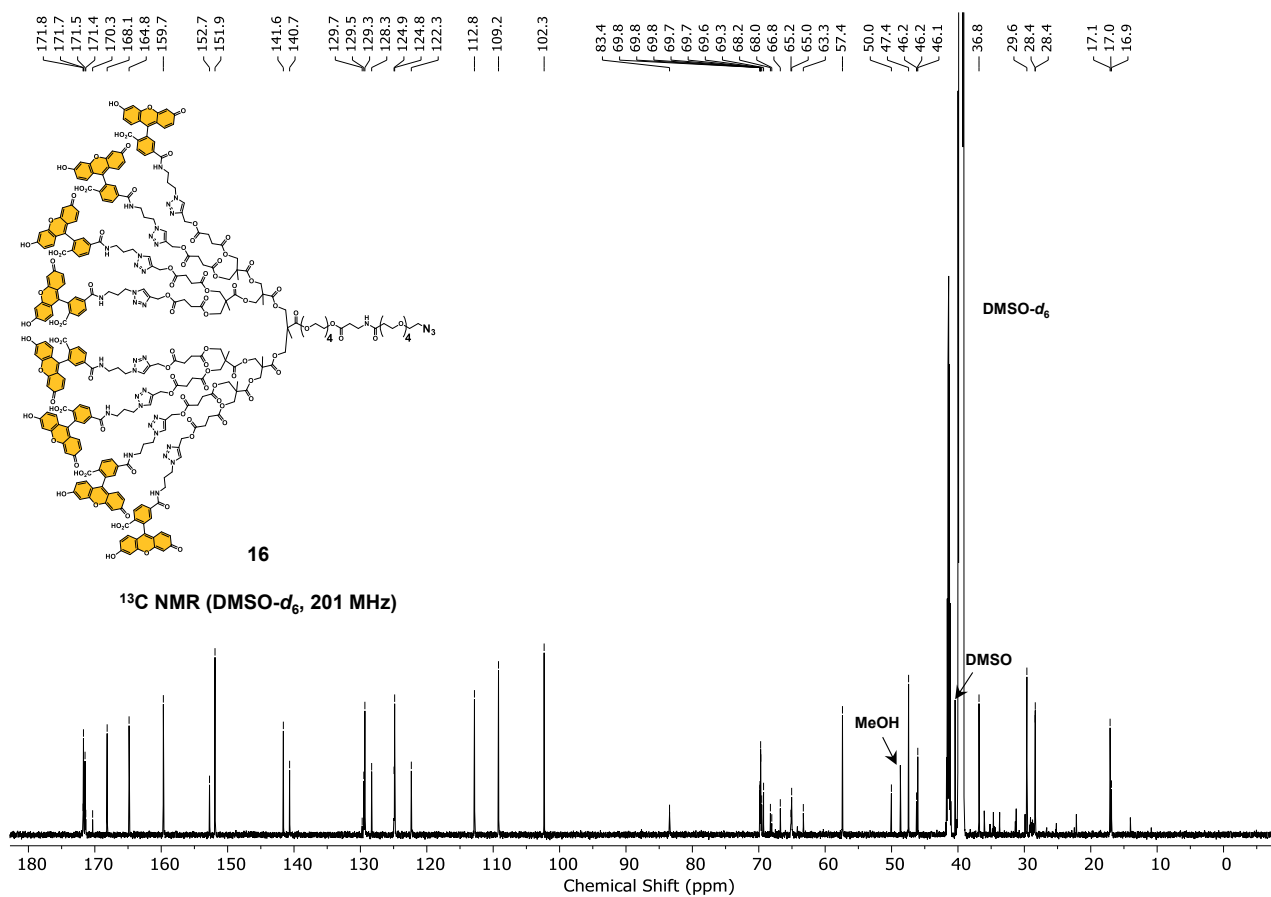
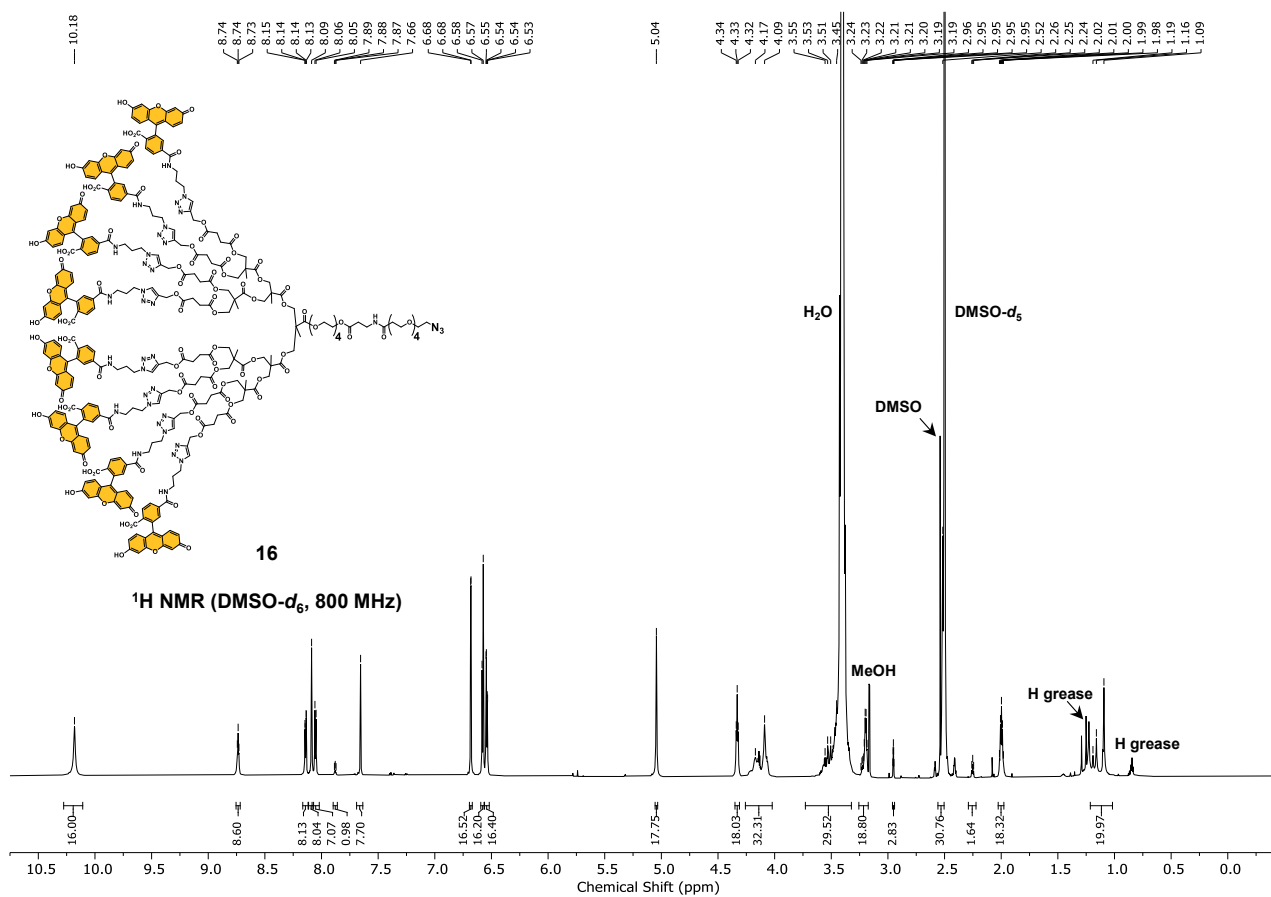
SUPPORTING INFORMATION



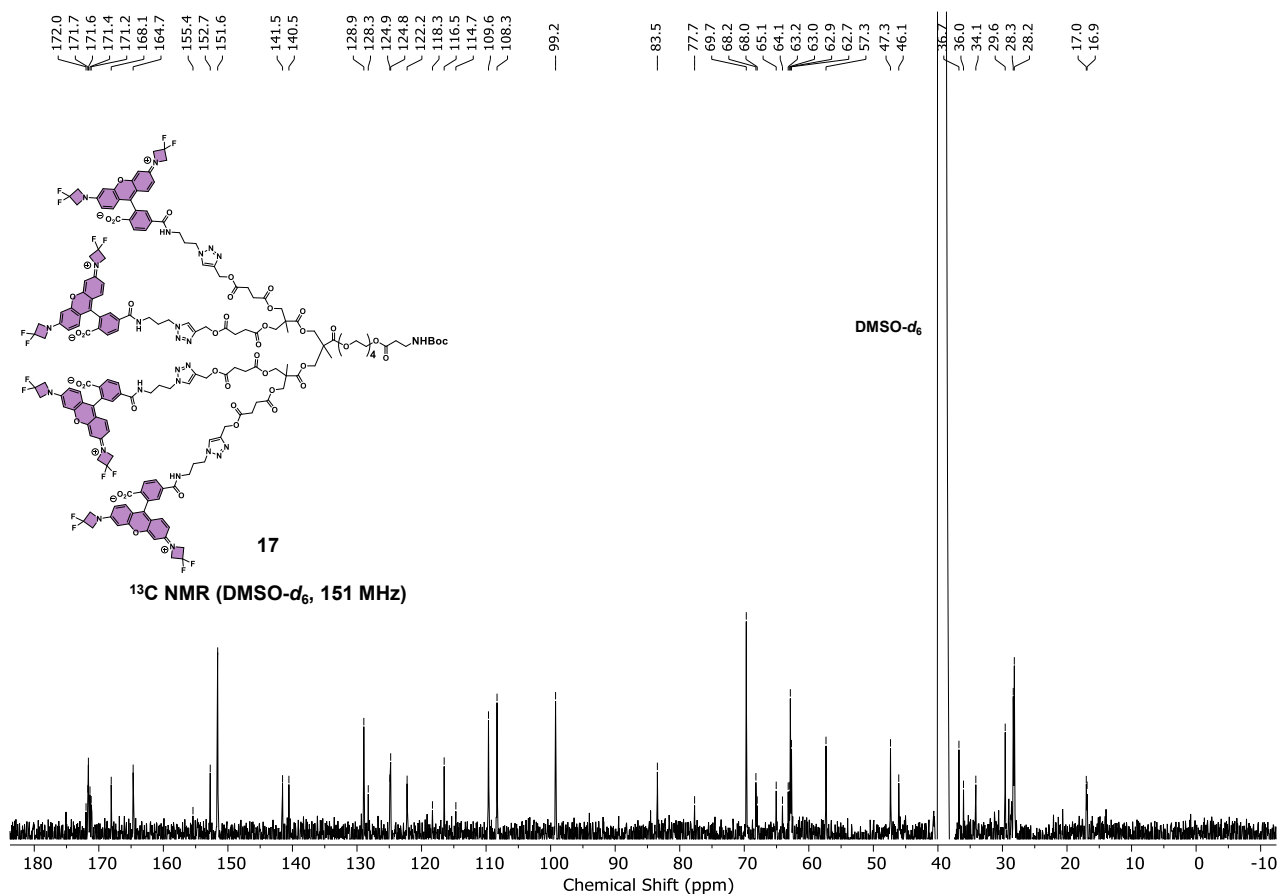
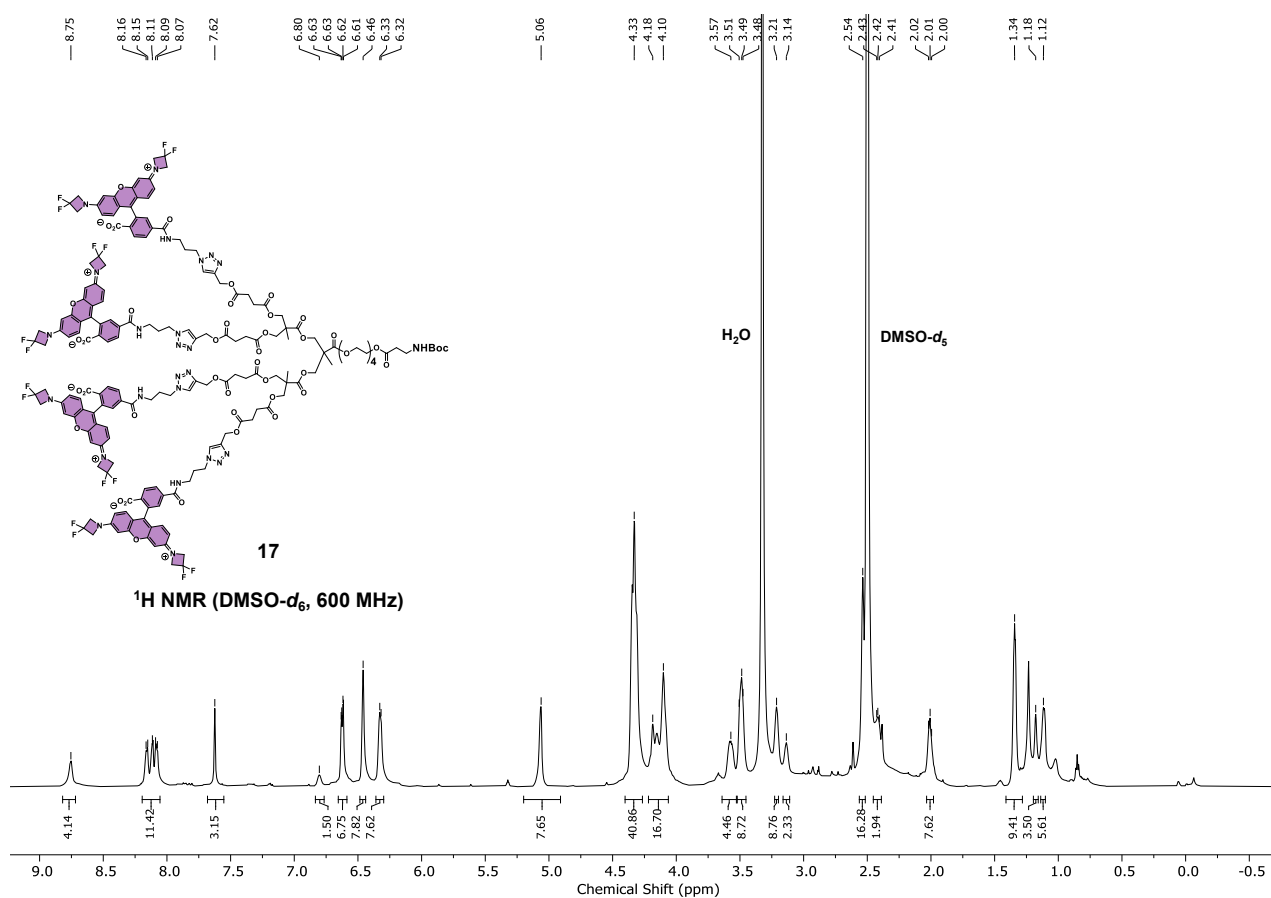
SUPPORTING INFORMATION

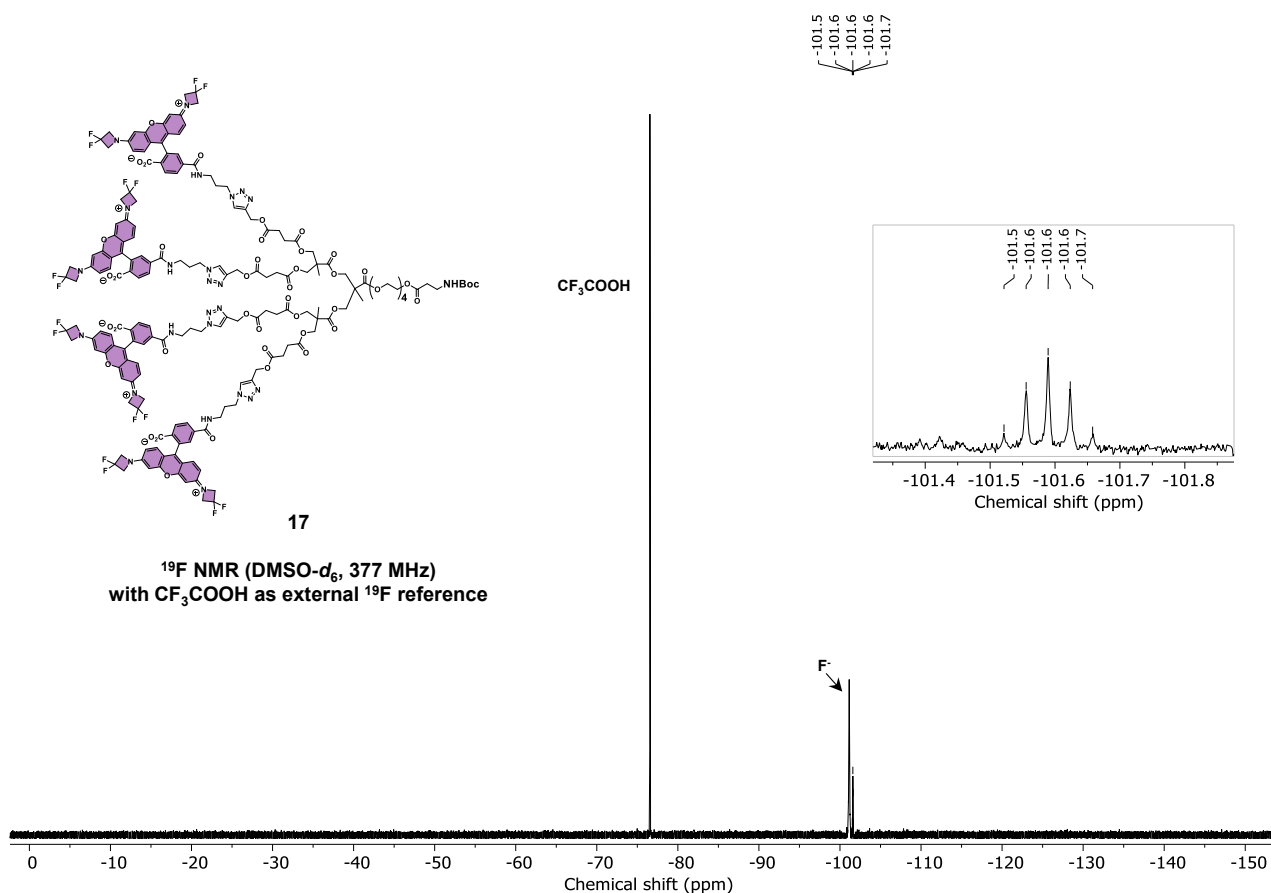


SUPPORTING INFORMATION



SUPPORTING INFORMATION





NOTE: The resonance at -101.1 ppm was tentatively assigned as soluble ionic fluoride (F^-).^[4,5]

9. References

- [1] F. Parenti, F. Tassinari, E. Libertini, M. Lanzi, A. Mucci, *ACS Omega* **2017**, *2*, 5775–5784.
- [2] G. Y. Wiederschain, *The Molecular Probes Handbook. A Guide to Fluorescent Probes and Labeling Technologies*, Springer, **2011**.
- [3] M. Beija, C. A. M. Afonso, J. M. G. Martinho, *Chem. Soc. Rev.* **2009**, *38*, 2410–2433.
- [4] A. Sadoc, M. Body, C. Legein, M. Biswal, F. Fayon, X. Rocquefelte, F. Boucher, *Phys. Chem. Chem. Phys.* **2011**, *13*, 18539–18550.
- [5] A. Rehmer, K. Scheurell, E. Kemnitz, *J. Mater. Chem. C* **2015**, *3*, 1716–1723.

10. Author Contributions

L. M. C. Conceptualization (**Equal**); Investigation and Methodology (**Lead**); Formal Analysis (**Lead**); Data Curation and Validation (**Lead**); Preparation of the Manuscript Draft (**Lead**).

F. S. Investigation and Methodology (**Supporting**); Formal Analysis (**Supporting**); Data Curation and Validation (**Supporting**); Preparation of the Manuscript Draft (**Supporting**); Supervision (**Supporting**).

A. C. Data Curation and Validation (**Supporting**); Preparation of the Manuscript Draft (**Supporting**); Supervision (**Supporting**).

S. S. Conceptualization (**Equal**); Supervision (**Supporting**).

T. C. Conceptualization (**Supporting**); Funding Acquisition (**Supporting**); Project Administration (**Supporting**).

T. F. Conceptualization (**Supporting**); Funding Acquisition (**Lead**); Project Administration (**Lead**); Supervision (**Lead**).

8.2 NMR Spectra for Unpublished Work

